

University of Kentucky

UKnowledge

Theses and Dissertations--Mining Engineering

Mining Engineering


2021

OXIDATION PRETREATMENT FOR ENHANCED LEACHABILITY OF RARE EARTH ELEMENTS FROM BITUMINOUS COAL SOURCES

Tushar Gupta

University of Kentucky, tushargupta2504@gmail.com

Author ORCID Identifier:

 <https://orcid.org/0000-0002-7985-2622>

Digital Object Identifier: <https://doi.org/10.13023/etd.2021.120>

[Right click to open a feedback form in a new tab to let us know how this document benefits you.](#)

Recommended Citation

Gupta, Tushar, "OXIDATION PRETREATMENT FOR ENHANCED LEACHABILITY OF RARE EARTH ELEMENTS FROM BITUMINOUS COAL SOURCES" (2021). *Theses and Dissertations--Mining Engineering*. 60.

https://uknowledge.uky.edu/mng_etds/60

This Doctoral Dissertation is brought to you for free and open access by the Mining Engineering at UKnowledge. It has been accepted for inclusion in Theses and Dissertations--Mining Engineering by an authorized administrator of UKnowledge. For more information, please contact UKnowledge@lsv.uky.edu.

STUDENT AGREEMENT:

I represent that my thesis or dissertation and abstract are my original work. Proper attribution has been given to all outside sources. I understand that I am solely responsible for obtaining any needed copyright permissions. I have obtained needed written permission statement(s) from the owner(s) of each third-party copyrighted matter to be included in my work, allowing electronic distribution (if such use is not permitted by the fair use doctrine) which will be submitted to UKnowledge as Additional File.

I hereby grant to The University of Kentucky and its agents the irrevocable, non-exclusive, and royalty-free license to archive and make accessible my work in whole or in part in all forms of media, now or hereafter known. I agree that the document mentioned above may be made available immediately for worldwide access unless an embargo applies.

I retain all other ownership rights to the copyright of my work. I also retain the right to use in future works (such as articles or books) all or part of my work. I understand that I am free to register the copyright to my work.

REVIEW, APPROVAL AND ACCEPTANCE

The document mentioned above has been reviewed and accepted by the student's advisor, on behalf of the advisory committee, and by the Director of Graduate Studies (DGS), on behalf of the program; we verify that this is the final, approved version of the student's thesis including all changes required by the advisory committee. The undersigned agree to abide by the statements above.

Tushar Gupta, Student

Dr. Rick Honaker, Major Professor

Dr. Jhon Silva, Director of Graduate Studies

OXIDATION PRETREATMENT FOR ENHANCED LEACHABILITY OF RARE
EARTH ELEMENTS FROM BITUMINOUS COAL SOURCES

DISSERTATION

A dissertation submitted in partial fulfillment of the
requirements for the degree of Doctor of Philosophy in the
College of Engineering at the University of Kentucky

By
Tushar Gupta
Lexington, Kentucky
Director: Dr. Rick Honaker, Professor of Mining Engineering
Lexington, Kentucky
2021

Copyright © Tushar Gupta 2021
<https://orcid.org/0000-0002-7985-2622>

ABSTRACT OF DISSERTATION

OXIDATION PRETREATMENT FOR ENHANCED LEACHABILITY OF RARE EARTH ELEMENTS FROM BITUMINOUS COAL SOURCES

Rare earth elements (REEs) are critical components in advanced electronics, clean energy technologies, and national energy and economic security. The global supply situation of these strategically valuable elements remains critical as the market is largely monopolistic. Thus, to alleviate the dependence on global imports, investments are being made in the research and development of innovative and cost-effective technologies for the indigenous processing and recovery of REEs from alternate sources that are cheap and abundant. Numerous research findings have identified potential benefits and proven the technological feasibility of extracting and selectively concentrating REEs from coal byproducts such as preparation plant rejects and acid mine drainage among other sources.

Given the relatively low grades, the chemical cost associated with hydrometallurgical extraction of REEs from coal-derived feedstocks is excessively high for commercial extraction. Recent studies have been successful in increasing REE recovery and leaching kinetics by oxidation pretreatment of the coal-based feed. However, the reasons behind the positive oxidation effects have yet to be systematically studied to provide an understanding of the mineralogical changes and to utilize the knowledge for process development. Therefore, the current investigation aimed to comprehensively study the effect of oxidation parameters on the leaching characteristics of REEs contained in coal-based feedstocks. Low and high-temperature oxidation methods were evaluated and assessed to quantify their impacts on the recovery of REEs as well as the extraction of common contaminant elements (aluminum, calcium, and iron) found in a coal-derived pregnant leach solution.

Initially, the effect of low-temperature plasma (LTP) was analyzed for improving the REE leaching recovery from coal coarse rejects. The refuse material originating from the West Kentucky No.13 (WK-13) and Fire Clay coal seams were oxidized by LTP and leached separately using different lixiviants, i.e., deionized water,

0.1M ammonium sulfate, and 1.2M sulfuric acid, at 75°C in a sequential manner. LTP pretreatment was found to significantly enhance REE leaching characteristics for the low ash content, light density fractions of the WK-13 with selectivity towards the heavy REEs that are of critical importance. High heavy REE recovery values from the 1.60 specific gravity (SG) float fraction were positively correlated with a decrease in organic content which was achieved by an increase in LTP treatment time and using both a mild 0.1M ammonium sulfate solution and 1.2M sulfuric acid as lixiviants. This finding indicated a strong affinity of the heavy REEs with the dispersed mineral matter existing within the organic material, which was partially liberated during the LTP treatment. The improvement in REE leachability can be attributed to increased porosity and surface area by LTP treatment as confirmed from surface area analysis and scanning electron micrographs. However, LTP had a limited effect on the high-ash content, heavy-density fractions and provided no significant improvement in leaching characteristics. Similarly, the LTP treatment of the Fire Clay provided no significant improvement in high ash density fractions and marginal benefits for the 1.60 float fraction, which suggests differences in the mode of occurrence of the REEs between the two coal sources.

Secondly, calcination at 600-800°C for two hours significantly improved REE leachability for all density fractions in both coals under standard acid leaching conditions. The majority of the heavy REEs were found to be marginally affected by thermal treatment. Additionally, a strong correlation between the light REEs and aluminum suggested a possible association of light REEs with clays. Test results from the parametric program performed based on a Box-Behnken design were used for modeling and optimization of three operating parameters associated with the lab-scale calcination process (temperature (400-800°C), ramp rate (2-10°C/min) and hold time (0-120 min)). The calcination temperatures required for selectively improving REE recovery while minimizing the extraction of contaminant ions were found to be dependent on the mineral composition of the feed.

Subsequently, the potential of iron contamination removal from the hydrometallurgical process by calcination and magnetic separation was investigated. The calcined products at 400-500°C of the pyrite-rich 2.20 SG sink fraction of the WK-13 seam

provided an opportunity for REE enrichment in the tailings by magnetic separation. The magnetic fraction had a higher recovery of heavy REEs and iron as compared to the feed and the nonmagnetic fraction. The improvements in the heavy REE leaching characteristics resulted from the transformation of pyrites to intermediate hematite at high temperatures under the presence of oxygen. A novel flowsheet was proposed by integrating calcination and magnetic separation with a typical hydrometallurgical process for efficient extraction of REEs from a pyrite-rich feedstock.

Finally, the effect of calcination atmosphere (oxidizing/inert) on enhancing the REE leachability was evaluated at high temperatures. The REE recovery for high ash fractions (>2.00 SG) of a Fire Clay seam source was significantly improved at 1000°C under an inert atmosphere, which contrasted with the poor recovery values achieved under oxygen due to sintering of the clay surfaces. The benefits of the heavy REE leaching from the low ash density fractions were realized only when the organic matter was removed under an oxidizing environment suggesting the association of heavy REEs with the organic material. As a means of further identifying modes of occurrence, an excellent correlation was discovered between the leaching behavior of the bituminous coal sources and natural clay minerals in relation to the recovery of the heavy REEs and overall REE leaching kinetics. A characteristic exothermic peak for the phase transformation of meta kaolinite to mullite was observed for calcination under an inert environment for the density fractions of the two coal sources. Selectivity towards REEs associated with the clay samples was obtained by calcination at 500-800°C and using a short leaching time. Fe contamination can be controlled by converting the pyrite to crystalline hematite at temperatures >600°C using standard air and by calcination at lower temperatures (400-500°C) for Fe that is associated with clay minerals.

KEYWORDS: rare earth elements, optimization, high-temperature calcination, low-temperature plasma, TGA-DSC, magnetic separation

Tushar Gupta

(Name of Student)

05/03/2021

Date

OXIDATION PRETREATMENT FOR ENHANCED LEACHABILITY OF RARE
EARTH ELEMENTS FROM BITUMINOUS COAL SOURCES

By
Tushar Gupta

Dr. Rick Honaker

Director of Dissertation

Dr. Jhon Silva

Director of Graduate Studies

05/03/2021

Date

DEDICATION

To My father, Shri Vipin Gupta (1960-2018).
Thank you for giving me life and teaching me to own my decisions.
I Miss You, Papa.
Wish you were here.

ACKNOWLEDGMENTS

Firstly, I want to express my sincerest gratitude to my advisor Dr. Rick Honaker for his valuable support, motivation, and invaluable guidance throughout my Ph.D. candidacy. His attitude towards research and life has inspired me and contributed greatly to the success of this investigation. A big thank you to my graduate committee members Dr. Wencai Zhang, Dr. Jack Groppo, and Dr. Kozo Saito for their valuable time and profound help in completing the research. The doors to their offices were always open whenever I ran into a troubled spot in my life or my work.

I am genuinely grateful to the University of Kentucky and the Department of Mining Engineering for the opportunity to do my Ph.D. A special shoutout to Lauren Pennington and Caleb Matocha from the University of Kentucky for their long hours of hard work and assistance, and Jason Bakus and Ethan Davis from the Kentucky Geological Survey as their guidance and expertise played a crucial role in this project.

My greatest gratitude goes to my family, Mrs. Hemant Gupta, Mr. Mukesh Gupta, Mrs. Seema Gupta, Mrs. Anju Gupta, Mr. Rajeev Gupta, and my siblings Shristy, Purva, and Prakhar for their endless love and encouragement. A big thanks also go to my wife Shanu, who has loved me, cared for me, and persevered with me through thick and thin.

Special thanks are given to Dr. Alind Chandra, Anand Kumar, Dr. Ashish Ranjan, Shravani Prakhya, Neeraj Gupta, Ahmad Nawab, and Neha Gupta, I say thank you all for your friendship support in diverse ways throughout the last few years. I would finally like to thank all my fellow graduate students and faculty and staff at the University of Kentucky who made my stay in Lexington one of the most memorable and enjoyable experiences in my lifetime.

TABLE OF CONTENTS

ACKNOWLEDGMENTS	III
LIST OF TABLES	VIII
LIST OF FIGURES	X
CHAPTER 1. INTRODUCTION	17
1.1 Background	17
1.2 Objectives	19
1.3 Organization.....	20
CHAPTER 2. LITERATURE REVIEW	22
2.1 Rare Earth Elements	22
2.1.1 Classification of REEs	22
2.1.2 REE Resources.....	23
2.1.3 Applications and end-use of REEs	25
2.1.4 Global demand and Supply of REEs	26
2.2 REE processing.....	27
2.2.1 Physical Beneficiation	27
2.2.1.1 Bastnaesite	27
2.2.1.2 Monazite	29
2.2.1.3 Xenotime.....	30
2.2.2 Hydrometallurgical Processing.....	31
2.2.2.1 Bastnaesite	31
2.2.2.2 Monazite	33
2.2.2.3 Xenotime.....	34
2.2.2.4 Ion- Adsorbed Clays	35
2.3 REEs in Coal.....	36
2.3.1 Extraction of REEs from coal.....	37
2.4 Low-temperature Plasma	46
2.5 Minerals of coal deposits	52
2.6 Decomposition of major coal minerals	54

2.6.1	Quartz.....	54
2.6.2	Pyrite.....	55
2.6.3	Clay Minerals.....	59
CHAPTER 3. MATERIALS AND METHODS.....		62
3.1	Introduction.....	62
3.2	Materials	62
3.2.1	Coal Refuse Samples	62
3.2.2	Chemicals.....	72
3.3	Experimental Apparatus and Procedures	73
3.3.1	Low-Temperature Plasma.....	73
3.3.2	Calcination Tests.....	75
3.3.3	Leaching Tests	75
3.3.4	Magnetic Separation	77
3.4	Analytical Tools.....	78
3.4.1	XRD	78
3.4.2	TGA-DSC	79
3.4.3	ICP-OES	81
3.4.4	BET Analysis	83
3.4.5	Scanning Electron Microscope (SEM)	85
CHAPTER 4. LOW-TEMPERATURE PLASMA.....		86
4.1	Introduction.....	86
4.2	Materials and Methods.....	88
4.2.1	Materials	88
4.2.2	Methods.....	89
4.2.2.1	Sample Characterization	89
4.2.2.2	Low-Temperature Plasma Tests	90
4.2.2.3	High-Temperature Calcination Tests.....	91
4.2.2.4	Leaching Tests	92
4.2.2.5	Mineralogy and REE analysis.....	92
4.3	Results and Discussions.....	93
4.3.1	Low-Temperature Plasma Tests	94

4.3.2	High-Temperature Calcination Tests	103
4.4	Conclusions.....	106
CHAPTER 5. HIGH-TEMPERATURE CALCINATION.....		108
5.1	Introduction.....	108
5.2	Materials and Methods.....	109
5.2.1	Materials	109
5.2.2	Methods.....	110
5.2.2.1	Calcination: Lab-Scale.....	110
5.2.2.2	Acid Leaching Tests	112
5.3	Results and Discussions.....	112
5.3.1	Batch Calcination Tests	112
5.3.2	Parametric Optimization Study.....	123
5.4	Conclusions.....	137
CHAPTER 6. PROCESS DEVELOPMENT FOR REMOVAL OF IRON FROM FEED 139		
6.1	Introduction.....	139
6.2	Materials and Methods.....	141
6.2.1	Materials	141
6.2.2	Methods.....	143
6.2.2.1	Calcination Tests.....	143
6.2.2.2	Magnetic Separation Tests.....	143
6.2.2.3	Acid Leaching Tests	144
6.2.2.4	Scanning Electron Microscope (SEM) Analysis	144
6.3	Results and Discussions.....	145
6.3.1	Pyrite Characterization.....	145
6.3.2	Magnetic Separation	147
6.4	Leaching Experiments	150
6.5	Novel Process Flow Sheet Development.....	155
6.6	Conclusions.....	158
CHAPTER 7. EFFECT OF CALCINATION ENVIRONMENT		160
7.1	Introduction.....	160

7.2	Materials and Methods.....	162
7.2.1	Materials	162
7.2.2	Methods.....	167
7.2.2.1	Calcination Tests.....	167
7.2.2.2	Acid Leaching Tests	168
7.2.2.3	DSC Analysis.....	168
7.3	Results and Discussions.....	169
7.3.1	Acid Leaching Tests	169
7.3.2	DSC Analysis.....	175
7.4	Calcination and leaching of mineral clay and pyrites.....	180
7.5	Conclusions.....	190
CHAPTER 8.	CONCLUSIONS.....	192
CHAPTER 9.	RECOMMENDATIONS FOR FUTURE WORK	196
REFERENCES	197
VITA	209

LIST OF TABLES

Table 2.1. Minerals that contain REEs and occur in economic or potentially economic deposits [9] (Ln=Lanthanide Element).	24
Table 2.2. List of REEs and their major end-use in the industry. (Modified from [9])....	26
Table 2.3. A summary of monazite and bastnasite roasting reactions [36].	42
Table 2.4. Common minerals found in coal and their elemental compositions [116].	53
Table 3.1. REE concentrations in each segment obtained from a core sample of the West Kentucky No.13 coal seam [61].	64
Table 3.2. The elemental concentration (ppm) of REEs+Sc+Y for the density fractionated samples of West Kentucky No.13 on a dry, ash basis.	69
Table 3.3. The elemental concentration (ppm) of REEs+Sc+Y for the density fractionated samples of Fire Clay on a dry, ash basis.	69
Table 3.4. XRF analysis of major and minor phases for the density fractions of the WK-13 and Fire Clay samples on an ash basis.	70
Table 3.5. Details of the chemicals and minerals used in the current study.	73
Table 3.6. The standard deviation for the measurement of rare earth elements and the contaminants using ICP-OES [61].	83
Table 4.1. Proximate analysis of the density fractions of the West Kentucky No.13 and Fire Clay refuse.	89
Table 4.2. Summary of the analytical techniques used.	90
Table 4.3. Results of the pore volume and surface area analysis for the feed and plasma-treated ash of 1.60 SG float and 2.20 SG sink material of West Kentucky No.13 refuse treated for 32 hours.	103
Table 5.1. Levels of Independent variables and their ranges for Box-Behnken design.	111
Table 5.2. Input factors and the results of the Box- Behnken experimental design for 1.60 SG float and 2.20 SG sink of West Kentucky No.13.	124
Table 5.3. Correlation matrix of the major response variables with the input variables used in the calcination studies of the West Kentucky No.13 sample.	125
Table 5.4. Set of optimum parameter values for the desired goals of the response variables from the Box-Behnken Design and the value of other output variables for 1.60 SG float of West Kentucky No.13 (Cont.=Total Contaminants).	128

Table 5.5. Set of optimum parameter values for the desired goals of the response variables from the Box-Behnken Design and the value of other output variables for 2.20 SG sink of West Kentucky No.13 (Cont.=Total Contaminants).	129
Table 5.6. Input factors and the results of the Box- Behnken experimental design for 1.60 SG float and 2.20 SG sink of Fire Clay.	131
Table 5.7. Correlation matrix of the major response variables with the input variables used in the calcination studies of Fire Clay sample.	131
Table 5.8. Set of optimum parameter values for the desired goals of the response variables from the Box-Behnken Design and the value of other output variables for 1.60 SG float of Fire Clay (Cont.=Total Contaminants).	134
Table 5.9. Set of optimum parameter values for the desired goals of the response variables from the Box-Behnken Design and the value of other output variables for 2.20 SG sink of Fire Clay (Cont.=Total Contaminants).	135
Table 5.10. The minimum values for artificial variable Relative Concentration (RC) for achieving maximum selectivity for REE recovery from the two coal sources.....	137
Table 7.1. The weight distribution of the (a) West Kentucky No.13 and (b) Fire Clay coarse refuse samples in different density fractions.	162
Table 7.2. Proximate analysis of the density fractions of the West Kentucky No.13 and Fire Clay refuse.	163
Table 7.3. XRF analysis of major and minor phases for the density fractions of the West Kentucky No.13 and Fire Clay samples on an ash basis.	164
Table 7.4. REE concentrations (ppm) by ICP-OES in each density fraction of West Kentucky No.13 coarse refuse on a dry, ash basis.....	165
Table 7.5. REE concentrations (ppm) by ICP-OES of different density fractions of Fire Clay samples.	165
Table 7.6. Details of the mineral samples used in the current study. (For Illite: x represents the variable amount of water that this group could contain)	166
Table 7.7. XRF analysis of major and minor phases for the mineral samples on an ash basis (* Iron for pyrite is reported as % Fe).....	166
Table 7.8. REE concentrations (ppm) by ICP-OES of mineral samples used in the study.	166

LIST OF FIGURES

Figure 2.1. Rare earth elements in the periodic table (shaded in orange).....	22
Figure 2.2. Lanthanide contraction in lanthanide series elements. The ionic radius decreases with increasing atomic numbers [28].	23
Figure 2.3. The distribution of global rare earth production and US consumption in 2020, the production data adapted from USGS Mineral Commodity Summary 2021.....	25
Figure 2.4. Simplified flowsheet for the physical beneficiation of bastnaesite at Mountain Pass, U.S. [40].....	28
Figure 2.5. Physical beneficiation of monazite in beach sand minerals [20].	30
Figure 2.6. Production of rare earth chlorides from bastnasite (Kruesi and Duker) [49].	31
Figure 2.7. Hydrometallurgical recovery schemes for the extraction of REEs from bastnaesite ore concentrate after physical beneficiation [20].....	33
Figure 2.8. Monazite processing flowsheet to recover rare earth elements by alkali treatment [20].....	34
Figure 2.9. Schematic flow sheet of three typical processes for the extraction of rare earth elements from xenotime [20].	35
Figure 2.10. Effect of pH on REE recovery from thickener underflow fine refuse (TUF) sample using 0.1 mol/L (NH ₄) ₂ SO ₄ and nitric acid for pH adjustment [15].....	39
Figure 2.11. Improvement in REE leaching recovery after thermal activation pretreatment of the de-carbonized -180 μm middlings material and five hours of leaching using 1.2 mol/L sulfuric acid solution at 75°C [15].	40
Figure 2.12. Recovery of REEs from low-temperature plasma-treated coal under various leaching conditions for 5 hours. (acid Leaching with sulfuric acid at final pH of 0; salt leaching with ammonium sulfate at final pH of 3; water leaching with deionized water at final pH of 3) [15].....	41
Figure 2.13. Leaching characteristics of total REEs, LREEs, and HREEs from the middlings (Mids) and coarse refuse (CR) as a function of reaction time and calcination temperature: (a), (b), and (c) are the total REEs, light REEs, and heavy REEs recovery values, respectively, for the Pocahontas No. 3 middlings sample and (d), (e) and (f) are likewise for the coarse refuse sample [36].....	43
Figure 2.14. TGA-DSC curve for the roasting process at a heating rate of 10 °C min ⁻¹ magnetic tailings mixed with CaO and coal [92].....	44

Figure 2.15. The concentration of the TREE (in black) and primary contaminants (in blue) in the PLS are generated from different coal sources. The numbers in bold represent the relative concentration (RC) of the contaminants to the TREES in the solution [61].	45
Figure 2.16. Schematic of the SX process procedure used to separate rare earth elements from the contaminant elements in the pregnant leach solutions from six coal sources [61]	46
Figure 2.17. Schematic diagram of RF low-temperature plasma ashing apparatus: (A) oxygen tank; (B), (F) needle valve; (C), (E) flow meter; (D) three-way juncture; (G) Pyrex tube; (H) MacLeod gauge; (I) three-way stopcock; (J) rotary pump; (K) High Frequency coil; (L) coaxial cable, 75 Ω impedance; (M) specimen; (VC) variable air condenser [108].	48
Figure 2.18. Oxygen plasma treatment on organic surface [102].	49
Figure 2.19. Oxidation of pyrite mixture with graphite as a function of RF Power after 24 hours of LTA [115].	51
Figure 2.20. SiO ₂ phase diagram illustrating the changes in the quartz during heating [119].	55
Figure 2.21. Decomposition products of pyrite in the air [126]	57
Figure 2.22. Thermal phase transition of pyrite [130].	57
Figure 2.23. Magnetic recovery of heat-treated mineral pyrite sample [133].	58
Figure 2.24. Mineral phases detected (through XRD analysis) after thermal treatment for 1 h at temperatures up to 1000°C, and the corresponding magnetization at 1600 kA m ⁻¹ of the heat-treated pyrite [133].	58
Figure 2.25. Coal deposit with the underclay below the coal and a sandstone host rock (Photo Courtesy: Mike Fitzpatrick from Flickr) [139].	59
Figure 2.26. SEM-BSE images of underclay with REE-bearing minerals. Framboidal pyrite and clay with La, Ce, Nd (left). Pore-filling clay in siderite and examples of REE phosphate minerals identified (right) [134].	60
Figure 2.27. Thermal decomposition of the kaolin [142].	60
Figure 3.1. Locations of coal preparation plants in the U.S. where the coarse refuse samples were collected for the tests.	62
Figure 3.2. Sampling locations for the coal preparation sites. (a) West Kentucky No.13 and (b) Fire Clay.	63
Figure 3.3. Cross-section of the Fire Clay coal seam and corresponding REE content on a dry, whole sample basis [61].	65

Figure 3.4. A sweep-belt sampler used to collect representative samples from the coarse refuse process stream of a coal preparation plant.	66
Figure 3.5. Schematic of the laboratory sample preparation process used on the West Kentucky No.13 and Fire Clay coarse refuse samples collected from the two processing plants.	67
Figure 3.6. The weight percent distribution of the West Kentucky No.13 and Fire Clay coarse refuse samples in different density fractions.	68
Figure 3.7. REE concentration for composite West Kentucky No.13 and Fire Clay coarse refuse samples on a dry, whole mass, and ash basis.	70
Figure 3.8. LECO TGA-701 Thermogravimetric analyzer.	71
Figure 3.9. Proximate analysis of the density fractions of the West Kentucky No.13 and Fire Clay coarse refuse samples.	71
Figure 3.10. Total sulfur concentrations on a dry basis in the density fractions of the two coarse refuse sources.	72
Figure 3.11. Setup of the PE-100 RIE low-temperature plasma unit at the University of Kentucky.	74
Figure 3.12. Benchtop muffle furnace used for calcination tests.	75
Figure 3.13. Apparatus for leaching tests with controlled temperature, stir speed, and condensation rates.	77
Figure 3.14. L-4-20 Eriez wet magnetic separator.	78
Figure 3.15. XRD instrument used for mineralogy analysis.	79
Figure 3.16. LINSEIS STA with water vaporizer with 5 sample gases and 1 balance purge service at the University of Kentucky.	81
Figure 3.17. ICP-OES apparatus at Kentucky Geological Survey at used for elemental characterization of the aqueous phase.	82
Figure 3.18. Instrumentation used for surface area and pore volume analyses.	84
Figure 3.19. Simplified process steps of a BET analysis [152].	84
Figure 3.20. The FEI Quanta 250 used for SEM analysis.	85
Figure 4.1. XRD patterns of the untreated density fractionated samples of (a) West Kentucky No.13 and (b) Fire Clay–refuse sample. (●-Kaolinite; ▲ -Quartz; ◇-Pyrite, and ◊ - Illite).	93
Figure 4.2. REE Distribution based on specific gravity for (a) West Kentucky No.13 and (b) Fire Clay refuse samples.	94

Figure 4.3. Moisture, carbon, and ash contents of the (a) West Kentucky No.13 and (b) Fire Clay density fractions after 32 hours of LTP treatment. (PT=Plasma Treated)	96
Figure 4.4. XRD patterns of the LTP treated, density fractionated samples of (a) West Kentucky No.13 and (b) Fire Clay–refuse sample. (●-Kaolinite; ▲ -Quartz; ◇-Pyrite, and ◊ - Illite).	96
Figure 4.5. REE recovery from the LTP treated West Kentucky No.13 (a) 1.60 SG float, (b) 1.60x1.80 SG, (c) 1.80x2.20 SG, and (d) 2.20 SG sink samples using 0.1M ammonium sulfate at 75°C for 5 hours.	99
Figure 4.6. REE recovery from the LTP treated West Kentucky No.13 (a) 1.60 SG float, (b) 1.60x1.80 SG, (c) 1.80x2.20 SG, and (d) 2.20 SG sink samples using 1.2M sulfuric acid at 75°C for 5 hours.	100
Figure 4.7. REE recovery from the LTP treated Fire Clay (a) 1.60 SG float, (b) 1.60x1.80 SG, (c) 1.80x2.20 SG, and (d) 2.20 SG sink samples using 1.2M sulfuric acid at 75°C for 5 hours.	101
Figure 4.8. SEM micrographs depicting particles with increased porosity and surface area for the LTP treated (a)1.60 SG float and (b) 1.60x1.80 SG density fractions of West Kentucky No.13.	103
Figure 4.9. REE recovery from the calcination of West Kentucky No.13 (a) 1.60 SG float, (b) 1.60x1.80 SG, (c) 1.80x2.20 SG, and (d) 2.20 SG sink samples using 1.2M sulfuric acid at 75°C for 5 hours.	104
Figure 4.10. REE recovery from the calcination of Fire Clay (a) 1.60 SG float, (b) 1.60x1.80 SG, (c) 1.80x2.20 SG, and (d) 2.20 SG sink samples using 1.2M sulfuric acid at 75°C for 5 hours.	106
Figure 5.1. Acid leaching test results with 1.2M H ₂ SO ₄ at 75°C for the 1.60 SG float of West Kentucky No.13 calcined at different temperatures in air.	114
Figure 5.2. Acid leaching test results with 1.2M H ₂ SO ₄ at 75°C for the 1.60x1.80 SG of West Kentucky No.13 calcined at different temperatures in air.	115
Figure 5.3. Acid leaching test results with 1.2M H ₂ SO ₄ at 75°C for the 1.80x2.20 SG of West Kentucky No.13 calcined at different temperatures in air.	116
Figure 5.4. Acid leaching test results with 1.2M H ₂ SO ₄ at 75°C for the 2.20 SG sink of West Kentucky No.13 calcined at different temperatures in air.	117
Figure 5.5. Acid leaching test results with 1.2M H ₂ SO ₄ at 75°C for the 1.60 SG float of Fire Clay calcined at different temperatures in air.	119
Figure 5.6. Acid leaching test results with 1.2M H ₂ SO ₄ at 75°C for the 1.60x1.80 SG of Fire Clay calcined at different temperatures in air.	120

Figure 5.7. Acid leaching test results with 1.2M H ₂ SO ₄ at 75°C for the 1.80x2.20 SG of Fire Clay calcined at different temperatures in air.....	121
Figure 5.8. Acid leaching test results with 1.2M H ₂ SO ₄ at 75°C for the 2.20 SG sink of Fire Clay calcined at different temperatures in air.	122
Figure 5.9. Response surface for the association of (a) LREE and (b) HREE recovery (%) of the calcined (i) 1.60 SG float and (ii) 2.20 SG sink fraction of West Kentucky No.13 as a function of main and interaction effects of the significant variables	126
Figure 5.10. Response surface for the association of (a) Al, (b) Ca, and (c) Fe concentration of the calcined (i) 1.60 SG float and (ii) 2.20 SG sink fraction of West Kentucky No.13 as a function of main and interaction effects of the significant variables.	127
Figure 5.11. Response surface for the association of (a) LREE and (b) HREE recovery (%) of the calcined (i) 1.60 SG float and (ii) 2.20 SG sink fraction of Fire Clay as a function of main and interaction effects of the significant variables	132
Figure 5.12. Response surface for the association of (a) Al, (b) Ca, and (c) Fe concentration of the calcined (i) 1.60 SG float and (ii) 2.20 SG sink fraction of Fire Clay as a function of main and interaction effects of the significant variables.	133
Figure 5.13. Actual vs predicted plots for the 1.60 SG float and 2.20 SG sink fractions of West Kentucky No.13 and Fire Clay, respectively.....	136
Figure 6.1. Process diagram of the sample preparation process from the coarse refuse material collected from the processing plant treating WK-13 seam coal.	142
Figure 6.2. Composition and REE makeup of the 2.20 SG sink fraction of WK-13 coarse refuse material.....	142
Figure 6.3. XRD analysis of the untreated 2.20 SG sink fraction of WK-13 (● -Kaolinite; ▲ -Quartz; □ -Pyrite).	143
Figure 6.4. Micrographs of various pyrite types in the 2.20 SG sink fraction of the WK-13 coarse refuse material. (a) regular spherical shaped clusters (b) composite mineral agglomerates, (c) large hexagonal crystals, and (d) small grain crystal clumps.....	146
Figure 6.5. The mass yield obtained from magnetic separation tests on calcined products of 2.20 SG sink of WK-13 generated at three temperatures under a field strength of 11500 Gauss.....	147
Figure 6.6. The collected magnetic and nonmagnetic fractions obtained from the magnetic separation of WK-13 2.20 SG sink fraction calcined at 400°C and 500°C.	148
Figure 6.7. XRD analysis of the magnetic and tailing fraction of the 2.20 SG sink fraction of WK-13 calcined at 400°C (●-Kaolinite; ○-Illite, ▲ -Quartz; ◇ -Hematite).	149

Figure 6.8. REE Concentration (ppm) in the magnetic and nonmagnetic fractions of 2.20 SG sink of WK-13 calcined at 400°C and 500°C.....	150
Figure 6.9. Mass yield of magnetic separation tests at varying magnetic field intensities for 2.20 SG sink of WK-13 calcined at 400°C.....	150
Figure 6.10. Acid leaching test results with 1.2M H ₂ SO ₄ for 2.20 SG sink calcined products at different temperatures. (Mags=Magnetic; N. Mag=Nonmagnetic; N. Mag-RC=Nonmagnetic fraction Re-Calcined at 600°C)	153
Figure 6.11. Acid leach test results with 1.2M H ₂ SO ₄ for the 2.20 SG sink calcined at different temperatures. (Mags=Magnetic; N. Mag=Nonmagnetic; N. Mag-RC=Nonmagnetic fraction Re-Calcined at 600°C)	154
Figure 6.12. SEM analysis of the 2.20 SG sink of WK-13 calcined at 400°C. EDX analysis suggesting the formation of iron oxide and the crystal structure of pyrite being intact.	156
Figure 6.13. Flowsheet for single-stage calcination followed by magnetic separation in the hydrometallurgical extraction of REEs from coal-based feedstocks.....	157
Figure 7.1. DSC Sensor setup for LINSIES STA analysis.....	169
Figure 7.2. Leaching recovery for the light and heavy REEs for the (a) 1.80 SG float, (b) 1.80x2.00 SG, (c) 2.00x2.20 SG, and (d) 2.20 SG sink fractions of West Kentucky No.13 calcined at 600°C for 2 hours under different atmospheric conditions. (UT=Untreated, IN=Inert, OX=Oxidizing, IN+OX= Inert followed by Oxidizing). The number in red represents the % ash content in the calcined product.	171
Figure 7.3. Leaching recovery for the light and heavy REEs for the (a) 1.60 SG float, (b) 1.60x1.80 SG, (c) 1.80x2.00 SG, (d) 2.00x2.20 SG, and (e) 2.20 SG sink fractions of Fire Clay calcined at 600°C for 2 hours under different atmospheric conditions. (UT=Untreated, IN=Inert, OX=Oxidizing, IN+OX= Inert followed by Oxidizing. The number in red represents the % ash content in the calcined product.	173
Figure 7.4. Leaching recovery for the light and heavy REEs for the mineral (a) Kaolinite (b) Illite samples calcined at 600°C for 2 hours under different atmospheric conditions. (UT=Untreated, IN=Inert, OX=Oxidizing, IN+OX= Inert followed by Oxidizing.	174
Figure 7.5. Leaching recovery for the light and heavy REEs for density fractions of Fire Clay calcined at 600°C and 1000°C for 2 hours under an inert environment.	175
Figure 7.6. The thermogravimetric and differential scanning calorimetric (TGA-DSC) curves for (a) 1.80 SG float, (b)1.80x2.00 SG, (c) 2.00x2.20 SG, and (d) 2.20 SG sink fractions of density fractions of West Kentucky No.13 (Exo Up: Heating rate =10°C/min) (OX=Oxidizing, IN=Inert).....	178
Figure 7.7. The thermogravimetric and differential scanning calorimetric (TGA-DSC) curves for the (a) 1.60 SG float, (b) 1.60x1.80 SG, (c) 1.80x2.00 SG, (d) 2.00x2.20 SG,	

and (e) 2.20 SG sink fractions of density fractions of Fire Clay (Exo Up: Heating rate =10°C/min) (OX=Oxidizing, IN=Inert).....	179
Figure 7.8. Acid Leaching Tests with 1.2M H ₂ SO ₄ for mineral Kaolinite sample calcined at different temperatures for 2 hours (a) LREE Recovery, (b) HREE Recovery, (c) Al, (d) Ca & (e) Fe.....	182
Figure 7.9. The thermogravimetric and differential scanning calorimetric (TGA-DSC) curves of mineral kaolinite (Exo Up: Heating rate =10°C/min, Oxidizing Conditions). 183	183
Figure 7.10. XRD Patterns of untreated kaolinite clay and calcinated at 400°C, 600°C, and 800°C for 120 minutes (○- Kaolinite).	183
Figure 7.11. Acid leaching test results using 1.2M H ₂ SO ₄ for mineral Illite sample calcined at different temperatures for 2 hours (a) LREE Recovery, (b) HREE Recovery, (c) Al, (d) Ca & (e) Fe.....	185
Figure 7.12. The thermogravimetric and differential scanning calorimetric (TGA-DSC) curves of mineral illite (Exo Up: Heating rate =10°C/min, Oxidizing Conditions).	186
Figure 7.13. Acid Leaching Tests with 1.2M H ₂ SO ₄ for mineral Pyrite sample calcined at different temperatures for 2 hours (a) LREE Recovery, (b) HREE Recovery, (c) Al, (d) Ca & (e) Fe	188
Figure 7.14. The thermogravimetric and differential scanning calorimetric (TGA-DSC) curves of mineral pyrite (Exo Up: Heating rate =10°C/min, Oxidizing Conditions).	189
Figure 7.15. XRD Patterns of untreated mineral pyrite and calcinated at 400°C, 600°C, and 800°C for 120 minutes (◇- Pyrite; ◆-Hematite).	189
Figure 7.16. The thermogravimetric and differential scanning calorimetric (TGA-DSC) curves of the mineral calcite (Exo Up: Heating rate =10°C/min, Oxidizing Conditions).	190

CHAPTER 1. INTRODUCTION

1.1 Background

The rare earth elements (REEs) are a class of 15 elements of the lanthanide series ranging from lanthanum (atomic no. 57) to lutetium (atomic no. 71) along with two transition elements scandium (atomic no. 21) and yttrium (atomic no. 39). The REEs have critical applications in sophisticated high-tech products due to their unique optical, catalytic, and chemical properties. Although substitutes are available for many applications, they are less effective. Thus, REEs are vital raw materials in the modern-day manufacturing economy. Given the annual demand of around 150,000 tons of REEs, the global REE market relies primarily on exports from China which produced 58% of the world's rare earth oxides (REO) in 2020 [1]. With a 100% import reliance on domestic consumption, the U.S. imported 110 million worth of finished REE products in 2020 primarily from China, Japan, and Malaysia. Therefore, to negate any potential economic impact due to unforeseen export restrictions and international trade wars, substantial efforts are being made for the development of cost-effective technology for indigenous production of REEs.

The U.S. is reevaluating the possibility of production from existing REE deposits and opportunities are being widely explored for extraction of REEs from alternate non-conventional resources that are cheap and abundantly available [2]. Over the last few years, coal has been extensively investigated as one of such promising resources as REEs have been found in low and high-rank coals, parting material, roof, and floor host rock, preparation plant rejects, thickener underflow, and acid mine drainage samples in concentrations up to and exceeding 1000 ppm [3, 4]. A study conducted by Luttrell et al. suggested that the coarse coal rejects being produced at operating coal processing facilities contain enough REEs to meet the U.S. annual REE demand [5]. Investigations have been focused primarily on coal by-products and acid mine drainage that can eliminate mining costs to offset the high costs of grinding and liberation of the finely dispersed REEs. Exploiting the difference in magnetic, electrostatic, and physiochemical characteristics of REE-bearing minerals contained in coal by physical extraction methods has been

investigated and found to be minimally effective in most cases [6-10]. Alternatively, findings from a significant number of studies conducted on the recovery and concentration of REEs from coal-based feedstocks advocate the feasibility of hydrometallurgical extraction over physical separation methods [11-17]. The REEs in coal can be dissolved in an aqueous phase by acid leaching and can be concentrated by liquid-liquid extraction methods to produce a high-grade mixed REO product which can be further processed to separate the individual REEs.

However, with the low concentration of REEs in the coal-derived feed and low recovery from subsequent extraction/separation process, maximizing REE recovery at every step is vital for the economic viability of the process. Oxidation pretreatment is a common practice in the REE industry for transforming conventional REE-bearing minerals into more leachable forms thus increasing REE recovery, improving leaching kinetics, and enabling the use of milder leaching conditions [10, 18]. Calcination with chemical additives at high temperatures (500-800°C) has been found to convert the conventional REE minerals into more leachable REE oxides, chlorides, or sulfates [7, 19, 20]. However, unlike traditional REE minerals that have homogeneity in the mode of occurrence, REEs in coal have varied modes of association such as with carbonates and phosphate minerals, as well as with ion-absorbed clays and organic compounds [12, 21-24]. Without pretreatment before leaching, the finely dispersed REEs associated with non-uniform mineralogy result in poor leaching characteristics of the REEs despite harsh leaching conditions.

For this study, oxidation pretreatment was utilized to pretreat the coal feedstock for the purposed of liberation, release, oxidation, and/or activation of the REEs from the organic matter in coal and/or from the minerals that were embedded in coal. Low and high-temperature oxidation methods were evaluated in this study to understand the effect of atmosphere conditions (oxidizing/ reducing) and temperature and to identify the association of REEs with the common minerals present in coal. During the initial test program, oxidation pretreatment using low-temperature plasma (LTP) was analyzed for studying the REE leaching characteristics from different density fractions of two bituminous coal sources. Subsequently, the potential value added by calcination

pretreatment was investigated for improving the REE leaching recovery from the coal-based feedstock. Based on the results of parametric tests, calcination parameters were optimized for high selectivity towards REEs and rejection of contaminant ions such as Al, Ca, and Fe. To reduce the contamination of iron in the leaching operation, pyrite sources were transformed to iron oxides and separated from the calcination products by exploiting the subtle difference in the magnetic properties using magnetic separation. Additionally, the association of REEs with coal pyrites was also established. Finally, the role of atmospheric conditions in calcination provided key information in fundamentally understanding the effect of the oxidation processes on the leachability of REEs contained in coal. The mode of REE association with clays was identified and the phase changes in minerals associated with coals were studied using differential scanning calorimetry (DSC). The information obtained was vital for the process design and the integration of an oxidation unit operation in the hydrometallurgical circuit, before leaching, for elevated REE production from coal and coal byproducts.

1.2 Objectives

The overall goal of the study was to integrate an oxidation pretreatment process with a hydrometallurgical processing circuit to enhance the recovery of REEs from coal and coal byproducts. The potential for value addition is through liberation, oxidization, or activation of the REEs embedded in the different density fractions of the coal. The key findings from the lab-scale characterization and optimization studies can be scaled to overcome the challenges for a pilot plant-scale continuous operation. The objectives of the research work were:

1. A comprehensive review of (a) the association of REEs in coal, (b) application of calcination in the processing of conventional REE resources, (c) use of low-temperature plasma (LTP) for coal oxidation, (d) effect of calcination on coal oxidation for elevated REE recovery and (d) phase transformations of common minerals found in coal by thermal treatment;
2. A parametric study of the LTP to evaluate the effect of oxygen plasma treatment on the REEs liberation and leaching performance. The resulting improvement on REE

- leachability and leaching selectivity was used to quantify the benefits of LTP on REE recovery from coal. The data obtained will be used to fundamentally understand the mechanism of LTP treatment;
3. A systematic study to evaluate the effects of calcination temperature and duration on the leaching recoveries of REEs and the concentration of common contaminant elements found in a pregnant leach solution (PLS) derived from a coal feedstock;
 4. Optimization of calcination conditions for the different density fractions of the coal seam and establish a numerical relationship between the significant input and output variables;
 5. Development of a process for the removal of iron from the feed by transforming the host pyrite to a magnetic product by controlled calcination and magnetic separation;
 6. Evaluate the association of REEs in common minerals found in coal and understand the phase transformations due to calcination treatment; and
 7. Evaluation of calcination atmosphere impacts on the improvements in REE leachability on the various density fractions of the coal deposit.

1.3 Organization

The dissertation is organized into nine chapters. The first chapter introduces the background, project goals, and objectives of the study. The second chapter provides a detailed review of the existing literature describing the current state of global REE trade, the occurrence of convention REE deposits and their extraction methods, REEs contained in coal, and the efforts made to date for their extraction. The second chapter also summarizes the effect of thermal and oxidation treatment on the common minerals found in coal. The third chapter covers the origin and preparation details of the test samples and the various experimental methods and analytical techniques used in the study. It delineates sample characterization methods, leaching operation, low and high-temperature oxidation treatments, and other experimental procedures. The chapter also describes the analytical tools and instruments used for quantitative elemental analysis, thermogravimetric

assessments, and mineralogical studies. Analysis of the test results and a detailed discussion of the findings are provided in chapters four to seven. Chapter four covers the studies performed using the novel LTP system with the major fundamental findings. Chapter five includes the optimization of the calcination process and chapter six focuses on the removal of iron contamination from leaching feed. Both the chapters attempt to add value to the existing pilot-scale facility by increasing revenue and lowering the operational costs. Chapter seven provides a comprehensive understanding of the effect of thermal and oxidative treatment on leaching characteristics of REEs associated with common coal minerals. Chapters eight and nine provide a summary and conclusions from the study and recommendations for future studies related to this topic, respectively.

CHAPTER 2. LITERATURE REVIEW

2.1 Rare Earth Elements

2.1.1 Classification of REEs

Despite the misnomer, the REEs are abundantly available in the earth's crust, but are finely disseminated and do not normally occur in concentrations that are amenable for commercial exploitation. The 17 REEs (Figure 2.1) are chemically coherent and are found in close association with each other in a rare earth deposit and separating individual elements from each other is cost exhaustive [20]. The REEs are classified based on their atomic number as 'light rare earth elements' (LREEs) and 'heavy rare earth elements' (HREEs). As per United States Geological Survey, LREEs are elements lanthanum to gadolinium (atomic number 57 to 64) [25]. Although yttrium has a lower atomic number than LREEs, it is classified as an HREE as it exhibits chemical and physical associations with HREEs. Thus, the HREEs are yttrium and elements terbium to lutetium (atomic number 39 & 65 to 71) [22, 26]. Scandium is also classified as an LREEs owing to its low atomic number [4, 27].

	1A	2A	3A	4A	5A	6A	7A	8	1B	2B	3B	4B	5B	6B	7B	0		
1	1 H															2 He		
2	3 Li	4 Be									5 B	6 C	7 N	8 O	9 F	10 Ne		
3	11 Na	12 Mg									13 Al	14 Si	15 P	16 S	17 Cl	18 Ar		
4	19 K	20 Ca	21 Sc	22 Ti	23 V	24 Cr	25 Mn	26 Fe	27 Co	28 Ni	29 Cu	30 Zn	31 Ga	32 Ge	33 As	34 Se	35 Br	36 Kr
5	37 Rb	38 Sr	39 Y	40 Zr	41 Nb	42 Mo	43 Tc	44 Ru	45 Rh	46 Pd	47 Ag	48 Cd	49 In	50 Sn	51 Sb	52 Te	53 I	54 Xe
6	55 Cs	56 Ba	L	72 Hf	73 Ta	74 W	75 Re	76 Os	77 Ir	78 Pt	79 Au	80 Hg	81 Tl	82 Pb	83 Bi	84 Po	85 At	86 Rn
7	87 Fr	88 Ra	A															
		L	57 La	58 Ce	59 Pr	60 Nd	61 Pm	62 Sm	63 Eu	64 Gd	65 Tb	66 Dy	67 Ho	68 Er	69 Tm	70 Yb	71 Lu	
		A	89 Ac	90 Th	91 Pa	92 U	93 Np	94 Pu	95 Am	96 Cm	97 Bk	98 Cf	99 Es	100 Fm	101 Md	102 No	103 Lr	

Figure 2.1. Rare earth elements in the periodic table (shaded in orange).

The REEs exhibit similar chemical properties due to lanthanide contraction which is the steady and significant decrease in the ionic radius with the increase in atomic

number. Lanthanide contraction results from the imperfect shielding of electrons by one another in the same subshell. In the lanthanide series, the number of electrons in the 4f-orbital and the nuclear charge increase with an increase in atomic number. Due to the shape of the f-orbital the magnitude of the effective nuclear charge experienced by the electrons increases and results in a steady decrease in ionic size across the lanthanide series. Therefore, lanthanum has the largest radius while lutetium has the smallest (Figure 2.2). The ionic radii of yttrium and its compounds are closely associated with heavier lanthanide elements such as erbium and holmium. Therefore, yttrium is classified as a heavy REE as it has similarities in outer electronic configuration and exhibits similar chemical properties. Scandium on the other hand has a small ionic radius and the atomic configuration does not experience lanthanide contraction. Thus the chemistry and properties of Scandium are different from that of the lanthanide elements [9, 20].

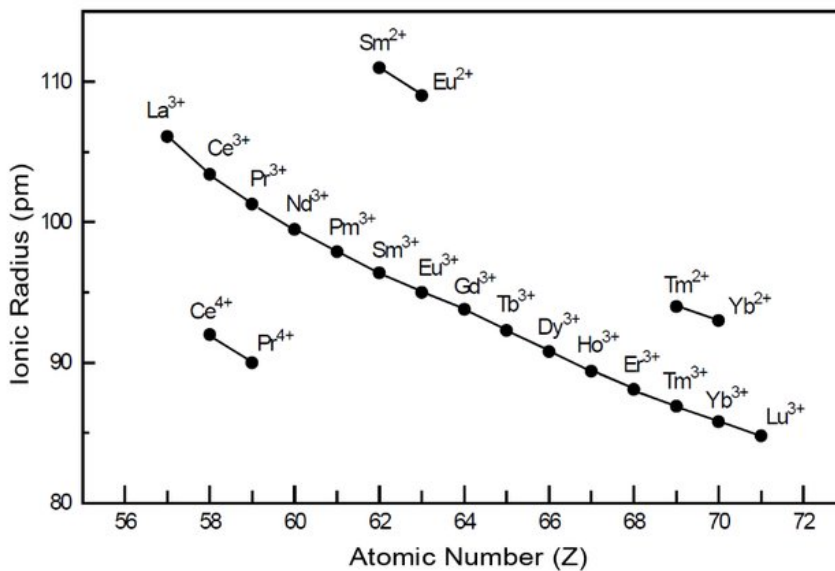


Figure 2.2. Lanthanide contraction in lanthanide series elements. The ionic radius decreases with increasing atomic numbers [28].

2.1.2 REE Resources

Except for radioactive promethium (atomic no. 61), all other REEs occur in nature. They are found abundantly in the earth's crust and are 200 times more plentiful than gold [20, 29]. Their crustal concentration is similar to that of common industrial metals such as copper, molybdenum, zinc, and tin. However, the REEs are termed 'rare'

because they have very little tendency to be concentrated in commercially viable ore deposits. They are found in more than 200 minerals but commonly occur as carbonates, oxides, phosphates, and silicates. A summary of the REE minerals with economic potential is provided in Table 2.1.

Table 2.1. Minerals that contain REEs and occur in economic or potentially economic deposits [9] (Ln=Lanthanide Element).

Mineral	Chemical Formula	REO (%)
Aeschnynite	(Ln,Ca,Fe,Th)(Ti,Nb) ₂ (O,OH) ₂	36
Allanite (orthite)	(Ca, Ln) ₂ (Al,Fe) ₃ (SiO ₄) ₃ (OH)	30
Anatase	TiO ₂	3
Ancylite	SrLn (CO ₃) ₂ (OH)•H ₂ O	46
Apatite	Ca ₅ (PO ₄) ₃ (F, Cl, OH)	19
Bastnasite	LnCO ₃ F	76
Brannerite	(U,Ca,Ln)(Ti,Fe) ₂ O ₆	6
Britholite	(Ln, Ca) ₅ (SiO ₄ , PO ₄) ₃ (OH, F)	62
Cerianite	(Ce, Th) O ₂	81
Cheralite	(Ln, Ca, Th) (P, Si) O ₄	5
Churchite	YPO ₄ •2H ₂ O	44
Eudialyte	Na ₁₅ Ca ₆ (Fe,Mn) ₃ Zr ₃ (Si,Nb)Si ₂₅ O ₇₃ (OH,Cl,H ₂ O) ₅	10
Euxenite	(Ln,Ca,U,Th)(Nb,Ta,Ti) ₂ O ₆	< 40
Fergusonite	Ln (Nb, Ti) O ₄	47
Florencite	Ln ₁₃ (PO ₄) ₂ (OH) ₆	32
Gadolinite	LnFeBe ₂ Si ₂ O ₁₀	52
Huanghoite	BaLn (CO ₃) ₂ F	38
Hydroxylbastnasite	LnCO ₃ (OH, F)	75
Kainosite	Ca ₂ (Y, Ln) ₂ Si ₄ O ₁₂ CO ₃ •H ₂ O	38
Loparite	(Ln,Na,Ca)(Ti,Nb) ₃	36
Monazite	(Ln, Th) PO ₄	71
Mosandrite	(Ca,Na,Ln) ₁₂ (Ti,Zr) ₂ Si ₇ O ₃₁ H ₆ F ₄	< 65
Parisite	CaLn ₂ (CO ₃) ₃ F ₂	64
Samarskite	(Ln,U,Fe) ₃ (Nb,Ta,Ti) ₅ O ₁₆	12
Synchisite	CaLn (CO ₃) ₂ F	51
Thalenite	Y ₃ Si ₃ O ₁₀ (OH)	63
Xenotime	YPO ₄	61
Yttrotantalite	(Y,U,Fe)(Ta,Nb)O ₄	< 24

Bastnasite, monazite, xenotime, and ion-adsorption clays together constitute about 95% of the total REE ore reserves. Bastnasite is a fluocarbonate mineral with about 70% REO content and is primarily rich in the LREEs. The Bayan Obo Mine owned and operated by the Baotou Iron and Steel Group in China and Mountain Pass Mine

owned by MP Materials in the U.S. constitute the largest economic resources of REEs globally. Monazite is a phosphate mineral also rich in LREEs. However, monazite deposits are accompanied by significant quantities of uranium and thorium which require safe disposal of tailings and restrict the exploitation of individual REEs available. Xenotime and ion-adsorption clays are important sources of yttrium and another heavy group of REEs but account for a much smaller part of the total production [30].

2.1.3 Applications and end-use of REEs

In the age of rapid economic growth, the demand for consumer products such as electronics, electric vehicles, flat-screen televisions, and cell phones has increased exponentially. Additionally, permanent magnets and catalysts have become increasingly important for applications in life science equipment, petroleum refining, automotive, and defense applications. The most common area for the end-use of REE in the United States in 2020 was in catalysts (75%) (Figure 2.3). REEs were also widely used in the metallurgy industry for alloys and ceramic industry which together accounted for about 15% of the total end-use. The major applications of REEs are summarized in Table 2.2.

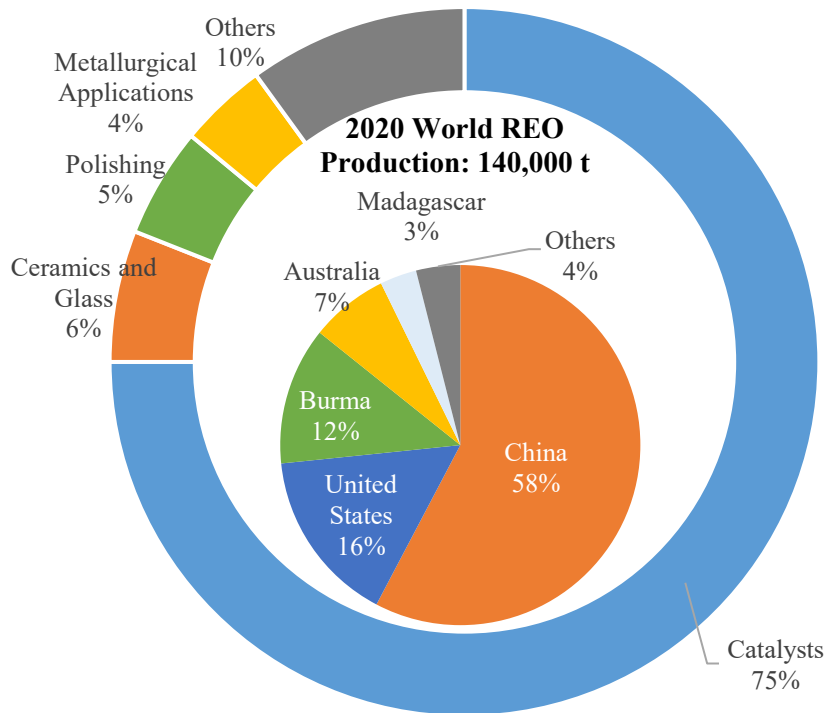


Figure 2.3. The distribution of global rare earth production and US consumption in 2020, the production data adapted from USGS Mineral Commodity Summary 2021.

Table 2.2. List of REEs and their major end-use in the industry. (Modified from [9])

Light REEs	Applications
Scandium	Ceramics, lasers, and phosphors
Lanthanum	FCC catalysts for petroleum refining, hybrid engines, and night vision goggles
Cerium	Glass polishing, phosphors, and catalysts
Praseodymium	Magnets for wind turbines, optical fibers, and strengthening agents for alloys
Neodymium	Lasers, glass tinting, dielectrics, and permanent magnets
Promethium	Pacemakers, watches, and compact fluorescent bulbs
Samarium	Nuclear reactors, aerospace equipment, and radiation treatments in cancer
Europium	Fluorescent lighting, computer screens, and fluorescent lamps
Gadolinium	Healthcare applications, MRIs, X-ray cassettes, and computer tomography
Heavy REEs	Applications
Yttrium	Cancer treatment drugs, superconductors, and lighting phosphors
Terbium	X-ray screens, color televisions, and fluorescent lighting
Dysprosium	Nuclear reactors, energy-efficient vehicles, and hard computer disks
Holmium	Adds color to glass, microwave equipment, and nuclear control rods
Erbium	Glass coloring, lasers for medical use, and fiber optic communication systems
Thulium	Crystals, X-rays, and lasers in medical and dental applications
Ytterbium	Fiber optics, cancer treatments, and strengthening stainless steel
Lutetium	The dopant in garnet crystals, petroleum refining, and meteorites aging

2.1.4 Global demand and Supply of REEs

The processing of conventional REE ores requires ultrafine grinding of the ore and extraction by acid leaching. The hydrometallurgical extraction produces a large volume of toxic tailings that require permanent storage and possess long-term environmental risks. In the 1990s, about 14 countries including the U.S., India, Australia, China, and Malaysia produced REEs. However, when cheap REEs were readily available in the international market primarily supplied by China, the REE consumers slowly drifted towards the import of the raw material and finished REE products. The U.S. was once self-sufficient in the indigenous production of REEs but now relies fully on imports for net apparent domestic consumption. Over the last two decades, China supplied REEs at prices that the nations across the globe were happy to pay. However, frequent price fluctuations and the implementation of export quotas presented a huge economical risk in the international market. The supply uncertainties and monopolistic control of such an important raw material forced many countries to re-evaluate the possibility of indigenous REE production and to ramp up production from sites that are already actively producing.

Currently, the majority of the REEs are produced from Bastnaesite. The use of Monazite despite the relatively higher concentration of HREEs will be limited until an environmentally sound and cost-effective method to dispose of the radioactive waste is developed. However, monazite-bearing sands are a lucrative resource in a long term due to abundant supply. In the year 2020, about 140,000 tons of REOs were produced worldwide with China (58%), U.S. (16%), Burma (12%), Australia (7%), and Madagascar (3%) being the major REE producers (Figure 2.3) [1]. As global economies move towards more energy-efficient and environmentally friendly technologies the demand for REEs is expected to rise [31]. The sales of electric vehicles and renewable energy technologies will fuel the demand for more efficient batteries. Future growth in the demand for REEs is projected as the sales of fiber optics, permanent magnets, and electronic devices will increase steadily over the next years [32].

2.2 REE processing

The grade and mineralization of the REE ore determine the selection of appropriate physical and chemical mineral processing methods. The cutoff grade for bastnaesite and monazite for industrial exploitation is about 2% while about 0.15% for ion adsorbed clays [33]. For conventional REE ore deposits, the run-off mine material is firstly concentrated by physical beneficiation methods such as communication, gravity separation, electrostatic separation, and froth flotation. The concentrated ore is then subjected to hydrometallurgical extraction by acid/base leaching with or without a calcination pretreatment. The REEs in the pregnant leach solution is finally extracted by liquid-liquid separation and selective precipitation. A roasting step followed by a selective precipitation step produces a mixed REO product [34, 35].

2.2.1 Physical Beneficiation

2.2.1.1 *Bastnaesite*

Bastnaesite production surpassed monazite production in 1965 with the development of Bayan Obo and Mountain Pass deposits [20, 36]. A simplified flowsheet for the Mountain Pass mine is outlined in Figure 2.4. The ore contains 60% calcite (CaCO_3), 20% barite (BaSO_4), and 10% silica (SiO_2) as gauge minerals along with the

10% bastnaesite ore [37]. The runoff mine material contains 7.7% REO by weight which is crushed in a jaw crusher in series with a cone crusher and a rod mill. The rod mill product is later fed to a classifier in a closed circuit with a conical ball mill. The classifier product is processed by a series of rougher and flotation cells and is finally enriched to a 70% REO concentrate [38]. Before rougher flotation, the ore is conditioned in six different steps with steam being bubbled through each of the treatment tanks. Sodium silicate, sodium hexafluorosilicate, and lignin sulfonate are used as depressants. Fatty acids (oleic) or hydroxamic acid are used as collectors and the total conditioning time is 2 hours. The conditioned slurry (~35% w/v) is pumped to the rougher flotation cell bank which produces a float concentrate of about 30% REO. The four-stage cleaner flotation bank treats the float from the rougher cells at 50% solids w/v and the tailings of the cleaner cells are recirculated in the cleaning circuit. The concentrate from the scavenger circuit is reintroduced to the rougher feed after size reduction. The tailings from the scavenger and rougher circuit constitute the overall process tailings and contain an average of 2% REOs. The product from the cleaner flotation circuit is dewatered and contains approximately 60-70% REOs [39]. The recovery of the overall process is about 90%.

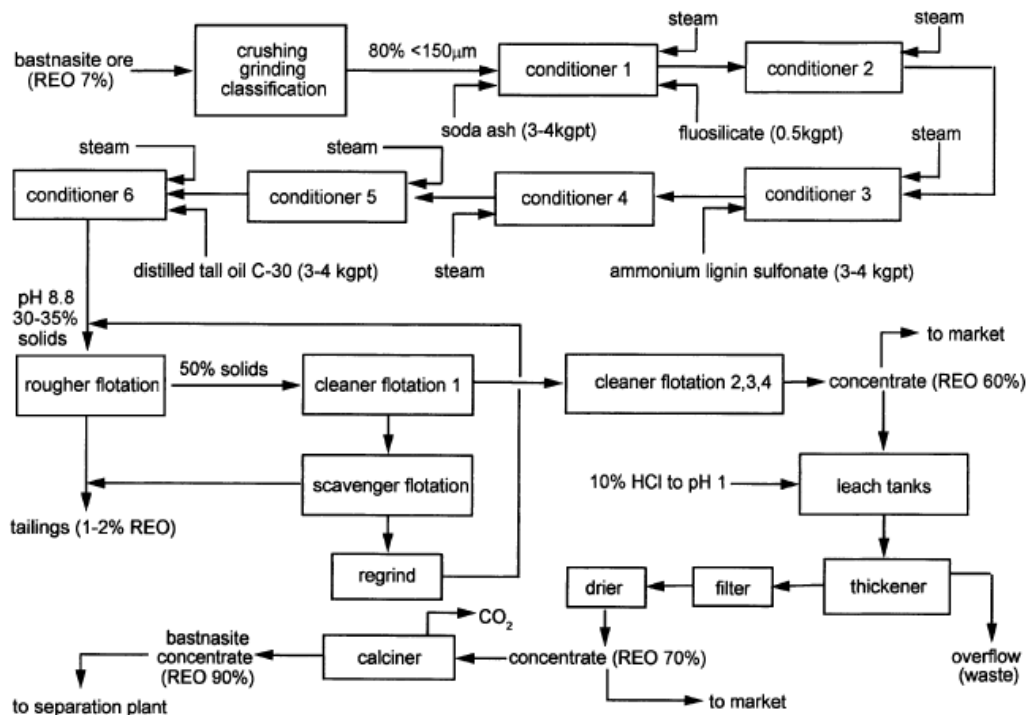


Figure 2.4. Simplified flowsheet for the physical beneficiation of bastnaesite at Mountain Pass, U.S. [40].

The Bayan Obo Mine in Inner Mongolia is the world's largest REE deposit where bastnaesite occurs together with monazite and iron-bearing ores such as hematite and magnetite (Fe_2O_3), magnetite (Fe_3O_4), and rutile (TiO_2). The REEs concentrated in the nonmagnetic tailings are reduced to $<74 \mu\text{m}$ by grinding and flotation is carried out after the addition of Na_2CO_3 as pH regulator, Na_2SiO_3 and NaSiF_6 as gangue depressants for iron and silicates and hydroxamic acid as collector at 5-6 pH range. The iron minerals, niobium, and silicates are pumped to separate iron beneficiation and niobium recovery circuit from the bottom of the flotation cells. The concentrate from the bulk flotation circuit contains a bastnaesite and monazite mix with a 56% REO content. The bastnaesite and monazite are separated using a shaking table due to the difference in their specific gravity. The shaking table separation yields two concentrate fractions; the primary bastnaesite product is 68% REO concentrate and a secondary concentrate containing monazite with 45% REO assay. The overall recovery of REE is about 72% from the primary ore while the rest is lost in tailings [20, 41].

2.2.1.2 *Monazite*

Monazite is a rare earth-thorium phosphate that contains 4-12% of naturally occurring radioactive elements along with 70% REEs by weight [42, 43]. Monazite is found mostly as a placer deposit or beach sand and is recovered as a byproduct of the processing of ilmenite, rutile, zircon, and cassiterite. The Bayan Obo deposit also contains significant quantities of monazite. The beneficiation processes usually involve separation into its constituents using density separation followed by electrostatic and magnetic methods, but Monazite or other minerals in beach sand deposits are separated and concentrated after coarse grinding via gravity separation, flotation, electrostatic separation, and/or magnetic processes (Figure 2.5) [44]. The process varies from location to location and depends on the mineralogical and chemical composition of the deposit. Wet gravity separation methods remove about 90% of the gangue minerals such as quartz and mica which are relatively less dense than the REE minerals. Ilmenite due to its magnetic susceptibility is magnetically separated from other minerals in the process. Rutile due to its higher electrical conductivity is separated from zircon. Further, non-magnetic zircon is separated from the magnetic monazite by magnetic separation [35]. Froth flotation of

monazite using fatty acid or phosphoric acid collectors has also been reported in some cases [45]. Depressants like sodium silicate, sodium sulfide, and sodium oxalate have been used to selectively float monazite and depress zircon and rutile in the tailings [46].

2.2.1.3 Xenotime

Xenotime is a rare-earth phosphate mineral with high yttrium content and low light REE concentration. The thorium content in xenotime is lower than monazite however it has more impurities such as iron and silicon [47]. Since both monazite and xenotime are phosphate minerals, they are essentially treated the same way. However, as compared to monazite which has 9-fold coordination, xenotime has a regular 8-fold crystalline structure and tends to incorporate the HREEs that have a smaller atomic radius as compared to the LREEs [48].

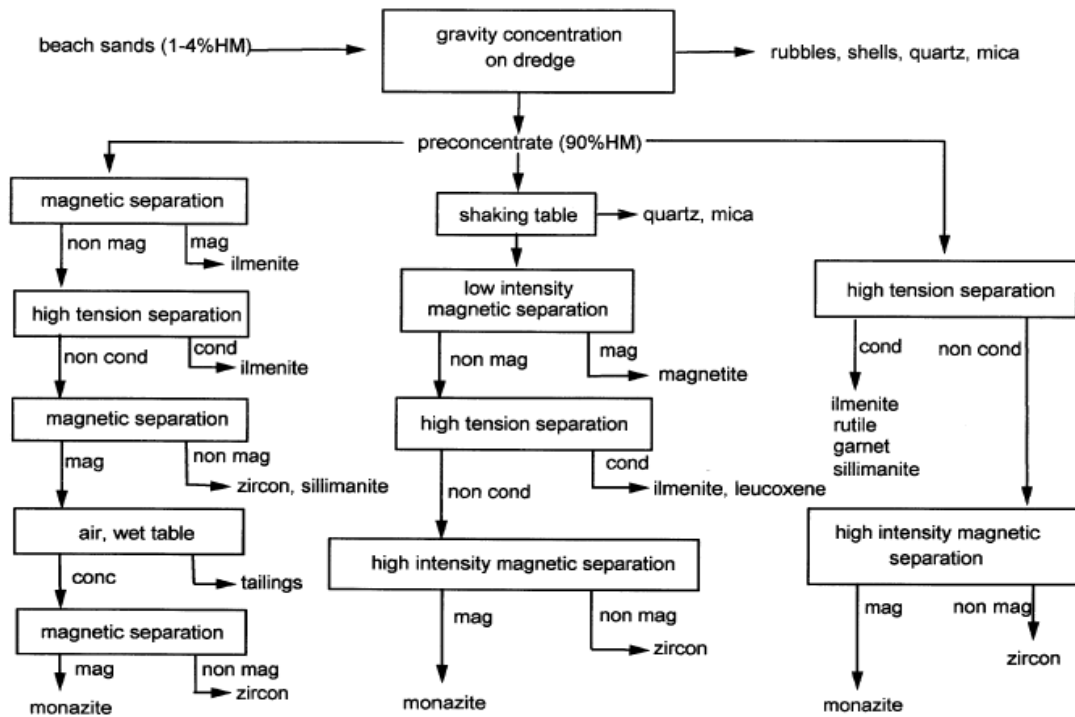


Figure 2.5. Physical beneficiation of monazite in beach sand minerals [20].

2.2.2 Hydrometallurgical Processing

2.2.2.1 Bastnaesite

The bastnaesite concentrate produces by the crushing, grinding, classification, and floatation of the primary ore undergoes acid digestion with hydrochloric acid to produce several REE chlorides as per the process developed by Kruesi and Duker, 1965 [49]. In the process, the bastnasite concentrate is attacked by 30% HCl followed by neutralization to produce mixed rare earth chlorides at 93°C (Figure 2.6) (Eq. 2-1).

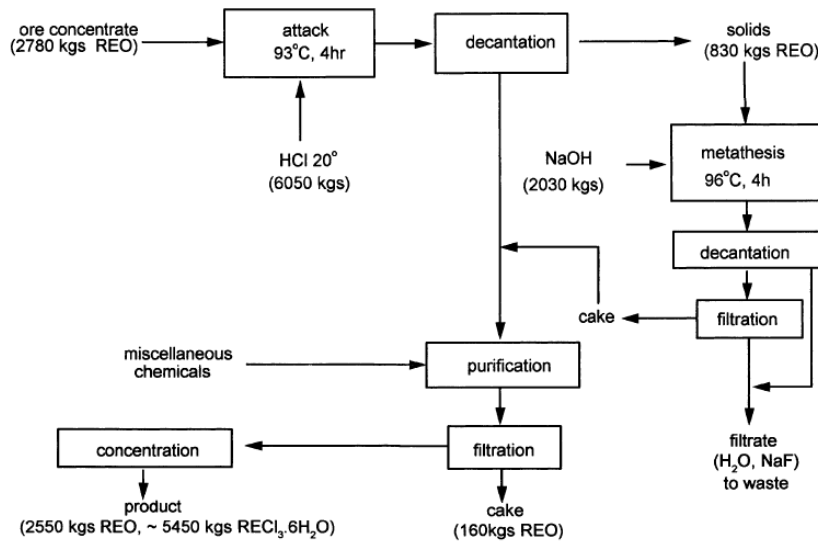
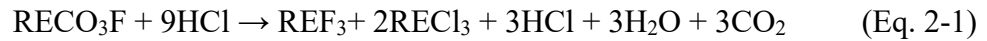
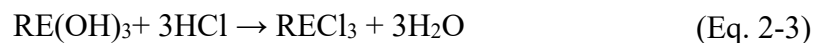
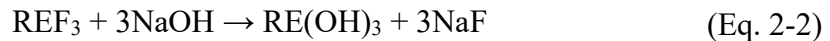


Figure 2.6. Production of rare earth chlorides from bastnasite (Kruesi and Duker) [49].

The filter cake containing the REE chlorides is digested with sodium hydroxide to produce rare earth hydroxides (Eq. 2-2) & (Eq. 2-3). The REE hydroxides are purified by the addition of hydrochloric acid and subsequently, iron and lead are precipitated.

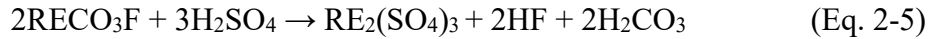


The solution with dissolved REE chlorides is concentrated by evaporation and the waste solids are filtered and discarded. The process has an REO recovery rate of 92%.

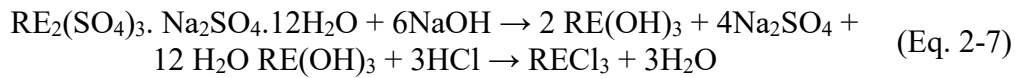
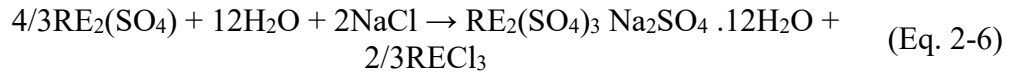
In the Goldschmidt process, the bastnasite ore direct is directly chlorinated at a high temperature (1,200°C) to produce an anhydrous REE chloride (Eq. 2-4). In the furnace, RE fluorocarbons are converted to chlorides by gaseous chlorine as per the following reaction (Figure 2.7) [50].



In an alternate processing scheme, at the Bayan Obo deposit, the bastnaesite concentrate is roasted with 98% sulfuric acid that destroys the fluoro-carbonate matrix, and REEs are converted to their sulfates (Eq. 2-5).



The REE sulfates are precipitated as double sodium sulfates by leaching with water and sodium chloride and then converted to REE hydroxides by digestion in strong NaOH solution and redissolved in hydrochloric acid (Eq. 2-6) & (Eq. 2-7). The dissolved REEs are eventually separated into individual REEs using solvent extraction [51].



Additionally, the bastnaesite ore can be calcined 800-900°C and subsequently digested in 57% nitric acid after size reduction. The dissolved REEs can be extracted by solvent extraction using tributyl phosphate (TBP) with 98% total REE recovery [20].

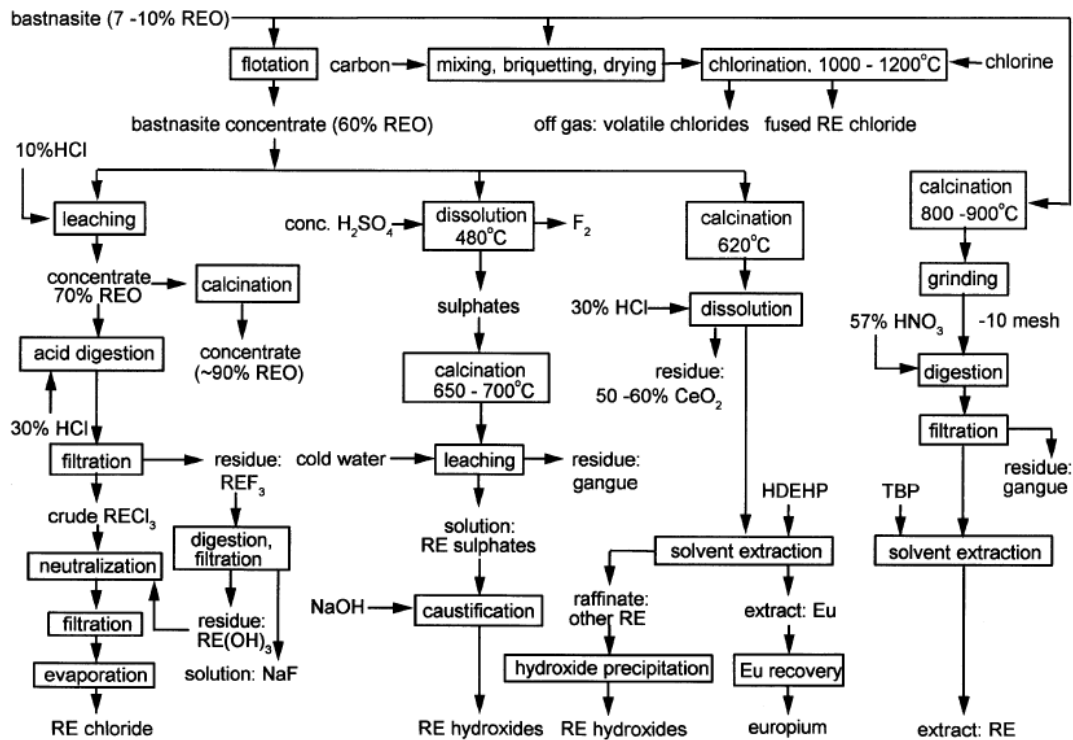


Figure 2.7. Hydrometallurgical recovery schemes for the extraction of REEs from bastnaesite ore concentrate after physical beneficiation [20].

2.2.2.2 Monazite

The primary step to recover REEs from monazite and removal of thorium is acid or alkali treatment [20, 48, 52]. The acid treatment uses concentrated sulfuric acid to non-selectively dissolve the REEs and thorium at high temperatures. The LREEs and thorium are separated using double sulfate precipitation, in which cerium and other light REEs precipitate, while thorium, yttrium, and other HREEs stay in the solution. The HREEs are further separated from thorium by solvent extraction using TBT as an extractant. Rare earth hydroxides are formed by the addition of NaOH to the LREE precipitate and the hydroxides are further purified by fractional precipitation. This acid treatment method was extensively used in the U.S. but is no longer in commercial use.

The alkali treatment process developed by Rhône-Poulenc using caustic soda (NaOH) has been a more popular process for monazite processing as REEs are precipitated in the form of hydroxides in the cake and trisodium phosphate (Na_3PO_4) is

generated as a byproduct [53]. The monazite concentrate from physical beneficiation is ground to 50 μm and is treated with caustic soda/sodium hydroxide at 140°C (Figure 2.8) (Eq. 2-8). The resulting REE hydroxides are dissolved in nitric acid and the process recovers 90% of the total REEs contained in monazite (Eq. 2-9).

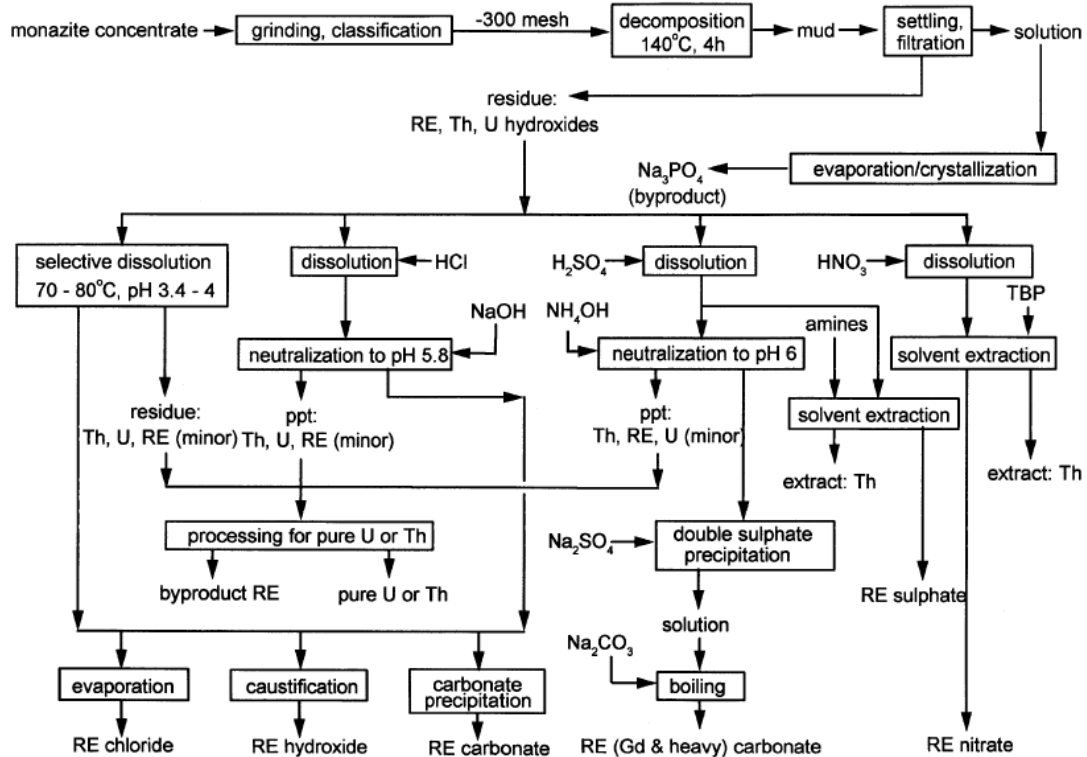
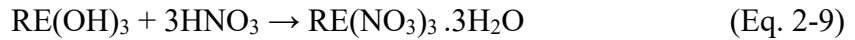
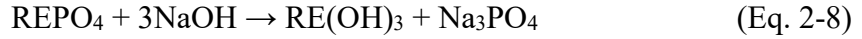


Figure 2.8. Monazite processing flowsheet to recover rare earth elements by alkali treatment [20].

2.2.2.3 Xenotime

Xenotime is a valuable phosphate deposit owing to the high yttrium and HREEs content which have critical and strategic importance. Processing of Xenotime concentrate involves milling followed by roasting in a furnace. The roasted product is digested with concentrated sulfuric acid (93%) at 250-300°C. This converts the rare earth phosphates to water-soluble rare earth sulfates, which are then leached using cold water for better recovery. REEs from the rare earth sulfate solution are precipitated by oxalic

acid ($\text{H}_2\text{C}_2\text{O}_4$) followed by calcination of REE oxalates to convert them to mixed REOs (Figure 2.9).

In an alternative process, the size-reduced xenotime is fused with molten caustic soda at 400°C [54] or by roasting with sodium carbonate at 900°C [55] for several hours. After leaching out the phosphates, the residual REE hydroxides are leached with small quantities of nitric or hydrochloric acid which dissolves the REEs leaving behind gangue such as silica and cassiterite. The dissolved REEs are then recovered by oxalic acid precipitation and calcinated after filtration.

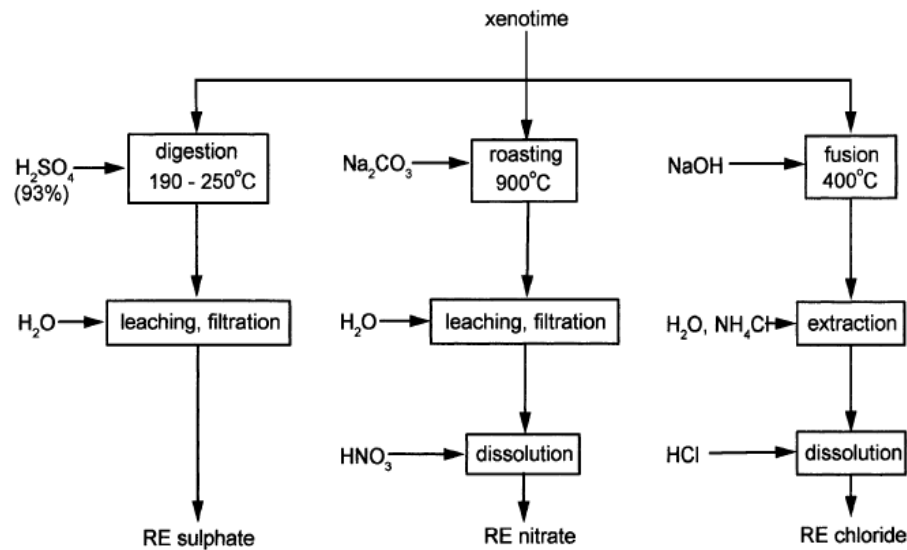
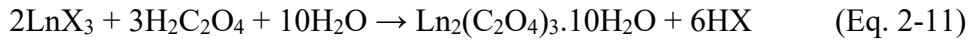


Figure 2.9. Schematic flow sheet of three typical processes for the extraction of rare earth elements from xenotime [20].

2.2.2.4 Ion-Adsorbed Clays

Although ion-adsorption type deposits are substantially lower grade than other REE minerals, the low REE content is largely offset by the inexpensive mining and processing along with the very low concentration of radioactive elements. They are formed by the weathering of igneous rocks (like granite) that contain REE-bearing minerals. Due to surface weathering the REE minerals are decomposed and ionized REEs are adsorbed onto the negatively charged surfaces of clay minerals such as kaolinite and halloysite [56, 57]. The absorbed REEs are recovered by leaching with concentrated inorganic salt of

monovalent cations as ammonium sulfate and sodium chloride. During leaching the physisorbed REEs are easily desorbed and substituted by monovalent cations and the REEs are transferred to the solution and are recovered by oxalic acid precipitation [58] (Eq. 2-10) & (Eq. 2-11).



Where $\text{M}=\text{Na}^+$ or NH_4^+ and $\text{X}=\text{SO}_4^{-2}$ or Cl^-

Mineable ion-adsorption type deposits are exclusively found in abundance in southern china. The continuous advancement in REE extraction from ion-adsorbed clays included batch leaching with NaCl followed by heap leaching methods with ammonium sulfate. Additional s efforts have been made for in situ leaching methods with ammonium sulfate [59, 60]. In situ methods provide the benefit of reduced environmental impact and can be used effectively for low-grade deposits and also for secondary recovery from tailings of previous leaching operations [57, 61].

2.3 REEs in Coal

Coal and coal-based byproducts are enriched in trace elements and can potentially be used as a source for both HREEs and LREEs. Coals with high REE concentrations have been discovered in Pavlovka and Rakovka coal deposits in Russia (300-1000 ppm REEs) [21, 62, 63], Appalachian deposits in the U.S. (500-4000 ppm REEs) [23, 64], Sydney Basin in Nova Scotia, Canada (72-483 ppm REEs) [65], Sichuan basin deposits in China [66, 67], and others across the globe [68-72]. The global average concentration of the REEs is 68.5 ppm in coal [3]. Due to the volatile REE prices, the REEs contained in coal have a significant economic potential even if the REEs are partially recovered. REE concentrations of 300 ppm on a dry, whole mass basis have been set as the cut-off by the U.S. Department of Energy for a coal-based resource to qualify as a feedstock for most of its funded research projects [21, 27, 63, 72-75].

REEs are mainly concentrated in coal in the form of accessory phosphates minerals (such as monazite and xenotime), sedimentary minerals (monazite, xenotime, zircon), or clay minerals (kaolinite, Illite) [3, 73, 76]. The occurrence of REEs in coals can

be in association with pyroclastic minerals like monazite and xenotime from a volcanic origin, diagenetic and epigenetic minerals that are a result of precipitation or recrystallization, and/or with organic compounds [21, 62, 76]. A study by Lin et. al. [77] suggests that about 25% of the REEs contained in the feed coal are associated with the organic matter with relatively higher concentrations of HREEs. Seredin [63] suggested that REEs mostly occur in REE enriched coals as crystallized grains of REEs, usually, 0.5-5 mm in diameter, deposited during sedimentation and in adsorbed forms on the organic matter or clay minerals. Hower et al. found that REEs in coal from eastern Kentucky is mainly in the form of REE-rich phosphates, like monazite, which is of authigenic origin judging from the fact that the monazite commonly in-fills cracks in clays and cells in clarain and vitrain. The monazite occurs in very small (<2 mm) irregularly shaped particles [23, 24, 64]. According to Seredin, most of the REEs in coal (70-80%) are present in the lightest density fraction (<1.40 specific gravity) [63].

2.3.1 Extraction of REEs from coal

The traditional rare earth minerals are recovered by primary physical beneficiation followed by metallurgical extraction of elements. REEs beneficiation and recovery from coal sources have thus been widely investigated using traditional commercial physical separation methods. However, REE mineral grains in coal are in a very small particle size range and are disseminated in the cracks and pores of the coal and host rock matrix which require ultrafine grinding for liberation. Thus, the complex nature of the occurrence, composition, and distribution of REEs in coal and coal combustion products possess significant economic and operational limitations of the conventional mineral processing techniques (e.g., gravity separation, froth flotation, magnetic separation, etc.). Exploiting the difference in magnetic, electrostatic, and physiochemical characteristics of REE-bearing minerals by physical extraction methods has been investigated and found to be ineffective in most cases [3, 12, 16, 78-82]. Gravity separation methods have been used to separate clean coal from heavy density material. However, significant benefits in REE enrichment have not been realized. Although a few successful attempts to concentrate REEs using froth flotation have been made, the commercial use of

the process is restricted by the need for ultrafine grinding for liberation of the finely disseminated REE minerals [78, 79, 83].

On the other hand, extraction, and concentration of REEs from coal-based feedstock have been proven to be technologically feasible by hydrometallurgical extraction methods such as leaching and solvent extraction [6, 11, 13-15, 17, 61, 84-86]. Hydrometallurgical methods such as acid leaching and ion exchange are normally utilized to process the resources in which the REEs have no specific mineral form or the REE minerals are in the ultrafine size range. A basic hydrometallurgical process has three distinct steps: 1) extraction of metal ions from the concentrated solid feed into aqueous solution by leaching with an acidic/basic reagent, 2) concentration of the dissolved metal in the solution using liquid-liquid extraction processes like selective precipitation and solvent extraction and 3.) recovery of metals using electrochemical processes like electrowinning, etc. [87-89]. The recovery of the REEs and rejection of the contaminants (Al, Ca, and Fe) is very critical for hydrometallurgical extraction as the economic viability of the process depends upon the efficiency of every step of the extraction process.

Selective leaching is the most critical aspect of the hydrometallurgical extraction of REEs from the coal-based feedstock. Owing to the very low concentration of REEs in the feed (~300 ppm), the pregnant solution generated in the leaching process has a very small amount of dissolved REEs (<25ppm) and large quantities of dissolved contaminants (>10000 ppm). Such a makeup of the leachate renders the downstream processes such as solvent extraction uneconomical. Therefore, the oxidation pretreatment step integrated into the hydrometallurgical extraction circuit can increase REE recovery, lower acid consumption, and decrease the concentration of contaminants going into the solvent extraction feed.

Selective precipitation is based on the different solubility products of the complexes formed by REEs and other contaminants with precipitants such as oxalic acid, ammonium hydroxide, and sodium sulfate. Rare earth species can be precipitated out as oxalates with oxalic acid (pH 1-4), while other metal species (iron, aluminum, titanium) remain in solution as soluble oxalate complexes. In a solvent extraction process, rare earth

cations are selectively transferred into the organic phase by using a selective extractant such as di-(2-Ethylhexyl) phosphoric acid (D2EHPA). A portion of the contaminants reporting to the organic phase along with REEs can be eliminated using a scrubbing process and REEs staying in the scrubbed organic phase are stripped out using a strongly acidic solution (e.g., 6 M HCl). Final solid products can be generated by roasting rare earth precipitates obtained from the stripping solution. Sellable products with more than 99.99% of REO can also be achieved under optimized operating conditions.

Detailed studies following the first phase of REE characterization studies have been focused primarily on the hydrometallurgical extraction of REEs from coal. The effect of different leaching reagents, temperatures, durations, etc. has been studied in detail [13, 15]. Investigations carried out using 0.1M ammonium sulfate as leaching reagent at pH of 5 for 24 hours resulted in poor leaching recovery values of ~10% total REEs. However, the significant differences in the recovery of Heavy and light REEs provided indirect evidence of a difference in the mode of occurrence between the two REE groups [15]. Significant improvements in REE recovery were observed upon decreasing the solution pH suggesting a pH-dependent solubility of REEs contained in coal (Figure 2.10).

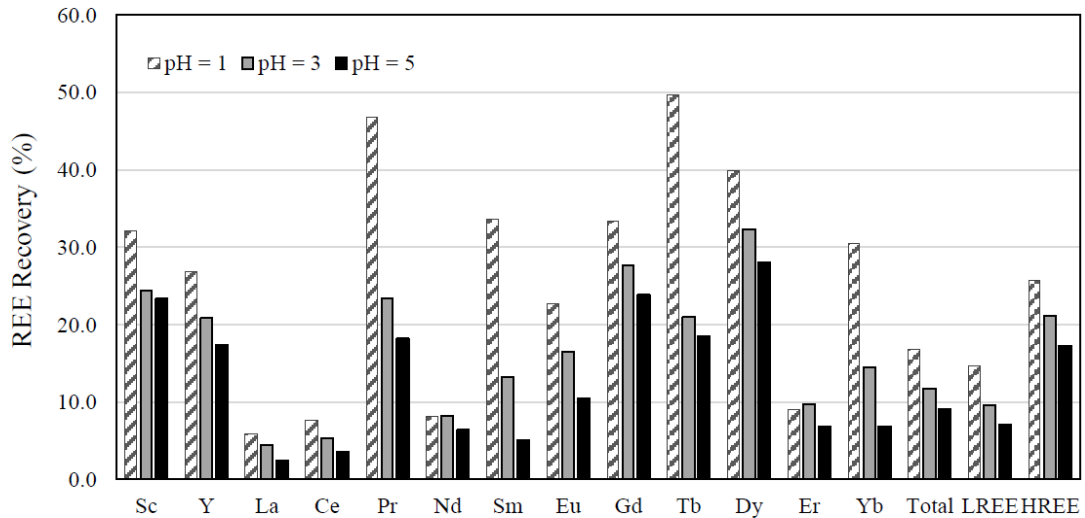


Figure 2.10. Effect of pH on REE recovery from thickener underflow fine refuse (TUF) sample using 0.1 mol/L (NH₄)₂SO₄ and nitric acid for pH adjustment [15].

However, owing to the poor leaching characteristics of the REEs contained in coal thermal pretreatment with and without chemical additives has also been explored. Yang recovered 74% of REEs using 1.2M sulfuric acid from calcination products of thickener underflow material calcined at 750°C for 2 hours. The improvement of 43 absolute percentage points primarily resulted from the increase in LREE leachability as compared to HREEs for which the increase was only 8% (Figure 2.11). Also, alkaline treatment using 8M NaOH before acid leaching with 1.2M sulfuric acid was found to improve REE recovery from 22% to 75%. However, both thermal and chemical pretreatment steps were found to significantly affect the leaching characteristics of LREEs over those of the HREEs.

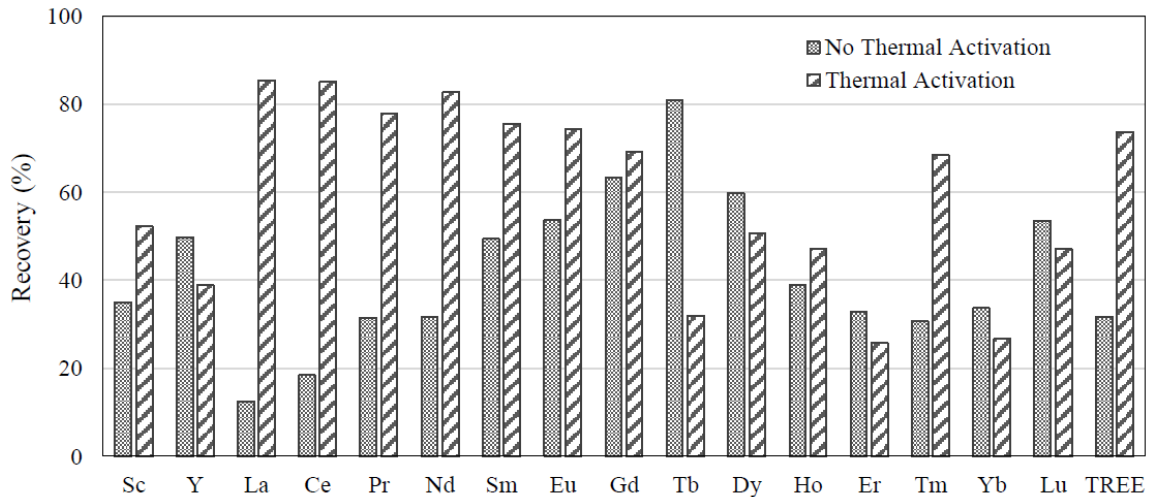


Figure 2.11. Improvement in REE leaching recovery after thermal activation pretreatment of the de-carbonized -180 μm middlings material and five hours of leaching using 1.2 mol/L sulfuric acid solution at 75°C [15].

Leaching tests with sulfuric acid at pH of 0, ammonium sulfate salt solution at pH of 3, and deionized water at pH of 3 were carried out for the coal sample decarbonized with LTP. The results after 5 hours suggested the following order of leaching recovery acid: leach > salt leach > water leach (Figure 2.12). However, the high recovery of critical elements such as Sc, Nd, and Dy provided an opportunity to recover REEs by using LTP as a pretreatment method. The LTP can be utilized to pretreat the feedstock

samples to liberate, release, oxidize and/or activate the rare-earth elements from organic matter in coal or minerals that are embedded in coal.

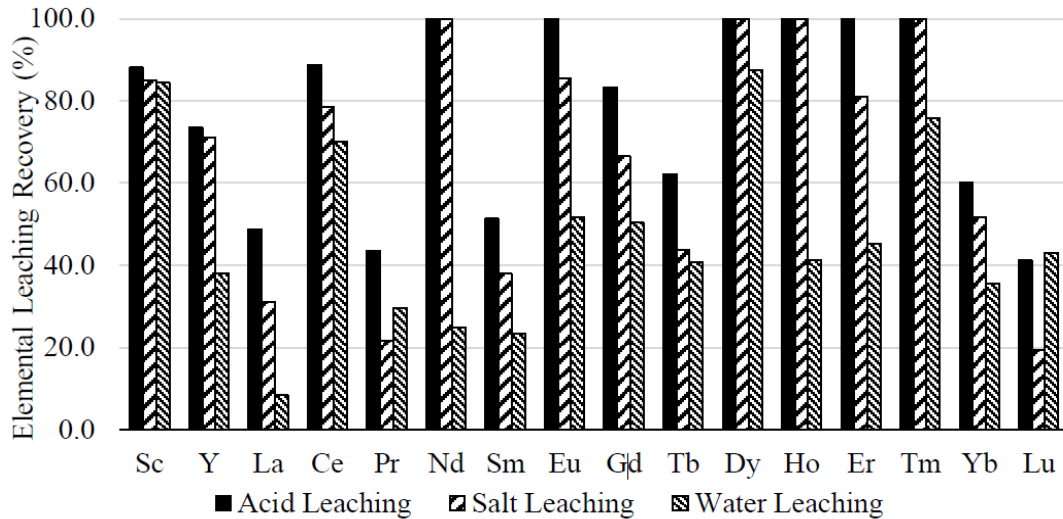


Figure 2.12. Recovery of REEs from low-temperature plasma-treated coal under various leaching conditions for 5 hours. (acid Leaching with sulfuric acid at final pH of 0; salt leaching with ammonium sulfate at final pH of 3; water leaching with deionized water at final pH of 3) [15]

Since the mode of association REEs with mineral phases in coal is very heterogeneous, thermal treatment in an oxidizing or inert atmosphere can be used to convert the REE minerals to more soluble REE compounds. Additionally, the structure of the host particle can be altered by thermal decomposition and/or phase transformation to provide enhanced REE liberation from the coal organic matrix and an improved diffusion rate of lixiviate to the particle core during the subsequent leaching operation. Calcinators are mature, commercially available technologies that exist as rotary drum units or fluidized-bed systems and can treat high throughput capacities. Oxidation pretreatment is very effective in transforming REE-bearing minerals into more leachable forms [10, 18]. A summary of roasting reactions of conventional REE minerals with and without reagent addition has been summarized in Table 2.3. The high-temperature roasting decomposes or transforms the carbonates and phosphates into more soluble oxides, sulfates, and chlorides.

Table 2.3. A summary of monazite and bastnasite roasting reactions [36].

Reactant	Reaction	Temperature	Time
None	$\text{REEFCO}_3 \rightarrow \text{REEOF} + \text{CO}_2(\text{g})$	500 °C	NA
	$3\text{REEOF} \rightarrow \text{REEF}_3 + \text{REE}_2\text{O}_3$	850 °C	NA
None	$\text{REEPO}_4(\text{s}) \rightarrow \text{REEPO}_4(\text{l})$ (melting)	~2000 °C	NA
NaOH	$\text{REEPO}_4 + 3\text{NaOH} \rightarrow \text{REE}(\text{OH})_3 + \text{Na}_3\text{PO}_4$	400 °C	120 min
NaOH plus milling	$\text{REEPO}_4 + 3\text{NaOH} \rightarrow \text{REE}(\text{OH})_3 + \text{Na}_3\text{PO}_4$	No roasting	120 min
CaO-C	$2\text{REEFCO}_3 + \text{CaO} \rightarrow \text{REE}_2\text{O}_3 + \text{CaF}_2 + 2\text{CO}_2(\text{g})$	380–431 °C	60 min
	$4\text{CeO}_2 + 2\text{C} + \text{O}_2 \rightarrow 2\text{Ce}_2\text{O}_3 + 2\text{CO}_2(\text{g})$		60 min
	$6\text{REEPO}_4 + 9\text{CaO} + \text{CaF}_2 \rightarrow 2\text{Ca}_5\text{F}(\text{PO}_4)_3 + 3\text{REE}_2\text{O}_3$	605–716 °C	NA
CaO-NaCl-CaCl ₂	$4\text{CeO}_2 + 2\text{C} + \text{O}_2 \rightarrow 2\text{Ce}_2\text{O}_3 + 2\text{CO}_2(\text{g})$		
	$2\text{REEFCO}_3 + 3\text{CaO} \rightarrow \text{REE}_2\text{O}_3 + \text{CaF}_2 + 2\text{CaCO}_3$	425–560 °C	
	$2\text{REEPO}_4 + 3\text{CaO} \rightarrow \text{REE}_2\text{O}_3 + \text{Ca}_3(\text{PO}_4)_2$	630–700 °C	NA
CaO-NaCl-CaCl ₂	$6\text{REEPO}_4 + 9\text{CaO} + \text{CaF}_2 \rightarrow 3\text{REE}_2\text{O}_3 + 2\text{Ca}_5\text{F}(\text{PO}_4)_3$		
	$2\text{REEPO}_4 + 3\text{CaO} \rightarrow \text{REE}_2\text{O}_3 + \text{Ca}_3(\text{PO}_4)_2$	650–780 °C	60 min
Ca(OH) ₂ -NaOH	$2\text{REEFCO}_3 + \text{Ca}(\text{OH})_2 \rightarrow \text{REE}_2\text{O}_3 + \text{CaF}_2 + 2\text{CO}_2(\text{g}) + \text{H}_2\text{O}(\text{g})$	700 °C	30 min
	$2\text{REEPO}_4 + 3\text{Ca}(\text{OH})_2 \rightarrow \text{REE}_2\text{O}_3 + \text{Ca}_3(\text{PO}_4)_2 + 3\text{H}_2\text{O}(\text{g})$	630 °C	30 min
MgO-C-Cl ₂	$2\text{REEFCO}_3 + \text{MgO} \rightarrow \text{REE}_2\text{O}_3 + \text{MgF}_2 + 2\text{CO}_2(\text{g})$	700 °C	120 min
	$4\text{CeFCO}_3 + 2\text{MgO} + \text{O}_2 \rightarrow 4\text{CeO}_2 + 2\text{MgF}_2 + 4\text{CO}_2(\text{g})$		
	$2\text{REEPO}_4 + 3\text{MgO} \rightarrow \text{REE}_2\text{O}_3 + \text{Mg}_3(\text{PO}_4)_2$		
	$2\text{CeO}_2 + 4\text{C} + 3\text{Cl}_2 \rightarrow 2\text{CeCl}_3 + 4\text{CO}(\text{g})$		
	$2\text{REE}_2\text{O}_3 + 3\text{C} + 3\text{Cl}_2 \rightarrow 2\text{REECI}_3 + 3\text{CO}_2(\text{g})$		
MgO-NH ₄ Cl	$\text{REEPO}_4 + 3\text{C} + 3\text{Cl}_2 \rightarrow \text{REECI}_3 + \text{POCl}_3(\text{g}) + 3\text{CO}(\text{g})$		
	$2\text{REEFCO}_3 + \text{MgO} \rightarrow \text{REE}_2\text{O}_3 + \text{MgF}_2 + 2\text{CO}_2(\text{g})$		
	$4\text{CeFCO}_3 + 2\text{MgO} + \text{O}_2 \rightarrow 4\text{CeO}_2 + 2\text{MgF}_2 + 4\text{CO}_2(\text{g})$	600 °C	80 min
	$2\text{REEPO}_4 + 3\text{MgO} \rightarrow \text{REE}_2\text{O}_3 + \text{Mg}_3(\text{PO}_4)_2$		
	$\text{MgF}_2 + \text{Mg}_3(\text{PO}_4)_2 \rightarrow 2\text{Mg}_2\text{FPO}_4$		
Charcoal	$\text{NH}_4\text{Cl} \rightarrow \text{NH}_3(\text{g}) + \text{HCl}(\text{g})$		
	$\text{REE}_2\text{O}_3 + 6\text{HCl} \rightarrow 2\text{REECI}_3 + 3\text{H}_2\text{O}$		
	$2\text{CeO}_2 + 8\text{HCl} \rightarrow 2\text{CeCl}_3 + 4\text{H}_2\text{O} + \text{Cl}_2$	500 °C	25 min
Na ₂ CO ₃	$2\text{REEPO}_4 + 5\text{C} \rightarrow \text{REE}_2\text{O}_3 + \text{P}_2(\text{g}) + 5\text{CO}(\text{g})$		
	$2\text{REEFCO}_3 + \text{Na}_2\text{CO}_3 \rightarrow \text{REE}_2\text{O}_3 + 2\text{NaF} + 3\text{CO}_2(\text{g})$	1400 °C	120
Na ₂ CO ₃	$4\text{CeFCO}_3 + 2\text{Na}_2\text{CO}_3 + \text{O}_2 \rightarrow 4\text{CeO}_2 + 4\text{NaF} + 6\text{CO}_2(\text{g})$	348-466 °C	NA
	$2\text{REEPO}_4 + 3\text{Na}_2\text{CO}_3 \rightarrow \text{REE}_2\text{O}_3 + 2\text{Na}_3\text{PO}_4 + 3\text{CO}_2(\text{g})$	578-653 °C	NA
Na ₂ CO ₃ plus milling	$2\text{LaPO}_4 + 3\text{Na}_2\text{CO}_3 \rightarrow \text{La}_2\text{O}_2\text{CO}_3 + 2\text{Na}_3\text{PO}_4 + 2\text{CO}_2$	450–500 °C	120
	$\text{La}_2\text{O}_2\text{CO}_3 \rightarrow \text{La}_2\text{O}_3 + \text{CO}_2(\text{g})$	625-725 °C	

Zhang and Honaker reported preferential LREE recovery using 1.2 M HCl (80-90%) for the Pocahontas No. 3 coal source after calcination at 600°C. Also, an insignificant increase in the recovery of HREEs was observed and was attributed to the

inability of thermal decomposition of HREE bearing phosphate minerals at 600°C. The findings suggested faster leaching kinetics after calcination of both the middling and the high ash sample of the feed (Figure 2.13). An interesting finding was the decrease of HREE recovery with the increase in temperature beyond 600°C, which was a result of HREEs associated with sulfide minerals that transformed into oxides like hematite which have lower solubility [36].

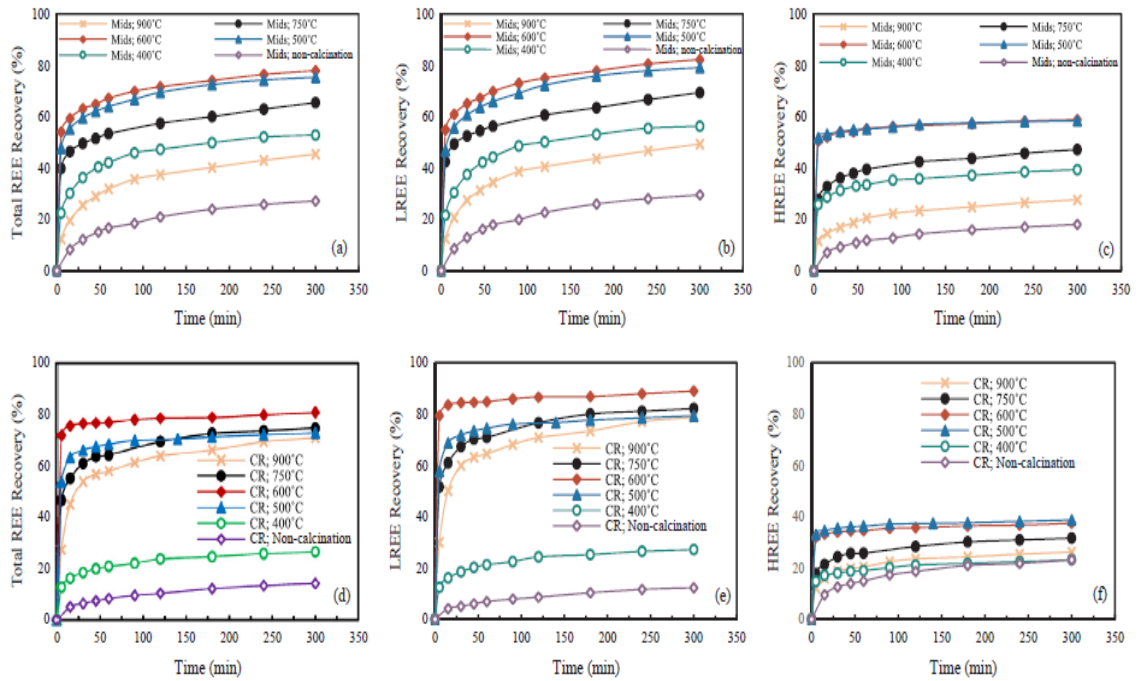


Figure 2.13. Leaching characteristics of total REEs, LREEs, and HREEs from the middlings (Mids) and coarse refuse (CR) as a function of reaction time and calcination temperature: (a), (b), and (c) are the total REEs, light REEs, and heavy REEs recovery values, respectively, for the Pocahontas No. 3 middlings sample and (d), (e) and (f) are likewise for the coarse refuse sample [36].

Zhang and Honaker studied the mode of occurrence of REEs with bituminous coal samples using calcination at 600°C followed by sequential extraction. It was found that the majority of REEs in untreated coal was in an insoluble form and after calcination, more soluble REE metal oxides were detected [90]. Zhang and Honaker also studied the effect of calcination on the recovery of REEs and other critical elements such as cobalt, chromium, lithium, manganese, strontium, and vanadium using 1.2 M HCl acid solution [91]. The recovery of REEs and critical elements increased from 24% to about

80-90% post calcination at 600-750°C for 2 hours in an oxidizing atmosphere. The major findings were the increase of LREE recovery after calcination which was initially in an insoluble form. Ji et. al. studied the effect of organic acids as lixiviants for the leaching recovery of REEs from the West Kentucky No.13 coal seam. The study reported improvements in the recovery of HREEs and Sc with the use of citric acid and DL-malic acid [17]. Various studies have been performed on the impact of thermal activation on the leaching kinetics of REEs however such studies have been limited to set temperature values and under an oxidizing environment. Additionally, a detailed investigation of the observed benefits has not been explored based on the changes in the mineralogy of the parent feed material [17, 36, 91].

Yuan et al. studied the phase transformation and decomposition of REE-bearing minerals with the addition of CaO during roasting. The TGA-DSC method showed that the decomposition of REEs was a two-step process (Figure 2.14) [92]. The endothermic peak from 380°C to 431°C corresponded to phase change and decomposition of rare earth carbonates. Secondly, the phosphate minerals decomposed in the temperature range of 605°C-716°C. The decomposition products were the oxides and fluorides of the host minerals. The study also delineated that low-temperature bastnasite decomposition progressed as a chemical reaction while the high-temperature step of monazite decomposition was controlled by diffusion.

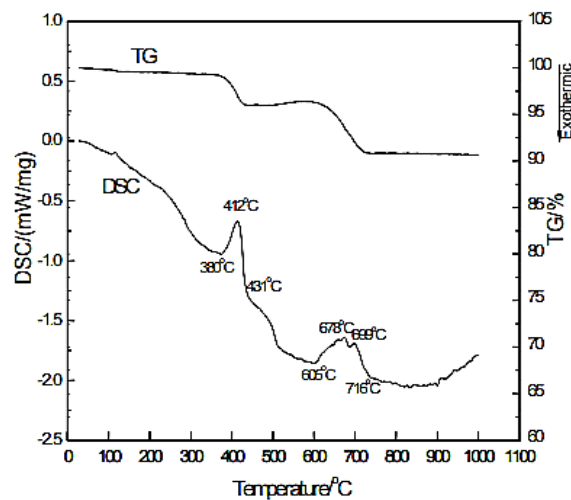


Figure 2.14. TGA-DSC curve for the roasting process at a heating rate of 10 °C min⁻¹ magnetic tailings mixed with CaO and coal [92].

The separation techniques which are used for producing mixed REO concentrate from conventional sources cannot be effectively applied in the coal-based leachates because of the significantly different compositions. Numerous findings suggest that the coal-based leachate contains significantly high concentrations of the contaminant elements while having relatively low concentrations of REEs (Figure 2.15). A higher concentration of contaminants negatively impacts the efficiency and cost of the solvent extraction process and downgrades the final product. Chandra, 2019 [61] developed a solvent extraction rougher and cleaner circuit using 5% Di-(2-Ethylhexyl) phosphoric acid (DEHPA) in kerosene as extractant to separate the REEs from the contaminants and produce a high purity REE product (Figure 2.16). The use of 5% dialkyl phosphinic acid (Cynex 272) in kerosene was proposed for the selective extraction of scandium from the original leachate solution with about 85% recovery was obtained.

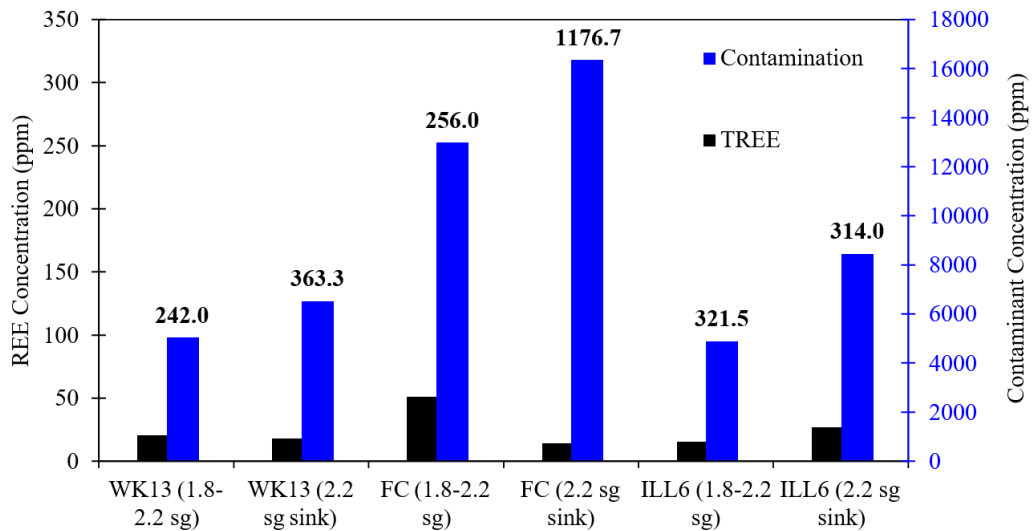


Figure 2.15. The concentration of the TREE (in black) and primary contaminants (in blue) in the PLS are generated from different coal sources. The numbers in bold represent the relative concentration (RC) of the contaminants to the TREEs in the solution [61].

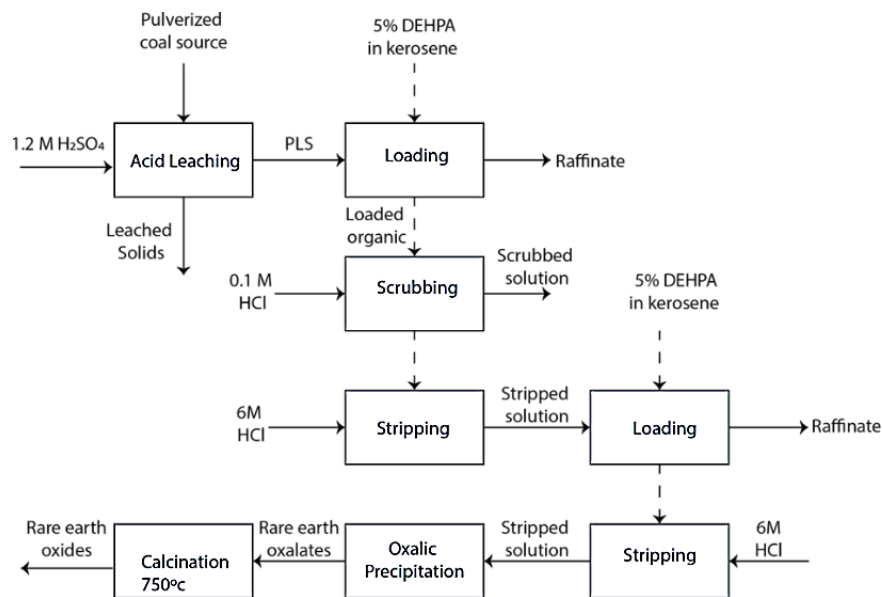


Figure 2.16. Schematic of the SX process procedure used to separate rare earth elements from the contaminant elements in the pregnant leach solutions from six coal sources [61]

Additional novel attempts have also been made to recover the REEs associated with coal byproducts by bioleaching to eliminate the use of acid leaching [93-95] and by bio-absorption for selective extraction of REEs from PLS solutions [96]. These efforts highlight the utility of benign techniques for the sustainable recovery of REEs to diversify the supply chain.

2.4 Low-temperature Plasma

Plasma is considered as the fourth state of matter other than solid, liquid, and gas, which is formed by striking a gas with enough energy to ionize gas molecules as a mixture of ions, electrons, and neutral particles [97, 98]. In the past century, plasma treatment technology has been developed and utilized in various fields of applications, especially in the field of material processing. Plasma treatment has been applied to surface modification and deposition, surface activation, material syntheses, waste decomposition, refining, extractive metallurgy, pyrometallurgy, etc. [97-104]. Plasma can be artificially generated by applying an electric field on a gas, which provides accelerated electrons in the gas environment and collides with the gas molecules and atoms. The collision causes excitation of the electrons and forms a partial or complete ionization of the gas [97]. The

electrical energy carried by electrons is converted to thermal energy. Two types of plasma are categorized in this process [102, 105, 106]:

1. Thermal plasma: the temperature of electrons is the same as the heavy particles such as ions and neutrals ($T_e \sim T_h$) reaching local thermodynamic equilibrium, usually produced at high pressure ($>10\text{kPa}$) with high temperature (2,000-20,000 K).
2. Non-equilibrium plasma (cold plasma): the temperature difference between an electron and heavy particles is significant ($T_e \gg T_h$), usually produced in a low-pressure environment with less electron density. In this case, the plasma temperature could be as low as 40~50 °C to as high as 300°C.

Typical thermal plasma applications include plasma torch welding/ cutting, spray coating, metal/ ceramics/ nanoparticle synthesis, extractive metallurgy, smelting/ refining metallurgy, hazardous waste destruction [105]. In 1961, Gleit and Holland developed a pretreatment method using low-temperature oxygen plasma to decompose organic substances before elemental analysis [107]. The original design used a radio frequency (RF) discharge technique to generate electrically excited oxygen. Figure 2.17 shows a schematic diagram of an RF plasma treatment apparatus in a later study reported by Hozumi et al. [108]. A radiofrequency coil is wrapped around a hard glass tube and energized with a high-frequency current to create an electromagnetic field that generates energy to remove electrons from oxygen atoms. The free electrons, which contain higher energy, bombard the remaining oxygen molecules injected into the tube and cause partial ionization [97].

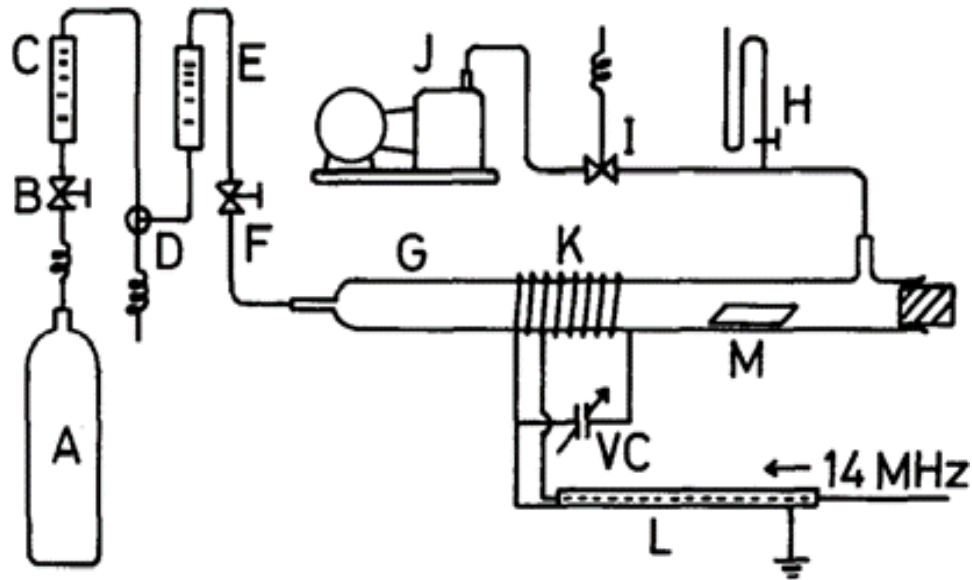
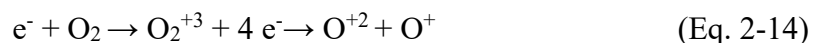
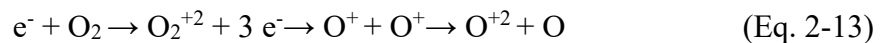
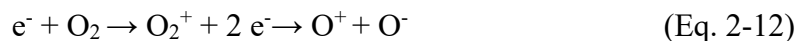


Figure 2.17. Schematic diagram of RF low-temperature plasma ashing apparatus: (A) oxygen tank; (B), (F) needle valve; (C), (E) flow meter; (D) three-way junction; (G) Pyrex tube; (H) MacLeod gauge; (I) three-way stopcock; (J) rotary pump; (K) High Frequency coil; (L) coaxial cable, 75 Ω impedance; (M) specimen; (VC) variable air condenser [108].

Other than the RF discharge technique, direct-current glow discharge excitation was developed as an alternative way of generating oxygen plasma. The reaction chamber is in a vacuum environment between two Ni electrodes under various power levels. The electric current passes through a chamber filled with oxygen gas and ionizes the gas to singlet form. The use of a larger chamber or several chambers in parallel for larger treatment capacity was also suggested in their study if other parameter values remained constant. The color of the discharge in the ashing chamber is blue during the oxidation process and will turn into violet color which is the color of the pure oxygen discharge indicating that the oxidation process is complete [109].

The ionization and dissociation of oxygen molecules by electron bombardment can be described in the following three expressions adapted from McConkey et al. [110] (Eq. 2-12), (Eq. 2-13) & (Eq. 2-14);



The first electron dissociation of oxygen atom requires 12.1 eV of energy (1 eV = 96.5 J/mol). The reactions in Eq. 1 are most likely to take place whereas Eq. 2 and 3 are lower probabilities. The first step reaction in Eq. 1 has an 80% possibility to occur whereas the second step has about a 20% chance due to the different energy absorption mechanisms of oxygen molecules [110].

A simplistic mechanism of the LTA process on organic surfaces is shown in Figure 2.18. As the mixture of ionized oxygen gas reaches the surface of particles, the singlet oxygen particle tends to chemically react with the radical hydrogen of the alkyl group. The reaction is merely happening at the interface between solid and gaseous phases and the organic material at the surface is gradually peeled away and the process continues into the deeper layers of the solid surfaces. The kinetic rate of this process is controlled mainly by the concentration of oxygen.

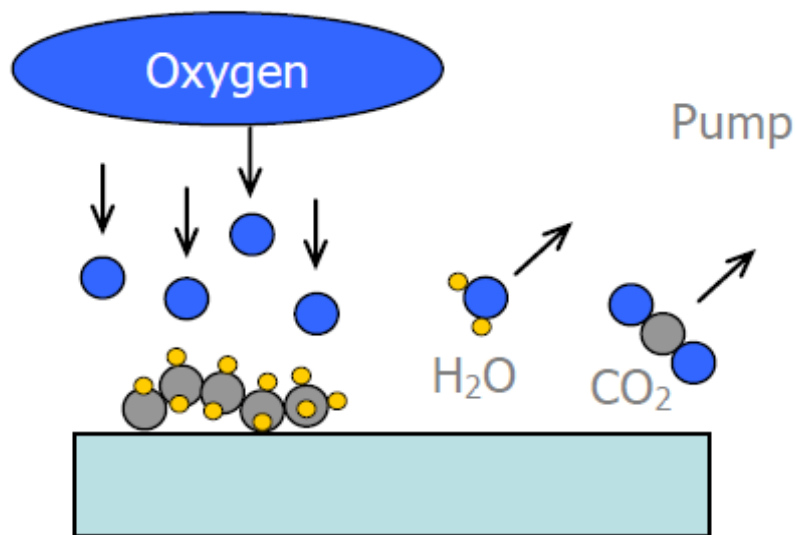


Figure 2.18. Oxygen plasma treatment on organic surface [102].

Low-temperature ashing (LTA) is a process in which a coal sample is exposed to oxygen activated by a radio-frequency oscillator. These highly charged ions chemically activate the surrounding gases and produce a highly charged chemically reactive environment that can be used for the combustion of organic matter at low temperatures. An oxygen plasma utilizes oxygen to produce plasma for the oxidation of organic matter present in coal into its basic combustion products CO₂ and H₂O [102]. This

oxidation, however, occurs at a very low temperature as compared to conventional burning. The oxidation process is initiated by the high kinetic energy of the free electrons. Due to the low temperature, the mineral matrix of the minerals present in the coal such as Illite, kaolinite, pyrite, and quartz remain intact. This process serves to ash the coal sample, liberating and concentrating the mineral matter associated with the coal as the organic material is oxidized. LTP treatment theoretically renders the mineral matrix unaltered after the removal of the carbon matter. This residue has been found to show higher leaching recoveries in literature [13, 102, 111].

The LTP ashing technique has been widely incorporated with analytical procedures as an ashing method to determine mineral matter content and mineralogy structure in coal and coal byproducts [109, 112]. Some studies compared the inorganic constituents of samples using various ashing methods and concluded that the low-temperature ashing (LTA) procedure provided accurate analyses on elements with high volatility, such as mercury, zinc, lead, arsenic, and manganese [113]. Allen et. al. investigated the microstructure change of coal in LTP using an LTA-504 unit obtained from LFE Corporation [114]. The microstructure of the LTP ash was strongly correlated to the mineral matter which was originally present in the organic matrix of the coal. The partial oxidation of pyrite during the ashing was also observed. A “gauze” appearance of individual ash particles was observed which was likely to be a three-dimensional network where denser particles were suspended in the ash matrix. These denser particles were the same types of mineral inclusions as those in the raw coal. The ash particles were more agglomerates of quartz, clay, and pyrite. Pyrite remained relatively undisturbed in the ashing process based on XRD analysis, however, the Fe:S ratio of the ash sample was higher than the ratio of the original pyrite composition.

Miller et al. however reported that undesired reactions such as oxidation of pyrite to hematite and fixation of organic sulfur as sulfates also occur during LTP treatment of coals. They quantified the amount of pyrite burnt and found a linear relationship with the RF Power of the treatment (Figure 2.19) [115]. The gas phase in the LTP equipment is stagnant and thus samples need to be withdrawn from the chamber periodically and stirred

to expose fresh surfaces [111, 115]. Miller also observed that organic sulfur was released as SO₃ or reacted with carbonates present to form fixed sulfates.

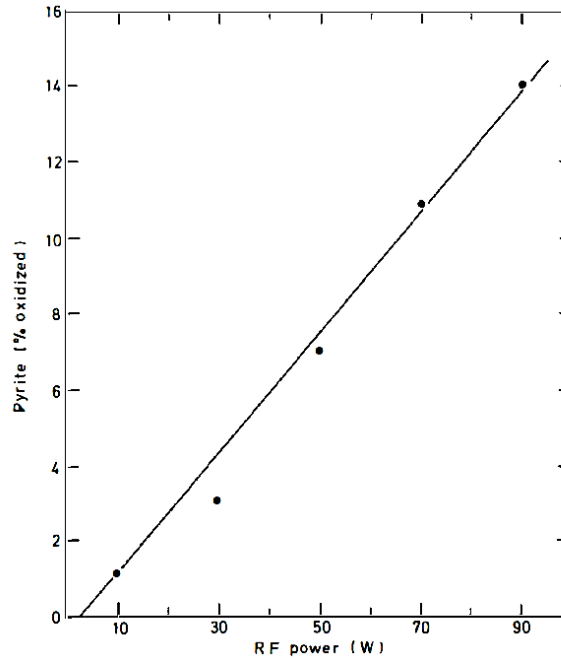


Figure 2.19. Oxidation of pyrite mixture with graphite as a function of RF Power after 24 hours of LTA [115].

Gleit and Holland evaluated the effect of pressure, flow, and power on oxidation rates. It was reported that the oxidation rate is a function of the exposed surface and decreases as the surface becomes covered with a mineral residue. At high oxygen flow rates, the decomposition is independent of the oxygen flow rate. Thus, an optimum saturation of oxygen will have the required kinetic energy in the free electrons for efficient performance. Oxidation rate increased linearly with power in the range of 120 to 300 watts and for specimens with larger surface areas, the change in rate with increased power is greater. The intensity of the intense blue glow of the oxygen plasma is a good visual representation of oxidizing power. The discharge could not be maintained when less than 120 watts were delivered to the induction coil [107].

2.5 Minerals of coal deposits

Coal is a heterogeneous mix of organic and inorganic mineral compounds. The organic content is derived from the carbon matter inherited from the plants. The inorganic matter is derived from sedimentation, minerals from original vegetation, and deposition by the movement of air and water. About 120 mineral forms have been identified to be present in coal out of which 33 occur in most coal deposits (Table 2.4). Quartz, pyrite, clays, calcite, and siderite are the most common minerals associated with coal. These minerals and other minor minerals usually contain the bulk of the 76 naturally occurring trace elements. However, most of those elements usually are present in only trace concentrations (ppm). Extracting and concentrating the trace elements organically associated with coal is very difficult using conventional mineral processing operations that remove the mineral matter from the organics. Organically bound trace elements can be released only by burning off the carbon matter, or by harsh chemical leaching, which is uneconomical and impractical in many cases. On the other hand, trace elements associated with clays or pyrite can be concentrated by crushing and washing and subsequently extracted by acid leaching. The minerals commonly occur as single mineral crystals or clusters of mineral crystals intermixed and interbedded with other mineral forms and organic matter. The minerals are found to fill void spaces in the coal with mineral grains ranging from submicron sizes to a few inches. When the coal is burned, most of the mineral matter and trace elements are concentrated in the ash. However, some minerals like pyrite break down into gaseous compounds and are emitted as flue gas. Iron in the pyrite reacts with oxygen to produce iron oxide (hematite, magnetite) and becomes part of the ash residue. Trace elements also separate from the organic or mineral matter when coal is burned. Most become part of the ash, but a few of the more volatile elements, such as mercury and selenium, are partly emitted in the gaseous exhaust [116].

Table 2.4. Common minerals found in coal and their elemental compositions [116].

Mineral	Chemical composition
Major Mineral Constituents (In general order of abundance)	
Quartz	SiO ₂
Kaolinite	Al ₂ Si ₂ O ₅ (OH) ₄
Illite	KAl ₄ (AlSi ₇ O ₂₀) (OH) ₄
Montmorillonite	(0.5Ca, Na) _{0.7} (Al,Mg,Fe) ₄ [(Si,Al) ₄ O ₁₀] ₂ (OH) ₄ · nH ₂ O
Chlorite	(Mg, Al, Fe) ₁₂ [(Si, Al) ₈ O ₂₀] (OH) ₁₆
Pyrite	FeS ₂ (May contain As, Cd, Co, Hg, Ni, Sb, and Se)
Calcite	CaCO ₃
Siderite	FeCO ₃ (May contain Mn)
Minor Mineral Constituents	
Analcime	NaAlSi ₂ O ₆ · H ₂ O
Apatite	Ca ₅ (PO ₄) ₃ (OH, F, Cl)
Barite	BaSO ₄
Chalcopyrite	CuFeS ₂
Clausthalite	PbS
Crandallite Group	
Crandallite	CaAl ₃ (PO ₄) ₂ (OH) ₅ · H ₂ O
Florencite	CeAl ₃ (PO ₄) ₂ (OH) ₆
Gorceixite	BaAl ₃ (PO ₄) ₂ (OH) ₅ · H ₂ O
Goyazite	SrAl ₃ (PO ₄) ₂ (OH) ₅ · H ₂ O
Dolomite	CaMg (CO ₃) ₂
Feldspars	(Ca,K,Na)AlSi ₃ O ₈
Galena	PbS
Marcasite	FeS ₂ (May contain the same elements as pyrite)
Monazite	(Ce,La,Y,Th,Nd)PO ₄
Rutile/Anatase	TiO ₂
Sphalerite	ZnS (May contain Cd.)
Xenotime	YPO ₄
Zircon	Zr [SiO ₄]
Trace Mineral Constituents	
Chromite	FeCr ₂ O ₄
Gibbsite	Al (OH) ₃
Gold	Au
Gypsum	CaSO ₄ · 2H ₂ O
Halite	NaCl
Magnetite	Fe ₃ O ₄
Muscovite	KAl ₂ (AlSi ₃ O ₁₀) (OH) ₂

2.6 Decomposition of major coal minerals

The most critical aspect of hydrometallurgical extraction of REEs is their concentration in the PLS. However, the concentration of contaminant ions in the PLS is equally if not more vital as their leaching behavior influences the ionic strength of the lixiviants and can result in lower REE recoveries. For coal-based leachates, the primary contaminants are aluminum, calcium, and iron. As the REEs exhibit similar chemical characteristics, their extraction requires the exploitation of subtle differences in basicity resulting from the difference in their ionic radius. Trivalent metal ions, Al^{+3} and Fe^{+3} , have been found to unfavorably affect the precipitation efficiency of REEs [84]. Calcium when present in a sulfate system can precipitate as gypsum [$\text{CaSO}_4 \cdot 2\text{H}_2\text{O}$] and allow for coprecipitation of REE ions on its surface [15]. Therefore, the ratio of contaminants to the total REE concentration influences the extraction efficiency and determines the cost of the solvent extraction and selective precipitation processes. The higher ratios tend to negatively impact the purity of the final product and require higher acid costs in solvent extraction stripping and higher base costs in selective precipitation. A low concentration of contaminant ions in the hydrometallurgical circuit will eliminate the need for multistage solvent extraction and will produce a higher-grade product [61].

Calcination of the coal-based feedstock is effective in improving the leaching recoveries and reaction kinetics of the REEs [17, 36, 91]. The benefits are obtained by converting the REEs to more soluble forms and/or by liberating the REE-minerals encapsulated within the mineral matter. The high-temperature calcination pretreatment however also oxidizes the gangue minerals and allows for the higher dissolution of contaminant ions primarily aluminum, calcium, and iron in the PLS [84]. Al and Fe are primarily associated with aluminosilicate clays and pyrites found as major minerals in coal. Calcium on the other hand originates from trace quantities of calcite found in coal beds.

2.6.1 Quartz

Quartz in coal originates from inherent ash and out of seam host rock dilutions. Quartz is relatively unreactive and has a very high thermal and acid stability

[117, 118]. When quartz is heated the crystalline structure changes to different polymorphs depending upon the pressure and temperature as shown in the phase diagram in Figure 2.20 [119]. When heated at atmospheric pressure α -quartz is quickly transformed to β quartz at 573°C but the transformation is reversed upon cooling. With a melting point of about ~1800°C, no significant increase in volume is observed by thermal treatment in air and under an inert atmosphere. Additionally, studies have found that the REE and trace element content in quartz is two to three orders of magnitude lower than the upper crustal abundance [120, 121].

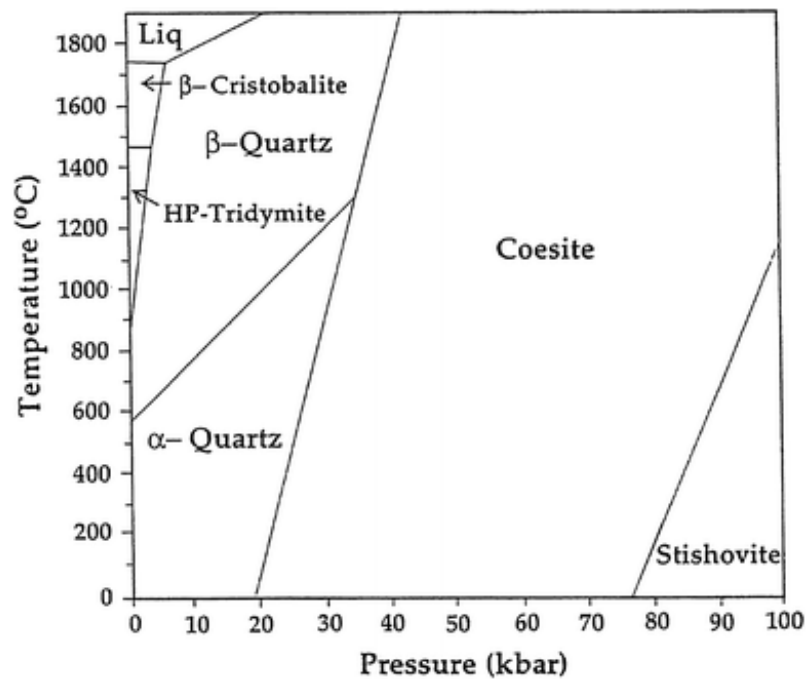


Figure 2.20. SiO₂ phase diagram illustrating the changes in the quartz during heating [119].

2.6.2 Pyrite

Pyrite is one of the most important coal minerals and is a major source of trace elements such as sulfur, arsenic, cadmium, mercury, chromium, etc. that are of environmental concern. Pyrites in coal exist as small clusters called framboids that have a well defined size range and characteristic morphology. They also occur as massive pyrite grains with angular morphology within the microfractures of the coal seam [122]. While massive pyrite can be removed from the coal by washing, the framboidal pyrites due to their small particle size are not efficiently removed [123]. Because framboidal pyrite is

fine-grained and pyrites exhibit paramagnetic properties, traditional separation methods have very little applicability.

Pyrite readily decomposes upon heating in a furnace and converts to pyrrhotite (FeS), magnetite (Fe_3O_4), and hematite (Fe_2O_3) depending upon the temperature, oxygen concentration, flow, and particle size. The decomposition of pyrite in the air starts at 300-400°C with the formation of pyrrhotite and hematite. The amount of hematite and pyrrhotite increases with the increase in temperature. At 800-900°C, almost all the pyrite was ultimately oxidized to hematite with trace amounts of detectable pyrrhotite. By 1100°C the small quantities of magnetite present at lower temperatures were oxidized to hematite. The corresponding thermal transformation process of pyrite in an air environment can be simply summarized as pyrite \rightarrow pyrrhotite \rightarrow magnetite \rightarrow hematite [124, 125] (Figure 2.21). When the pyrite was heated in a 2% O_2 atmosphere, more pyrrhotite was formed than in the air atmosphere and the temperature range over which pyrrhotite is stable is greatly increased. As the partial pressure of oxygen was reduced, at 1100°C magnetite was the major phase due to the limited presence of limited oxygen while pyrrhotite and hematite were detectable in trace quantities [126, 127]. In a completely inert atmosphere, no iron oxides were expected to form and the pyrrhotite was stable over a wide temperature range and converted to magnetite over 1000°C due to the trace amounts of oxygen present in the commercial N_2 source.

The formation of pyrrhotite from pyrite is the starting point of the reaction where the sulfur vapor diffuses through the pyrrhotite layer. The thermal decomposition process is diffusion-controlled and the conversion of pyrite to pyrrhotite follows the unreacted core model [128, 129]. Pyrrhotite and magnetite are intermediate products of the oxidation from pyrite to hematite and SO_2 are released during the thermal decomposition [130] (Figure 2.22). However, the decomposition temperature of pyrite from coal is 100°C lower than mineral pyrite due to the hydrogen donation ability of the host hydrocarbons [131, 132]. The impact related to the leaching behavior of the trace elements associated with pyrites in oxidizing and inert environments during thermal phase transition is complicated and not been understood fully.

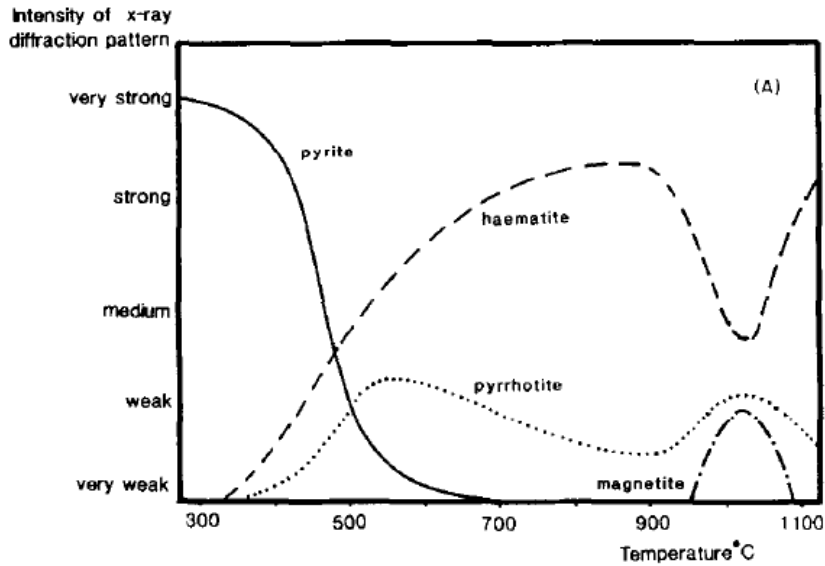


Figure 2.21. Decomposition products of pyrite in the air [126]

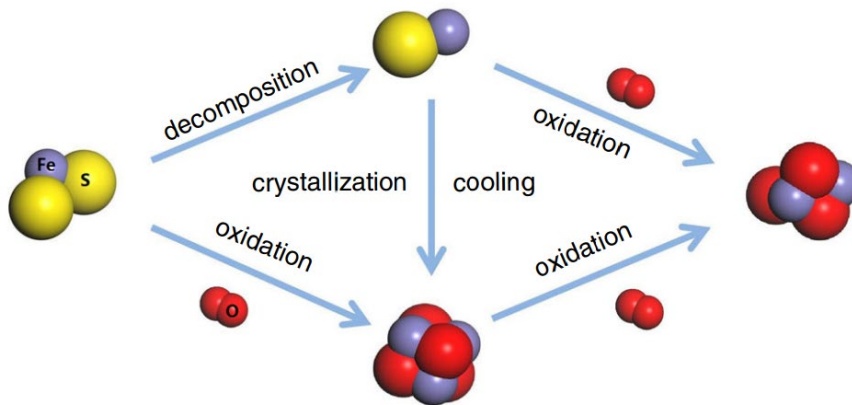


Figure 2.22. Thermal phase transition of pyrite [130].

In some studies, pyrite exhibited both paramagnetic and ferromagnetic properties. Thermal treatment can increase the magnetic susceptibility of pyrite minerals and provide an avenue for recovery by magnetic separation. It was found that the magnetic fraction remained about 20% up to 200°C and increased considerably when the treatment temperature was 400°C (Figure 2.23). It is at 400°C that new phases were detected by XRD (Figure 2.24). For mineral pyrites, the magnetic recovery reaches about 95% at higher temperatures suggesting the formation of magnetic iron oxide [133].

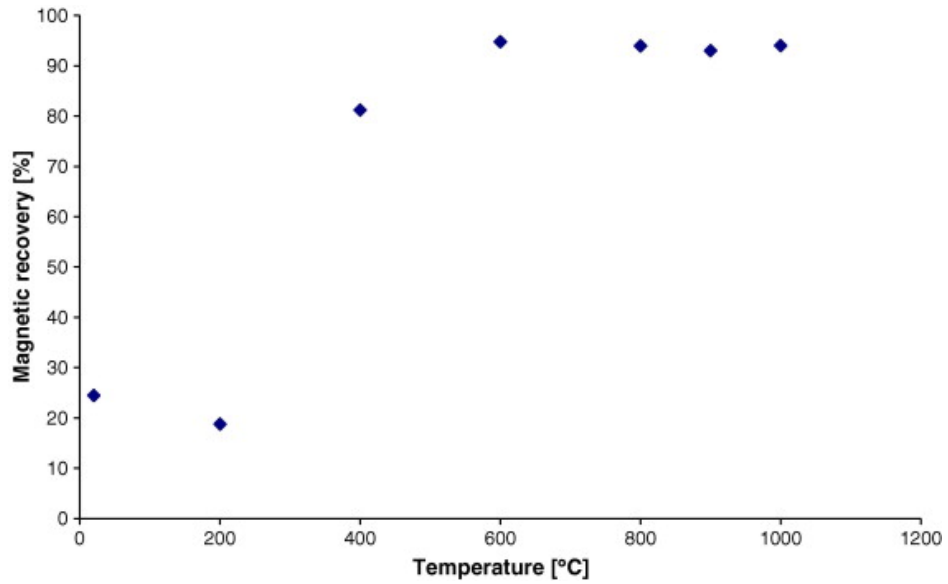


Figure 2.23. Magnetic recovery of heat-treated mineral pyrite sample [133].

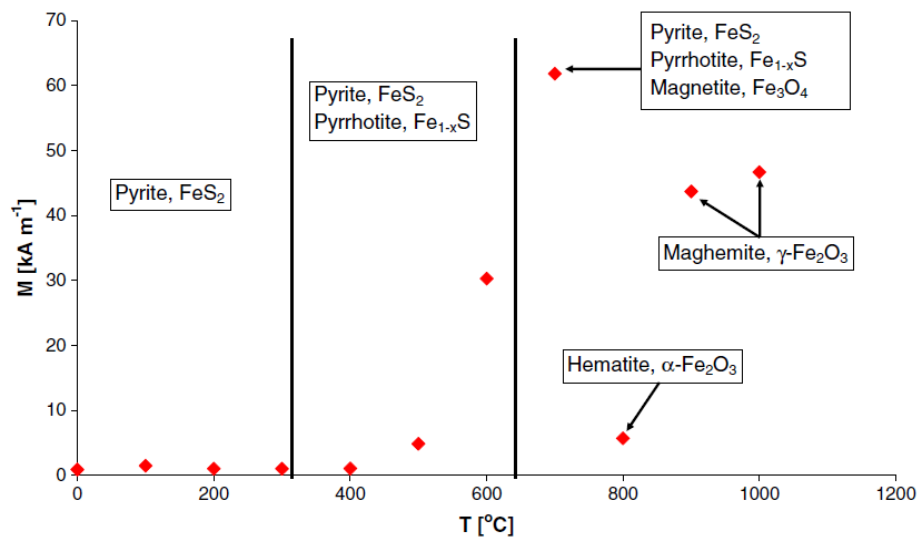


Figure 2.24. Mineral phases detected (through XRD analysis) after thermal treatment for 1 h at temperatures up to 1000°C, and the corresponding magnetization at 1600 kA m₁ of the heat-treated pyrite [133].

2.6.3 Clay Minerals

The clays that form the floor of the coal seam are called under-clays and can be a potential host to ion adsorbed REEs (Figure 2.25). Clay minerals such as kaolinite, halloysite, and Illite have been identified to be present in bulk along with quartz in the underclay samples of Appalachian basin coal deposits [134-137]. Scanning electron microscope analysis has identified 1–20 μm -long mineral crystals of REE phosphate minerals such as monazite and xenotime in the interparticle pore space of the underclay (5 wt.%) (Figure 2.26). Additionally, REE-bearing minerals have also been seen to be present in clay-hosted pyrites present in the coal deposits (1 wt.%) [138]. As such the majority of the REE minerals species are the ones that have a high concentration of LREEs.

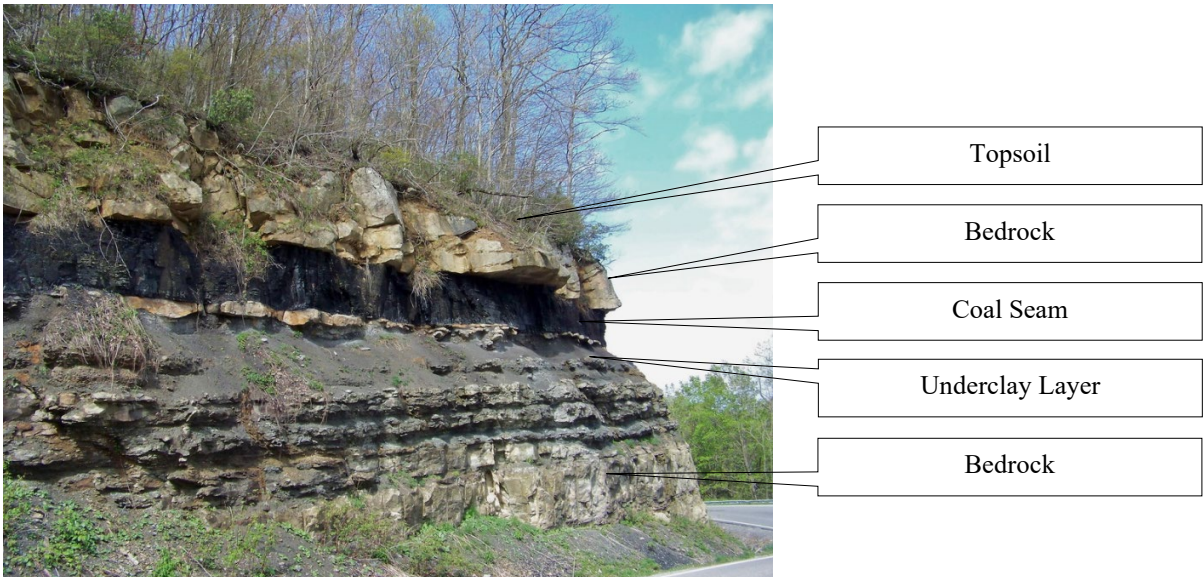


Figure 2.25. Coal deposit with the underclay below the coal and a sandstone host rock (Photo Courtesy: Mike Fitzpatrick from Flickr) [139].

Ion-adsorbed clays are an important source of HREEs are mainly in the form of ions that have been adsorbed onto the surfaces of the alumina silicate minerals such as kaolinite and Illite. Kaolinite is a major mineral present in coal and is insoluble in dilute mineral acids in the hydrated form. However, upon drying (650°C -850°C) kaolinite gets converted to the amorphous form metakaolin which has a high solubility in weak acids [140, 141]. At temperatures >900°C metakaolin crystallizes to form mullite which is acid insoluble.

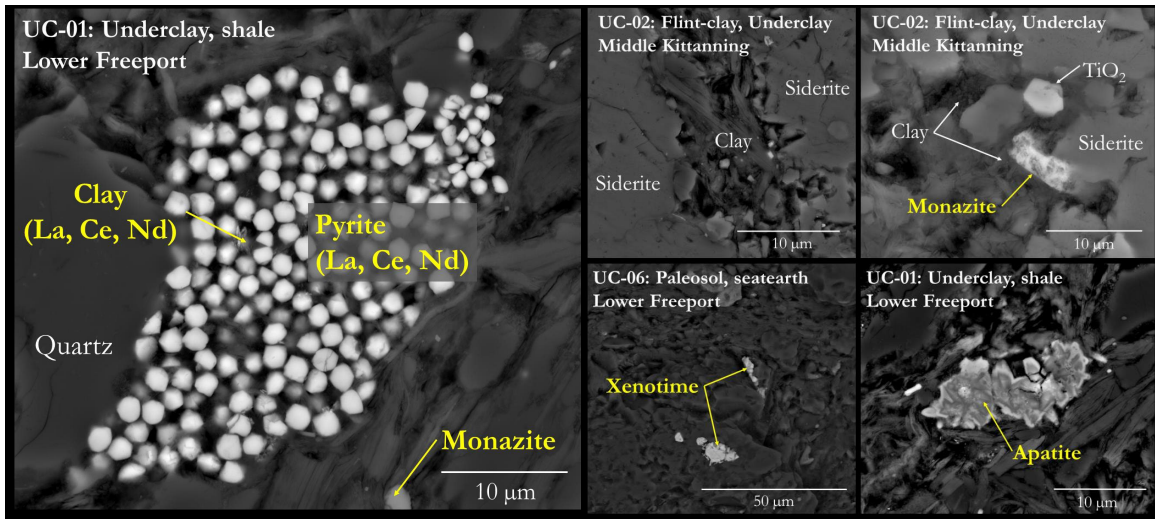


Figure 2.26. SEM-BSE images of underclay with REE-bearing minerals. Framboidal pyrite and clay with La, Ce, Nd (left). Pore-filling clay in siderite and examples of REE phosphate minerals identified (right) [134].

When a kaolinite sample was heated under nitrogen with a heating rate of 10°C/min the dihydroxylation of the sample occurred at 519°C with a weight loss of about 12%. A secondary phase transformation was observed at 991°C where metakaolin was converted to pseudo-mullite (Figure 2.27) [142].

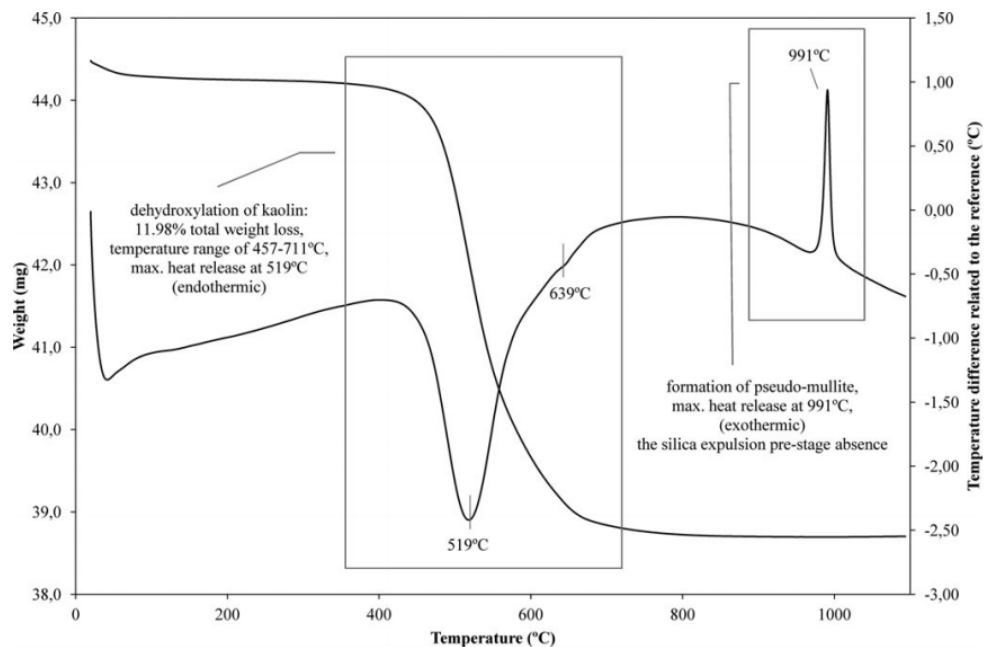
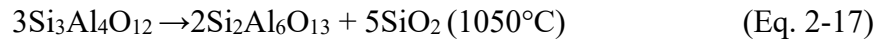
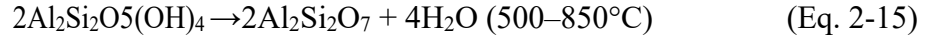


Figure 2.27. Thermal decomposition of the kaolin [142].

A study on a Nigerian kaolinite sample outlines the transformation of native kaolinite to amorphous metakaolin to the typical mullite/cristobalite (Eq. 2-15), (Eq. 2-16) & (Eq. 2-17). The study found the dihydroxylation temperature to be 528°C with a weight decrease of 14.4% [143]. The findings from BET surface area analysis on the native kaolinite sample and calcined products at 750°C and 1050°C suggested a decrease in surface area with an increase in temperature.



Sintering of kaolinite clays has been reported at a temperature range of 900-1050°C when heated in the air [144]. Upon heating the kaolinite transforms to an intermediate amorphous metakaolin phase which recrystallizes with shrinkage in volume. Wang et. al found that the solubility of kaolinite increases with leaching temperature and the leaching kinetics are time-dependent [145].

CHAPTER 3. MATERIALS AND METHODS

3.1 Introduction

The experimental findings presented in Chapters 4 through 6 have been produced using common materials, experimental apparatus, and procedures. This chapter will provide more in-depth details related to the materials and methods relative to the brief descriptions provided in each of the subsequent chapters.

3.2 Materials

3.2.1 Coal Refuse Samples

Based on previous studies, the majority of the REEs reported to the coarse refuse streams of coal preparation plants [5, 146]. As such, coarse refuse samples were collected as the feed for the study from processing plants treating West Kentucky No.13 (WK-13) (Illinois Basin) and Fire Clay (Central Appalachian Coal Basin) seam coals. The sources were identified in a previous U.S. Department of Energy project (DE-FE0027035) as containing over 300 ppm of total REEs on a dry, whole sample basis (Figure 3.1).



Figure 3.1. Locations of coal preparation plants in the U.S. where the coarse refuse samples were collected for the tests.

The WK-13 seam material is classified as bituminous coal and is primarily used as feed for coal-powered electric power plants. Before entering the coal preparation plant, the raw coal feed is crushed to a top particle size of 75 mm (3-inches) and screened to obtain a 75-mm x 16 mesh size fraction that is cleaned using 1220-mm (48-inch) diameter dense medium cyclones. The material finer than 16 mesh is classified to create a nominal 16 x 100 mesh size fraction that is treated using spiral concentrators. The material finer than 100 mesh material reports to the plant fine reject stream through the thickener underflow. A simplified flowsheet for the coal cleaning operation showing the sampling location is provided in Figure 3.2 (a). The 1800 tph preparation plant located in Webster County, Kentucky treats coal from room-and-pillar underground mining in the WK-13 coal seam. The seam is relatively thick which limits out-of-seam rock dilution by the operations of continuous miners. Therefore, the coarse refuse samples collected for the study predominantly originated from the parting material. This parting material has been reported to contain elevated concentrations of REEs (Table 3.1) [61].

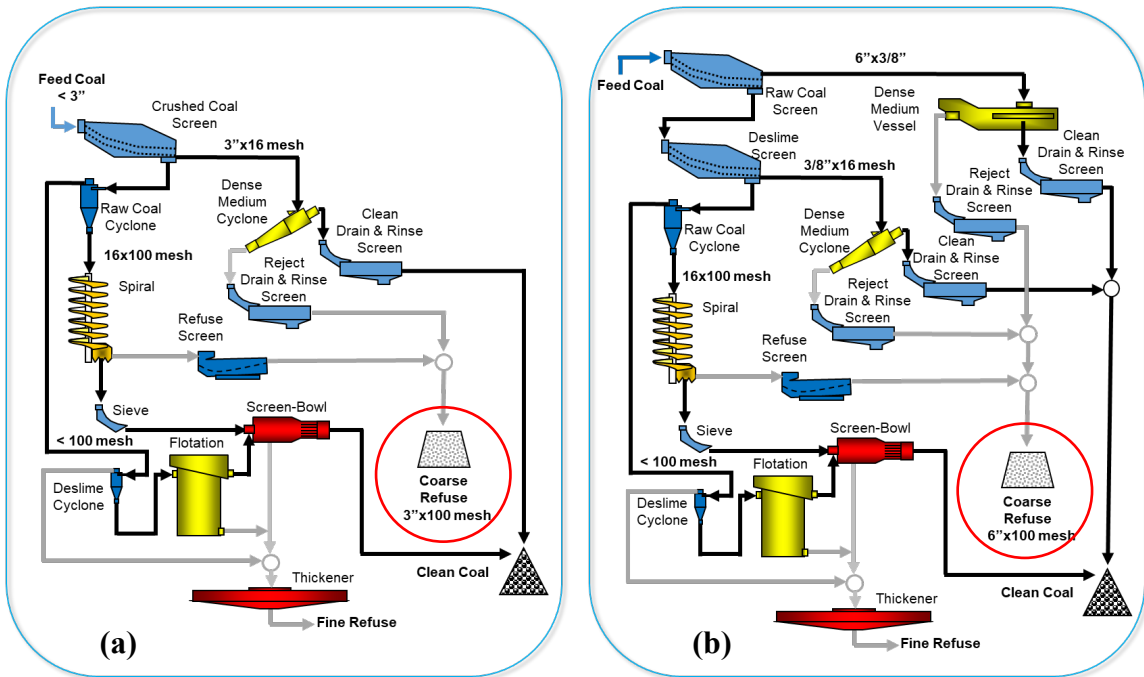


Figure 3.2. Sampling locations for the coal preparation sites. (a) West Kentucky No.13 and (b) Fire Clay.

Table 3.1. REE concentrations in each segment obtained from a core sample of the West Kentucky No.13 coal seam [61].

Description	Lithology	REE ash-basis (ppm)			REE whole mass -basis (ppm)			HREE/ LREE
		TREE	LREE	HREE	TREE	LREE	HREE	
Roof	Rock	259.5	218.2	41.3	239.1	201.0	38.1	0.19
Roof	Rock	277.6	237.1	40.5	256.5	219.0	37.4	0.17
Parting	Claystone	212.1	173.8	38.4	174.2	142.7	31.5	0.22
Parting	Claystone	1143.9	988.8	155.2	928.9	802.9	126.0	0.16
Parting	Claystone	362.7	317.5	45.2	322.1	282.0	40.1	0.14
Parting	Claystone	456.2	394.7	61.5	398.6	344.9	53.8	0.16
Parting	Claystone	334.5	287.5	47.1	265.0	227.7	37.3	0.16
Floor	Rock	389.8	286.2	103.6	334.7	245.8	89.0	0.36
Floor	Rock	161.2	135.9	25.2	143.3	120.9	22.4	0.19
	Composite	349.2	294.2	55.0	308.5	259.9	48.6	0.19

The Fire Clay coal seam is a high-quality bituminous coal source that is generally used as fuel for coke ovens, boilers, and pulverized coal combustion (PCC) units. The plant uses a dense medium vessel to clean 150-mm x 10-mm (6-inch x 3/8 inch) material, a dense medium cyclone to treat the 10-mm x 16 mesh fraction and spiral concentrators for the 16 x 100 mesh fraction. The size fraction finer than 100 mesh reports to the fine coal waste. A simplified flowsheet for the coal cleaning operation is provided in Figure 3.2 (b). The Leatherwood preparation plant is in Perry County, Kentucky operated by the Blue Diamond Division of Blackhawk Mining. The plant treats 1400 tph of run-of-mine coal from the Fire Clay coal seam also known as Hazard No. 4. This seam is well studied and documented to contain high concentrations of REE resulting from the deposition of volcanic ash during the coalification process. Channel samples of the host rock and bottom bench of the coal seam have been found to contain REEs greater than 400 ppm (Figure 3.3). The operations using a continuous miner produces significant amounts out of seam dilution due to the relatively low height of the coal seam. This REE enriched host rock is subsequently removed by dense media separation at the preparation plant and discarded primarily in the coarse reject stream.

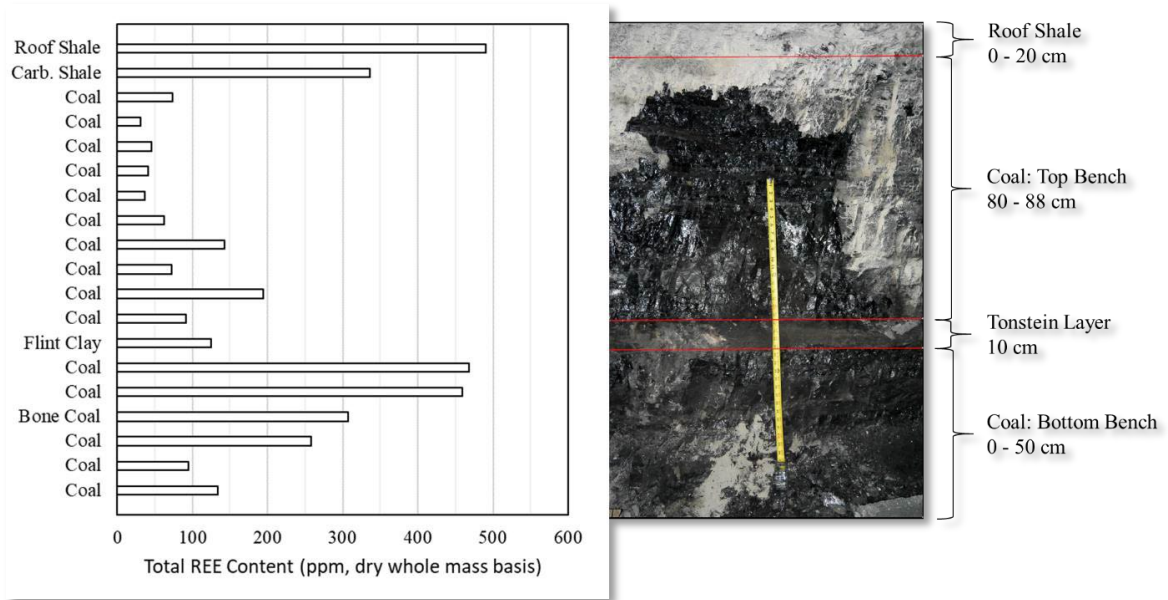


Figure 3.3. Cross-section of the Fire Clay coal seam and corresponding REE content on a dry, whole sample basis [61].

The coarse refuse belts were collected taken incrementally every 20 minutes using inline sweep belt samplers as depicted in Figure 3.4. The coarse refuse material was comprised of the rejects from the dense media separation units and spiral concentrators. The samples were collected over a three-hour operating period with 10 kg increments taken every 20 minutes with each sweep. Each sample increment was placed into 200-liter barrels and transported to coal labs at the University of Kentucky for further processing and use in the research program.

The samples were air-dried and subsequently, density fractionated at three specific gravity (SG) cut points, i.e., 1.60 SG, 1.80 SG, and 2.20 SG, which produced four density fractions (i.e., 1.60 SG float, 1.60x1.80 SG, 1.80x2.20 SG, and 2.20 SG sink). A schematic of the sample preparation is shown in Figure 3.5. The samples of different density fractions come from different segments of the coal seam. The heaviest density fraction primarily represents roof and floor material, while the lightest density fraction (1.60 SG float) is likely derived from interlayers between the coal segments. Therefore, the mineralogy of REEs in these density fractions may be distinctly different.



Figure 3.4. A sweep-belt sampler used to collect representative samples from the coarse refuse process stream of a coal preparation plant.

A lab-scale float-sink system using ultrafine magnetite was utilized to create the heavy medium to avoid chemistry changes that may occur if organic liquids or salt solutions were used as the medium. Fine magnetite was mixed with tap water to obtain the targeted medium density. To maintain suspension of the magnetite, air was injected into the slurry thereby creating the required agitation. Coarse reject material was placed into the heavy medium and float material was collected using a strainer. After density fractionation, all density fractions were wet screened to remove the magnetite. The final products were air-dried instead of mechanical oven drying to minimize oxidization. The dry solids in each density fraction were crushed using a laboratory jaw crusher followed by a hammer mill and subsequently pulverized to achieve a top particle size of 180 μm (80

mesh) for use as feed for the test program. Particle size reduction after the float-sink tests and drying provided fresh particle surfaces for the calcination and leaching experiments.

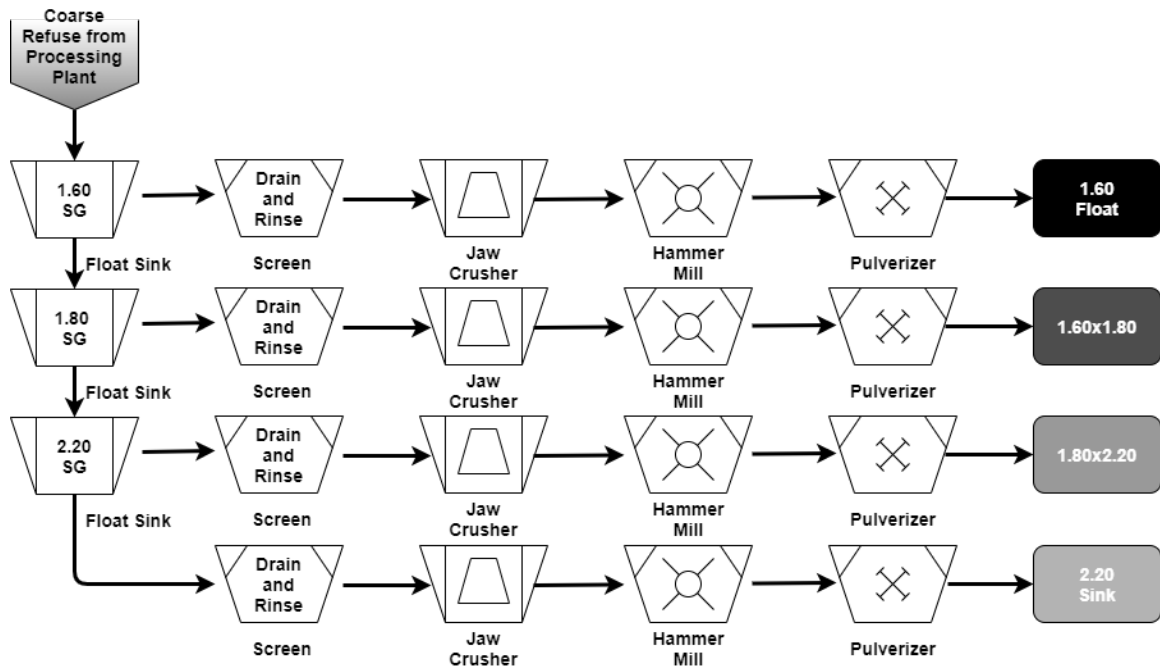


Figure 3.5. Schematic of the laboratory sample preparation process used on the West Kentucky No.13 and Fire Clay coarse refuse samples collected from the two processing plants.

Both coarse refuse samples were predominantly comprised of material heavier than 2.20 SG representing more than 70% of the total mass yield for both sources (Figure 3.6). The material lighter than 1.80 SG is generally referred to as middling or mixed-phase particles comprised of unliberated coal and rock. The mass yield of this material was about 9% for WK-13 and approximately 2% for the Fire Clay source. The low mass yield of the middling material (<1.80 SG) is indicative of the relative amounts in the raw coal feed in the plants, the high SG separations utilized in the plants, and the excellent cleaning efficiencies provided by the dense medium separation processes.

The trace concentrations of REEs in the coarse refuse samples were measured by ashing and digesting the samples in concentrated acid in preparation for elemental analysis in an inductively coupled, optical electron spectrometer (ICP-OES) following the ASTM D6357-11 method. For each batch of 50 samples, a standard solid sample supplied by the National Institute of Standards and Technology (NIST) of the U.S.

Department of Commerce was digested together with the precipitates. A more detailed description of the ICP-OES analysis and the data quality checks used in the investigation is provided in a later section of this chapter.

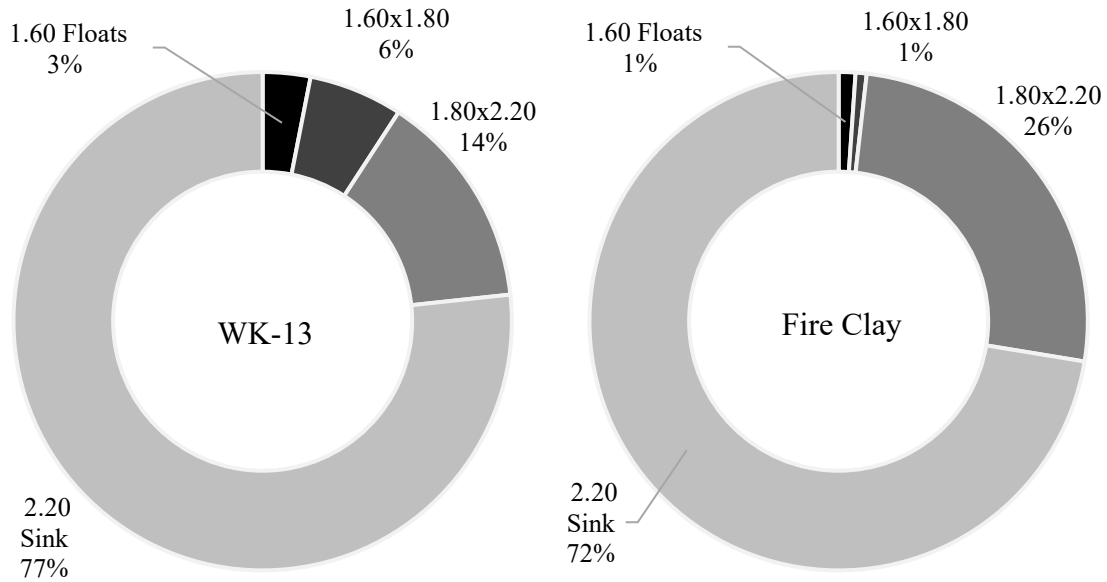


Figure 3.6. The weight percent distribution of the West Kentucky No.13 and Fire Clay coarse refuse samples in different density fractions.

The result from the investigation of REEs+Sc+Y present in the feed sources is provided in Table 3.2 and Table 3.3. REEs in the two samples contained critical elements such as Sc, Pr, Nd, Sm, and Y (~40%) that are vital components in permanent magnets and superconductors. The concentration of Sc was found to decrease with increasing specific gravity and both sources contained higher concentrations of LREEs than HREEs. Also, the abundance of elements with even atomic numbers in the analyses aligns with the Oddo-Harkins Rule (i.e., the abundance of elements with an even number of protons is higher than its neighbors with an odd number of protons). The trend of the total REEs follows the trend of distribution of LREEs in these samples. Figure 3.7 shows a comparison between the REE concentrations of the two composite samples. The Fire Clay composite sample has a total REE concentration higher than 300 ppm while the WK-13 composite sample falls slightly below 250 ppm on a dry, whole sample basis.

Table 3.2. The elemental concentration (ppm) of REEs+Sc+Y for the density fractionated samples of West Kentucky No.13 on a dry, ash basis.

Specific Gravity	Sc	La	Ce	Pr	Nd	Sm	Eu	Gd	LREEs
1.60 SG float	31.4	44.8	84.8	18.9	47.0	17.3	3.2	12.6	260.0
1.60x1.80 SG	25.6	49.8	97.8	18.0	51.0	16.4	2.7	11.6	272.9
1.80x2.20 SG	19.4	68.6	141.3	19.6	67.8	16.8	2.6	11.4	347.5
2.20 SG sink	17.2	52.1	106.8	16.7	53.9	15.4	2.1	10.2	274.3
Composite	18.4	54.0	110.5	17.2	55.5	15.7	2.3	10.5	284.1
Specific Gravity	Y	Tb	Dy	Ho	Er	Tm	Yb	Lu	HREEs
1.60 SG float	47.8	5.0	5.3	0.0	4.8	1.0	9.1	5.2	78.2
1.60x1.80 SG	39.0	3.4	4.4	0.0	4.5	0.9	7.1	4.1	63.3
1.80x2.20 SG	32.2	1.2	5.7	0.7	5.0	0.9	4.7	1.8	52.3
2.20 SG sink	26.8	1.6	3.1	0.0	4.1	0.6	4.4	2.7	43.4
Composite	29.0	1.8	3.6	0.1	4.3	0.7	4.8	2.7	46.9

Table 3.3. The elemental concentration (ppm) of REEs+Sc+Y for the density fractionated samples of Fire Clay on a dry, ash basis.

Specific Gravity	Sc	La	Ce	Pr	Nd	Sm	Eu	Gd	LREEs
1.60 SG float	30.0	138.6	313.0	35.9	136.5	28.7	4.4	24.1	711.3
1.60x1.80 SG	15.6	72.3	158.6	18.6	71.6	15.3	2.0	12.7	366.7
1.80x2.20 SG	13.1	59.8	130.8	15.7	60.5	13.0	1.5	10.5	304.9
2.20 SG sink	13.2	56.2	119.3	15.5	57.4	12.8	1.4	10.0	285.8
Composite	13.4	58.1	124.7	15.8	59.2	13.0	1.5	10.3	296.0
Specific Gravity	Y	Tb	Dy	Ho	Er	Tm	Yb	Lu	HREEs
1.60 SG float	64.0	0.6	19.2	3.8	8.4	2.3	6.7	0.8	105.7
1.60x1.80 SG	34.6	0.3	9.5	2.0	5.9	1.2	4.0	0.4	57.8
1.80x2.20 SG	28.5	0.3	7.5	1.6	4.9	0.9	3.4	0.4	47.6
2.20 SG sink	27.3	0.5	6.8	1.2	4.5	0.9	3.5	0.8	45.4
Composite	28.1	0.5	7.1	1.3	4.7	0.9	3.5	0.7	46.7

Elemental information regarding major, minor, and trace elements was studied using XRF (X-ray fluorescence) analysis. For the WK-13 density fractionated samples, oxides of Si, Al, and Fe contributed to more than 90% of the total ash (Table 3.4). Elements such as Ca, Mg, Na, K, Mn, P, Ti, Ba, and Sr were also present in trace amounts. On the other hand, the Fire Clay sample was predominantly composed of Si and Al. Fe and K were found in minor amounts while other elements were present in trace quantities.

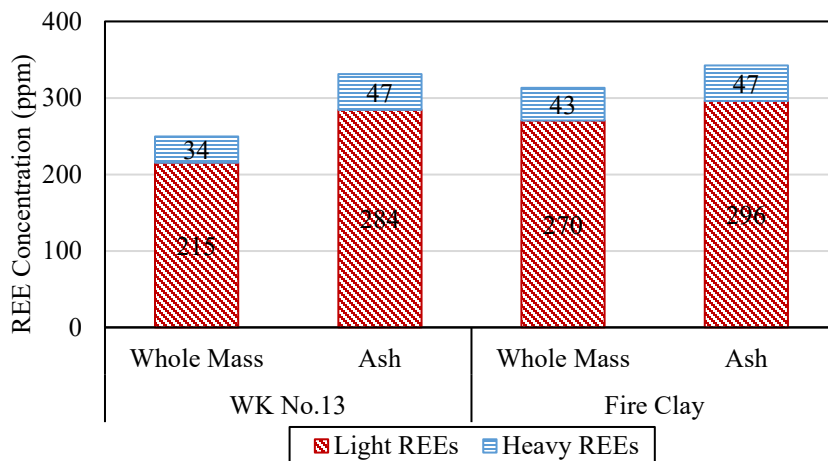


Figure 3.7. REE concentration for composite West Kentucky No.13 and Fire Clay coarse refuse samples on a dry, whole mass, and ash basis.

Table 3.4. XRF analysis of major and minor phases for the density fractions of the WK-13 and Fire Clay samples on an ash basis.

Specific Gravity	SiO ₂ (%)	Al ₂ O ₃ (%)	Fe ₂ O ₃ (%)	CaO (%)	MgO (%)	Na ₂ O (%)	K ₂ O (%)	MnO (%)	P ₂ O ₅ (%)	TiO ₂ (%)	BaO (%)	SrO (%)
West Kentucky No.13												
1.60 SG float	38.9	18.8	33.8	1.6	0.8	0.0	2.2	0.0	0.2	0.9	0.4	0.1
1.60x1.80 SG	42.0	20.6	27.3	2.0	1.0	0.0	2.5	0.0	0.2	0.9	0.3	0.1
1.80x2.20 SG	52.4	25.5	12.9	0.9	1.1	0.1	3.1	0.0	0.3	1.0	0.2	0.1
2.20 SG sink	53.3	22.9	18.3	1.0	1.3	0.5	3.3	0.1	0.3	0.9	0.1	0.1
Fire Clay												
1.60 SG float	59.9	26.9	4.0	0.6	1.0	0.2	2.8	0.0	0.4	1.5	0.1	0.1
1.60x1.80 SG	61.3	24.8	4.0	0.4	1.2	0.3	3.3	0.0	0.2	1.2	0.1	0.0
1.80x2.20 SG	66.0	25.8	4.4	0.4	1.4	0.5	3.6	0.0	0.1	1.0	0.1	0.0
2.20 SG sink	65.0	23.9	6.4	0.6	1.5	0.5	3.8	0.1	0.1	0.9	0.1	0.0

Proximate analyses were performed on the density fractionated samples using a thermogravimetric analyzer (TGA-701) manufactured by LECO Corporation (Figure 3.8). Multiple replicate tests were done over the project period and the average moisture, ash, and carbon content of the four density fractions were measured for both sources [147]. The proximate analysis results of the four density fractions are shown in Figure 3.9. The error bars on the ash and carbon content represent the standard deviation from the mean values. The samples were inherently dry and had low moisture content. The weighted average organic matter content decreased with increasing specific gravity.



Figure 3.8. LECO TGA-701 Thermogravimetric analyzer.

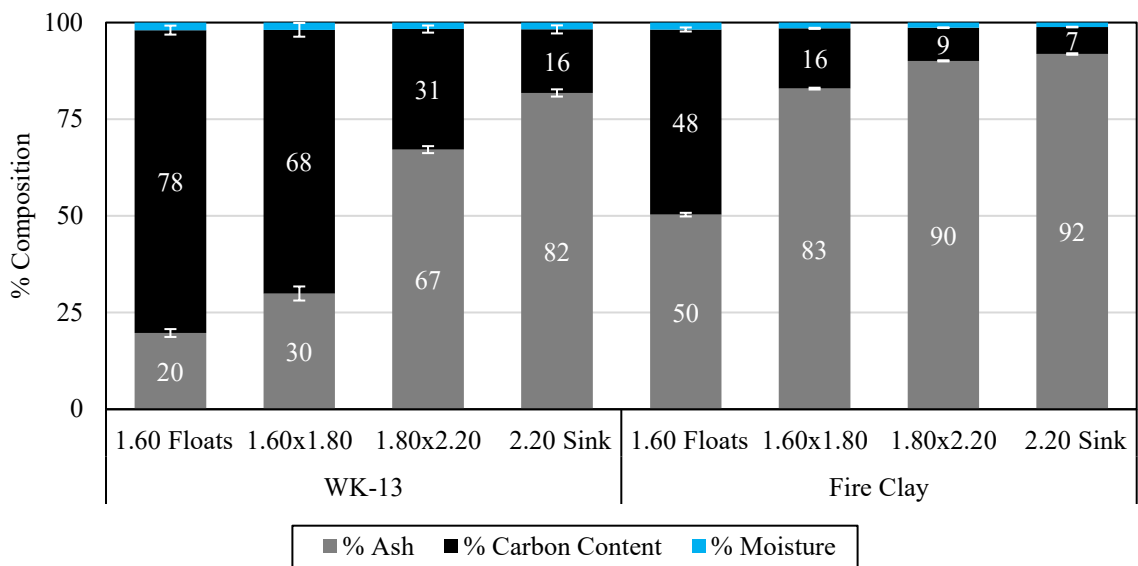


Figure 3.9. Proximate analysis of the density fractions of the West Kentucky No.13 and Fire Clay coarse refuse samples.

Total sulfur analysis of the density fractionated samples was performed using a LECO Sulfur Analyzer following the ASTM method D2492-02 [148]. The total concentration includes various forms of sulfur present in coal, i.e., pyritic, organic, sulfate as well as elemental. As shown in Figure 3.10, the density fractions of WK-13 samples have high sulfur content. The Fire Clay coarse refuse, on the other hand, had a very low concentration of sulfur. The difference in sulfur concentration of the two samples suggests

the difference in depositional environments when the two coals were formed. Generally, low-sulfur coal deposits develop in freshwater environments whereas high-sulfur deposits come from brackish swamps or marine-influenced environments. The heavy density 2.20 SG sink fraction of WK-13 has >10% sulfur content which may be due to the presence of pyrite in the sample. The typical specific gravity of natural pyrite ranges from 4.80 – 5.10. As such, free or mixed-phase particles with high pyrite concentration typically report to the heaviest density fraction after a float-sink separation.

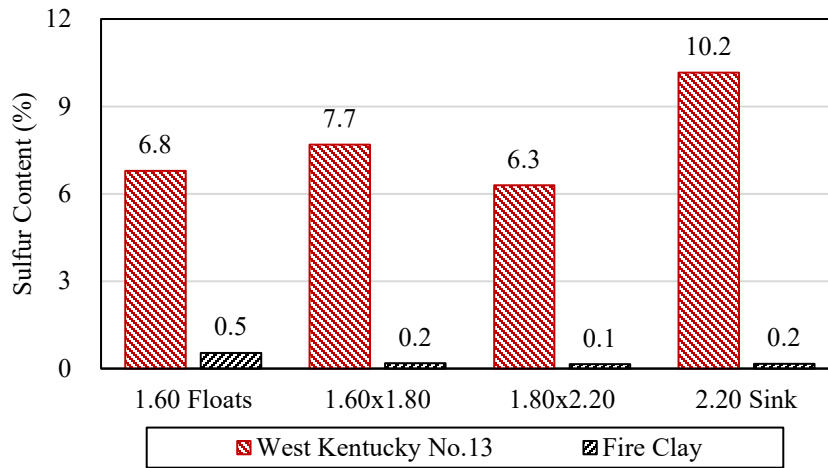


Figure 3.10. Total sulfur concentrations on a dry basis in the density fractions of the two coarse refuse sources.

3.2.2 Chemicals

Trace metal grade sulfuric acid and American Chemical Society (ACS) grade ammonium sulfate salt for acid and salt leaching tests, respectively, were used as lixivants for leaching tests. No chemical additives were used in the calcination tests. The molarity of the acid solutions was modified using deionized water with a resistivity of 18.2 MΩ·cm at 25°C as per the ASTM D1193-06 standard [149]. High purity pure mineral specimens of pyrite, kaolinite, Illite, calcite, and quartz were used for TGA-DSC analysis. The details of all the chemicals and mineral samples used in the study are provided in Table 3.5.

Table 3.5. Details of the chemicals and minerals used in the current study.

Name	Formula	Molar Weight (gm)	Purity Grade	Source
Chemicals				
Sulfuric acid	H ₂ SO ₄	98.08	> 99.9%	Fisher Sci
Hydrochloric acid	HCl	36.46	> 99.9%	Fisher Sci
Nitric acid	HNO ₃	63.01	> 99.9%	Fisher Sci
Ammonium Sulfate	(NH ₄) ₂ SO ₄	132.14	> 99.9%	Fisher Sci
Mineral Specimens				
Kaolinite	Al ₂ Si ₂ O ₇ .2H ₂ O	258.16	>99.9%	Fisher Sci
Pyrite	FeS ₂	119.98	> 99.9%	Fisher Sci
Quartz	SiO ₂	60.08	> 99.9%	Fisher Sci
Illite Shale	(K, H) Al ₂ (Si, Al) ₄ O ₁₀ (OH) ₂ - xH ₂ O	-	> 85.0%	Ward's Science
Calcite	CaCO ₃	100.09	>99.99	Fisher Sci

3.3 Experimental Apparatus and Procedures

3.3.1 Low-Temperature Plasma

The benchtop low-temperature plasma (LTP) system used for the study was model number PE-100 RIE manufactured by Plasma Etch Inc., Carson City Nevada. The instrument incorporates a 305H x305W x305D mm³ (12 H x 12 W x 12 D in³) aluminum vacuum chamber resistant to plasma etching. The chamber houses a 230W x 230D mm² (9 W x 9 D in²) reactive ion etching (RIE) electrode that creates a potential difference that ionizes the gases inside the chamber to create plasma. Uniform plasma is generated through a 0-600W 13.56 MHz direct contact radio frequency (RF) power supply with a variable power setting. The vacuum controller sets the vacuum conditions inside the aluminum chamber by a 2-stage direct drive oil pump with an oil mist filter. The oxygen gas flow controller and water-cooling temperature controller provide adjustments and control to the gas flow rate and the temperature of the base electrode plate, respectively. The setup of the equipment is shown in Figure 3.11. The entire system is operated by Plasma Etch, Inc. software preloaded on a laptop for fully automatic system control, operation, process sequencing, and multiple recipe storage.

For the low-temperature plasma treatment, the samples were uniformly spread on a watch glass of 15 cm diameter and were treated for different treatment times.

Based on the results of parametric tests, the RF power was set at 450 watts and the O₂ flow rate was maintained at 40 cc/min. This set of input variables were selected sample was placed on the base plate and the oxygen flow was initiated after the chamber was pumped down to a vacuum of 0.3 torrs. The RF power generator starts after the O₂ flow has stabilized at the set point. The potential difference ionizes the oxygen present in the chamber and creates a highly oxidizing plasma. As a quality control measure, the chamber was cleaned with compressed air after every batch treatment. The temperature of the sample was monitored with an infrared temperature gun to ensure that the temperature inside the plasma chamber was less than 100°C.

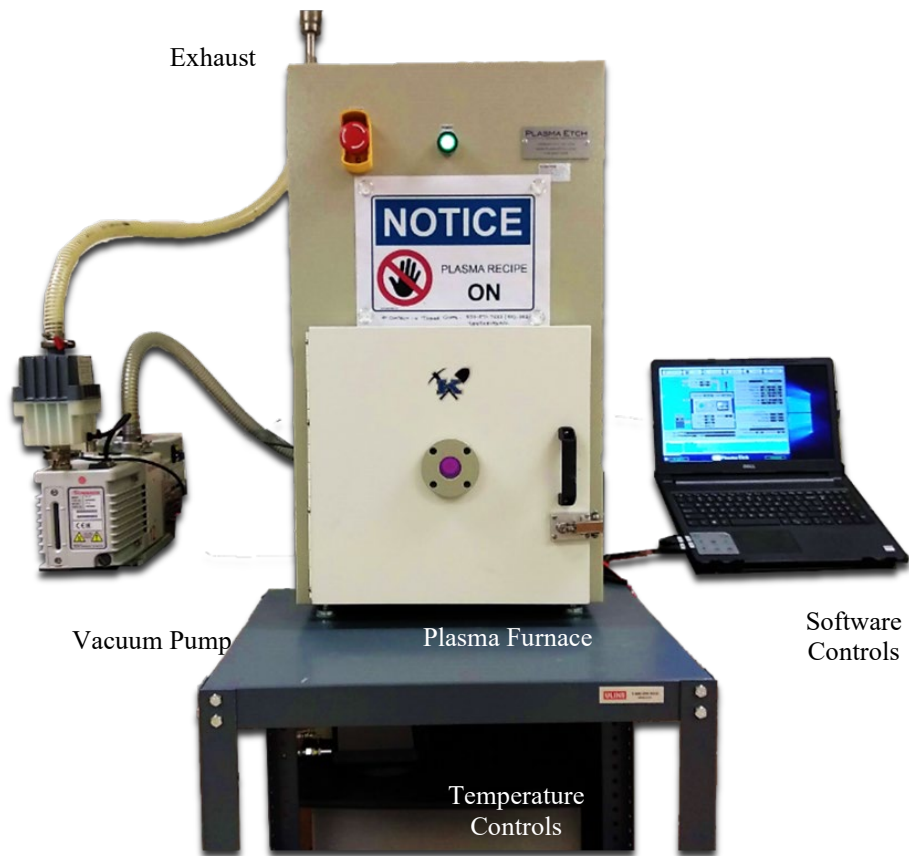


Figure 3.11. Setup of the PE-100 RIE low-temperature plasma unit at the University of Kentucky.

3.3.2 Calcination Tests

Calcination tests were carried out in a lab-scale Thermolyne F6020C-80 muffle furnace (Figure 3.12) manufactured by Thermo Scientific, USA at different temperatures, hold times, and heating rates. A representative 30g sample was evenly distributed into six crucibles for every batch (5g/crucible). No chemical additives were added, and static atmospheric conditions were used. After completion of the test, the furnace was allowed to gradually cool to room temperature at which time the samples were removed from the furnace. The calcined products were placed in a desiccator to prevent moisture adsorption before being transferred into sample bags and sealed. The samples were weighed and subjected to REE analysis and acid leaching tests.



Figure 3.12. Benchtop muffle furnace used for calcination tests.

3.3.3 Leaching Tests

REEs associated with the different density fractions of a given coal source may have distinct leachabilities due to the variation in rare earth mineralogy resulting from diverse geochemical and physical activities. The leaching experimental apparatus as shown in Figure 3.13 comprised of a magnetic hot plate, water bath, three-neck round bottom flask, and a reflux condensing system. Tap water flowing through the jacket of the condenser maintained the ambient pressure inside the reactor by condensing the evaporated liquid.

Leaching tests were performed on the feed and thermally treated (oxidized and inert) density fractions of the WK-13 and Fire Clay samples to assess the effect of different lixiviants (deionized water, 0.1M ammonium sulfate solution, and 1.2M sulfuric acid) at 75°C and a solid concentration of 1% weight by volume (w/v) in the three-neck round bottom flasks while maintaining the stirring speed constant. For every test, 15 ml representative samples were extracted at 10, 30, 60, 180, and 300 min from the start of the leaching process to provide the data needed to quantify leaching kinetics. The pH and temperature values of the leachate samples were measured by an Orion™ Versa Star Pro™ pH meter from Thermo Scientific, which was capable of pH measurements in the range of -2.000 to 20.000 under operating temperatures between -0.5°C to 105°C. Weights of the samples were recorded, and the liquid samples were cooled to room temperature to stop the leaching process. The leachate was filtered using a 0.45 µm PVDF membrane filter after centrifuging for 10 min at 4000 rpm to separate the liquid from the solids. The leaching tests were stopped at 300 min and the residual slurry was filtered using a 5 µm pore size filter paper. The filtrates were cooled to room temperature and their volumes were recorded. The filter cakes were dried in an oven at 60°C for 12 hours and the solid residual dry weights were recorded.

Leaching recovery (R, %) is the amount of REEs present in the feed that was dissolved in the solution during the leaching process. Leaching recovery (R, %) was calculated using the following equation:

$$R (\%) = \frac{C_L * V_L}{C_L * V_L + C_S * m_S} \quad (\text{Eq. 3-1})$$

where C_s (µg/g) and C_L (µg/ml) represent REE concentrations in the solid residual and final leachate, respectively; m_s (g) is the weight of the leaching solid residual; and V_L (ml) the volume of the final leachate solution. The differences between the back-calculated REE contents and the values measured directly by ICP-OES were within ±5%, indicating minor experimental errors. It is noted that all REE contents associated with solid samples are based on a dry whole sample basis.

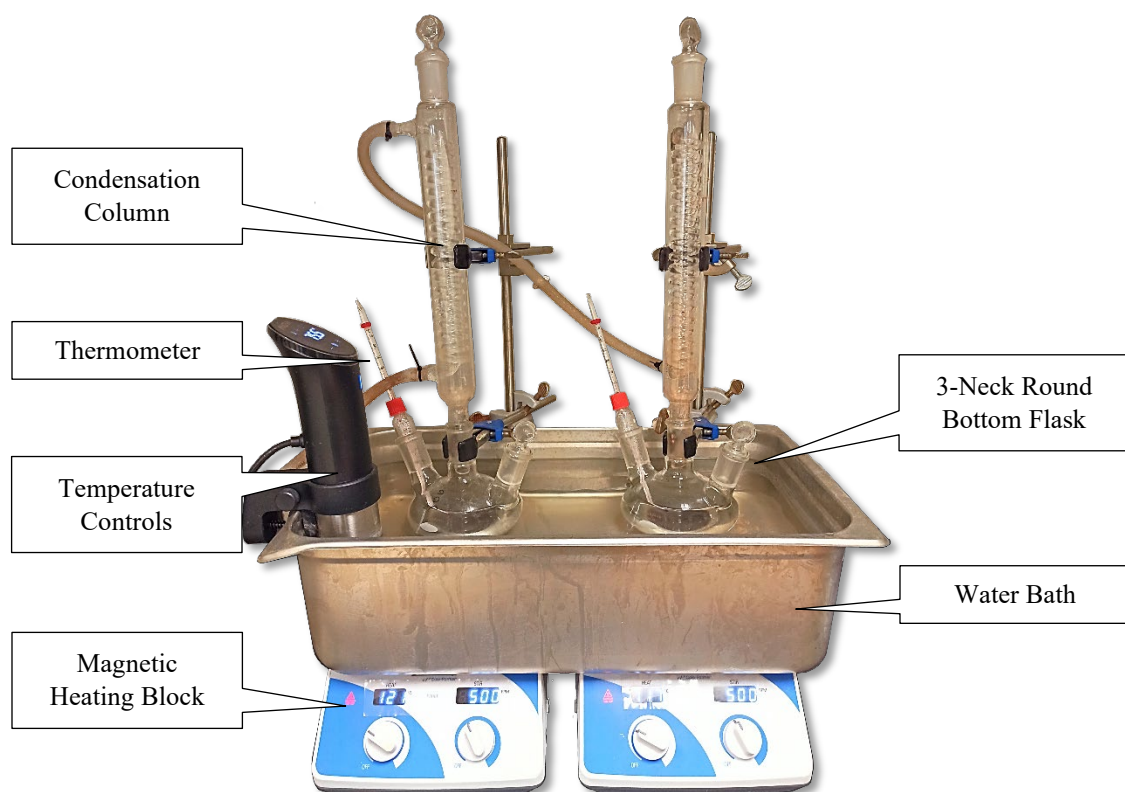


Figure 3.13. Apparatus for leaching tests with controlled temperature, stir speed, and condensation rates.

3.3.4 Magnetic Separation

Magnetic separation tests were performed on the calcined products of the 2.20 sink fraction of the WK-13 coal seam. A slurry of 10% w/v was introduced into the L-4-20 wet high-intensity magnetic separator (WHIMS) at various magnetic field strengths. The non-magnetic material in the feed slurry was passed through the metal matrix continuously and collected in a bucket. The magnetic material adhered to the matrix while the magnetic field was on. After all the feed was passed through the system, the magnetic field was turned off and the magnetic material was collected by washing with water (Figure 3.14). The magnetic and non-magnetic slurries were dewatered, air-dried, and subsequently split into subsamples for proximate and REE analysis. Magnetic separation tests were performed at 11500 gauss for the 2.20 SG sink fraction calcined that was pre-calcined at 400°C, 450°C, 500°C, and 600°C and mass yield values recorded.

Additional tests were carried out on the 2.20 SG sink material of WK-13 calcined at 400°C at magnetic field intensities ranging from 2500 to 11500 gauss.

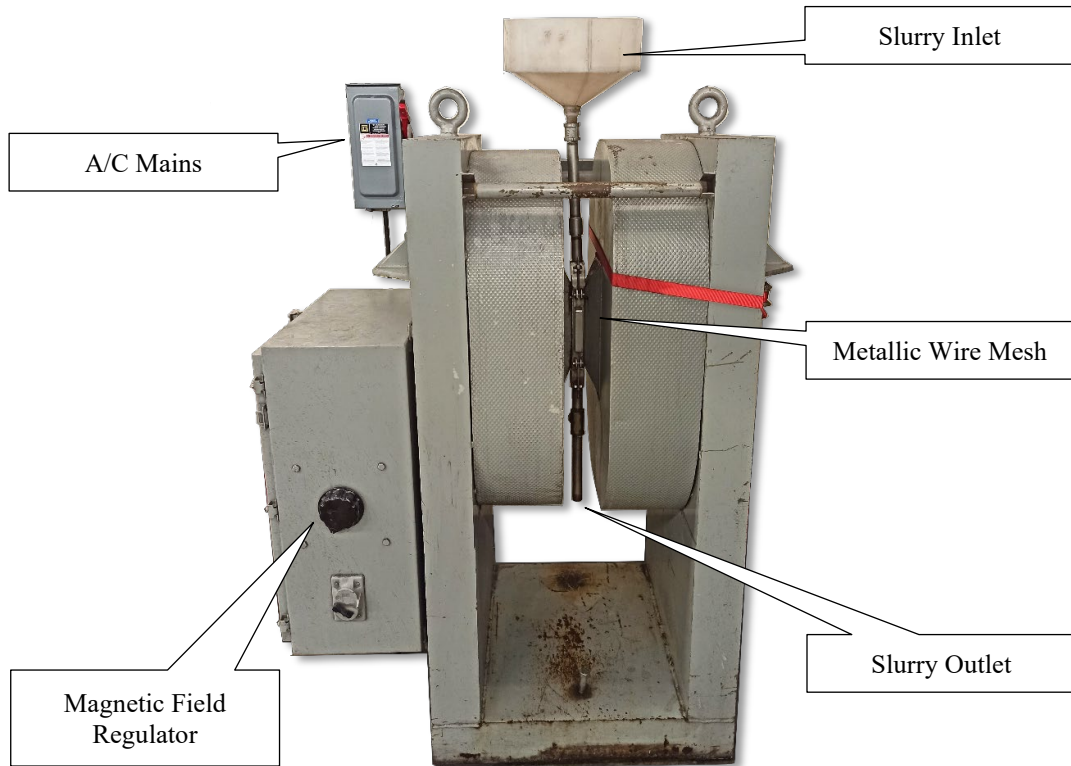


Figure 3.14. L-4-20 Eriez wet magnetic separator

3.4 Analytical Tools

3.4.1 XRD

X-ray diffraction (XRD) is a nondestructive analytical technique that is used to characterize the mineral composition of the density fractionated samples. A small amount of pulverized crystalline powder was packed in a sample holder and mounted on the AXS D8 DISCOVER Diffractometer, manufactured by Bruker, USA (Figure 3.15). Each scan was performed on 2θ values from 10° to 70° with a step size of 0.02° and a scan speed of $1^\circ/\text{min}$. The XRD spectrum was analyzed by EVA software to identify the major mineral phases and quantify their relative concentrations which were estimated based on mineral peak intensities. XRD analysis generally has a detection limit of $\sim 1\%$ by volume [150]. Therefore, no peaks above background noise will be detected in the diffraction pattern of a mineral present below this level.

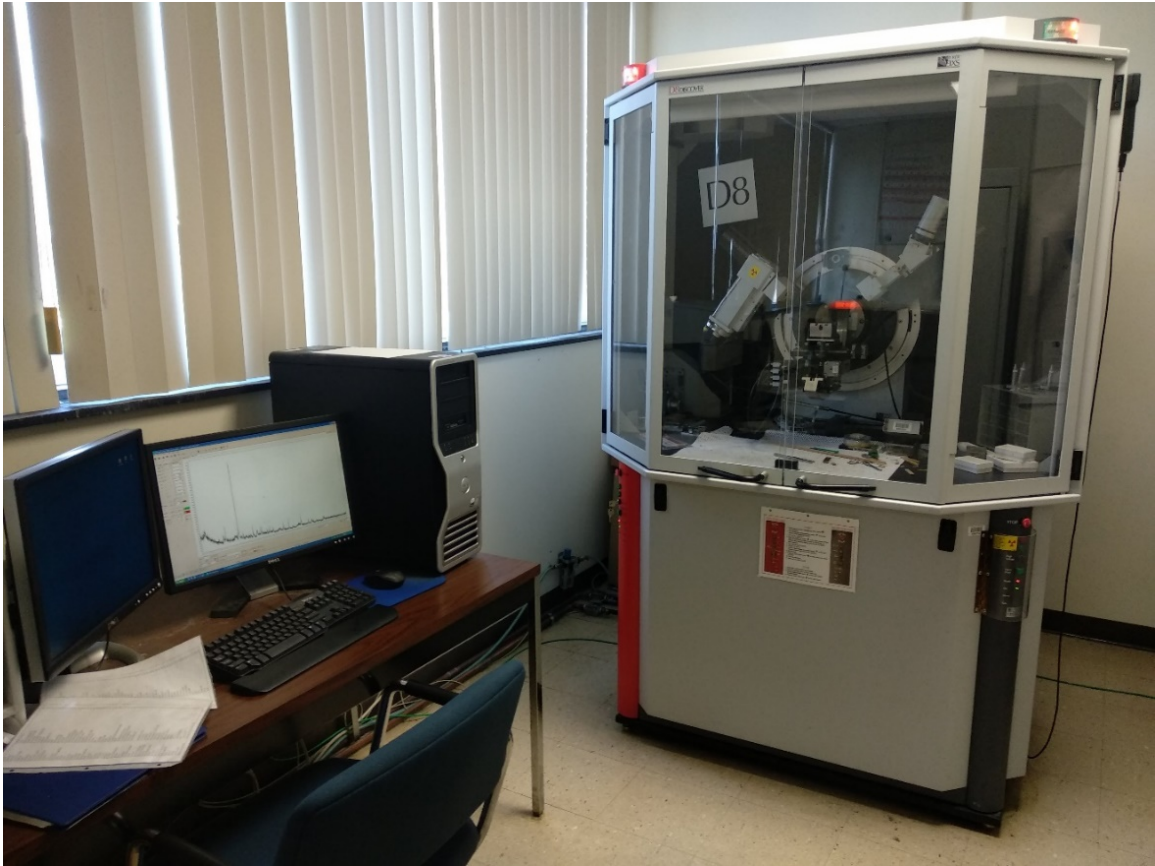


Figure 3.15. XRD instrument used for mineralogy analysis.

3.4.2 TGA-DSC

To evaluate the effect of calcination temperature, duration, and atmosphere on the leaching recoveries of REEs and critical elements, a Simultaneous Thermal Analyzer (STA) was installed at the University of Kentucky. The STA PT 1600 is a high-end simultaneous thermobalance from LINSEIS, Germany. The system offers unparalleled Thermogravimetric Analyzer (TGA) and Differential Scanning Calorimeter (DSC) resolution and can perform a multitude of thermal analyses under varying temperatures, environmental conditions, and gas mixtures.

Thermogravimetric analysis was performed for a temperature range of 25-1100°C at varying heating rates ranging from 1-15°C/min under oxidizing conditions (O_2 flow rate=100scc/min). Nitrogen was used as a purge gas. About 50 mg of sample was loaded into the sample crucible and placed into the STA chamber. A vacuum was pulled inside the chamber and was subsequently backfilled with inert gas before starting the

analysis. A closed-loop water chiller with an internal flow switch was connected to the furnace collar. The water vapor generator with heated coupling was installed which allowed for the use of wet gas into the furnace and provides control on the humidity inside the equipment (Figure 3.16). The gas mixer setup can be used to use any combination of gas concentrations and alter the chamber environment. The entire system was operated by software preloaded on a Think Centre windows 10 computer for fully automatic system control, operation, process sequencing, and data analysis. DSC analysis using the LINSEIS STA was also performed under oxidizing atmospheres on the pure mineral species commonly found in the WK-13 and Fire Clay deposits. This data was correlated with the changes observed for the different density fractions of the two coal sources to determine the phase transformations responsible for the change in REE recovery after calcination. An STA measures both, heat flow and weight change of a sample as a function of temperature and time under a controlled atmosphere and was used to understand the effect of calcination and calcination kinetics.

Systematic and random errors constitute the difference between a true value and an individual measurement. Systematic errors were rectified by carrying out a series of blank measurements. The results of the blank run were subtracted from the sample measurement to obtain the true measurement and relative mass loss. Three replicate tests were performed for each sample to account for the standard deviation in the data and the mean curve was generated to account for the variability in the sample.

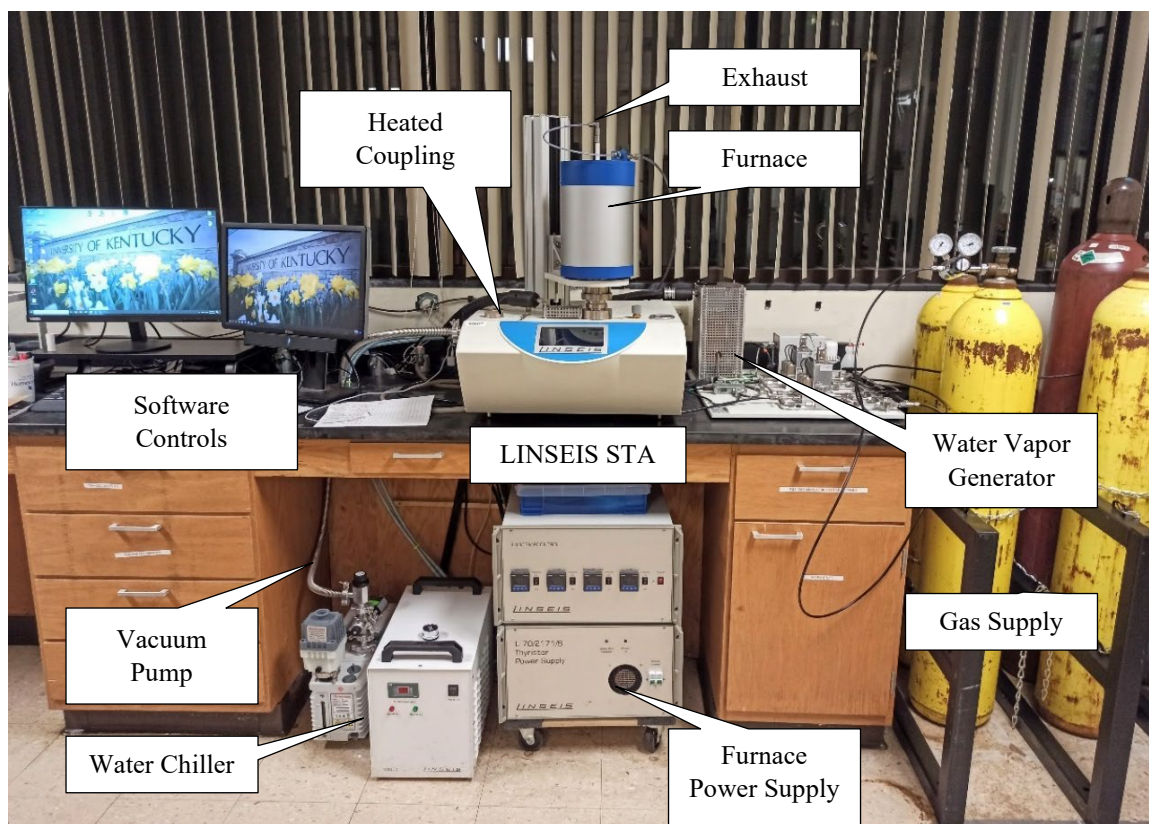


Figure 3.16. LINSEIS STA with water vaporizer with 5 sample gases and 1 balance purge service at the University of Kentucky.

3.4.3 ICP-OES

All aqueous samples from the leaching tests were directly analyzed by ICP-OES located at the Kentucky Geological Survey analytical laboratory. ICP-OES manufactured by Spectro Arcos (Figure 3.17) utilized a multi-element calibration standard VHGS-M68-1-100 manufactured by the LGC group for calibration. The concentration of all 17 REEs and major contaminant elements (aluminum, calcium, iron, etc.) typically present in the leachate generated from coal-based materials were analyzed. Additionally, the concentration of radioactive ions (uranium and thorium) was also analyzed to abide by the environmental and safety guidelines. The trace concentration of REEs in the solid samples was measured by ashing the samples and digesting them in concentrated acid for an ICP-OES analysis following the modified ASTM D6357-11 method [91]. The process involved ashing a 1 g representative sample at 500°C for 3 hours followed by digesting 100 mg of the ashed sample in 20 ml Aqua Regia (HCl: HNO₃ = 3:1 v/v). 20 ml of hydrofluoric acid was added to the tube and the solution was evaporated at 150°C. The

solid residue obtained post evaporation was dissolved in 10 ml nitric acid and 30 ml deionized water. After this process, the solids were completely digested. A sample was then analyzed by ICP-OES after making up the desired volume using DI water.



Figure 3.17. ICP-OES apparatus at Kentucky Geological Survey at used for elemental characterization of the aqueous phase.

The ICP-OES unit was calibrated using 0.0 ppm, 0.2 ppm, 1 ppm, and 10 ppm dilutions of the calibration standards. For elemental concentrations greater than the calibration range, the samples were diluted (10x and 100x) using 5% nitric acid to bring the concentration of the metals within the regression range. The calibration was verified by running two check standards that were sourced independently after every 20th sample to ensure that there was no inherent variability in the calibration. Three measurements were made for each sample for replication. The standard deviation associated with the analyzed elements was less than 0.05 ppm on a whole sample basis. The details of the standard deviation of individual elements are provided in Table 3.6.

Table 3.6. The standard deviation for the measurement of rare earth elements and the contaminants using ICP-OES [61].

Element	Standard Deviation (ppm)	Element	Standard Deviation (ppm)
Sc	0.0164	Tb	0.0135
Y	0.013	Dy	0.0108
La	0.0208	Ho	0.024
Ce	0.0117	Er	0.0126
Pr	0.0193	Tm	0.0237
Nd	0.0191	Yb	0.0174
Sm	0.017	Fe	0.0325
Eu	0.051	Al	0.0115
Gd	0.01765	Ca	0.0185

3.4.4 BET Analysis

Brunauer–Emmett–Teller (BET) measures surface area based on gas adsorption [151]. The BET surface area and pore volume analysis were performed by a technician at the Center for Applied Energy Research (CAER) associated with the University of Kentucky. A model 3 Flex manufactured by Micromeritics; USA was used for the analysis (Figure 3.18). A 100 mg representative dry solid sample was precisely weighed, sealed, and degassed using a vacuum while avoiding irreversible changes to the surface. The sample and reference tubes were evacuated, and a dead volume analysis was performed using an inert gas. The inert gas is used to correct the quantity of the adsorbate adsorbed and is removed by vacuum. The sample was then subjected to a slow flow of nitrogen for adsorption onto the particle surfaces. The pressure continues to fall until the adsorbate and the adsorptive are in equilibrium. The amount of adsorbate at equilibrium pressure is the difference between the amount of gas injected and the amount of adsorptive remaining in the gas phase. Pressure, temperatures, and dead volume of the system are required for the calculations. In the desorption step, a vacuum was applied to give the desorption isotherm. A simplified step process of the analysis is provided in Figure 3.19. The amount of nitrogen adsorbed and desorbed at the sample surface was plotted as a curve which was used to calculate the surface area and pore volume. The surface area of each sample was calculated using the BET method where the total volume was equal to the volume of nitrogen at a specific P/P_0 . P/P_0 is the ratio of partial pressure of the adsorbed substance to the saturated vapor pressure of the adsorbed gas. The determination of

specific surface area requires at least 3 measurements of adsorbed gas quantity each at different values of P/P_0 . The Barrett-Joyner-Halenda (BJH) method was utilized to calculate the pore size distribution using the adsorption and desorption isotherms. The BJH method assumes that pores have a cylindrical shape and liquid nitrogen condenses in the capillaries within the pores.



Figure 3.18. Instrumentation used for surface area and pore volume analyses.

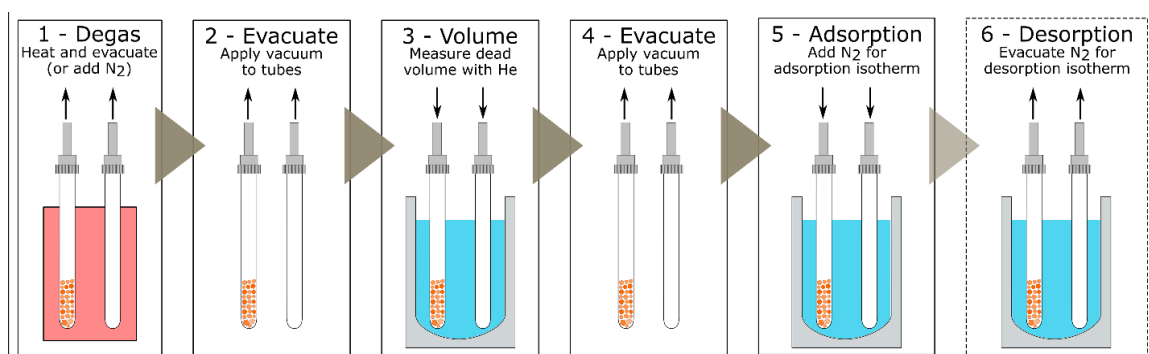


Figure 3.19. Simplified process steps of a BET analysis [152].

3.4.5 Scanning Electron Microscope (SEM)

The LTP and calcined products of the two coal sources were subjected to SEM analysis to examine the surface texture, particle topography, and mineralogical composition using an FEI Quanta 250 Scanning Electron Microscope (Figure 3.20) at the Electron Microscopy Center of the University of Kentucky. The samples were mounted on a sample holder using an electrically conductive double-sided carbon tape. Non conducting samples such as coal combustion products were coated with gold to a thickness of 7 nm to reduce beam penetration and allow for a sharper image. The elemental composition of the sample was determined by capturing the backscattered electrons and X-rays using a retractable energy-dispersive X-ray (EDX) Detector.

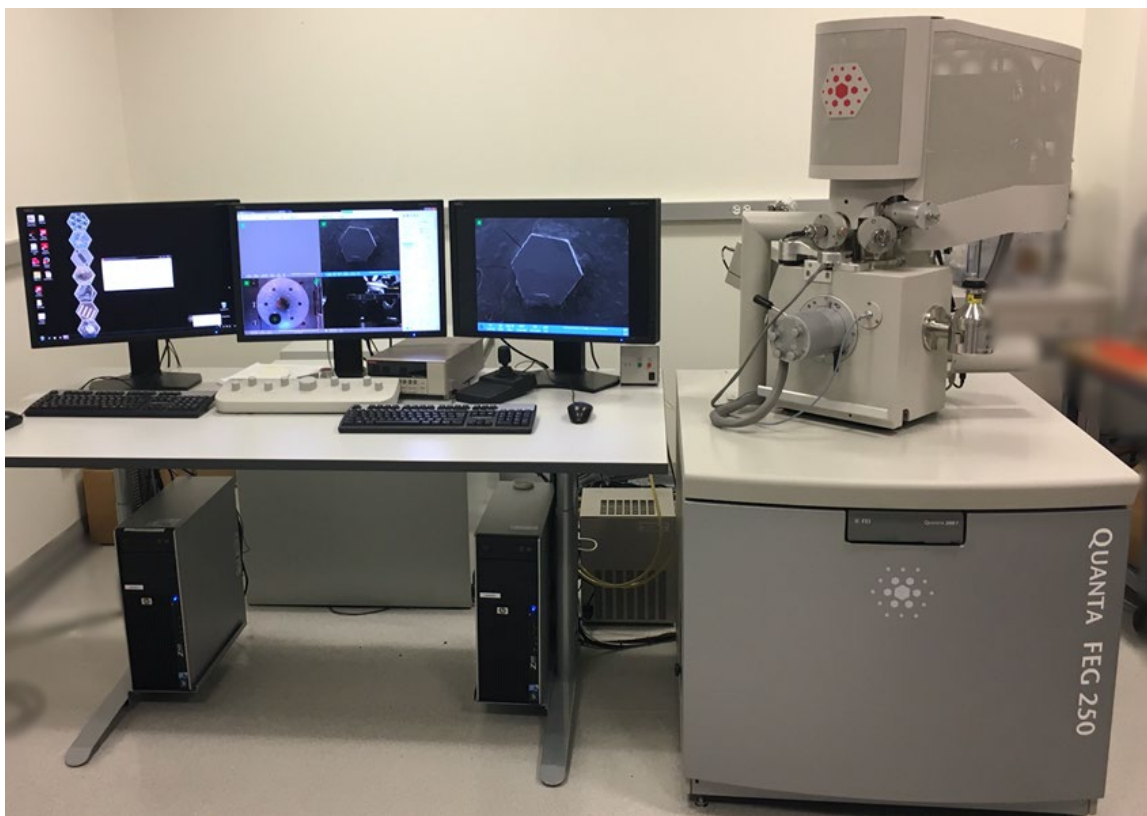


Figure 3.20. The FEI Quanta 250 used for SEM analysis.

CHAPTER 4. LOW-TEMPERATURE PLASMA

4.1 Introduction

The lanthanide elements of the periodic table, lanthanum (La) to lutetium (Lu) along with scandium (Sc) and yttrium (Y) are collectively called the REEs [20]. REEs are used in the manufacture of common consumer goods as well as are used in state-of-the-art applications. The dependence on these critical elements is primarily due to their unique magnetic, optic, and catalytic properties and due to the unavailability of a suitable substitute in select applications [30]. The REEs are mostly classified based on their atomic number as ‘light rare earth elements’ (LREEs) and ‘heavy rare earth elements’ (HREEs). The elements lanthanum to gadolinium are collectively called LREEs (atomic number 57 to 64). Yttrium is classified as an HREE as it exhibits chemical and physical associations with HREEs. Thus the HREEs are yttrium and elements terbium to lutetium (atomic number 39 & 65 to 71) [22, 26]. Scandium is categorized as an LREEs due to its low atomic number [4, 27].

With an impetus to produce REEs indigenously and alleviate the dependence on global imports, many countries are actively investing in technologies to extract REEs from alternate sources such as coal and its by-products. REEs have been found in low and high-rank coals, parting material, roof, and floor host rock, preparation plant rejects, thickener underflow, and acid mine drainage in concentrations up to a few tenths of a percentage point [3, 4]. REEs in coal has been identified to be present as carbonates and phosphate minerals, as well as in ion-absorbed and organic compounds [12, 21-24]. Investigations have been focused primarily on coal by-products and acid mine drainage that can eliminate mining costs to offset the high grinding and liberation costs of the finely dispersed REEs. Exploiting the difference in magnetic, electrostatic, and physiochemical characteristics of REE-bearing minerals by physical extraction methods has been investigated and found to be minimally effective in most cases [1, 15-22]. Alternatively, findings from a significant number of studies conducted on the recovery and concentration of REEs from coal-based feedstocks advocate the feasibility of hydrometallurgical extraction over physical separation methods [6-9, 11, 13, 78, 79].

However, despite satisfactory recovery values, the chemical cost associated with the use of strong leaching conditions is prohibitively high for commercial extraction of REEs from coal-derived feedstocks provided the generally low grades [8, 13].

Given the low concentrations of REEs in the feed coupled with the different modes of occurrences and low recoveries from subsequent extraction/separation processes, maximizing REE recovery at every unit operation is vital to minimize production costs. Oxidation pretreatment is very effective in transforming conventional REE-bearing minerals into more leachable forms thus increasing REE recovery, improving leaching kinetics, and enabling the use of milder leaching conditions [10, 18]. Roasting with chemical additives at high temperatures (500-800°C) has been found to convert the conventional REE minerals into more leachable REE oxides, fluorides, or sulfates [7, 19, 20]. However, for REEs contained in coal, the combustion at high temperatures (>800°C) has been found to create a vitrified glassy ash particulate that has poor leaching characteristics even under extreme leaching conditions [153]. Thus, the principal objective of the study is to investigate the effect of the Low-Temperature Plasma (LTP) oxidation process on the recovery of REEs, from coal byproducts in a hydrometallurgical processing circuit. The potential of value addition is by liberating, oxidizing, or activating the REEs embedded in the different density fractions of the coal. A low-temperature oxygen plasma utilizes oxygen to produce plasma for the oxidation of organic matter present in coal into its basic combustion products CO₂ and H₂O [102]. LTP oxidizes the sample at a lower temperature (<100°C) as compared to conventional calcination. This process serves to ash the coal sample, liberating and concentrating the mineral matter associated with the coal as the organic material is oxidized. A systematic study of understanding the benefits of LTP pretreatment as a potential pretreatment unit operation has not been performed for the REEs contained in coal [97, 98]. The hypothesis is that by implementing the plasma treatment, the surface property and pore structure of a coal particle can be altered. The open surface area is projected to increase which will provide enhanced REE liberation from the coal organic matrix and an improved diffusion rate of lixiviate to the particle core when exposed to subsequent leaching treatment.

Plasma treatment has been applied to surface modification and deposition, surface activation, material syntheses, waste decomposition, refining, extractive metallurgy, pyrometallurgy, etc. [97-106]. The LTP ashing technique has been widely incorporated with analytical procedures as an ashing method to determine mineral matter content and mineralogy structure in coal and coal byproducts [109, 112]. Allen et al. investigated the microstructure change of coal [114]. It was found that the microstructure of the low-temperature ash was strongly influenced by the mineral matter which was originally chemically bound in the organic matrix of the coal. Miller et al. reported that the gas phase in the LTP equipment is stagnant and thus samples need to be withdrawn from the chamber periodically and stirred to expose fresh surfaces [111, 115]. Gleit and Holland reported that the oxidation rate is a function of the exposed surface and decreases as the surface becomes covered with a mineral residue. Additionally, the intensity of the intense blue glow of the oxygen plasma is a good visual representation of oxidizing power [107]. LTP technology has been commercially utilized for surface treatment for chemical stability and the growth of vertical graphene for enhancing the strength of carbon fibers [154-157]

4.2 Materials and Methods

4.2.1 Materials

Previous studies have found that the majority of REEs associated with run-of-mine coal processed in a coal preparation plant reports to the refuse streams (REF) [5]. As such, two barrels of refuse samples were collected using belt sweep samplers at processing plants treating WK-13 and Fire Clay coal seam material. The samples were air-dried and subsequently, density fractionated at three specific gravity (SG) cut-points, i.e., 1.60 SG, 1.80 SG, and 2.20 SG prepared using ultrafine-magnetite, which produced four density fractions (i.e., 1.60 SG float, 1.60 x 1.80 SG, 1.80 x 2.20 SG, and 2.20 SG sink). After density separation, both the float and sink products were wet screened to remove the magnetite and air-dried instead of mechanical oven drying to minimize oxidization. Finally, the density fractionated samples were pulverized to 180 μm using a laboratory jaw crusher and hammer mill. The trace metal grade sulfuric acid and American Chemical

Society (ACS) grade ammonium sulfate salt for acid and salt leaching tests respectively were purchased from Fisher Scientific, USA

Given that the samples originated from the coarse waste streams of coal preparation plants, the abundance of the material existing in the high-ash 2.20 SG sink fraction was expected with more than 70% of the total mass yield for both sources. Significant differences in ash contents were found in the density fractions of the two samples (Table 4.1). The variability in the sulfur concentration of the two samples suggests a difference in depositional environments when the two coals were formed. The 2.20 SG sink fraction of the WK-13 source had greater than 10% total sulfur primarily due to the visible presents of pyrite (specific gravity=4.95) which reports primarily to the heavier density fractions in the density fractionation test.

Table 4.1. Proximate analysis of the density fractions of the West Kentucky No.13 and Fire Clay refuse.

Sample SG	% Moisture	% Ash	% Carbon Content	% Sulfur
West Kentucky No.13				
1.60 SG float	2.0	19.7	78.3	6.8
1.60x1.80 SG	1.9	29.9	68.2	7.7
1.80x2.20 SG	1.7	67.1	31.2	6.3
2.20 SG sink	1.8	81.8	16.4	10.2
Composite	1.8	74.6	23.6	8.9
Fire Clay				
1.60 SG float	1.8	50.3	47.9	0.5
1.60x1.80 SG	1.5	82.9	15.6	0.2
1.80x2.20 SG	1.3	90.1	8.6	0.1
2.20 SG sink	1.2	91.9	7.0	0.2
Composite	1.2	90.9	7.9	0.2

4.2.2 Methods

4.2.2.1 Sample Characterization

A summary of sample characterization methods used in the study is provided in Table 4.2. Proximate analyses (ASTM D3172) were performed on representative samples of each density fraction and their corresponding oxidation products using a thermogravimetric analyzer (TGA-701) manufactured by LECO Corporation. Total sulfur content (ASTM D4239) was quantified using a LECO SC-430 sulfur analyzer.

The total sulfur concentration included various forms of sulfur present in coal such as pyritic, organic, sulfate as well as elemental. X-ray diffraction (XRD) analysis was performed on the density-fractionated samples to characterize the mineralogy as a function of specific gravity using an AXS D8 DISCOVER Diffractometer. XRD provided mineralogical information that included components that represented greater than 1-2% volume of the total sample. As such, elemental information regarding major and minor elements was obtained using an AXS S4 Pioneer wXRF (X-ray fluorescence) analyzer. The REE concentrations in each fraction of the refuse samples were measured by ashing the samples and digesting them in concentrated acid for an ICP-OES analysis following the modified ASTM D6357-11 method as discussed by Zhang and Honaker, 2020 [91]. An SEM-EDX study of the plasma-treated density fractions of both the coal sources was conducted to evaluate the modifications of sample properties by oxidation pretreatment using an FEI Quanta 250 scanning electron microscope. The findings of the SEM image analysis were corroborated with the BET surface area and pore volume analysis.

Table 4.2. Summary of the analytical techniques used.

Analytical Facility	Facility Model and Origin	Purpose
BET Surface Area Analyzer	3-Flex, Micrometrics, USA	surface area and pore volume analysis
ICP-OES	Arcos ICP OES, Spectro, Germany	determining elemental content
Low-Temperature Plasma	PE 100-RIE, Plasma Etch Inc., USA	low-temperature plasma oxidation
Muffle Furnace	Thermolyne F6020C-80 Thermo Scientific, USA	high-temperature calcination
Scanning Electron Microscope	FEI Quanta 250, Thermo Scientific, Quanta USA	phase transformation and decomposition process
Sulfur Analyzer	SC-430, LECO Corporation USA	sulfur content
Thermogravimetric Analyzer	TGA-701, LECO Corporation USA	composition of coal, proximate analysis
X-ray Fluorescence	AXS S4 Pioneer wXRF, Bruker, USA	chemical composition
X-ray powder diffraction	AXS D8 DISCOVER Diffractometer, Bruker, USA	phase transformation and decomposition process

4.2.2.2 *Low-Temperature Plasma Tests*

The benchtop LTP system used for the study was model number PE-100 RIE manufactured by Plasma Etch Inc., Carson City Nevada. The instrument incorporates a 30-cm H x 30-cm W x 30-cm D aluminum vacuum chamber resistant to plasma etching. The chamber houses a 23-cm W x 23-cm D reactive-ion etching (RIE) electrode that

creates potential difference which ionizes the gases inside the chamber to create plasma. Uniform plasma is generated through a 0-600W 13.56 MHz direct contact radio frequency (RF) power supply with a variable power setting. The vacuum controller manipulates the vacuum conditions inside the aluminum chamber by a 2-stage direct drive oil pump with an oil mist filter. The oxygen gas flow controller and water-cooling temperature controller provide adjustments and control to the gas flow rate and the temperature of the base electrode plate, respectively. The operating system is Plasma Etch, Inc. software which provides automatic system control, operation, and process sequence storage.

Regarding the experimental program, a two-factorial parametric experimental test program was initially deployed to identify the significant operational factors (temperature, RF power, oxygen flow rate, treatment time) that were specific to the plasma treatment process. REE recovery using the standard leach conditions was utilized as the response variable to assess the effects of the plasma oxidation treatment. Based on the findings of the two-factorial parametric test, treatment time was found to be the most significant parameter for improving REE leachability in both the low and high SG fractions. Subsequently, a detailed test program was designed keeping RF Power at 450 Watts, oxygen flow rate at 40 ccs/min, and temperature at 80°C while varying treatment time over periods of 4, 8, 16, and 32 hours.

4.2.2.3 High-Temperature Calcination Tests

Calcination tests in the temperature range of 200-1000°C at intervals of 200°C were conducted to provide a comparison between low and high-temperature oxidation methods and to assess the effect of calcination temperature on the REE leachability. These tests were carried out in a laboratory-scale Thermolyne F6020C-80 muffle furnace manufactured by Thermo Scientific, USA. Batch samples from each SG fraction of the WK-13 and Fire Clay seam sources were used as feed for the tests. Representative samples were evenly spread in a crucible and calcined for 2 hours at various temperatures. After completion of the test, the furnace would gradually cool down to room temperature and the samples were collected. The calcined products were weighed and subjected to a standard leaching test using 1.2M sulfuric acid. REE recovery in the leaching tests was used as the response variable.

4.2.2.4 *Leaching Tests*

REEs associated with the different density fractions of a given coal source may have distinct leachabilities due to the variation in rare earth mineralogy resulting from different geochemical and physical activities. Leaching tests were performed on the feed and LTP treated density fractions of the WK-13 and Fire Clay samples to assess the effect of different lixiviants (deionized water, 0.1 M ammonium sulfate solution, and 1.2M sulfuric acid) at 75°C and a solid concentration of 1% w/v in three-neck round bottom flasks while keeping the stirring speed constant. For every test, a series of representative samples (15 mL) were collected at 10, 30, 60, 180, and 300 min of the leaching process to establish leaching kinetics. Weights of the samples were recorded, and leachate filtered using a 0.45 µm PVDF membrane filter after centrifuging for 10 min at 4000 rpm. The leaching tests were stopped at 300 min and the residual slurry was filtered using a 5 µm pore size filter paper. The filtrates were cooled to room temperature and their volumes were recorded. The filter cakes were dried in an oven at 60°C for 12 hours and the solid residual dry weights were recorded. The recovery was calculated as per (Eq. 3-1).

4.2.2.5 *Mineralogy and REE analysis*

Kaolinite ($\text{Al}_2(\text{Si}_2\text{O}_5)(\text{OH})_4$), quartz (SiO_2), and pyrite (FeS_2) were the three dominant minerals found in the WK-13 (Figure 4.1). For the low sulfur content Fire Clay sample, kaolinite, quartz, and illite/muscovite ($\text{KAl}_2(\text{Si}_3\text{AlO}_{10})(\text{OH})_2$) were the three dominant mineral phases. The ash associated with coal deposits is composed primarily of quartz. The XRD plot of the Fire Clay sample did not have a pyrite peak which was distinctly present in the WK-13 samples. This finding correlates with the low total sulfur content (<1%) for the Fire Clay material.

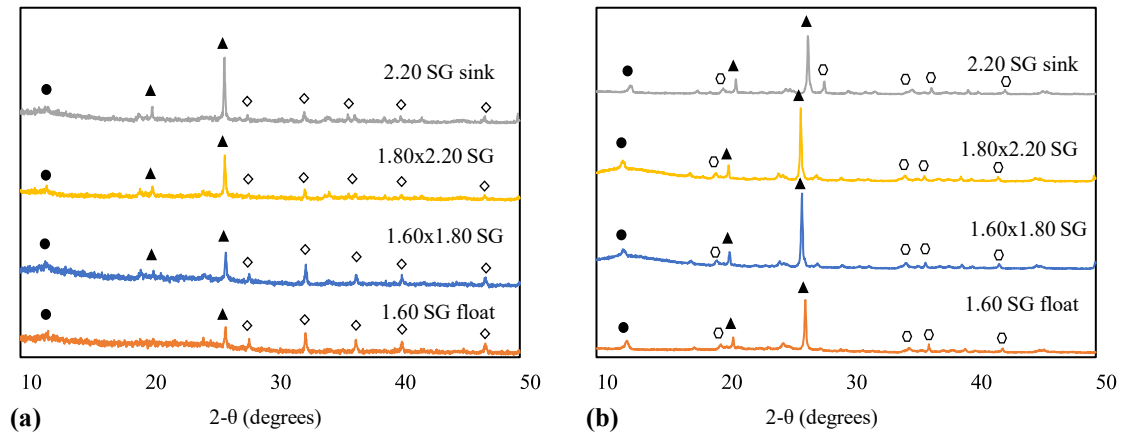


Figure 4.1. XRD patterns of the untreated density fractionated samples of (a) West Kentucky No.13 and (b) Fire Clay–refuse sample. (●-Kaolinite; ▲ -Quartz; ◇-Pyrite, and ○ - Illite).

4.3 Results and Discussions

The results from the REE analyses for the two feed sources revealed that the samples were dominated by cerium, lanthanum, and praseodymium (~56%) and critical elements such as yttrium and neodymium (~26%). Both samples contained higher concentrations of LREEs than HREEs (Figure 4.2). The REE distribution by SG for the two samples showed the potential of enrichment by a simple ashing process. On a whole mass basis, the higher SG fractions in the WK-13 source were found to have higher REE content than the low ash material. However, ashing the samples (1.60 SG float and 1.60x1.80 SG) enriched the REEs in the residual ash by about 200%. On the contrary, the low ash fraction (1.60 SG float) of the Fire Clay source had a total REE concentration greater than 400 ppm on a whole mass basis. As the SG fractions of the Fire Clay material (except for 1.60 SG float) were predominantly composed of ash material, the effect of ashing is not as pronounced as that seen for WK-13. For the 1.60 SG float fraction of the Fire Clay seam refuse, concentrations upwards of 800 ppm were obtained on an ash basis. This finding correlates to numerous previous studies that suggest that the middling fractions of the Fire Clay seam are rich in REEs [80]. The REEs in the middlings of fire Clay have been reported to be associated with the mineral matter and exist as finely dispersed monazite [24, 80]. This would necessitate the use of roasting assisted with chemical additives to extract the REEs associated with coal deposits.

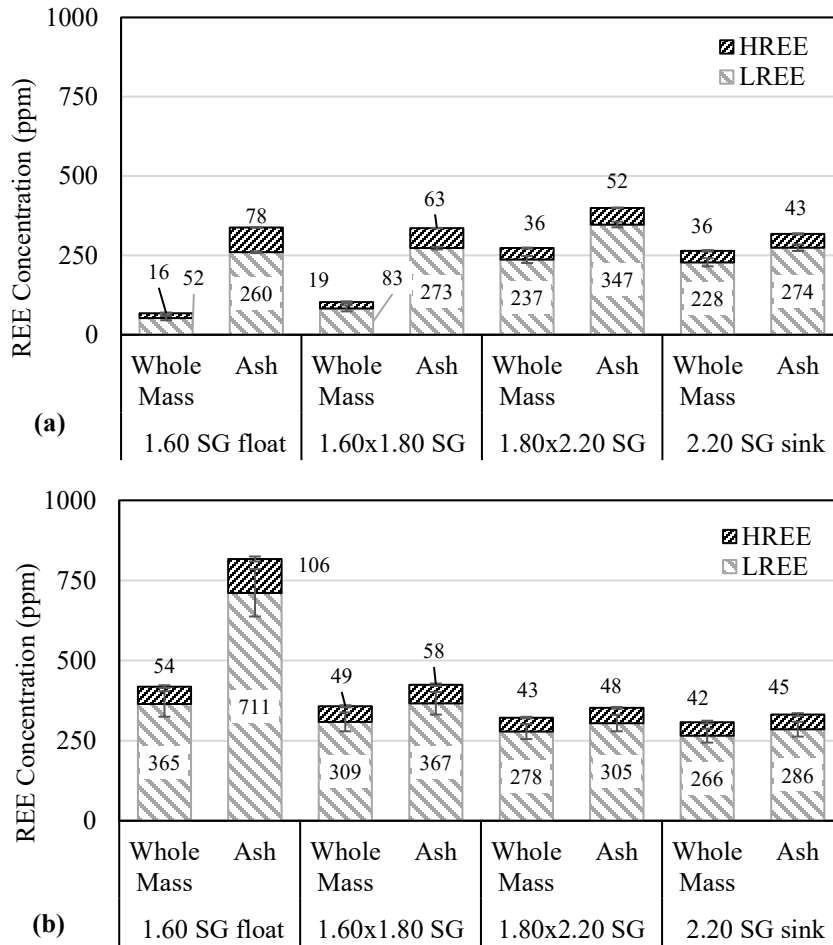


Figure 4.2. REE Distribution based on specific gravity for (a) West Kentucky No.13 and (b) Fire Clay refuse samples.

4.3.1 Low-Temperature Plasma Tests

A laboratory low-temperature oxygen plasma unit with the ability to control test conditions was used to optimize the operating parameters of the plasma treatment process (i.e., power, temperature, treatment time, etc.) to positively impact leaching characteristics. For the parametric tests, the samples were uniformly spread on a 15 cm diameter watch glass and subjected to the ionized oxygen plasma. It was observed that the top layer of the sample was more likely oxidized, while the under layers remained unchanged, which may have been due to limited exposure to the plasma. When the under layers of the sample was exposed to the LTP treatment, oxidization was more efficient, thereby improving organic matter removal. Based on the findings of the parametric test, treatment time was found to be the most significant parameter for improvement in the

leachability of REEs in both low and high ash density fractions. Therefore, a systematic test program was designed keeping RF Power at 450 Watts, oxygen flow rate at 40 ccs/min and temperature at 80°C, and treatment from 4 to 32 hours. The wide range of treatment time provided vital information on the minimum time required for observing a significant change in REE leachability.

Proximate analysis (moisture, carbon, and ash contents) was performed on the time-based LTP treated products of all the density fractions of WK-13 and Fire Clay (Figure 4.3). As shown in Figure 4.3 (a), the carbon contents of the lower density fractions (1.60 SG float and 1.60x1.80 SG) were decreased by plasma treatment, which corresponds to an elevation in the ash contents. Similarly, a significant increase in the ash content was seen for the 1.60 SG float fraction of the Fire Clay source (Figure 4.3 (b)). However, for the high-density fractions (1.80x2.20 SG. and 2.20 SG. sink), the carbon and ash contents changed by a very small amount even after 32 hours of LTP treatment. This observation suggests that plasma treatment has a very limited effect on high ash material. The degree of plasma treatment is directly proportional to the amount of carbon matter present in the sample. The abundance of ash-forming material masked the carbon matter present in the sample and thus reduced the effectiveness of its exposure to plasma.

XRD analysis of the LTP treated WK-13 and Fire Clay samples (Figure 4.4) did not show a change in mineral composition as compared to the feed material (Figure 4.1). The peak intensities of individual minerals were increased due to the partial removal of carbon matter from lower density fractions. The increase in ash content after LTP treatment as shown in Figure 4.3 was achieved by the removal of organic matter without altering the mineral matrix.

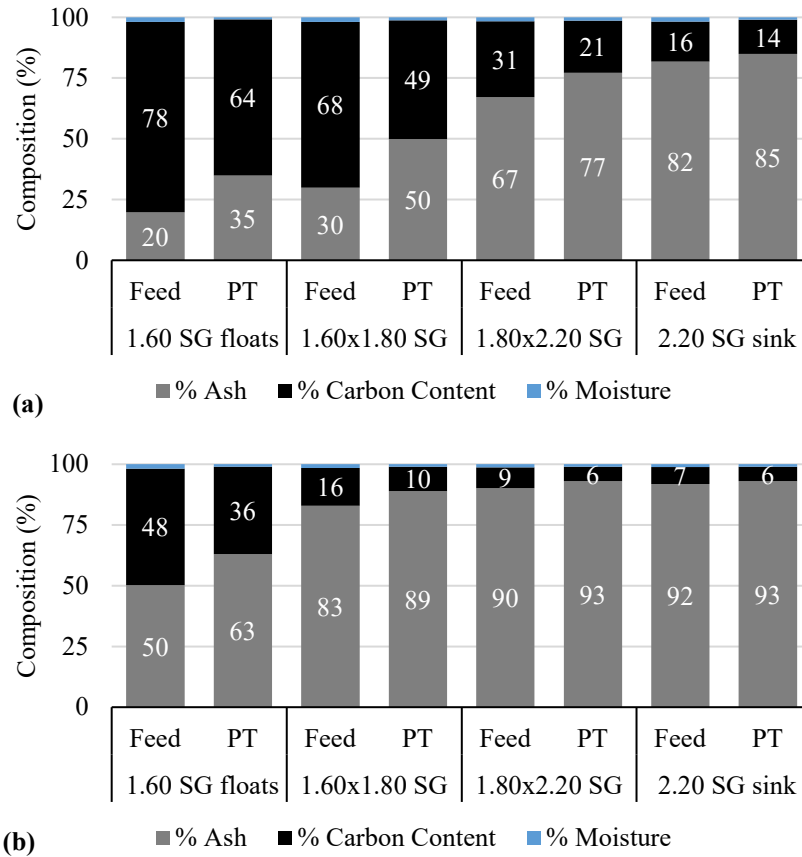


Figure 4.3. Moisture, carbon, and ash contents of the (a) West Kentucky No.13 and (b) Fire Clay density fractions after 32 hours of LTP treatment. (PT=Plasma Treated)

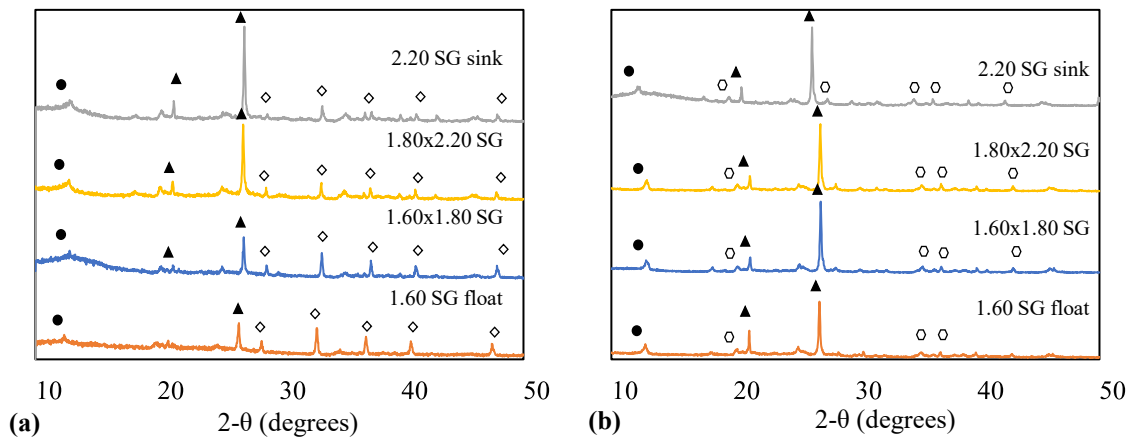


Figure 4.4. XRD patterns of the LTP treated, density fractionated samples of (a) West Kentucky No.13 and (b) Fire Clay-refuse sample. (● -Kaolinite; ▲ -Quartz; ◇ -Pyrite, and ○ - Illite).

The mode of occurrence of trace elements in coal determines their solubility in water. Most previous research shows a pH-dependent solubility of REEs. Thus, REEs in coal show good leachability in strong acids and poor leachability in neutral and mild conditions. The four density fractions of the WK-13 and Fire Clay refuse samples were treated by LTP for different time durations, and leaching tests were performed on the products using deionized water, 0.1M ammonium sulfate solution, and 1.2M sulfuric acid.

Water leaching is normally utilized for solid samples with high solubility. The LTP technique aims to utilize oxygen plasma to oxidize the carbon and access any water-soluble REEs. This can be followed by water leaching to dissolve the REEs into a liquid solution, which can be further processed using hydrometallurgical techniques. For leaching tests with DI water, no pH modifiers were used. The total REE recovery from all the density fractions of the WK-13 material with deionized water was found to be less than 10%, despite 32 hours of LTP treatment. However, the HREE recoveries for the 1.60 SG float and 1.60x1.80 SG fractions increased by 15% and 9% respectively. The nominal increase in the leachability of HREEs after plasma oxidization suggested that the HREEs associated with the clean coal matrix were converted to a water-soluble form. The final pH range for the leach solution of WK-13 material was 3.5-4.0. The natural acidity of the feed material by pyrite dissolution also assisted in the benefits of REE leachability. Alternatively, for all the density fractions of the Fire Clay seam, the total REE recovery by water leaching was found to be less than 1% and no significant effect of plasma treatment using neutral water as the lixiviant was observed. Thus, it was concluded that the poor leaching characteristics corresponded to the absence of water-soluble REE minerals in the LTP treated products of the Fire Clay source.

Salt leaching tests with 0.1M ammonium sulfate were also performed on the LTP treated density fractions. No pH adjustments were made, and the pH of the solution could drift naturally. pH values of 3.5 and 6.0 were recorded for the WK-13 and Fire Clay material respectively after completion of the salt leaching tests. The pH for the WK-13 was acidic due to the significant presence of pyrites in the feed. The Fire Clay material on the other hand showed high neutralization potential due to the presence of calcite and the absence of acid-forming pyrites. The REE recovery of the density fractions

of WK-13 is shown in Figure 4.5. For the 1.60 SG float and 1.60x1.80 SG density fractions, the REE recovery increased by extending the treatment period from 4 to 32 hours (Figure 4.5 (a) & Figure 4.5 (b)). For example, the total REE recovery of the 1.60 SG float fraction approximately increased by 11% points when the samples were treated for 32 hours (Figure 4.5 (a)). In an interesting find, the plasma treatment was found to have a significant effect on the recoveries of HREEs as compared to the LREEs. This finding suggests that HREEs have a higher affinity to the organic matter in coal relative to LREEs. However, it is difficult to prove whether the HREEs occurred as elemental forms or were finely dispersed in ash material. The results indicated that significant HREE recovery was achieved when the carbon was even partially removed by using ammonium sulfate as lixiviant. Therefore, salt leaching can be used to extract critical HREEs from LTP-treated low ash coals under mild and benign leaching conditions. This will save capital and operational costs associated with acids used in the leaching process.

However, the effect of LTP on the heavier density fraction of the WK-13 material was not as pronounced as that for the lower density fractions and salt leaching was found to be less efficient (Figure 4.5 (c) & Figure 4.5 (d)). Salt leaching tests were also performed on the LTP-treated Fire Clay density fractions. The effect of LTP treatment on both the light and heavy density fractions of the Fire Clay plasma treated material was insignificant as no improvement in REE recovery values was seen despite 32 hours of treatment. These findings could be the result of a different mode of occurrence and association of REEs in Fire Clay as compared to WK-13. Not to mention, the trace amounts of calcite present in the Fire Clay material have a neutralizing potential which could cause precipitation of the dissolved REEs and result in lower REE recoveries.

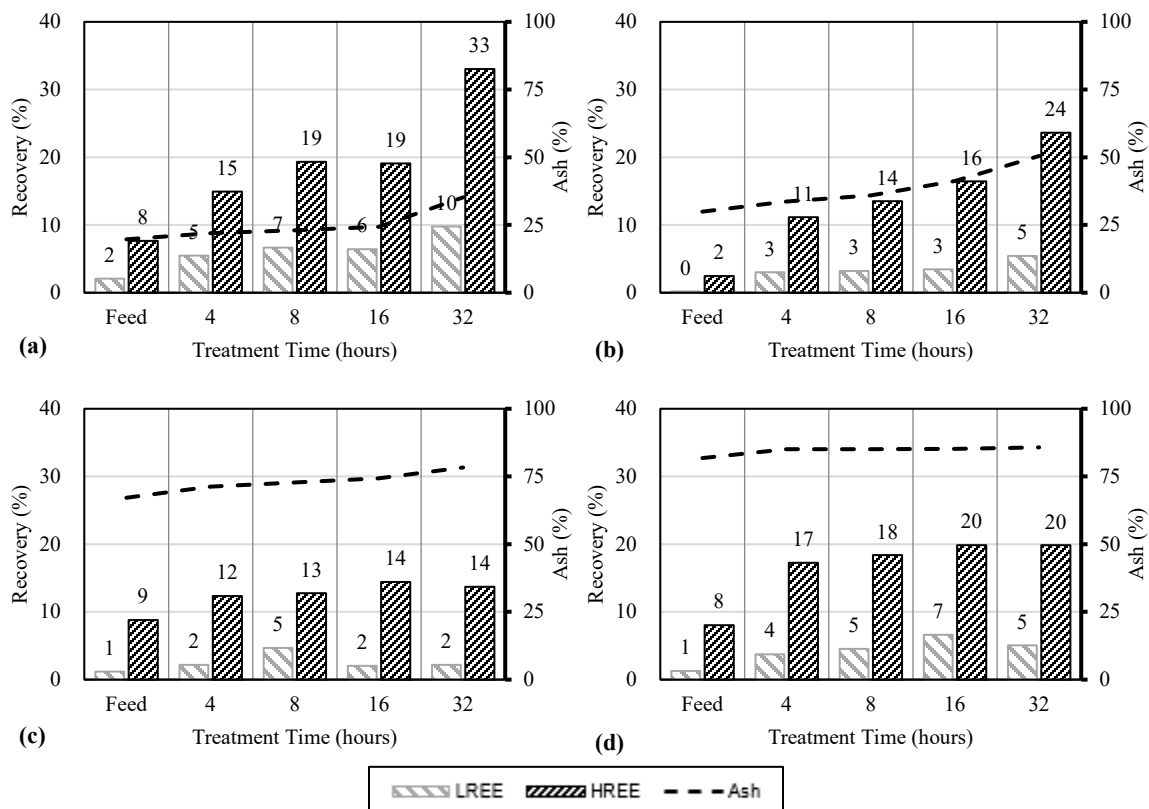


Figure 4.5. REE recovery from the LTP treated West Kentucky No.13 (a) 1.60 SG float, (b) 1.60x1.80 SG, (c) 1.80x2.20 SG, and (d) 2.20 SG sink samples using 0.1M ammonium sulfate at 75°C for 5 hours.

When 1.2M sulfuric acid was used, the total REE recovery of the WK-13 1.60 SG float fraction increased from 16% to 30% after 32 hours of LTP treatment (Figure 4.6(a)). The ash contents of the plasma-treated products were also increased from about 21% to 35% indicating enhanced oxidization of the organic matter. Similar improvements in REE leachability were also observed for the 1.60x1.80 SG fraction, which contained a medium level of ash material (Figure 4.6(b)). These results may be a result of REEs released from the carbonaceous components being removed during plasma treatment and the creation of access to REE-enriched, dispersed mineral matter such as clays that are dissolved by the strong acid solution. The recoveries of both LREEs and HREEs were not affected despite prolonged LTP treatment for the 1.80 x 2.20 SG, and 2.20 SG sink fractions (Figure 4.6(c) & Figure 4.6(d)). As such, the organic matter content played a critical role in the increase in REE recovery from coal by LTP oxidation. With an increase in treatment time, the HREE recovery was preferentially increased relative to LREEs for

the samples with less than 1.80 SG (Figure 4.6(a) and Figure 4.6(b)). This indicated that low-temperature treatment is more beneficial to HREEs and suggesting an association of HREEs with clean coal fraction of the seam. This association could be the result of the chelation of positively charged HREE ions onto the negatively charged surfaces of micro dispersed clays dating back to the origin of coal and movement of the organic humic acids [158].

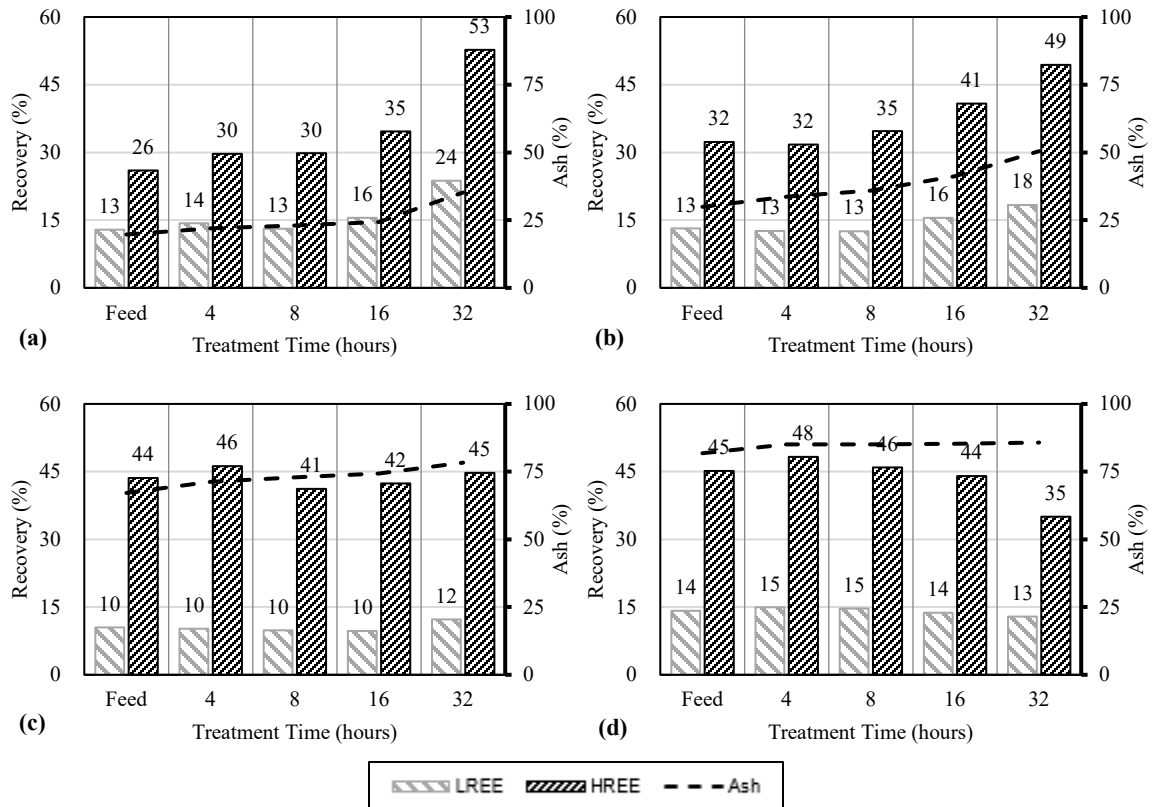


Figure 4.6. REE recovery from the LTP treated West Kentucky No.13 (a) 1.60 SG float, (b) 1.60x1.80 SG, (c) 1.80x2.20 SG, and (d) 2.20 SG sink samples using 1.2M sulfuric acid at 75°C for 5 hours.

Acid Leaching tests with 1.2M sulfuric acid at 75°C were also conducted on the LTP treated density fractions of the Fire Clay seam. As previously reported in Figure 4.3 (b), the ash contents of the plasma-treated products of Fire Clay were marginally increased indicating limited oxidization of the organic matter. For the 2.20 SG sink fraction, the recovery of both LREEs and HREEs was not affected even after prolonged treatment time (Figure 4.7(d)). For the 1.60 SG float fraction, which contained a relatively

higher amount of clean coal, total REE recovery was marginally increased by 11% points after low-temperature treatment for 32 hours (Figure 4.7(a)). Alternatively, REEs that were initially associated with the organic matter was dissolved as metal ions after the LTP treatment. However, due to the marginal effect, it can be deduced that more than 32 hours of treatment for the low-density fraction is required to get a significant impact on REE recovery values. Additionally, the effect on the 1.60x1.80 SG and the 1.80x2.20 SG density fractions were marginal (Figure 4.7(b) and Figure 4.7(c)). Overall, no selectivity was observed for HREEs in the LTP-treated Fire Clay material as it was observed for the WK-13 material. Findings from the WK-13 seam indicated that low-temperature treatment is more beneficial to HREEs as they have a higher affinity to the organic matter in coal relative to LREEs. However, such a relationship of HREEs with clean coal was not observed for the Fire Clay source.

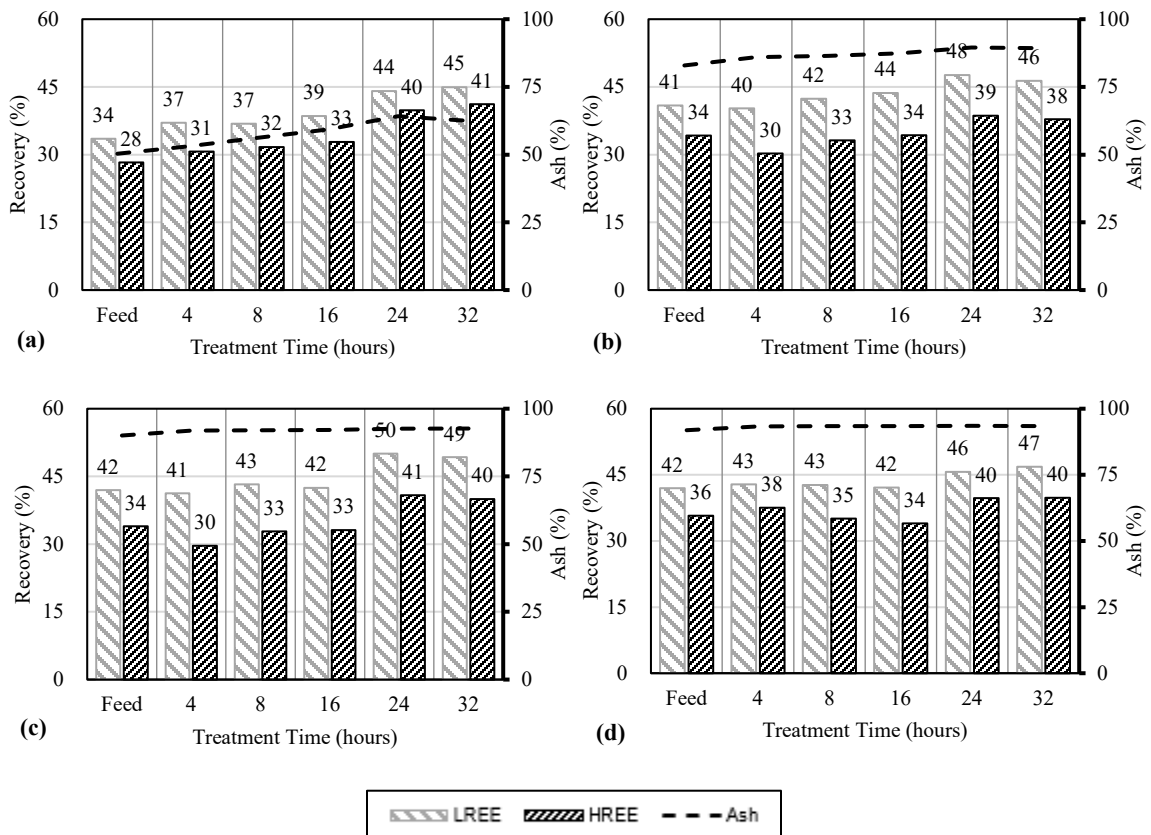


Figure 4.7. REE recovery from the LTP treated Fire Clay (a) 1.60 SG float, (b) 1.60x1.80 SG, (c) 1.80x2.20 SG, and (d) 2.20 SG sink samples using 1.2M sulfuric acid at 75°C for 5 hours.

The surface area and pore volume analysis of the feed, plasma-treated ash, and calcinated products of the 1.60 SG float and 2.20 SG sink fractions of the WK-13 refuse sample are provided in Table 4.3. The LTP ashing showed a 600% increase in the surface area of the 1.60 SG float density fraction after most of the organic material was removed. The total area and volume of the pores in the plasma-treated ash also increased significantly. This allowed the lixiviants to penetrate deeper into the solid matrix and dissolve the REEs that would otherwise have had remained inaccessible. The 2.20 SG sink fraction, however, showed an insignificant change in the surface area and pore volume. This density fraction was made up primarily of ash which remained unaffected by LTP treatment.

An SEM-EDX study of the plasma-treated density fractions of the coal sources was conducted to evaluate the modifications of surface properties by LTP treatment. Any changes in the texture and particle size could be used to assess the effect of LTP pretreatment for the liberation of REEs that are bound in microscopic size ranges in the coal matrix. As shown in Figure 4.8, particles with high porosity were observed in the plasma-treated 1.60 SG float density fraction of the WK-13 material. Such particles with improved surface area and porosity were absent in the untreated fraction. The surface texture of particles as seen in Figure 4.8 shows the effect of plasma treatment on the feed material that increases the surface area and pore volume and allows enhanced REE recovery. Particles had a honeycomb structure and evident signs of increased porosity at microscopic levels. When the carbon was partially removed, the pore structure of the coal samples expanded which increased the porosity and the lixiviants could dissolve the REEs locked inside the particle. This increase in porosity, surface area, and pore volume was also corroborated by BET and pore volume analysis reported in Table 4.3. LTP primarily oxidizes the organic material contained in the samples. There exists a strong positive correlation between organic content in the feed and the weight loss by oxidation in LTP treatment. Therefore, improvements in porosity and surface area were not observed for the 2.20 SG sink material.

Table 4.3. Results of the pore volume and surface area analysis for the feed and plasma-treated ash of 1.60 SG float and 2.20 SG sink material of West Kentucky No.13 refuse treated for 32 hours.

1.60 SG float			
	Feed	Plasma Ash	% Change
BET Surface Area (m ² /g)	1.2864	9.7513	658
Total Volume in Pores (cm ³ /g)	0.0031	0.0509	1542
Area in Pores (m ² /g)	0.3110	3.4140	998
Total Area in Pores (m ² /g)	0.6280	6.6270	955
2.20 SG sink			
	Feed	Plasma Ash	% Change
BET Surface Area (m ² /g)	7.8935	6.8527	-13
Total Volume in Pores (cm ³ /g)	0.0085	0.0092	8
Area in Pores (m ² /g)	4.0900	2.5710	-37
Total Area in Pores (m ² /g)	5.0120	3.5810	-29

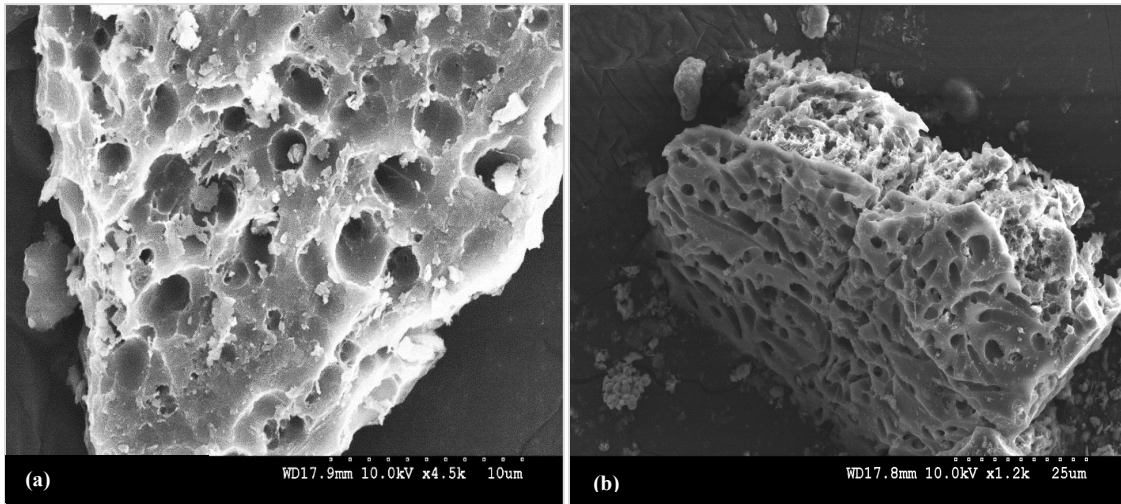


Figure 4.8. SEM micrographs depicting particles with increased porosity and surface area for the LTP treated (a) 1.60 SG float and (b) 1.60x1.80 SG density fractions of West Kentucky No.13.

4.3.2 High-Temperature Calcination Tests

High-temperature calcination for the WK-13 material was found to have a significant impact on the REE leaching characteristics (Figure 4.9). Exceptionally high total REE recoveries were found for samples calcinated at 600°C and 800°C. The improvement in leaching for the calcined samples peaked at 600°C but dropped substantially for higher temperature values for material lighter than 1.80 SG (Figure 4.9(a))

& Figure 4.9(b)). This increased recovery can be attributed to the liberation and conversion of hard-to-leach rare earth minerals to more soluble oxide forms after calcination which increases their leachability. For samples heavier than 1.80 SG, comparable leaching performance is observed at 600°C and 800°C. (Figure 4.9(c) & Figure 4.9(d)). The low leaching recoveries at 1000°C were likely due to sintering of the clays (e.g., Kaolinite and Illite) and formation of a glassy matrix due to the high temperature which isolated the entrapped REEs making them difficult to leach.

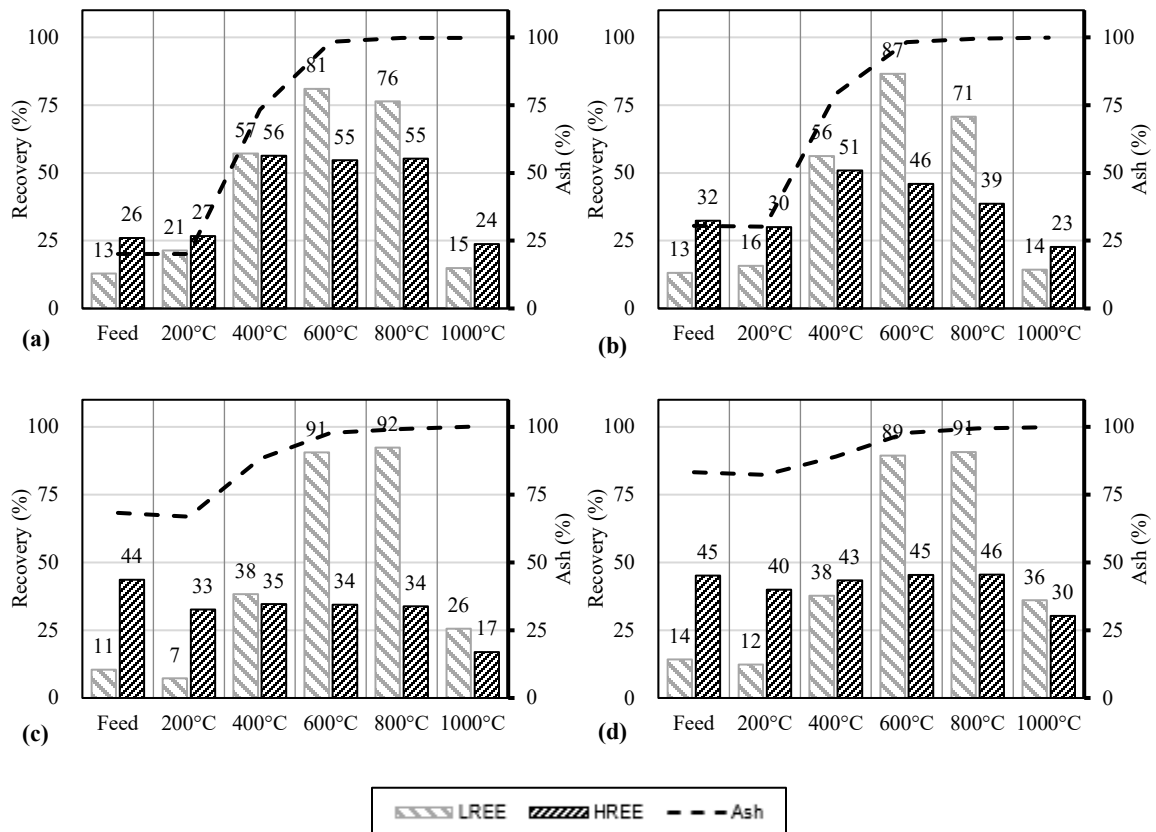


Figure 4.9. REE recovery from the calcination of West Kentucky No.13 (a) 1.60 SG float, (b) 1.60x1.80 SG, (c) 1.80x2.20 SG, and (d) 2.20 SG sink samples using 1.2M sulfuric acid at 75°C for 5 hours.

The trend of recovery of HREEs in the 1.6 SG float density fraction revealed that HREEs are liberated by the effect of high-temperature calcination. About 55% of the total HREEs dissolve into the leachate. However, the data suggests that HREEs in the heavier density fractions have a very different mode of occurrence where high-temperature calcination provided no significant effect on their recovery. This finding

suggests that a significant portion of the HREEs exists in an insoluble form, bound with the inert ash material which is very hard to leach. LREEs show consistency in the mode of occurrence across all density fractions and show very high recovery with values as high as 85%. High HREE recoveries found in the lower density fractions correspond to their association with the clean coal and middling fractions of the WK-13. Similar findings have been previously reported for the LTP studies (Figure 4.6(a) & Figure 4.6(b)). Total REE recoveries greater than 75% were observed after pretreatment using a temperature of 600°C. It was also observed that even partial carbon removal at 400°C released the HREEs bound with the organic matter and resulted in higher REE recoveries.

Calcination also had a significant impact on the REE leaching characteristics for the density fractions of the Fire Clay material (Figure 4.10). Calcination of the Fire Clay 2.20 SG sink sample, which comprises primarily of the ash material, increased the recovery values for total REEs by more than 20 absolute points at 600°C. The positive association of REE recovery and temperature maximizes the recovery at 600°C and flips to an inverse relationship post 600°C. Based on the results it can be concluded that the Fire Clay density fractions have higher amounts of insoluble REEs trapped in the solid matrix. The recovery of REEs increase with temperature but the effect of calcination is more pronounced for the lower density fractions with specific gravities less than 1.80. Also, the majority of HREEs in the Fire Clay material is hard to leach with lower recoveries despite calcination.

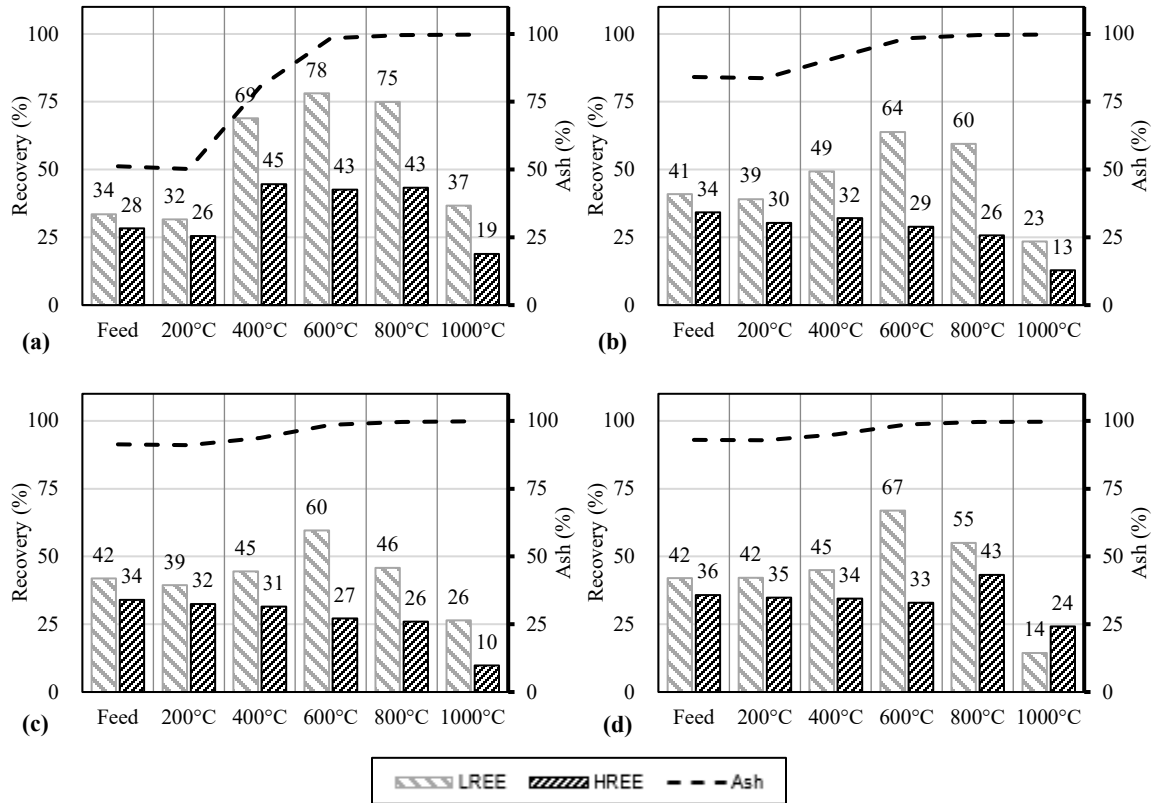


Figure 4.10. REE recovery from the calcination of Fire Clay (a) 1.60 SG float, (b) 1.60x1.80 SG, (c) 1.80x2.20 SG, and (d) 2.20 SG sink samples using 1.2M sulfuric acid at 75°C for 5 hours.

4.4 Conclusions

The discussed work evaluated the effect of plasma oxidation on the various density fractions of representative coarse coal refuse samples obtained from active coal preparation plants treating WK-13 and Fire Clay seam coal sources. LTP oxidation treatment provided a significant positive impact on the leachability of REEs associated with the WK-13 coal material using benign ammonium sulfate solution. The recovery improvements correlated to an ash content increase from LTP oxidation. Higher recoveries were observed for higher ash content changes in the 1.60 SG float fraction. Considering the relative recovery improvement differences, the HREEs have a strong affinity with carbonaceous material, which was removed during the LTP oxidation. Scanning electron microscope micrographs showed that the plasma oxidation treatment created a porous structure that had a higher volume of pores. The creation of a high surface area allowed for improved access for the lixiviants to react and extract the REEs bound in the organic

structure and the micro dispersed mineral matter. As such, LTP oxidation had no impact on REE recovery from the 2.20 SG sink fraction. LTP treatment was found to not affect the leachability of REEs contained in all the density fractions of a Fire Clay refuse sample when using untreated water and 0.1 M ammonium sulfate as lixiviants. This finding provides indirect evidence that there is little to no organic affinity of the REEs in the Fire Clay coal source. The improvement obtained when using a sulfuric acid solution was likely due to improved access to REE-enriched mineral matter and rare earth mineral grains that can be dissolved under low pH conditions.

High-temperature oxidation of the feed to the leaching process was also found to significantly enhance the leachability characteristics of both the light and heavy REEs comprised in the SG fractions of the WK-13 and Fire Clay refuse materials when performed under optimum temperatures. The recovery enhancement was especially significant for the LREEs contained in all density fractions whereas improvement in HREE extraction was primarily achieved for the 1.60 SG float fraction. The mechanisms that provided the leachability improvement by high-temperature oxidation include: i) release of the REEs (especially HREEs) from the organic matrix through the combustion of the organic material; ii) liberation of finely dispersed mineral matter which allows access to the acid leach solution; iii) decomposition of the rare earth bearing minerals.

CHAPTER 5. HIGH-TEMPERATURE CALCINATION

5.1 Introduction

The steady demand for rare earth elements (REEs) in clean energy technologies coupled with the risks in the global supply chain resulted in a surge of research initiatives to recover the REEs from non-conventional resources. Since 2011, efforts have been made to characterize and quantify the REEs in various coal deposits across the United States and explore the possibility of economical extraction by traditional as well as novel mineral processing methods [3-5, 23, 71, 79, 146, 159]. Findings from a significant number of studies conducted on concentration and recovery of REEs from coal-based feed advocate the feasibility of using hydrometallurgical extraction over physical separation methods [6-9, 11, 13, 14, 78, 79, 160]. However, the chemical cost for REE recovery from coal using strong leaching conditions is prohibitively high [8, 13, 61, 161]. This economic unviability is inherently a result of the finely dispersed nature of REE minerals and the low REE recoveries due to the varied modes of occurrences of REEs in coal [21-24].

Thermal treatment has been very effective in transforming conventional REE-bearing minerals such as bastnaesite and monazite into more leachable forms [8, 10, 18-20]. The high-temperature acidic/basic baking using sulfuric acid, ammonium chloride, sodium carbonate, etc. has been used extensively to enhance the recovery of REEs from the traditional REE-bearing ore. The high-temperature calcination supplemented by chemical additives decomposes or transforms the REE carbonates and phosphates into corresponding REE oxides, sulfates, and chlorides which have a higher solubility [3, 52, 162, 163]. Zhang and Honaker reported preferential recovery of light LREE using 1.2M HCl (80-90%) for the Pocahontas No. 3 coal source after calcination at 600°C. However, an insignificant increase in the recovery of HREE was observed and was attributed to the inability of thermal decomposition of HREE bearing phosphate minerals at 600°C. The study also reported faster leaching kinetics after calcination of both the middling and the high ash sample of the feed [36]. Similarly, significant benefits in the recovery of LREEs by acid leaching of coal calcination products have been reported in the literature [13, 86,

164]. The benefits were realized by decomposition of finely dispersed REE-bearing minerals and/or by liberation of REE minerals encapsulated in the interlayers of the clays associated with coal deposits. Additionally, calcination of coal refuse at 600-750°C was also found to benefit the recovery of other critical elements such as Li, Co, Ni, Mn, V, and Sr [17, 91, 165].

Although benefits in the leaching characteristics of REEs are achieved by calcination, the process also increases the concentration of contaminant ions in the pregnant leach solution [36, 61, 91]. This creates operational challenges in downstream selective precipitation and solvent extraction processes and renders the process cost inhibitive [84]. The studies performed to date on coal calcination have been performed at specific temperature set-points and therefore the wholesome effect of temperature on the REEs and contaminant ions has not been fully quantified. Additionally, a comprehensive study on the effects of other control variables has also not been conducted. Thus, by utilizing the results from a statistically designed set of experiments, this section aims to study the effect of calcination parameters to maximize REE recovery from coal refuse and minimize the concentration of contaminant ions such as Al, Ca, and Fe. To achieve this objective, the samples were calcined at temperatures ranging from 100°C to 1000°C and the results were used to narrow the upper and lower temperature boundaries for subsequent optimization studies. The value ranges for the other operational parameters were selected based on the equipment specifications. Secondly, based on the data obtained from the three-factor three-level statistical design of experiments, significant parameters were recognized, and empirical models were developed to finally optimize the process variables. Statistically designed test programs allowed for easier interpretation of results and minimization of systematic experimental errors.

5.2 Materials and Methods

5.2.1 Materials

Coarse refuse samples from two coal preparation plants processing WK-13 and Fire Clay seam coals were collected as the feed for the study. The samples were air-dried, and density fractionated using a lab-scale float-sink system where ultrafine

magnetite was mixed with tap water to prepare heavy mediums having specific gravity (SG) values of 1.60 SG, 1.80 SG, and 2.20 SG. The magnetite was continuously suspended in the heavy media by agitation using injected air. The density fractionated products were wet screened to remove the entrained magnetite. The clean coal fraction (1.60 SG float), middlings (1.60 SG x 1.80 SG, 1.80 SG x 2.20 SG), and high ash fraction (2.20 SG sink) were air-dried and finally pulverized to 180 μm using a combination of a jaw crusher and a hammer mill. Trace metal grade sulfuric acid was purchased from Fisher Scientific, US, and used for the acid leaching tests. Dilutions to test at lower acidity levels were achieved using deionized water with a resistivity of 18.2 $\text{M}\Omega\cdot\text{cm}$ at 25°C as per ASTM D1193-06 standard.

5.2.2 Methods

5.2.2.1 Calcination: Lab-Scale

Calcination tests were carried out in a lab-scale Thermolyne F6020C-80 muffle furnace manufactured by Thermo Scientific, USA at different temperatures, hold times, and heating rates. A representative 30g sample was evenly distributed into six crucibles for every batch (5g/crucible). No chemical additives were added, and static atmospheric conditions were used. After completion of the test, the furnace was gradually cooled to room temperature before extraction of the samples. The calcined products were weighed and subjected to REE analysis and acid leaching tests.

A test program based on a Box-Behnken statistical design was performed to quantify the main parameter and parameter interaction effects on the response variables. It also allows the development of a mathematical model to describe the process by assessing the statistical significance of the independent factors as well as the significance of the interactions between the factors [78, 166, 167]. The set of parameter values that provide an optimum performance can also be identified using multivariate analyses. The three independent input parameters selected for the study were temperature ($^{\circ}\text{C}$), heating rate ($^{\circ}\text{C}/\text{min}$), and hold time (min). The lower and upper bounds of the variables are presented in Table 5.1. The temperature range for the tests for selected based on the results of the parametric tests. The maximum value for heating ramp rate was selected based on a

controlled experiment where the increase in furnace temperature was measured with time. The maxima for hold time was based on the studies done previously by Zhang where a hold time of 120 minutes was used for complete oxidation of the feed [36]. Solid weight treated in every batch was kept constant to eliminate variability due to changing feed rate. The recovery (%) of REEs and the concentration of major contaminant ions (Al, Ca, and Fe (ppm)) were measured as response variables.

Table 5.1. Levels of Independent variables and their ranges for Box-Behnken design.

Factor	Name	Units	Minimum	Maximum	Mean
A	Temperature	°C	400	800	600
B	Ramp	°C/min	2	10	6
C	Hold Time	min	0	120	60

The three-factor, three-level Box-Behnken experimental configuration required 17 test runs to develop empirical models to relate REE recovery and contaminant concentration with the significant input parameters and to subsequently present the relationships as response surfaces. Design Expert-12 software was utilized to plan the experiments and perform the statistical analysis. The runs were randomized to minimize systematic error and ensure that the results were probabilistically independent. The significance of the empirical model was tested based on the p-values obtained from the Analysis of Variance (ANOVA). ANOVA is one of the most organized and logical approaches for analysis of a factorial design test to obtain vital information for understanding the process behavior [168-170]. Empirical equations were built to predict the response based on the individual and combined effects of the input variables. The significance of each parameter and their interactions were tested against the null hypothesis that the coefficient for the variable is null. The terms that obtain a p-value less than 0.05 in an overall F-test were considered significant [171]. All insignificant parameters were removed. The high adjusted R^2 value was used as a measure to determine the efficacy of the best-fit model to the data. Additionally, the models were tested against the following assumptions of regression:

1. Residual errors for the selected models were found to be independent;

2. Residual errors for the selected models were found to be distributed normally with a mean value of zero; and
3. The variance of errors for the selected models was found to be constant across all the observations.

5.2.2.2 *Acid Leaching Tests*

REEs associated with different density fractions may have distinct leaching characteristics due to the variation in rare earth mineralogy resulting from different geochemical and physical activities. Acid leaching tests on the feed and calcined products were performed in a three-neck round bottom flask with 1.2M sulfuric acid at 75°C for 5 hours at 1% w/v solid concentration. The test apparatus allowed for control over leaching temperature and stirring speed and was equipped with condensers to minimize volumetric losses due to evaporation. For every test, a series of representative samples (15 mL) were collected at 10, 30, 60, 180, and 300 min of the leaching process to establish the leaching kinetics. Weights of the samples were recorded for mass balance evaluation. The samples were centrifuged at 4000 rpm for 10 min to collect the supernatants which were filtered using a 0.45 μm PVDF membrane filter. The leaching tests were stopped at 300 min and the residual slurry was filtered using a 5 μm pore size filter paper. The filtrates were cooled down to room temperature and their volumes were recorded. The filter cakes were dried in an oven at 60°C for 12 hours and the solid residual dry weights were recorded. The recovery was calculated as per (Eq. 3-1).

5.3 Results and Discussions

5.3.1 Batch Calcination Tests

The calcination tests at varying temperatures were conducted to establish the upper and lower bound for optimizing the variable in the subsequent calcination optimization studies. The leaching recovery for light and heavy REEs along with the concentration of Al, Ca, and Fe for the calcination products of all the density fractions of West Kentucky No.13 at temperatures ranging from 100-1000°C is provided in Figure 5.1, Figure 5.2, Figure 5.3, and Figure 5.4. About 9-17% of the LREEs and about 32-43% HREEs were leached from the untreated density fractions of the WK-13. The higher recovery of the heavy REEs from the untreated 2.20 SG sink fraction (Figure 5.4) as

compared to the LREEs results in a higher concentration of HREEs in the acid mine drainage from the WK-13 rejects [172]. Significant benefits in the HREE recoveries were achieved after calcination from the 1.60 SG float fraction when the organic matter was fully removed, and the mineral matter was liberated at temperatures 400-600°C. The organic removal from the light density fraction by calcination results in the liberation of the finely dispersed mineral matter thereby providing enhanced interaction between the lixiviant and the mineral surface as explained by Zhang and Honaker [90]. There is also the possibility of organic association of REEs with humic acids in coal which form complexes with REE ions [158]. Based on the leaching characteristics exhibited by the HREEs there seem to be two maybe three modes of association as reflected by the leaching results of most density fractions. Some HREEs are organically associated that are released by the combustion process. Additionally, a large portion of HREEs are found to be unaffected by calcination at high temperatures and would require an acid baking process for chemical liberation. This could be a signature of the presence of xenotime in the mineral matrix.

However, the HREEs in the density fractions >1.80 SG showed no significant improvement in leaching kinetics and characteristics (Figure 5.3). This would suggest that a majority of HREEs in the high ash parting material of the WK-13 seam are hard to leach and/or strongly bound in minerals that are not affected by thermal treatment. The benefits in leaching characteristics of the LREEs for all the density fractions corresponded to the increase in temperature from 500-800°C. A similar increase in the concentration of aluminum was also observed suggesting a possible co-existence of LREEs in the clays associated with the coal deposits. Calcium in the PLS primarily originated from the calcite present in the coal deposit. This calcite is highly soluble and dissolves readily in an acidic solution. The decrease in leaching recoveries of all the species at temperatures greater than 800°C may be due to the sintering of the clay surfaces that makes the REEs hard to leach. Iron contamination in the PLS solution was found to be maximum from the leaching of samples calcinated at a temperature of 400°C. This observation was likely due to the decomposition of the pyrite and the formation of an intermediate iron oxide product at 400-500°C that is highly soluble.

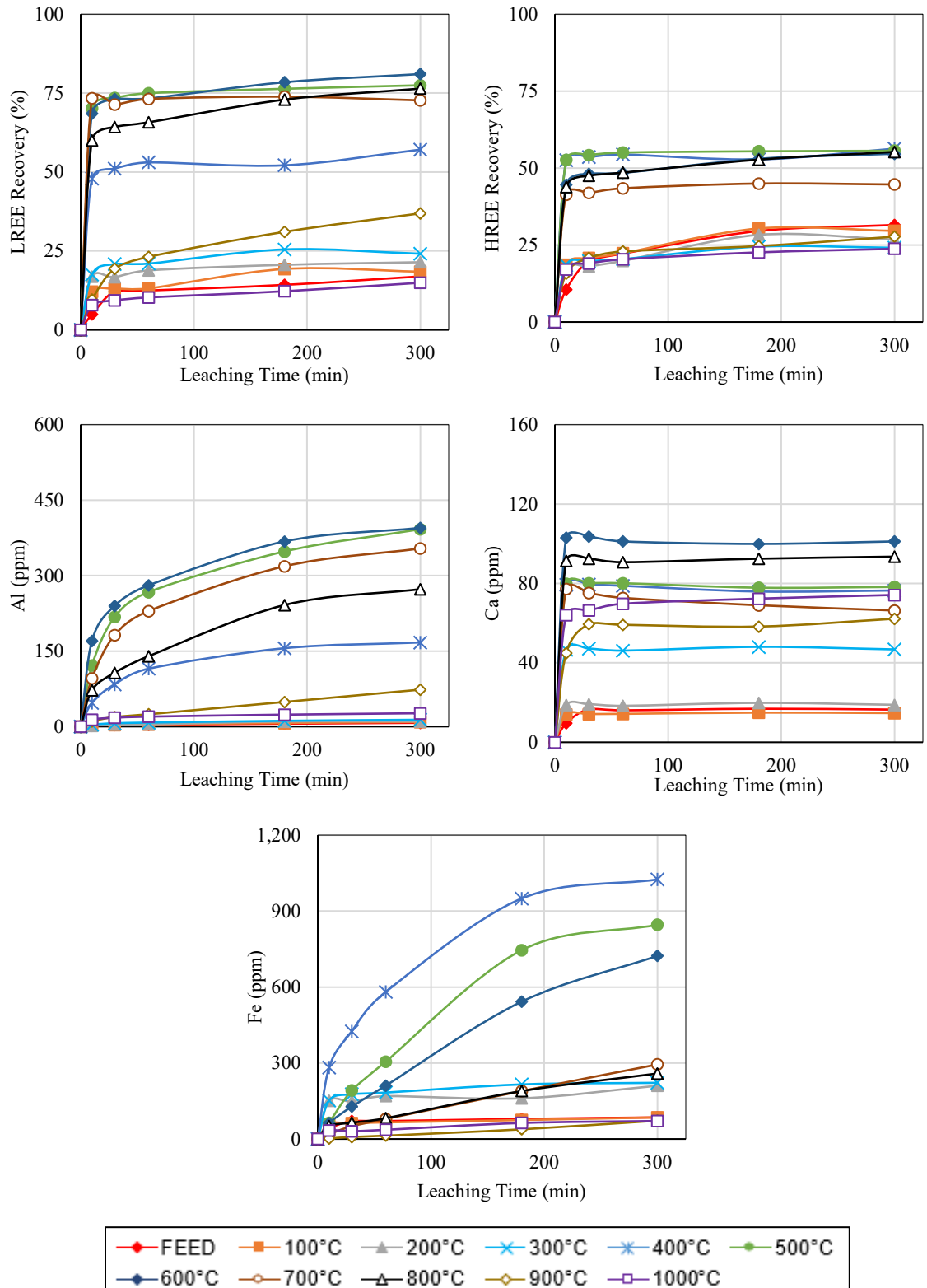


Figure 5.1. Acid leaching test results with 1.2M H₂SO₄ at 75°C for the 1.60 SG float of West Kentucky No.13 calcined at different temperatures in air.

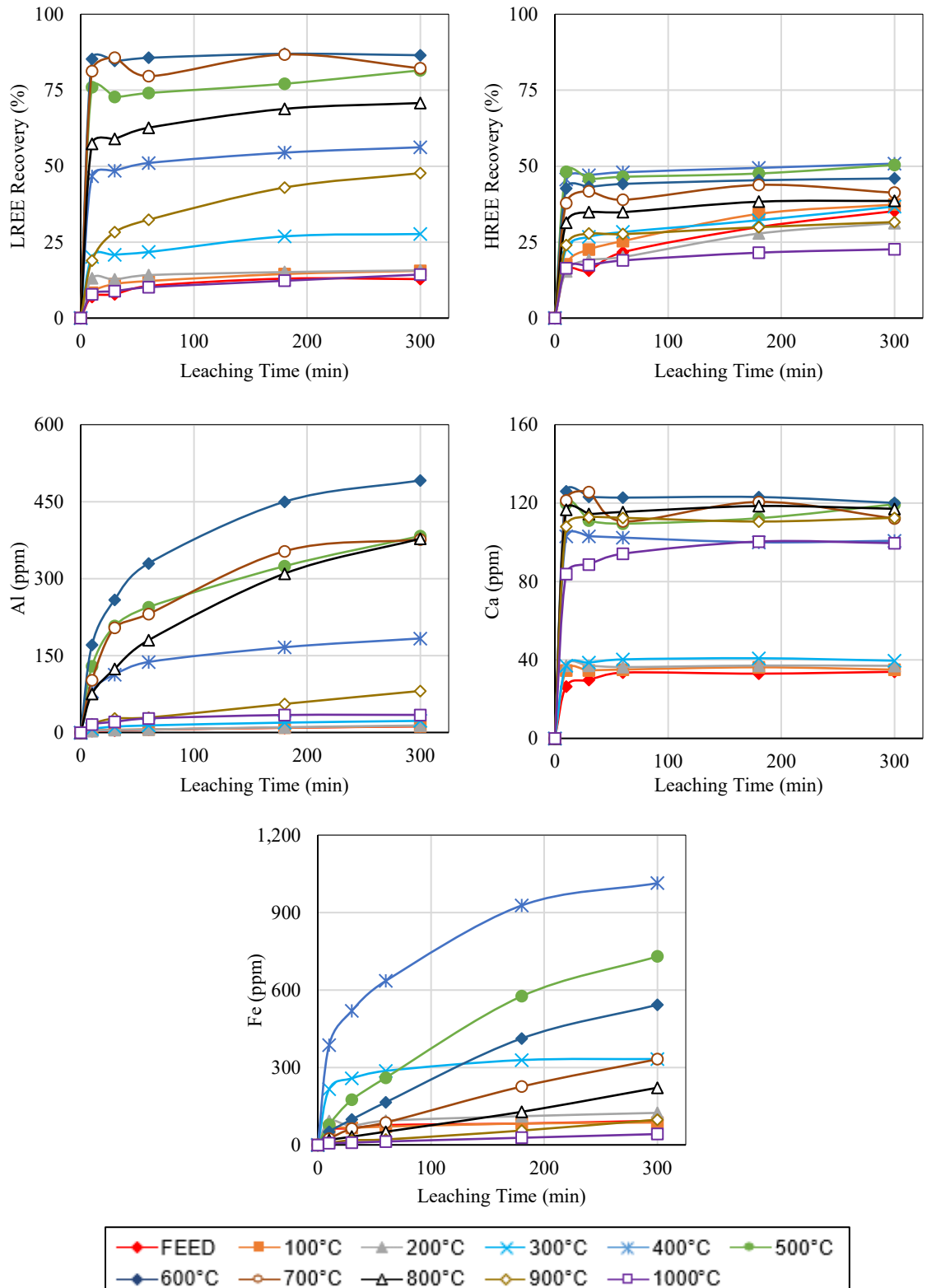


Figure 5.2. Acid leaching test results with 1.2M H₂SO₄ at 75°C for the 1.60x1.80 SG of West Kentucky No.13 calcined at different temperatures in air.

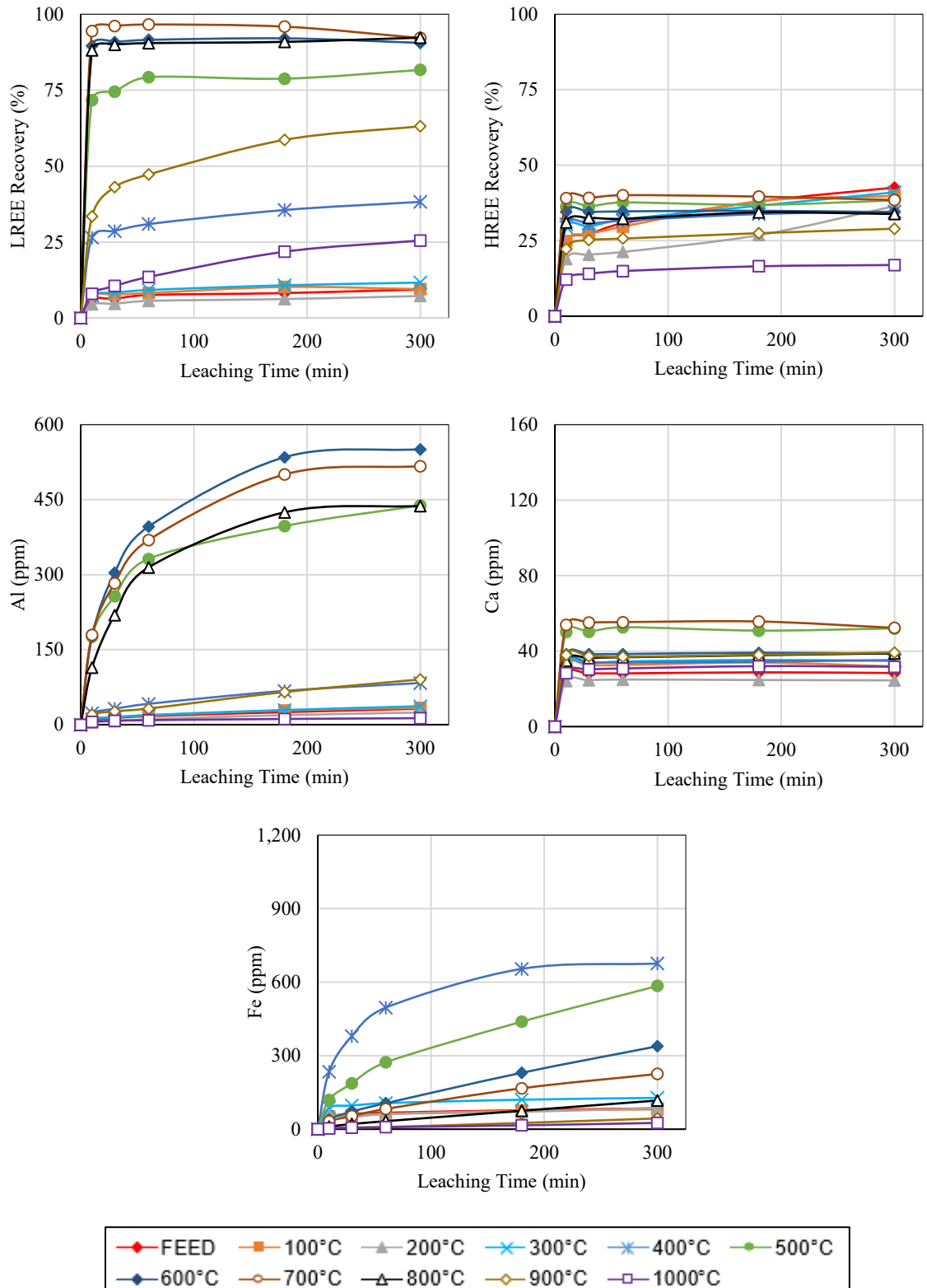


Figure 5.3. Acid leaching test results with 1.2M H₂SO₄ at 75°C for the 1.80x2.20 SG of West Kentucky No.13 calcined at different temperatures in air.

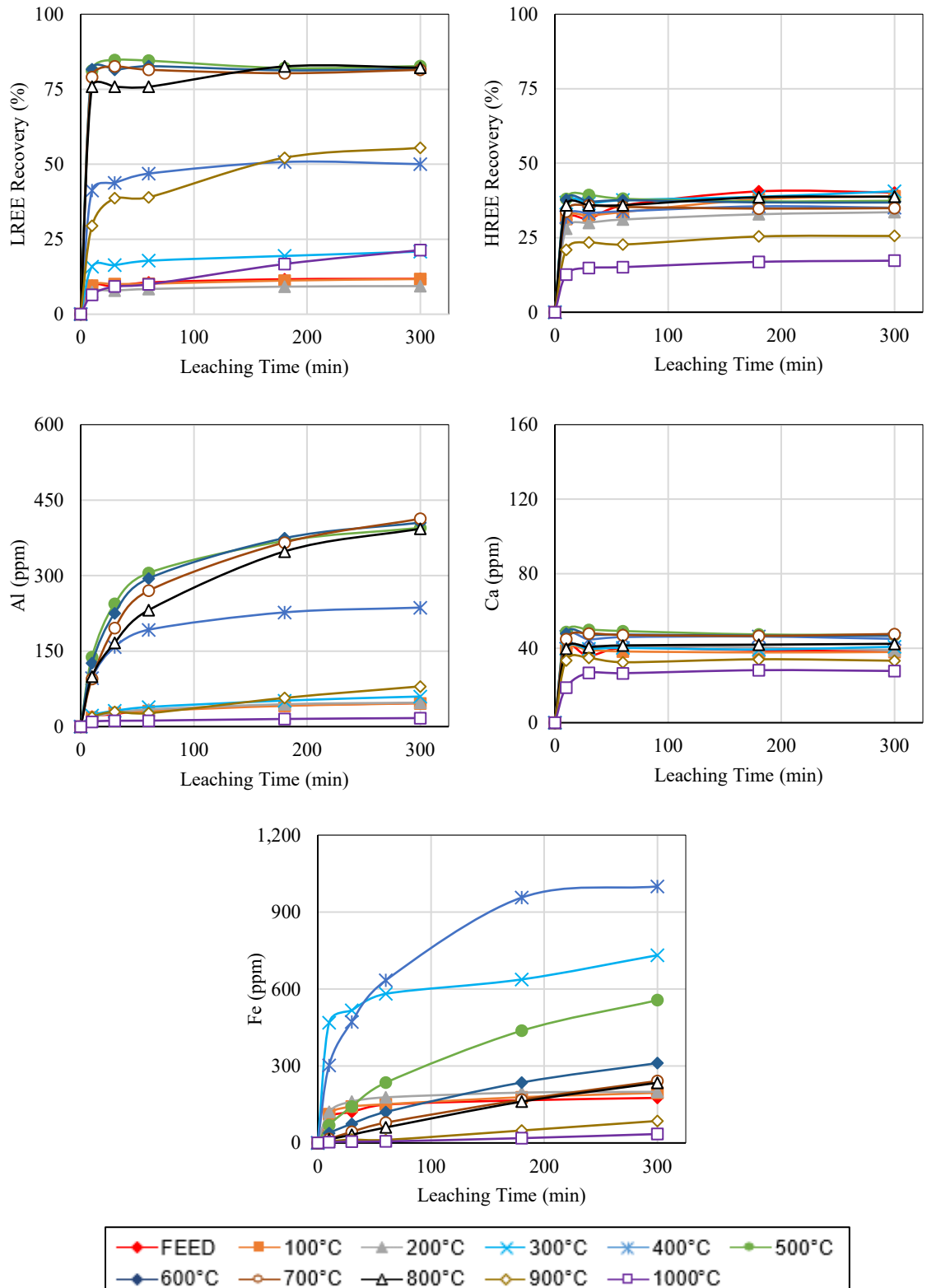


Figure 5.4. Acid leaching test results with 1.2M H₂SO₄ at 75°C for the 2.20 SG sink of West Kentucky No.13 calcined at different temperatures in air.

Calcination for the Fire Clay density fractions had a significant impact on the REE leaching characteristics. The leaching recovery for light and heavy REEs along with the concentration of Al, Ca, and Fe for the calcination products of all the density fractions of Fire Clay at temperatures ranging from 100-1000°C is provided in Figure 5.5, Figure 5.6, Figure 5.7, and Figure 5.8. The LREE recovery was improved significantly for all the density fractionated samples, especially the 1.60 SG float (from 34% to 77%) after high-temperature treatment at 500°C for 2 hours. However, for the other three density fractions, calcination at 600-700°C for 2 hours provided the highest leach recovery. The mineralogy and/or association characteristics of REEs are different in the Fire Clay from the WK-13 material owing to the better leaching kinetics of the former for an untreated sample. Calcination of the Fire Clay material at 600-800°C provides a general increase in the recovery of the REEs. The improvement in REE recovery, however, was not as pronounced as the impact on the WK-13 source. The leaching behavior of the HREEs associated with the heavy density fractions of Fire Clay was found to be unaffected by the high-temperature calcination process.

Based on the calcination results, high-temperature blank calcination was found to significantly affect the recovery of REEs, particularly the light REEs, and increase the concentration of contaminants (Al, Ca, and Fe) in the subsequent leaching unit operation. The benefits in REE leachability for both the coal seams were realized in the 400-800°C temperature range. Significant changes in the leaching behavior of Fe and Al were also observed within the same temperature values. Therefore, a subsequent test program was designed to optimize the input parameters for maximizing REE recovery and minimizing the concentration of contaminants in the leachate by keeping the lower and upper-temperature values at 400°C and 800°C, respectively.

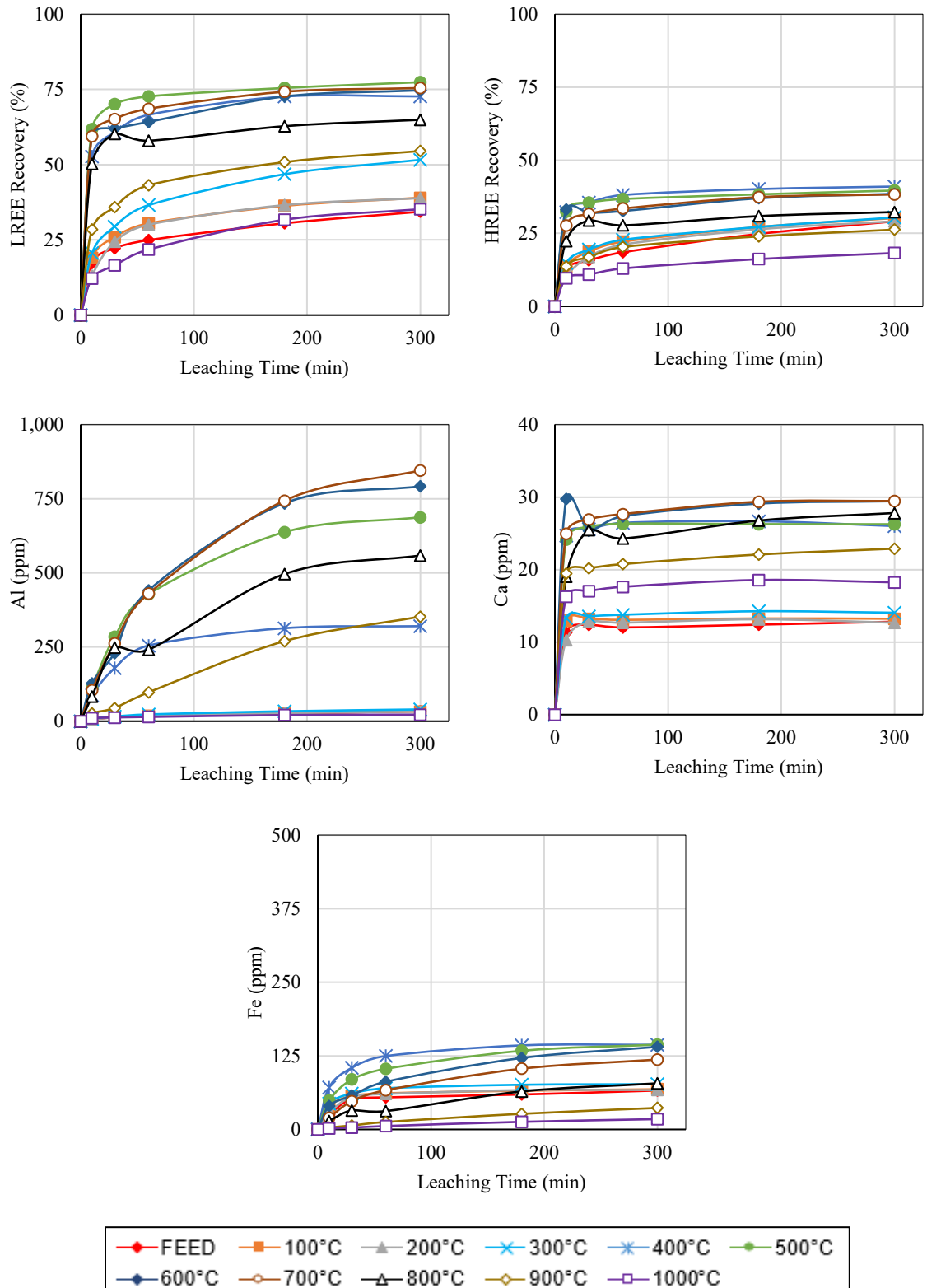


Figure 5.5. Acid leaching test results with 1.2M H₂SO₄ at 75°C for the 1.60 SG float of Fire Clay calcined at different temperatures in air.

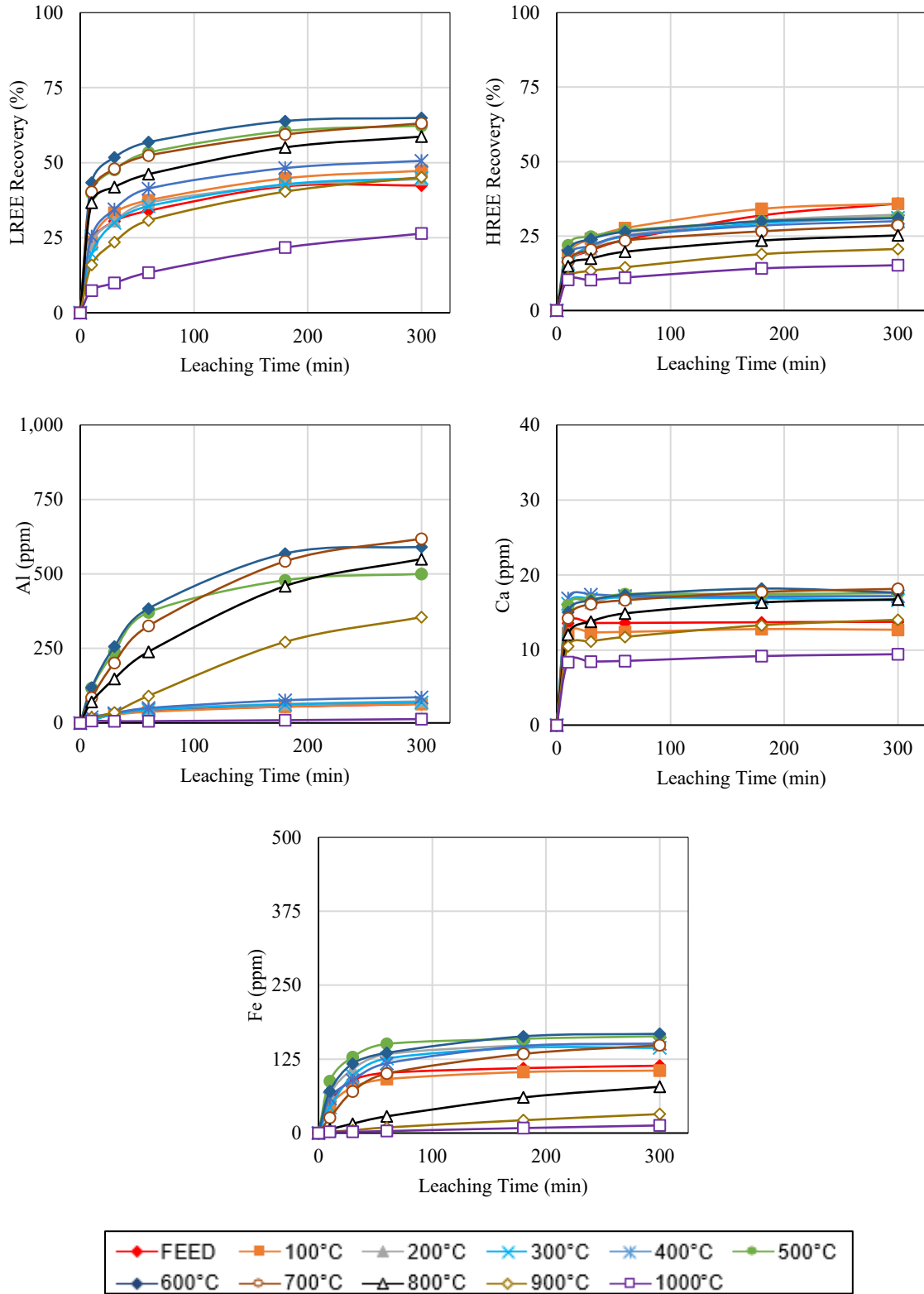


Figure 5.6. Acid leaching test results with 1.2M H₂SO₄ at 75°C for the 1.60x1.80 SG of Fire Clay calcined at different temperatures in air.

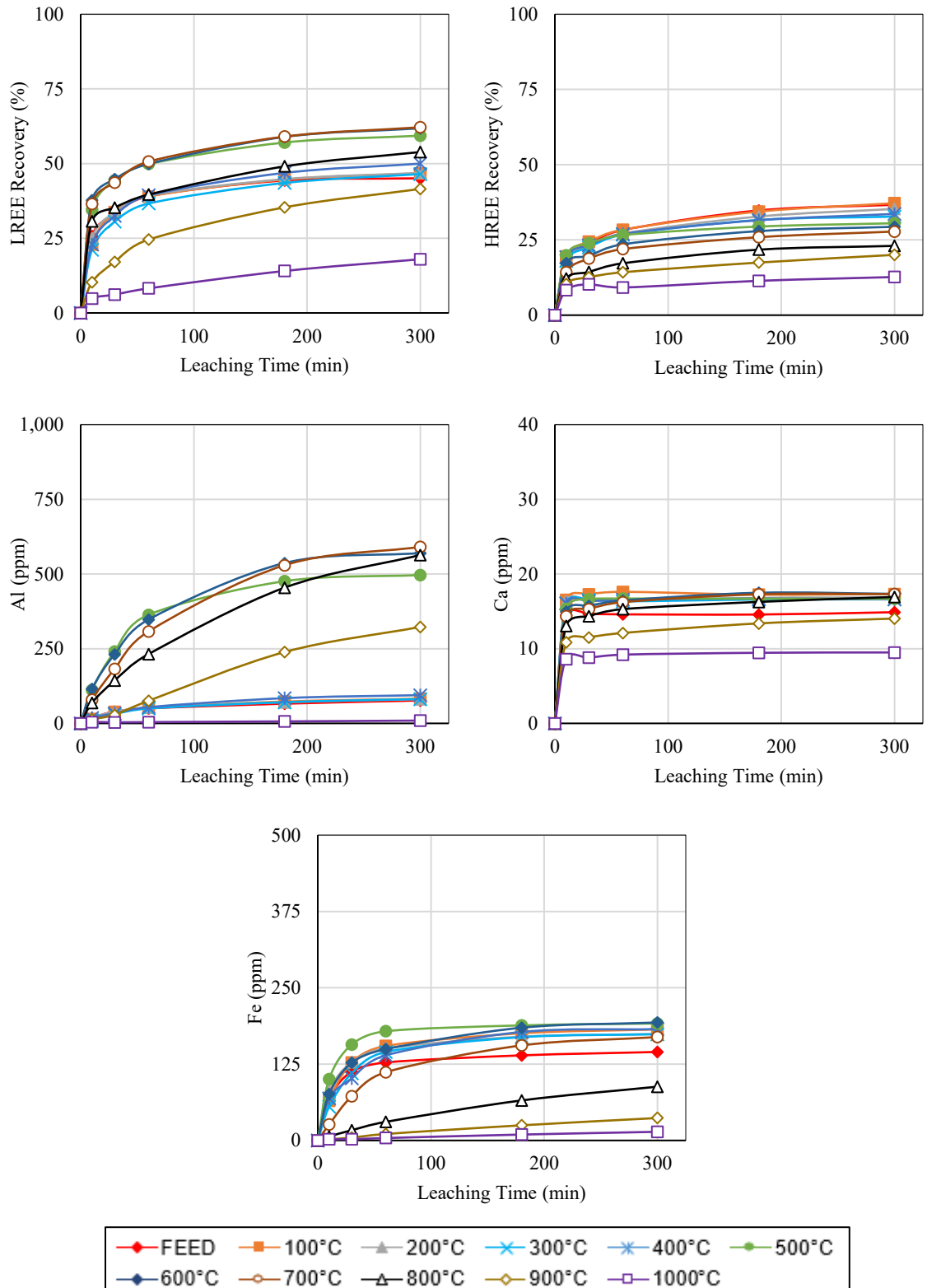


Figure 5.7. Acid leaching test results with 1.2M H₂SO₄ at 75°C for the 1.80x2.20 SG of Fire Clay calcined at different temperatures in air.

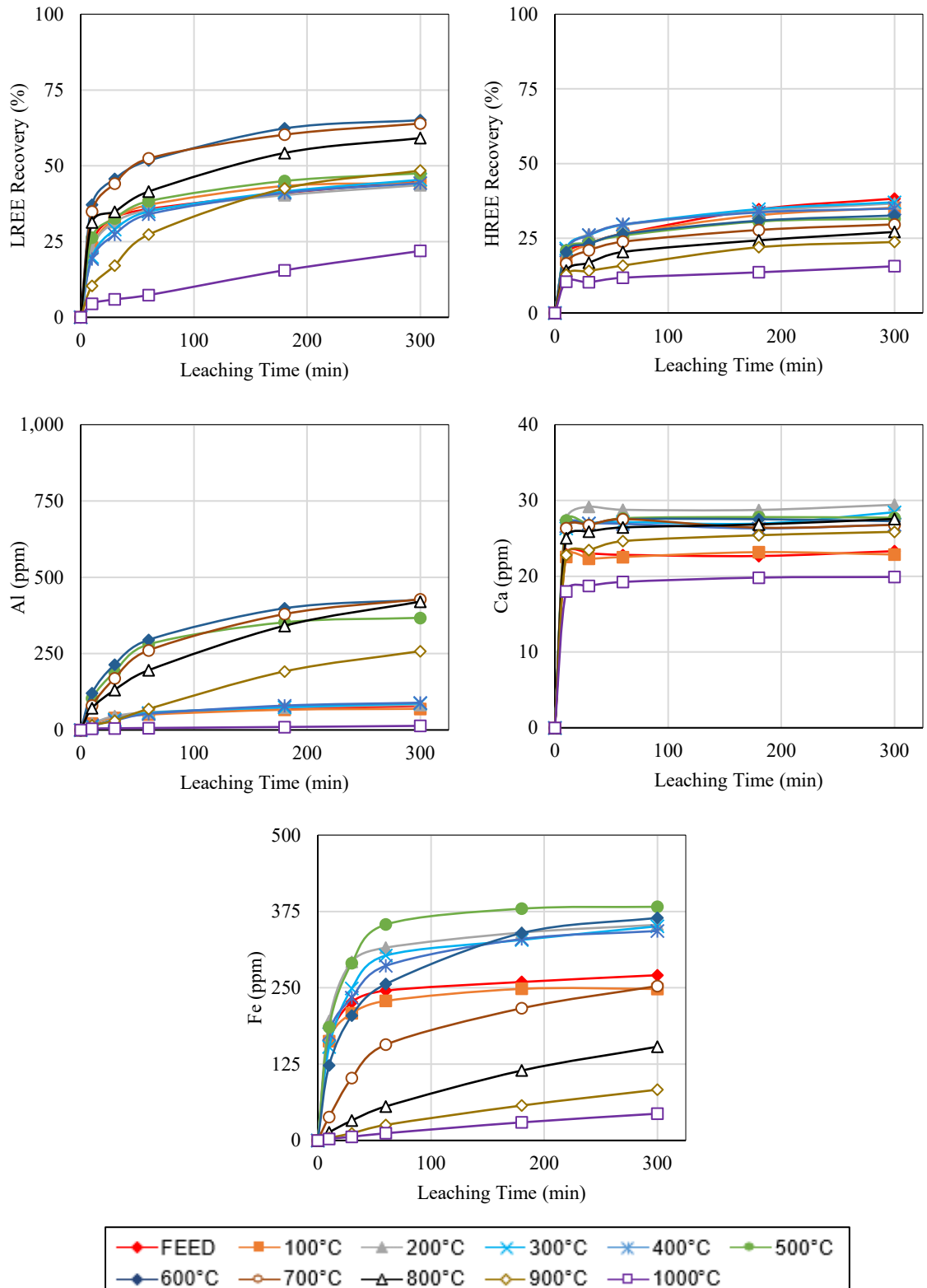


Figure 5.8. Acid leaching test results with 1.2M H₂SO₄ at 75°C for the 2.20 SG sink of Fire Clay calcined at different temperatures in air.

5.3.2 Parametric Optimization Study

The details of the calcination test conditions performed on the 1.6 SG float and 2.2 SG sink fractions of the WK-13 coarse refuse material are provided in Table 5.2. Significant benefits in the recovery of REEs were achieved for the 1.60 SG float fraction as compared to the 2.20 SG sink material at 400°C. The partial removal of organic matter associated with the lighter density fraction allowed for higher LREE and HREE recoveries at 400°C. However, exceptionally high LREE recoveries (>80%) were achieved at high calcination temperatures (600-800°C) for the 2.20 SG sink fraction. The difference in optimum calcination temperatures between the two density fractions could be due to the different modes of occurrence of the REEs.

Empirical models were developed that describe REE recovery as a function of the process parameter values. The 3-dimensional surface plots for the main and interaction effects are provided in Figure 5.9 and Figure 5.10. LREE showed a quadratic relationship with temperature (Figure 5.9.a-i & 5.a-ii). Higher HREE recovery in the 1.6 SG float fraction (Figure 5.9.b-i) as compared to the 2.2 SG sink fraction (Figure 5.9.b-ii) corresponds to an increase in the ash content by calcination and suggests an organic association. The recovery of HREE from calcined products of 2.20 SG sink fraction was marginally increased as compared to the feed but was unaffected by a further increase in temperature. The HREE recovery was found to be within the range of experimental error in the test program (Figure 5.9.b-ii). Thus, about 60% of heavy REEs remained locked in the WK-13 ash material and difficult to leach despite strong acid leaching conditions.

Table 5.2. Input factors and the results of the Box- Behnken experimental design for 1.60 SG float and 2.20 SG sink of West Kentucky No.13.

Run	Temp. (°C)	Heating Rate (°C/min)	Hold Time (min)	TREE (%)	LREE (%)	HREE (%)	Al (ppm)	Ca (ppm)	Fe (ppm)	TREE (%)	LREE (%)	HREE (%)	Al (ppm)	Ca (ppm)	Fe (ppm)
				1.60 SG float						2.20 SG sink					
				20	17	32	7	16	85	16	12	40	47	38	176
1	600	2	0	75	79	61	348	70	1265	79	85	41	356	42	781
2	600	6	60	67	71	52	357	71	731	77	84	37	408	45	564
3	600	6	60	66	71	51	379	74	731	77	83	38	404	45	581
4	600	6	60	73	77	58	410	74	972	77	83	38	401	44	560
5	400	6	120	56	55	57	113	50	1109	34	33	37	91	46	844
6	800	6	0	65	70	49	410	76	368	77	83	39	436	51	321
7	400	2	60	57	56	59	82	43	1039	31	30	36	85	45	995
8	400	6	0	53	54	52	51	26	797	28	27	35	71	43	861
9	600	6	60	66	69	53	385	81	694	75	80	40	381	48	798
10	600	2	120	67	71	54	383	78	817	74	80	37	431	52	869
11	800	2	60	58	62	43	373	69	363	72	78	37	464	53	283
12	800	6	120	57	60	45	352	70	225	72	77	35	429	49	218
13	400	10	60	50	49	52	89	40	775	34	33	36	84	42	841
14	800	10	60	50	53	37	280	73	129	75	81	39	422	50	219
15	600	10	0	64	68	51	346	68	913	72	77	37	382	49	905
16	600	6	60	61	66	48	369	71	935	75	81	39	435	51	682
17	600	10	120	61	64	48	349	76	379	61	64	48	349	76	379

The Pearson linear correlation values for the selected response and input variables are summarized in Table 5.3. Aluminum was found to have a strong positive relationship with temperature for both the density fractions. This can be attributed to the dehydration of clay minerals (kaolinite and Illite) which are the primary source of aluminum and are more leachable at higher temperatures. The decline in Al concentration at 800°C may be due to the conversation of metakaolin to mullite or aluminum-silicon spinel and amorphous silica, which has a lower solubility or due to sintering of clay at high temperatures (Figure 5.10.a-i) [144, 173, 174]. The presence of calcium in the leachate

was due to the trace amounts of calcite present in the WK-13 material. The increase in the concentration of calcium was most likely due to higher calcium content in calcined products (Figure 5.10.b-i & b-ii). Calcite decomposes at 800°C to form calcium oxide. Both of these species have high solubility in acidic solutions [175]. Iron in the feed was found to be present in the form of pyrites. The concentration of iron in the acid leachate shows an inverse relationship with temperature and heating rates. More iron was leached when the sample was treated at lower temperatures for a longer duration of time. The lower temperatures facilitated the formation of more soluble intermediate iron oxides which were converted to α -hematite at higher temperatures which have very low solubility (Figure 5.10.c-i & c-ii) [176]. The heating rate was found to be an insignificant parameter for final concentrations of Al and Ca which suggests that their solubility was driven solely by the setpoint temperature.

Table 5.3. Correlation matrix of the major response variables with the input variables used in the calcination studies of the West Kentucky No.13 sample.

	1.60 SG float					2.20 SG sink				
	LREE	HREE	Al	Ca	Fe	LREE	HREE	Al	Ca	Fe
Temperature	0.31	-0.65	0.75	0.73	-0.72	0.78	0.33	0.86	0.69	-0.87
Heating Rate	-0.35	-0.43	-0.08	-0.03	-0.35	0.00	0.00	-0.01	-0.04	-0.09
Hold Time	-0.20	-0.15	0.03	0.20	-0.22	0.00	-0.37	0.08	0.28	-0.08

From the results, it can be concluded that temperature is the most important parameter among the process parameters evaluated. The oxidative versus reductive environment effects will be presented and discussed in Chapter 7. The heating rate of the sample has an insignificant effect on the leachability of REEs as well as the concentration of contaminants. The hold time or residence time, however, plays a significant role, especially at high setpoint temperatures. A high temperature coupled with long residence times allows for the sintering of particles which subsequently reduces the REE recoveries [144, 173].

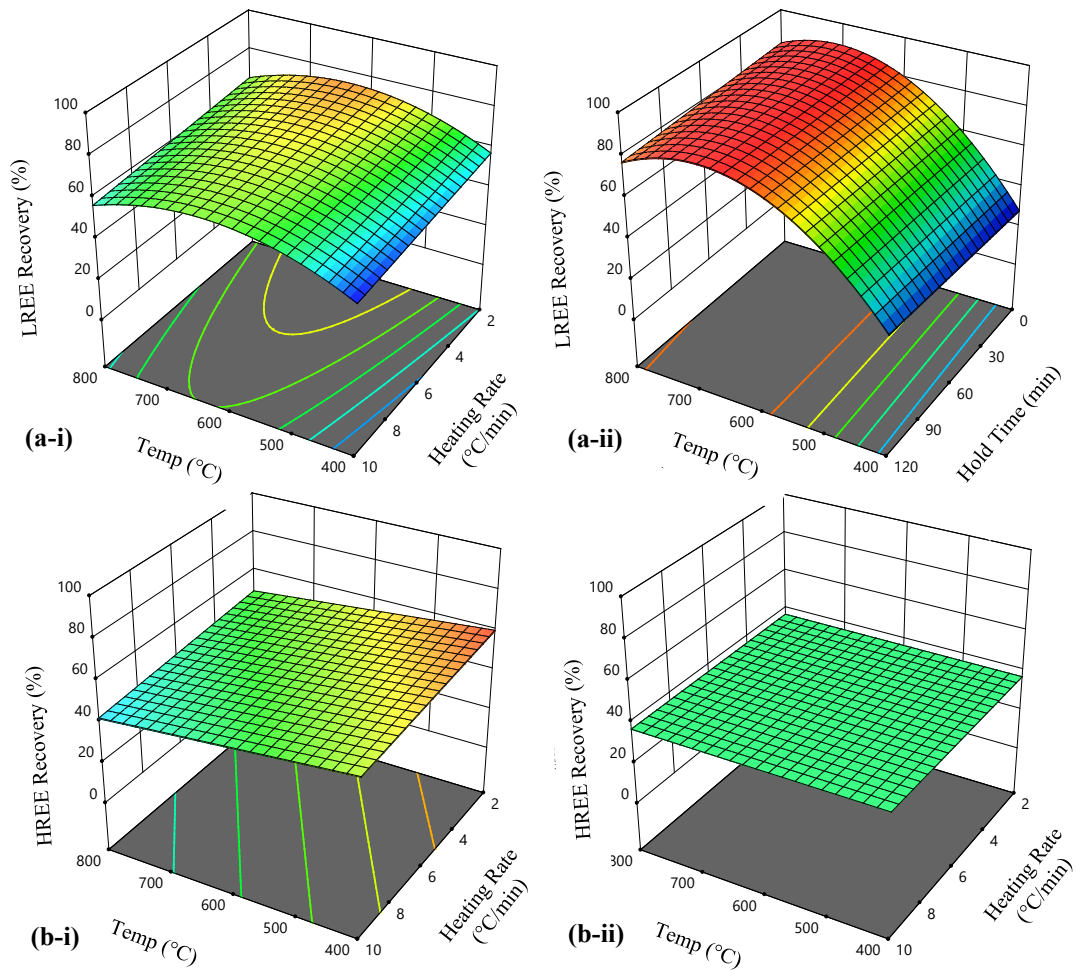


Figure 5.9. Response surface for the association of (a) LREE and (b) HREE recovery (%) of the calcined (i) 1.60 SG float and (ii) 2.20 SG sink fraction of West Kentucky No.13 as a function of main and interaction effects of the significant variables

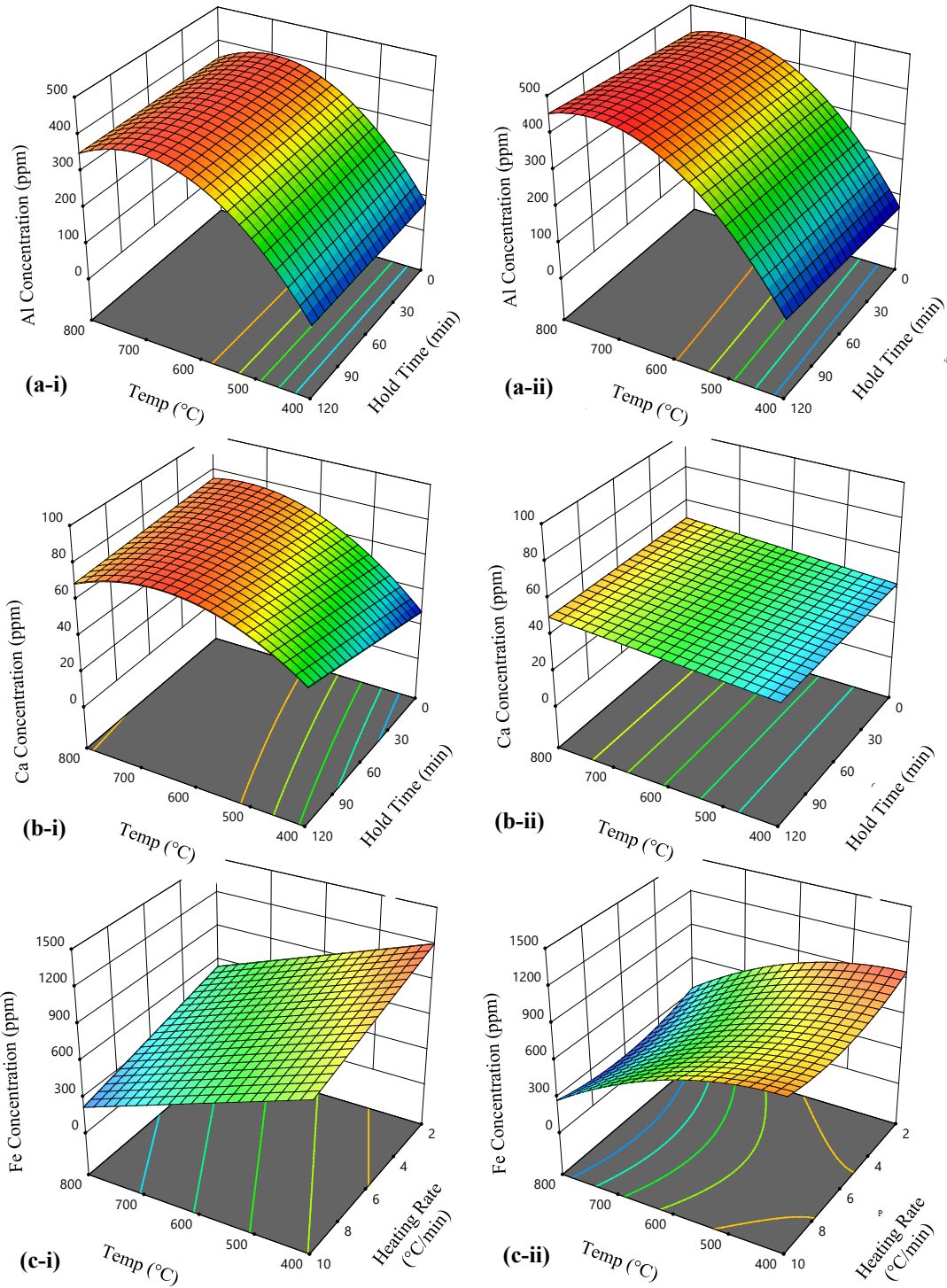


Figure 5.10. Response surface for the association of (a) Al, (b) Ca, and (c) Fe concentration of the calcined (i) 1.60 SG float and (ii) 2.20 SG sink fraction of West Kentucky No.13 as a function of main and interaction effects of the significant variables.

The optimization module of the Stat-Ease software was used to search for a combination of levels of inputs that can simultaneously satisfy the criteria placed on each of the response variables. The optimization algorithm uses the empirical models developed during the data analysis of the Box-Behnken design of experiments. The input factors are set to be “in range” and the combination of maximization/minimization criteria are assigned to the responses. Numerical optimization then uses the models to search the factor spaces for the best tradeoffs to achieve the desired goals. Considering the results from Table 5.4, the recovery of highly valued HREEs can be maximized at 400°C with a minimum concentration of Al and Ca in the pregnant leach solution. This set of input parameter values, however, allows for maximum contamination of Fe in the system and lower LREE recovery. Additional operational benefits can be realized if the iron in the calcined products can be removed by magnetic separation or by removing the pyrites in the feed using a density separator or froth flotation. The optimum conditions to maximize TREE recovery and minimize the total contaminants can be achieved at 776°C and a hold time of 84 minutes.

Table 5.4. Set of optimum parameter values for the desired goals of the response variables from the Box-Behnken Design and the value of other output variables for 1.60 SG float of West Kentucky No.13 (Cont.=Total Contaminants).

	Temp (°C)	Heating Rate (°C/min)	Hold Time (min)	TREEs (% Recovery)	LREEs (% Recovery)	HREEs (% Recovery)	Al (ppm)	Ca (ppm)	Fe (ppm)	Total Cont. (ppm)	Probability
Max LREEs	629	2	71	71	75	54	386	77	833	1296	0.87
Max HREEs	400	2	60	58	58	60	84	40	1210	1334	0.95
Max TREEs	616	2	10	71	75	54	379	72	854	1305	0.91
Max Al	689	2.5	110	69	73	52	400	78	710	1188	0.97
Max Ca	650	9	120	63	67	47	394	79	509	982	0.97
Max Fe	400	2	60	58	58	60	84	40	1210	1334	0.95
Min Al	400	2	60	58	58	60	84	40	1210	1334	0.91
Min Ca	400	6	0	54	54	57	84	28	1049	1161	0.97
Min Fe	800	10	60	53	57	42	354	72	230	656	0.91
Max TREEs Min Cont.	776	2	84	64	68	50	371	73	591	983	0.57

Similarly, optimization studies were conducted for the 2.20 SG sink fraction of the WK-13 (Table 5.5). The concentration of Al and Ca in the leachate was found to be maximum at higher temperatures. LREE was also found to be maximum in the higher temperature range. A TREE recovery of 79% could be achieved with a temperature set point of 800°C and a contaminant concentration of 983 ppm in solution. The high temperature facilitates low Fe dissolution in the leachate while maximizing the LREE recovery. While the optimum conditions for maximum REE recovery for both the coals require high temperatures (775-800°C), the 1.60 SG float fraction was found to need a higher hold time (residence). This was required for the complete removal of the combustible content and liberation of the REEs micro dispersed in the mineral matter contained in clean coal.

Table 5.5. Set of optimum parameter values for the desired goals of the response variables from the Box-Behnken Design and the value of other output variables for 2.20 SG sink of West Kentucky No.13 (Cont.=Total Contaminants).

	Temp (°C)	Heating Rate (°C/min)	Hold Time (min)	TREEs (% Recovery)	LREEs (% Recovery)	HREEs (% Recovery)	Al (ppm)	Ca (ppm)	Fe (ppm)	Total Cont. (ppm)	Probability
Max LREEs	626	9	3.5	77	85	38	409	48	663	1120	1.00
Max HREEs	400	10	60	32	31	38	83	44	904	1031	0.40
Max TREEs	624	3.2	16	79	84	38	410	48	701	1159	1.00
Max Al	789	2.3	55	76	81	38	442	51	355	848	1.00
Max Ca	626	8.3	11.4	78	85	38	410	48	642	1100	0.39
Max Fe	400	2	60	32	31	38	83	44	970	1097	0.74
Min Al	400	6	0	29	28	38	66	44	833	943	0.95
Min Ca	400	6	0	29	28	38	66	44	833	943	0.68
Min Fe	800	6.6	13	76	82	38	425	51	206	749	0.93
Max TREEs Min Cont.	800	2	3	79	83	38	423	51	343	749	0.95

The test conditions and respective output values for the 1.60 SG float and 2.20 SG sink fraction of Fire Clay material are provided in Table 5.6. The untreated density fractions (feed) of the Fire Clay had higher LREE and HREE recovery values as compared to their WK-13 counterparts. The effect of calcination on the 1.60 SG float fraction was found to be more profound than the 2.20 SG sink. The higher TREE recoveries result from the combustion of the carbon matter present in the sample which liberates or oxidizes the REEs contained in the organic matrix. On the other hand, a majority of REEs remain insoluble in the 2.20 SG sink of the Fire Clay material despite calcination treatment and strong acid leaching conditions. This difference in the leaching behaviors between the two feed sources suggests a very different mode of occurrence and association of the REEs in the mineral matrix. The LREEs in the 1.60 SG float show an improvement of about 50% points when calcined at 600-800°C with long residence times. Like the WK-13 material, the HREEs were relatively inert to the thermal treatment as the maximum HREE recovery obtained from the 1.60 SG float fraction was about 45%. Heating rate and hold time were found to be insignificant for all the response variables associated with the 2.20 SG sink material of Fire Clay. The lower recovery values for the Fire Clay material suggest that a large fraction of REEs in the Fire Clay 2.20 SG sink material are difficult to decompose under the investigated set of conditions.

The Pearson linear correlation values for the selected response and input variables are summarized in Table 5.7. Like WK-13, LREEs and Al show a strong positive correlation with temperature for both the density fractions. The HREEs and Fe in the 2.20 fraction are negatively correlated with temperature. In the absence of pyrite, the absolute concentration of Fe in the leachate is about 25% as compared to its corresponding fraction in WK-13 material. Figure 5.11.a-i & Figure 5.11.a-ii show that LREEs in both the density fractions have a strong positive association with the first and second-order terms of temperature.

Table 5.6. Input factors and the results of the Box- Behnken experimental design for 1.60 SG float and 2.20 SG sink of Fire Clay.

Run	Temp. (°C)	Heating Rate (°C/min)	Hold Time (min)	TREE (%)	LREE (%)	HREE (%)	Al (ppm)	Ca (ppm)	Fe (ppm)	TREE (%)	LREE (%)	HREE (%)	Al (ppm)	Ca (ppm)	Fe (ppm)
				1.60 SG float						2.20 SG sink					
Untreated Feed				34	34	29	34	13	66	44	45	38	79	23	271
1	600	2	0	70	74	41	779	28	188	56	60	32	429	29	338
2	600	6	60	69	73	40	826	28	149	53	57	28	444	30	339
3	600	6	60	70	74	41	898	29	158	49	53	27	411	28	313
4	600	6	60	70	75	41	871	29	148	53	57	28	430	28	320
5	400	6	120	63	66	42	149	24	156	36	38	29	85	25	289
6	800	6	0	68	73	39	931	30	110	52	56	26	349	27	190
7	400	2	60	63	66	41	99	21	120	43	44	38	92	26	284
8	400	6	0	55	58	35	68	17	96	40	41	34	82	25	262
9	600	6	60	73	77	43	903	29	165	61	65	37	329	27	283
10	600	2	120	77	81	47	978	30	170	56	60	29	339	27	282
11	800	2	60	78	81	49	977	30	94	54	58	26	407	28	162
12	800	6	120	70	74	40	986	30	90	51	55	26	399	27	153
13	400	10	60	64	67	43	121	22	131	40	42	32	83	26	302
14	800	10	60	64	68	35	968	30	87	58	62	29	393	27	159
15	600	10	0	71	75	41	879	29	157	52	56	30	344	26	335
16	600	6	60	71	76	41	962	30	151	54	58	29	381	27	329
17	600	10	120	69	74	38	626	27	132	56	60	30	368	27	298

Table 5.7. Correlation matrix of the major response variables with the input variables used in the calcination studies of Fire Clay sample.

	1.60 SG float					2.20 SG sink				
	LREE	HREE	Al	Ca	Fe	LREE	HREE	Al	Ca	Fe
Temperature	0.60	0.06	0.86	0.82	-0.35	0.75	-0.62	0.79	0.50	-0.64
Heating Rate	-0.26	-0.54	-0.05	-0.03	-0.19	-0.03	-0.13	-0.05	-0.28	0.04
Hold Time	0.23	0.3	0.02	0.15	0.00	0.00	-0.20	0.00	-0.12	-0.13

The 3-dimensional response surface of the contaminant ions in Figure 5.12 shows a quadratic relationship of Al and Fe with temperature. Calcium concentration in the leachate was within the range of experimental error and variability in the feed.

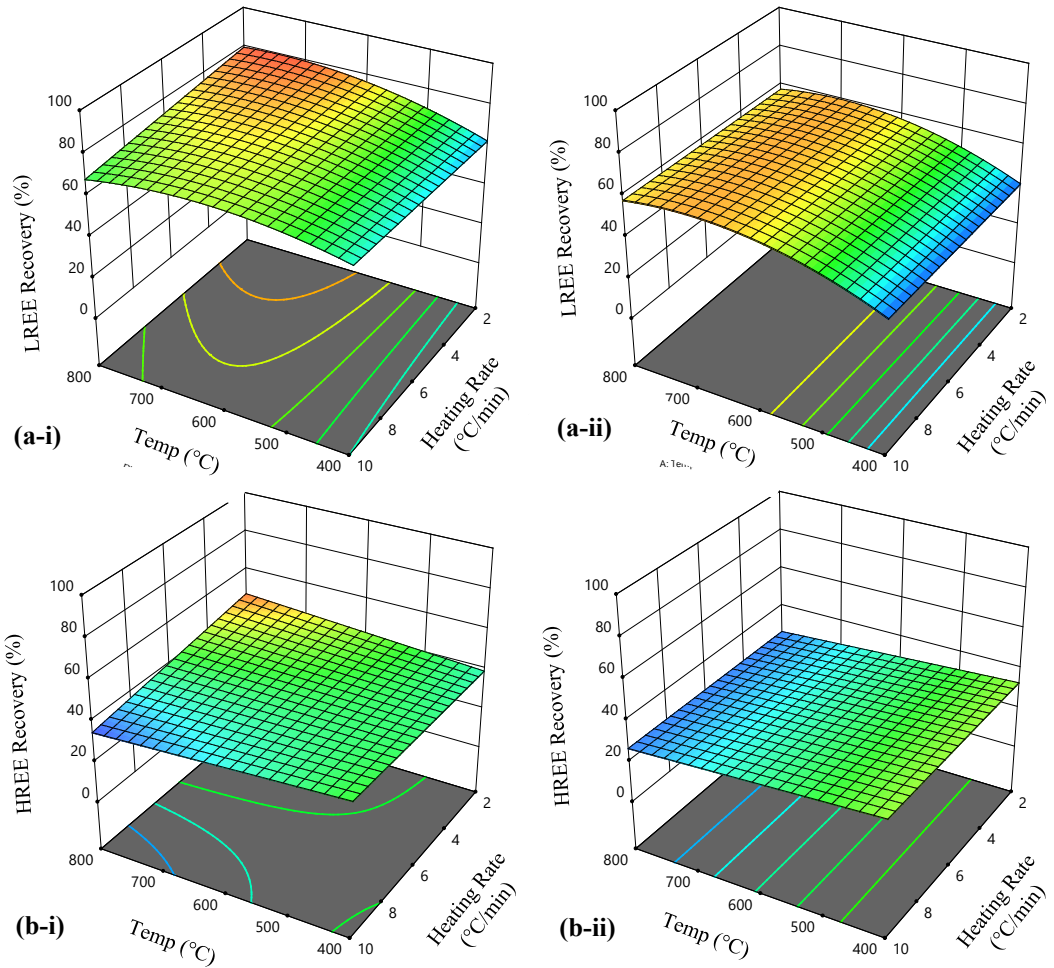


Figure 5.11. Response surface for the association of (a) LREE and (b) HREE recovery (%) of the calcined (i) 1.60 SG float and (ii) 2.20 SG sink fraction of Fire Clay as a function of main and interaction effects of the significant variables

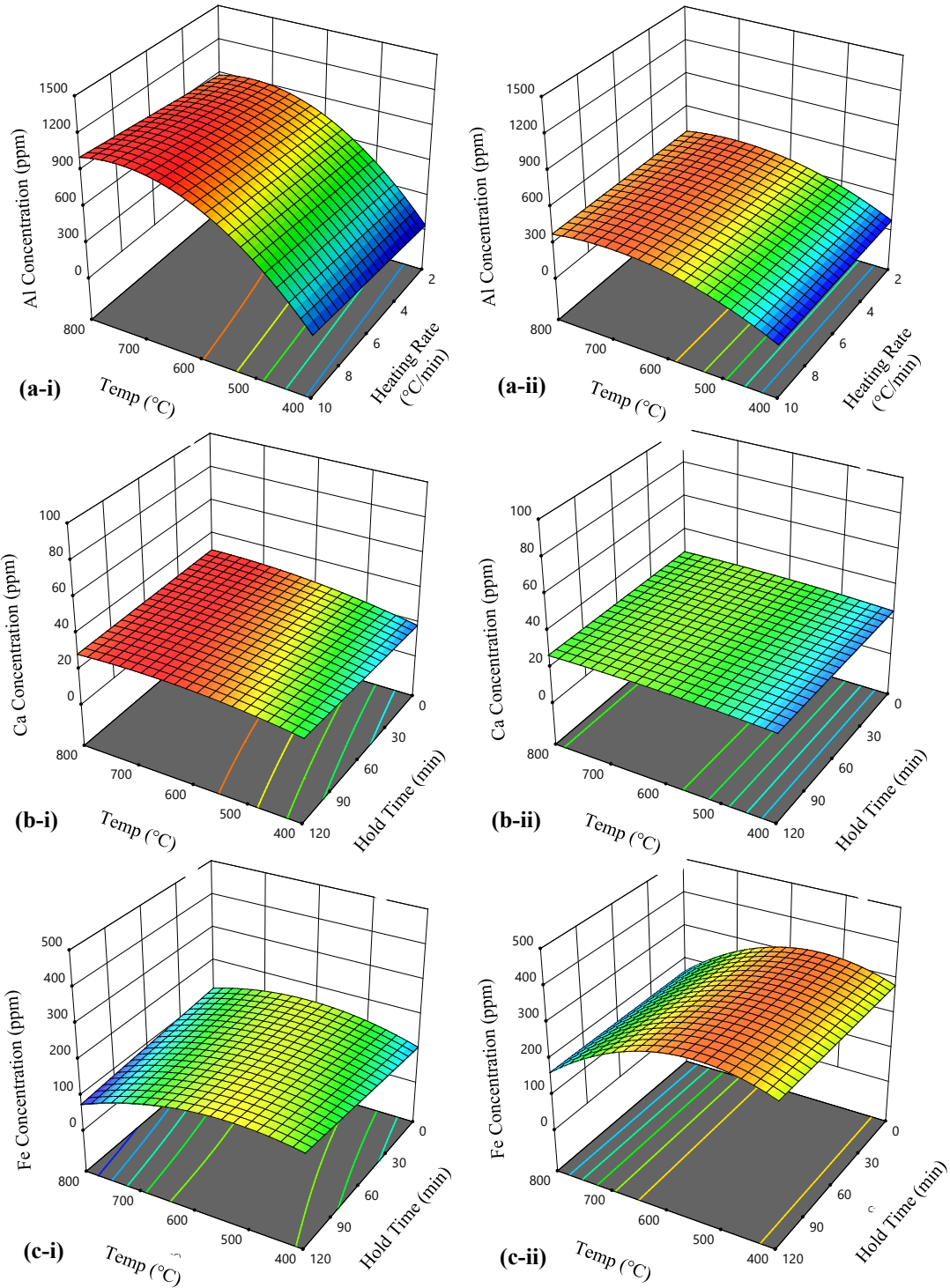


Figure 5.12. Response surface for the association of (a) Al, (b) Ca, and (c) Fe concentration of the calcined (i) 1.60 SG float and (ii) 2.20 SG sink fraction of Fire Clay as a function of main and interaction effects of the significant variables.

Due to the low sulfur content in the Fire Clay material, the contamination due to Fe was very small as compared to WK-13 material. Additionally, as the clays were not fully dehydrated, a small amount of Al was leached into the solution. Also, high TREE recoveries can be achieved at relatively lower temperatures keeping the contaminant ions in check. Although to achieve high LREE and HREE recovery values temperatures, >770°C are required for the 1.60 SG float (Table 5.8). Similarly, 700°C allows for high TREE recoveries for the 2.20 SG sink fraction. The association of Fe in the Fire Clay sample is possible as a substitution for aluminum in clays and therefore maximum Fe in solution occurs at temperatures that decompose clay minerals by dehydration thereby providing access to the interlayers (Table 5.9). Iron in aluminosilicate clays has also been found to be present as impurities of iron oxide [140, 177, 178].

Table 5.8. Set of optimum parameter values for the desired goals of the response variables from the Box-Behnken Design and the value of other output variables for 1.60 SG float of Fire Clay (Cont.=Total Contaminants).

	Temp (°C)	Heating Rate (°C/min)	Hold Time (min)	TREEs (% Recovery)	LREEs (% Recovery)	HREEs (% Recovery)	Al (ppm)	Ca (ppm)	Fe (ppm)	Total Cont. (ppm)	Probability
Max LREEs	773	2	19	76	80	44	934	31	121	1049	1.00
Max HREEs	800	2	120	76	80	52	1119	29	75	1207	0.59
Max TREEs	791	2.5	1	75	79	43	894	31	119	1006	1.00
Max Al	727	3.88	44	74	78	43	999	30	132	1114	1.00
Max Ca	737	9.3	37	67	72	37	1009	30	130	1194	1.00
Max Fe	524	6.4	120	69	73	42	646	28	164	822	0.76
Min Al	400	10	81	63	66	41	45	22	133	217	1.00
Min Ca	400	6	0	61	64	39	99	19	106	256	0.89
Min Fe	798	8.5	90	66	71	37	917	30	86	1056	1.00
Max TREEs Min Cont.	407	10	120	63	66	41	15	24	148	181	0.76

Table 5.9. Set of optimum parameter values for the desired goals of the response variables from the Box-Behnken Design and the value of other output variables for 2.20 SG sink of Fire Clay (Cont.=Total Contaminants).

	Temp (°C)	Heating Rate (°C/min)	Hold Time (min)	TREEs (% Recovery)	LREEs (% Recovery)	HREEs (% Recovery)	Al (ppm)	Ca (ppm)	Fe (ppm)	Total Cont. (ppm)	Probability
Max LREEs	694	6.9	82	56	60	28	424	28	267	719	0.57
Max HREEs	No solution										
Max TREEs	689	5.6	30	56	60	29	423	28	271	722	0.55
Max Al	700	9.4	57	56	60	28	424	28	263	715	0.94
Max Ca	672	4.2	47	56	60	29	421	28	282	731	0.61
Max Fe	534	9.8	111	51	55	31	321	27	325	673	0.92
Min Al	400	10	60	40	41	33	85	26	284	395	0.99
Min Ca	400	6	120	40	41	33	85	26	284	395	0.87
Min Fe	800	6	120	54	58	27	387	27	166	580	0.93
Max TREEs	800	6	0	54	58	27	387	27	166	580	0.51
Min Cont.											

In addition to the recovery of REEs and the concentration of contaminant elements in the calcination products of the two feed sources, an artificial variable called ‘Relative Concentration’ (RC), which is the ratio of the total concentrations of contaminant ions to REEs was created. RC is defined by the following expression:

$$\text{Relative Concentration (RC)} = \text{Total Contaminants} / \text{Total REE} \quad (\text{Eq. 5-1})$$

Relative Concentration is a measure of selectivity for the dissolution of REEs and rejection of the bulk of the contaminants. A lower RC value would result in higher REE ions in the solutions and relatively lower contaminant ions. Empirical models were developed for RC associated with the 1.60 SG and 2.20 SG sink fractions of the two feed sources. The actual and predicted values for the artificial variable are provided in Figure 5.13. The linear distribution of the actual and predicted values along with high R² and adjusted R² values suggest that the models were an excellent fit for the experimental data. The model was minimized to obtain the highest selectivity for each of the two density fractions for both sources and the results are presented in Table 5.10. The values for

maximum selectivity correlate well with the findings from the optimum set of parameter values for WK-13 (Table 5.4 and Table 5.5) and Fire Clay (Table 5.8 and Table 5.9).

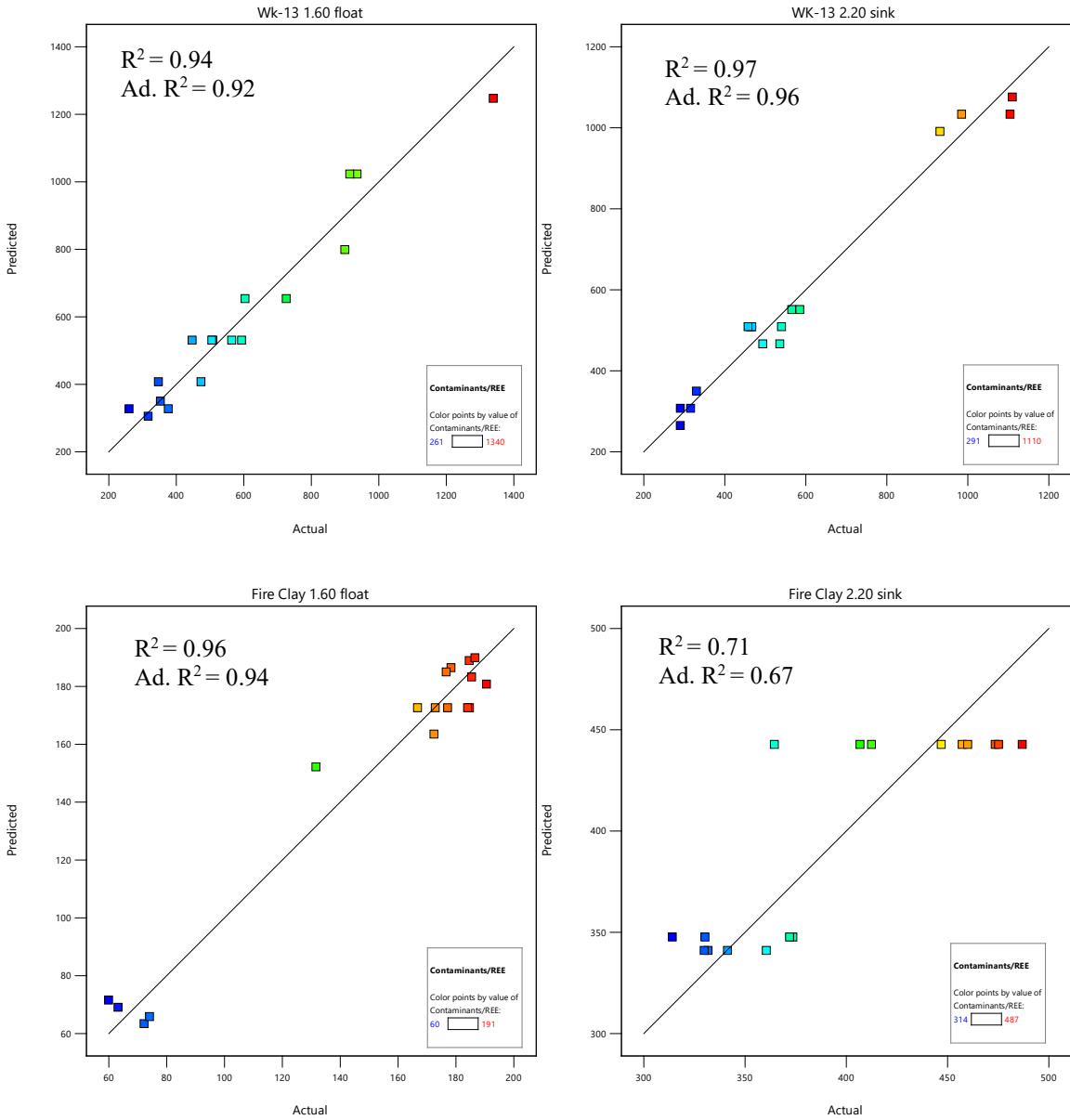


Figure 5.13. Actual vs predicted plots for the 1.60 SG float and 2.20 SG sink fractions of West Kentucky No.13 and Fire Clay, respectively.

Table 5.10. The minimum values for artificial variable Relative Concentration (RC) for achieving maximum selectivity for REE recovery from the two coal sources.

	Temp (°C)	Heating Rate (°C/min)	Hold Time (min)	TREEs (% Recovery)	LREEs (% Recovery)	HREEs (% Recovery)	Al (ppm)	Ca (ppm)	Fe (ppm)	Relative Concentration	Probability
West Kentucky No.13											
1.60 SG float	771	5	120	61	65	47	375	73	480	302	0.96
2.20 SG sink	799	10	86	74	78	38	445	51	261	289	1.00
Fire Clay											
1.60 SG float	404	8.5	88	62	65	41	63	22	135	60	1.00
2.20 SG sink	800	2	60	54	58	27	387	27	166	341	0.84

5.4 Conclusions

Calcination optimization tests using the Box-Behnken design of experiments were separately performed on the 1.60 SG float and 2.20 SG sink fractions of WK-13 and Fire Clay coal refuse material. To assess leachability, a standard test was utilized that used a 1.2M sulfuric acid solution as the lixiviant at 75°C for 5 hours with a 1% w/v solid concentration. The phase transformations of the common minerals found in coal deposits such as kaolinite, pyrite, and calcite resulted in the variability in leaching characteristics. For the low-density fractions, REE leachability was directly related to the removal of combustible content and liberation of the encapsulated REE minerals. For the high ash density fractions, the dehydration of clays and the oxidation of pyrites, and the decomposition of calcite contributed to the improvements in REE recovery.

The calcination performance generally increased with temperature from 500-800°C but declined for 900-1000°C due to sintering of the clays that hinders REE dissolution. Al concentration was found to be dependent primarily on temperature. At higher calcination temperatures higher amounts of Al were dissolved in the acid solution. Ca concentration due to the high reactivity of its parent minerals (calcite and calcium oxide) was high and remained unaffected by thermal activity. The optimum temperature to maximize total REE leaching recovery for WK-13 refuse material was found to be 616°C and 624°C for the 1.60 SG float and 2.20 SG sink fractions, respectively. However,

higher temperature values of 776°C and 800°C were observed when maximizing TREE recovery and minimizing total contaminant ion concentration simultaneously in the leachate. The benefits of calcinating at higher temperatures correspond to a -30% and -50% change in Fe concentration in 1.60 SG float and 2.20 SG sink fraction. This significant reduction was possibly due to the conversion of pyrites to α -hematite at higher temperatures.

The optimum temperature for maximizing the total REEs recovery from the Fire Clay material was found to be 791°C and 689°C for the 1.60 SG float and 2.20 SG sink fractions, respectively. The maximum TREE recovery from the 2.20 SG sink fraction was about 56% suggesting the majority of REEs especially HREEs in the high-density rock recovered from the Fire Clay seam is hard to leach. These locked REEs possibly occur as finely dispersed REE minerals that require the use of chemical additives for liberation during the calcination process. For optimizing the REE recovery and contaminant concentration, the best approach for the 1.60 SG fractions was thermal treatment at 407°C minimized the dissolution of Al from the clays. Calcinating the 2.20 SG sink fraction at 800°C provides the tradeoff between the operational gains of low contamination and losses on potential REE recovery. A cost-based analysis to compare the effect of calcination performance at 400°C and 800°C would provide economic insights into the merits of the calcination temperatures.

CHAPTER 6. PROCESS DEVELOPMENT FOR REMOVAL OF IRON FROM FEED

6.1 Introduction

Since the release of the U.S. Department of Energy Critical Mineral Strategy in 2011, coal sources have been extensively investigated as a potential resource for the extraction of REEs. The REEs in all major U.S. coal deposits have been characterized and efforts have been made to concentrate and/or extract REEs from coal-derived by-products such as plant reject, fly ash, bottom ash, and acid mine drainage [3-5, 9, 11, 78, 146, 160, 161]. The conventional REE minerals are primarily concentrated by physical mineral processing techniques such as gravity separation and froth flotation and are subsequently extracted by hydrometallurgical processes [7, 19, 20]. However, the varied mineralogy and ultrafine particle size of the REEs associated with coal limit the use of standard physical separation unit operations and rely largely on hydrometallurgical extraction [6, 11, 79]. Although, successful processes have been developed to produce a high-grade REE product from a coal-based feed by leaching, solvent extraction, and selective precipitation; the high reagent costs possess significant challenges in their economic viability.

The most critical aspect of hydrometallurgical extraction of REEs is their concentration in the PLS. However, the concentration of contaminant ions in the PLS is equally if not more vital as their leaching behavior influences the ionic strength of the lixiviants and can result in lower REE recoveries. For coal-based leachates, the primary contaminants are aluminum, calcium, and iron. As the REEs exhibit similar chemical characteristics, their extraction requires the exploitation of subtle differences in basicity resulting from the difference in their ionic radius. Trivalent metal ions, Al^{+3} and Fe^{+3} , have been found to unfavorably affect the precipitation efficiency of REEs [84]. Calcium when present in a sulfate system can precipitate as gypsum [$\text{CaSO}_4 \cdot 2\text{H}_2\text{O}$] and allow for co-precipitation of REE ions on its surface [15]. Therefore, the ratio of contaminants to the total REE concentration influences the extraction efficiency and ultimately the cost of solvent extraction and selective precipitation processes. The higher ratios tend to negatively impact the purity of the final product and require higher acid costs in solvent

extraction stripping and higher base costs in selective precipitation. A low concentration of contaminant ions in the hydrometallurgical circuit will eliminate the need for multistage solvent extraction, reduce chemical consumption and produce a higher-grade product [61].

Calcination of the coal-based feedstock is effective in improving the leaching recoveries and reaction kinetics of the REEs [17, 36, 91]. The benefits are obtained by converting the REEs to more soluble forms and/or by liberating the REE-minerals encapsulated within the mineral matter. The high-temperature calcination pretreatment however also oxidizes the gangue minerals and allows for the higher dissolution of contaminant ions primarily aluminum, calcium, and iron in the PLS [84]. Al and Fe are primarily associated with aluminosilicate clays and pyrites found as major minerals in coal. Calcium on the other hand originates from trace quantities of calcite found in coal beds. Coal deposits with high pyrite content contain appreciable amounts of both massive and fine-grained pyrites which are primarily differentiated by the size of mineralization [122]. While massive pyrite can be removed from the coal by washing, the framboidal pyrites due to their small particle size are not efficiently removed [123]. These pyrite framboids are responsible for iron contamination in the PLS and are a common host to trace elements such as Pb, As, Cd, and REEs [123, 179]. Because framboidal pyrite is fine-grained and pyrites exhibit paramagnetic properties, traditional separation methods have very little applicability. This work aims to characterize the pyrite present in coarse coal refuse from a bituminous coal source which is a potential feedstock for REE extraction and has over 250 ppm of REEs. The objective of the paper is to enhance the magnetic susceptibility of a pyrite-rich material by calcination and removal of iron by magnetic separation. Previously, studies investigating the phase transformations of coal pyrites have been performed. However, attempts to remove iron from the calcined products of coal for hydrometallurgical extraction of REEs have not been undertaken. The hypothesis for the potential benefits of such a process are:

1. Reduction of the concentration of contaminant ions in the PLS for economic benefits in the downstream concentration steps;

2. Benefits in the operational, environmental, and economical performance of the calcination operation;
3. Identification of a possible mode of association of REEs with pyrites;
4. The capture of SO₂ in the flue gas for sulfuric acid production.

6.2 Materials and Methods

6.2.1 Materials

Coal from the WK-13 seam located in the Illinois Coal Basin is extracted using room-and-pillar mining and treated in a coal preparation plant to produce a clean coal product that meets ash, sulfur, and heating value specifications. At a mining operation in western Kentucky, USA, a representative coarse refuse sample (75- mm x 0.15 mm) was collected in 18-kg increments using a sweep-belt sampler over a three-hour operating period. The sample was density fractionated using a lab-scale float-sink system using a magnetite-based medium having a specific gravity (SG) of 2.20. The 2.20 SG sink fraction was wet screened to remove the entrained magnetite, air-dried, and finally pulverized to finer than 180 µm using a jaw crusher and a hammer mill (Figure 6.1). This material, which was observed to be rich in pyrite, was used as the feed source for calcination and acid leaching tests. The WK-13 seam is relatively thick (2.4-m), which limits the host rock dilution during the extraction process. Therefore, the 2.20 SG sink fraction primarily originated from parting material within the coal seam. In previous studies, this parting material has been reported to contain a high concentration of REEs [61, 180]. Trace metal grade sulfuric acid was purchased from Thermo Scientific, USA, and was used to prepare 1.2M sulfuric acid solution by dilution with deionized water (ASTM D1193-06) for acid leaching tests.

The 2.20 SG sink density fraction was predominantly composed of inert ash material with very low inherent moisture content. The 16% combustible content possibly originated from the total sulfur content from pyrites and other sources along with carbonaceous shale which occurred as out-of-seam dilution. The thermal decomposition of pyrites occurs at 300-400°C. With a total REE concentration of 265 ppm on a whole

mass basis, the density fraction contains 86% LREEs and about 14% HREEs (Figure 6.2). X-ray diffraction (XRD) analysis was performed to characterize the sample mineralogy. Kaolinite [Al₂(Si₂O₅) (OH)₄], quartz [SiO₂], and pyrite [FeS₂] were the three dominant minerals found in the sink fraction of the WK-13 sample (Figure 6.3).

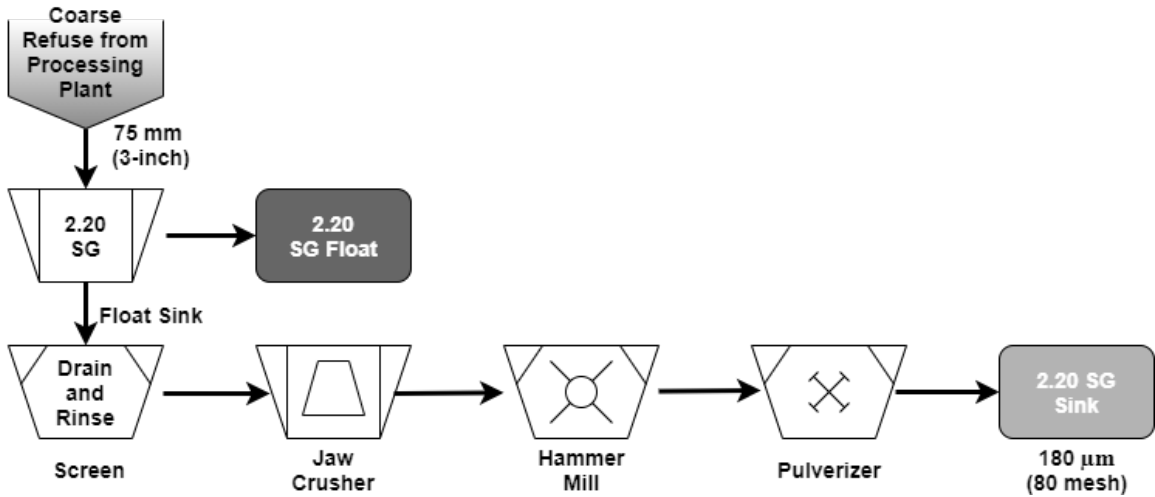


Figure 6.1. Process diagram of the sample preparation process from the coarse refuse material collected from the processing plant treating WK-13 seam coal.

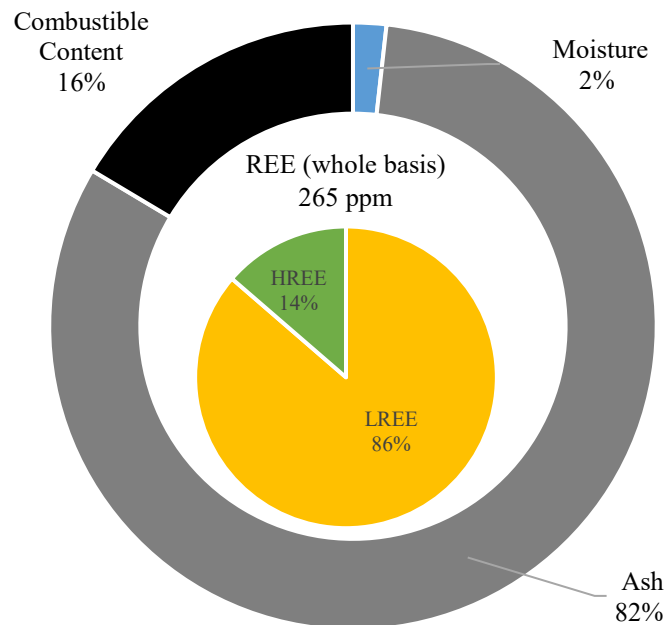


Figure 6.2. Composition and REE makeup of the 2.20 SG sink fraction of WK-13 coarse refuse material.

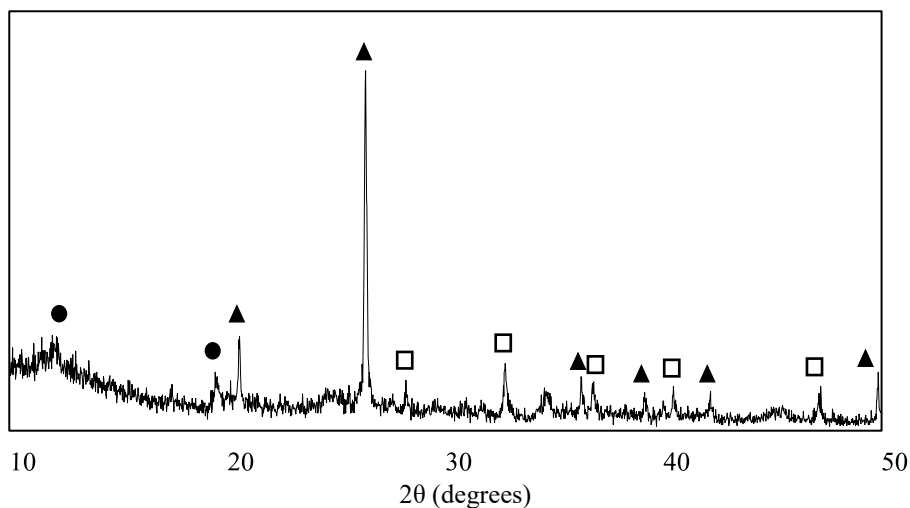


Figure 6.3. XRD analysis of the untreated 2.20 SG sink fraction of WK-13 (● -Kaolinite; ▲ -Quartz; □ -Pyrite).

6.2.2 Methods

6.2.2.1 Calcination Tests

Calcination tests were carried out in a lab-scale Thermolyne F6020C-80 muffle furnace manufactured by Thermo Scientific, USA at different temperatures. The samples were heated at a constant rate of 10°C/min and the temperature was maintained inside the furnace for 2 hours. A representative 30g sample was evenly distributed into six crucibles (5g/crucible). No chemical additives were added, and static atmospheric conditions were used. After completion of the test, the furnace was gradually cooled to room temperature. The calcined products were weighed and subjected to REE analysis and acid leaching tests.

6.2.2.2 Magnetic Separation Tests

Magnetic separation tests were performed on the calcined products of the 2.20 SG sink fraction of the WK-13 coarse refuse. A slurry of 10% w/v was introduced into an L-4-20 wet high-intensity magnetic separator (WHIMS) at various magnetic field strengths. The non-magnetic fraction of the feed slurry was collected into a bucket while feeding continuously. After all the feed was passed through the unit, the magnetic material that was adhered to a steel matrix was subsequently collected by turning off the magnetic

field and washing through the matrix and collected into a separate container (Figure 3.14). The magnetic and non-magnetic slurries were dewatered, air-dried, and subsequently split into subsamples for proximate and REE analysis. Magnetic separation tests using a field strength of 11500 gauss were performed on material that was calcined at temperatures of 400°C, 500°C, and 600°C. The mass yield values to the magnetic and non-magnetic product streams were recorded. Additionally, tests were carried out on 2.20 SG sink material calcined at 400°C at increasing magnetic field intensities from 2500 to 11500 gauss.

6.2.2.3 *Acid Leaching Tests*

Acid leaching tests on the feed and calcined products were performed under a set of standard conditions in a three-neck round bottom flask with 1.2M sulfuric acid at 75°C for 5 hours at 1% w/v solid concentration. The test apparatus shown in Figure 3.13 allows control over leaching temperature and stirring speed. The setup was equipped with condensers to minimize volumetric losses due to evaporation.

For every test, a series of representative samples (15 ml) were collected at 10, 30, 60, 180, and 300 min from the start of the leaching process to establish leaching kinetics. Weights of the samples were recorded for mass balance evaluation. The samples were centrifuged at 4000 rpm for 10 min to collect the supernatants which were filtered using a 0.45 µm PVDF membrane filter. The leaching tests were stopped at 300 min and the residual slurry was filtered using a 5 µm pore size filter paper. The filtrates were cooled to room temperature and their volumes were recorded. The filter cakes were dried in an oven at 60°C for 12 hours and the solid residual dry weights were recorded. The recovery was calculated as per (Eq. 3-1).

6.2.2.4 *Scanning Electron Microscope (SEM) Analysis*

The feed and magnetic separation products were subjected to SEM analysis to examine the surface texture, particle topography, and mineralogical composition using an FEI Quanta 250 Scanning Electron Microscope at the Electron Microscopy Center of the University of Kentucky. The samples were mounted on a sample holder using an electrically conductive double-sided carbon tape. Non-conducting samples were coated

with platinum to a thickness of 7 nanometers to reduce beam penetration and allow for a sharper image. The elemental composition of the sample was determined by capturing the backscattered electrons and X-rays using a retractable energy-dispersive X-ray (EDX) Detector.

6.3 Results and Discussions

6.3.1 Pyrite Characterization

A wide variety of pyrite forms were found in the SEM analysis of the untreated 2.20 SG sink material collected from the WK-13 coarse refuse. The sample contained regular framboidal pyrites with pyrite microcrystals ranging from 100 nm to 1 μm as well as massive pyrites ranging from 10-50 μm . Additionally, irregular pyrite aggregates were found associated with quartz and clay minerals as large compound particles (Figure 6.4). All pyrite crystals in the feed were found to be angular and with no observable porosity.

The total sulfur content of 9.7% in the 2.20 SG sink fraction primarily originated from pyrite. The sample was calcined at temperatures ranging from 100-1000°C and the calcined products were subjected to a dry magnetic separation using a handheld neodymium magnet. The calcination products between the temperatures of 400-600°C showed magnetic susceptibility while the calcinated material at all other temperatures was not affected by the application of an external magnetic field.

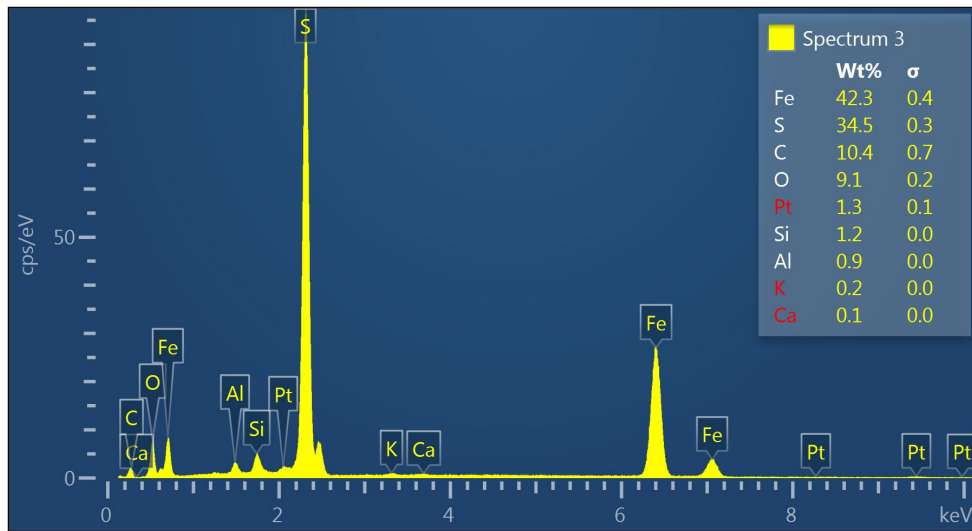
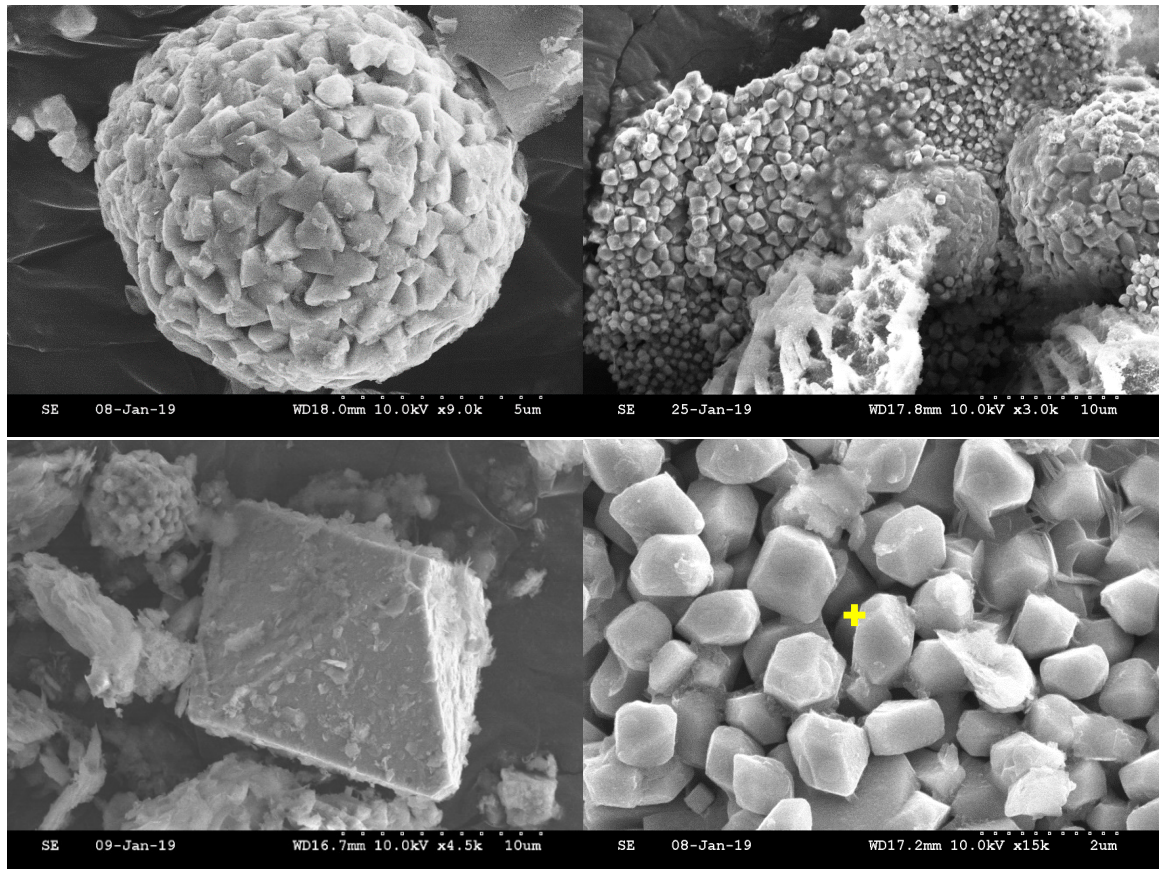


Figure 6.4. Micrographs of various pyrite types in the 2.20 SG sink fraction of the WK-13 course refuse material. (a) regular spherical shaped clusters (b) composite mineral agglomerates, (c) large hexagonal crystals, and (d) small grain crystal clumps.

6.3.2 Magnetic Separation

Subsequently, wet high-intensity magnetic separation tests were performed at the peak magnetic field intensity of 11500 gauss (1.15 Tesla). The mass yield for the magnetic separation tests of the calcination products at different temperatures is provided in Figure 6.5. The magnetic mass yield was maximum at 400°C where 81% iron was rejected to the magnetic fraction along with 23% of REEs. The mass yield and iron rejection decreased with an increase in calcination temperature. The magnetic and nonmagnetic fractions were collected, dewatered, and air-dried. The magnetic and nonmagnetic products were weighed and subjected to XRD, SEM, and REE analysis to determine the mineralogy and partitioning of REEs. Figure 6.6 shows the magnetic and nonmagnetic fractions of the calcined products at 400°C and 500°C collected by magnetic separation.

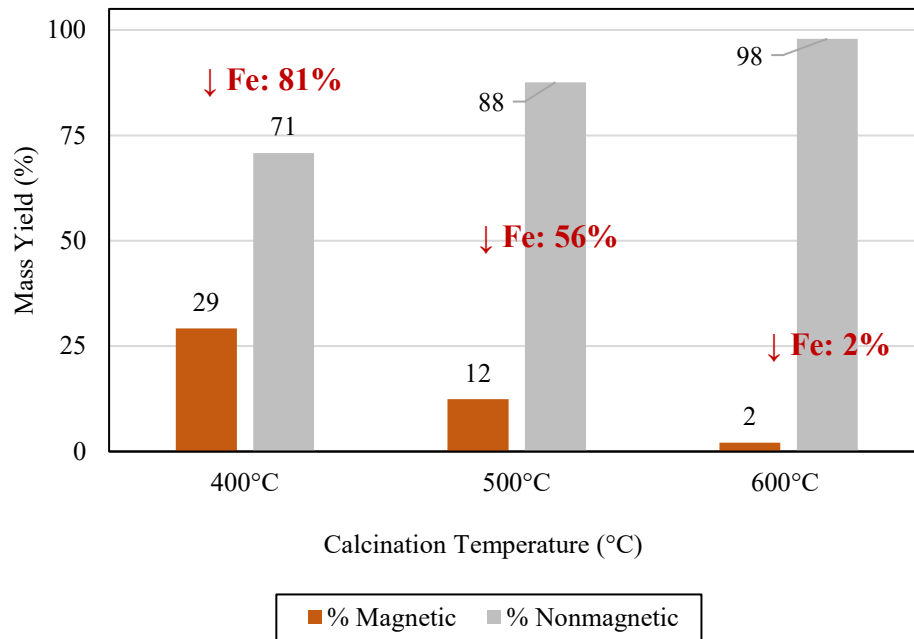


Figure 6.5. The mass yield obtained from magnetic separation tests on calcined products of 2.20 SG sink of WK-13 generated at three temperatures under a field strength of 11500 Gauss.

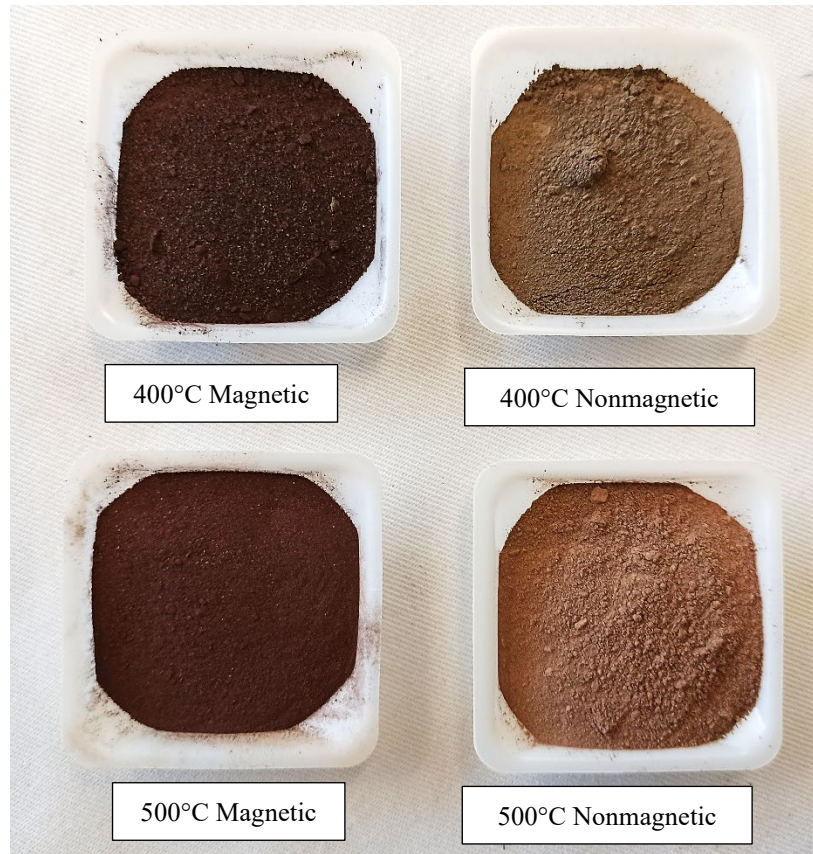


Figure 6.6. The collected magnetic and nonmagnetic fractions obtained from the magnetic separation of WK-13 2.20 SG sink fraction calcined at 400°C and 500°C.

The XRD analysis was performed to ascertain the mineral phases of the magnetic and tailings fraction and establish the changes in mineralogy because of calcination at 400°C (Figure 6.7). The major minerals found in the magnetic fractions were quartz [SiO₂], kaolinite [Al₂(Si₂O₅) (OH)₄], and hematite [Fe₂O₃]. As compared to the feed, the pyrite in the sample was transformed to hematite during the high-temperature calcination process in the presence of oxygen. Most of the iron-rich pyrite was converted to magnetic hematite and reported to the magnetic fraction. Moreover, the oxidation of pyrite aggregates associated with the mixed-phase particles in the feed resulted in the entrainment of quartz and kaolinite in the magnetic fraction due to incomplete liberation. It has been found previously that the change in the magnetic behavior of pyrite during thermal decomposition and oxidation is very complex and depends on factors such as temperature, oxygen concentration, and particle size [124, 181].

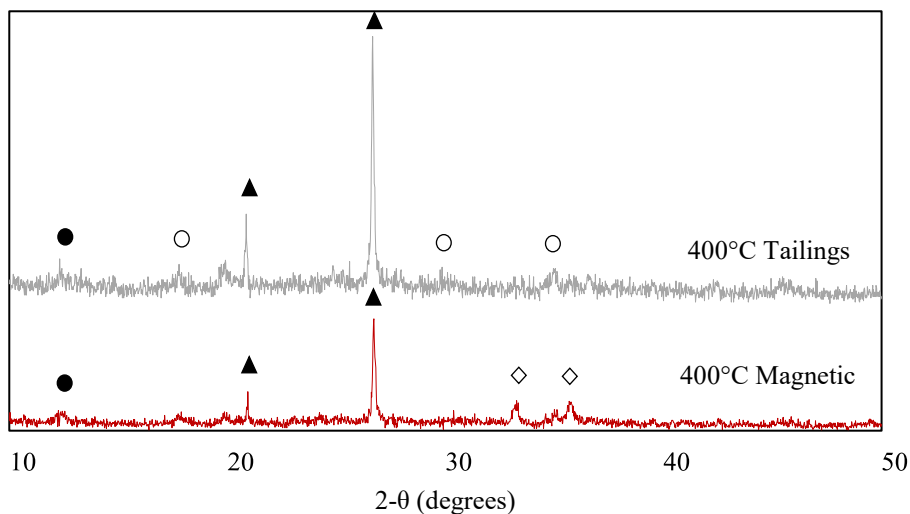


Figure 6.7. XRD analysis of the magnetic and tailing fraction of the 2.20 SG sink fraction of WK-13 calcined at 400°C (●-Kaolinite; ○-Illite, ▲ -Quartz; ◇ -Hematite).

ICP-OES analyses revealed that the nonmagnetic fraction contained higher concentrations of both light and heavy REEs. Therefore, magnetic separation of calcinated material can be viably used as a physical separation method for enriching REEs in the feed to the hydrometallurgical circuit (Figure 6.8). The REE contents in the nonmagnetic fraction of 2.20 SG sink calcined at 400°C increased by 15% as compared to the untreated feed. As most of the pyrite was converted to a magnetic oxide and removed by magnetic separation, the higher REE concentrations could be associated with other mineral forms in the feed, possibly clays. Similar explanations of the association of REEs with kaolinite and Illite minerals have been postulated by Moldoveanu and Papangelakis, Valian, and Zhang et. al [16, 26, 180].

Magnetic separation tests were also carried out on the calcination products of 400°C at varying magnetic field strengths. A 12% magnetic mass yield occurred using a field strength of 2400 gauss, suggesting that the iron oxide has higher sensitivity to an external magnetic field than the parent pyrite which has a weak response to a magnetic field. The magnetic fraction yield increased along with the rejection of iron from the tailings with an elevation in magnetic field strength suggesting that the pyrite crystals intermixed and interbedded with other mineral forms also reported to the magnetic stream when a sufficiently high magnetic field was applied (Figure 6.9).

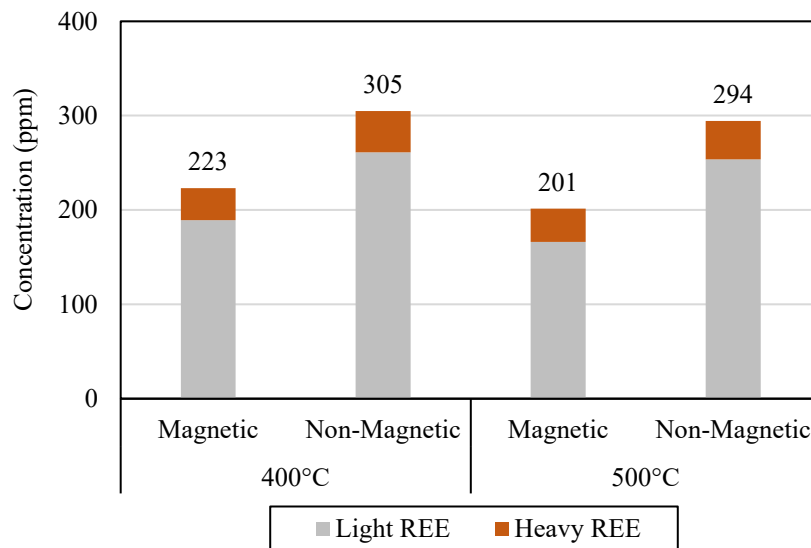


Figure 6.8. REE Concentration (ppm) in the magnetic and nonmagnetic fractions of 2.20 SG sink of WK-13 calcined at 400°C and 500°C.

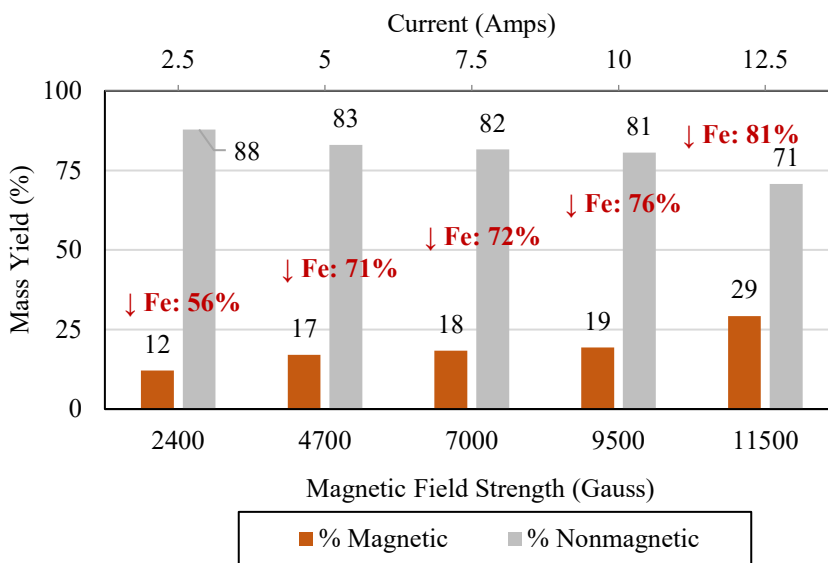


Figure 6.9. Mass yield of magnetic separation tests at varying magnetic field intensities for 2.20 SG sink of WK-13 calcined at 400°C.

6.4 Leaching Experiments

Leaching tests were carried out on the magnetic and nonmagnetic fractions of calcination products separated at 11500 gauss with 1.2M sulfuric acid at 75°C and 1%w/v solid concentration. Baseline values were established by leaching the untreated sample under the same set of leaching conditions. Additionally, calcination products of

400°C, 500°C, and 600°C were also subjected to acid leaching for comparison purposes. The recovery of LREEs and HREEs along with the concentration of Al, Ca, and Fe in the PLS was measured as the response. For a sample calcined at 400°C, the LREE recoveries were found to be approximately 35 absolute percentage points lower than those calcined at 600°C (Figure 6.10). The bulk of this difference in LREE recovery resulted from the variation in the recovery of lanthanum, cerium, and neodymium, which typically are the bulk of the elements comprising the LREEs. The HREE recovery, however, was found to be higher at 400°C with 40% yttrium and 55% dysprosium recovery. The concentration of Al in the PLS was higher at 600°C suggesting that the aluminosilicates were transformed to a more soluble form at 600°C. The increase in the leachability of Fe at 400°C as compared to the untreated material and the subsequent decrease at 600°C suggests that the pyrite was oxidized to a more stable oxide at 600°C which is harder to leach as compared to the more leachable form at 400°C. The concentration of calcium in the PLS was the same at the two calcination temperatures. Decomposition of calcium carbonate occurs in the 700-800°C temperature range and thus calcination at 400-600°C did not alter the mineralogy of calcite [175]. Overall, calcination of the feed at 600°C followed by acid leaching had better REE leaching results and lower total contaminant ion concentration than the sample calcined at 400°C.

When the calcination products at 400°C were separated into the magnetic and nonmagnetic fractions and leached separately, the hematite-rich magnetic fraction (400°C-Mags) showed higher HREE leaching recoveries as compared to the 600°C calcined material (600°C). However, the concentration of Al and Ca were considerably lower while the Fe concentration was elevated by more than 700%. This suggested that the magnetic fraction had easy-to-leach HREEs associated with the hematite. The 400°C-nonmagnetic material (400°C-N. Mag) had significantly lower (~50%) total REE recovery and a 48% lower concentration of contaminants in the PLS as compared to the 600°C calcined material. This observation can be used to develop an alternate process flowsheet by calcinating the feed at lower temperatures and removing the contaminant ions entering the hydrometallurgical circuit by magnetic separation. The cost analysis of the reagent dosage in downstream processing steps for using a 600°C calcined feed versus the operational costs of calcination at 400°C followed by magnetic separation will eventually

determine the preference of one process over the other. Additionally, for REE extraction from a feedstock with high pyrite content, the latter of the two abovementioned processes might be required to remove the excess iron contamination.

When the 400°C nonmagnetic material was recalcined at 600°C (400°C-N. Mag-RC), the recovery of LREE was found to increase and was like the calcination products of feed at 600°C. Additionally, with the removal of most of the pyrites as iron oxides in the magnetic fraction, the increase in the LREE recovery possibly originated from the REEs associated with clays. This hypothesis is supported by the identical Al concentration trends achieved for the 400°C tailings fraction re-calcined at 600°C and the 2.20 SG sink feed calcined at 600°C. The lower HREE recoveries, however, were partly due to the loss of highly leachable HREEs to the magnetic fraction.

On the other hand, the LREE recovery for the samples calcined at 500°C and 600°C were found to be similar (Figure 6.11). No benefits of calcination at the two temperatures were observed for the HREE recovery as compared to the untreated feed. The calcination products had similar leaching characteristics for Al and Ca for both the temperature values. However, the recovery of Fe was higher for 500°C as compared to 600°C suggesting a more leachable form of iron oxide at 500°C which, when subjected to a higher temperature, was transformed to more stable mineralogy. When the magnetic separation products from 500°C calcination were leached, significant dissolution of Fe was observed for the magnetic fraction (500°C-Mags) suggesting the phase transformation of pyrite to hematite also improved the leaching characteristics of Fe. Higher HREE recoveries were observed for the HREEs associated with the magnetic fraction as compared to all other samples. This finding suggests that HREEs were associated with the pyrite and were converted to more leachable forms when calcined at 500°C. The non-magnetic fraction (500°C-N. Mag) of the 500°C had similar total contaminants to 600°C and showed similar leaching characteristics concerning the REEs. The above observations suggest that calcination at 500°C followed by magnetic separation and leaching had no significant benefit over the calcination at 600°C.

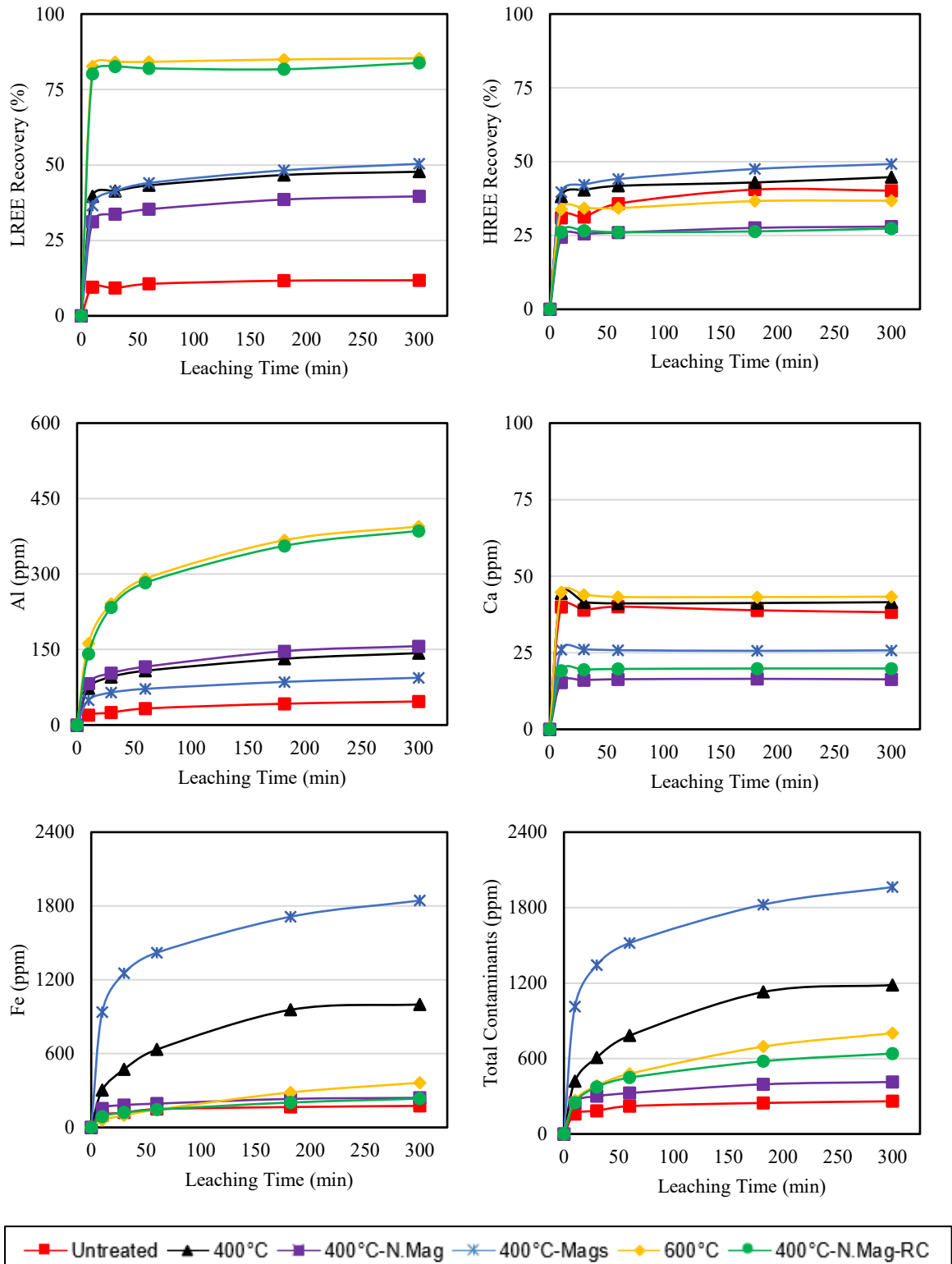


Figure 6.10. Acid leaching test results with 1.2M H₂SO₄ for 2.20 SG sink calcined products at different temperatures. (Mags=Magnetic; N. Mag=Nonmagnetic; N. Mag-RC=Nonmagnetic fraction Re-Calcined at 600°C)

In the acid leaching tests, the magnetic fraction for the samples calcined at 400°C and 500°C was found to have better leaching characteristics based on higher HREE recovery values and lower concentrations of Al and Ca. The increase in the HREE recoveries correlated well with an increase in Fe concentration in the PLS. The initial decomposition of the pyrite particles resulted in the formation of iron oxide identified as hematite by XRD analysis of the magnetic fractions (Figure 6.7). However, based on the physical evidence provided by SEM analysis of the magnetic fractions, it is suggested that, at lower temperatures, pyrite microcrystals oxidized and were converted to porous iron oxide clusters with no melting and little dimensional change (Figure 6.12). Energy dispersive X-ray (EDX) analyses of the calcined massive pyrite suggest a Fe/O ratio closer to hematite. The increased porosity of the hematite layer is suggestive of a significant mass transfer by sulfur evolution through the pores of the particle as SO₂. When the internal pressure exceeds the cohesion stress of the hematite rim, the particles cleave, leading to fissures. Evidence shows completely decomposed pyrite particles exhibiting massive fissures, which supports this hypothesis (Figure 6.12). Opening of these channels within the particle assists in the dissolution of associated HREEs as observed in the acid leaching tests.

6.5 Novel Process Flow Sheet Development

The current flowsheet developed by the researchers at the University of Kentucky [14, 161] utilizes a conventional hydrometallurgical approach for REE extraction. This process for REE recovery principally incorporates six major processing steps, (1) concentration of REEs by physical separation, (2) calcination of the concentrated feed at 600°C, (3) dissolution of REEs into solution by acid leaching, (4) REE concentration by solvent extraction or by selective precipitation followed by redissolution, and (5) oxalic acid precipitation to recover REE oxalates and (6) roasting to convert them to REE oxides. With objectives to develop an economically viable process for REE recovery from a coal-based feedstock, the optimization of the unit operations and overall process flowsheet is required.

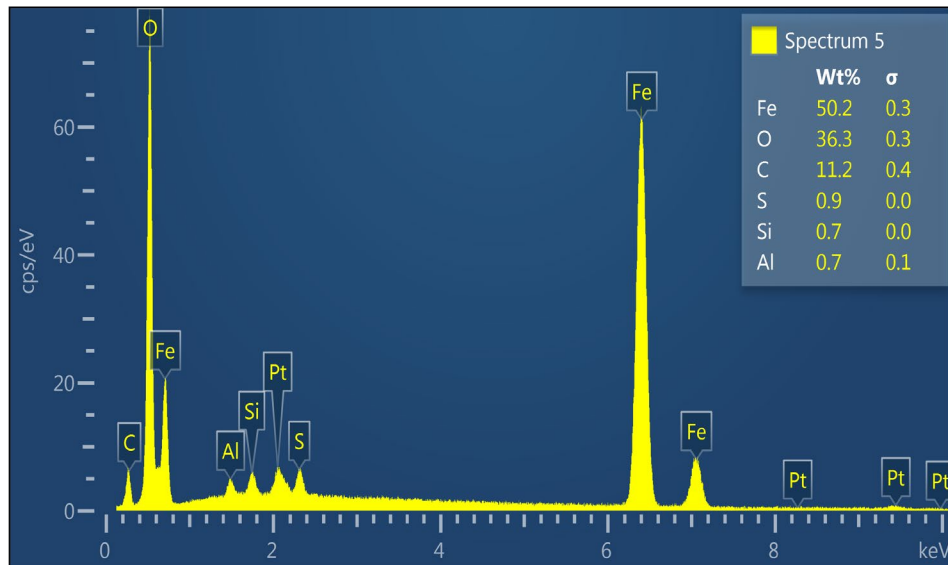
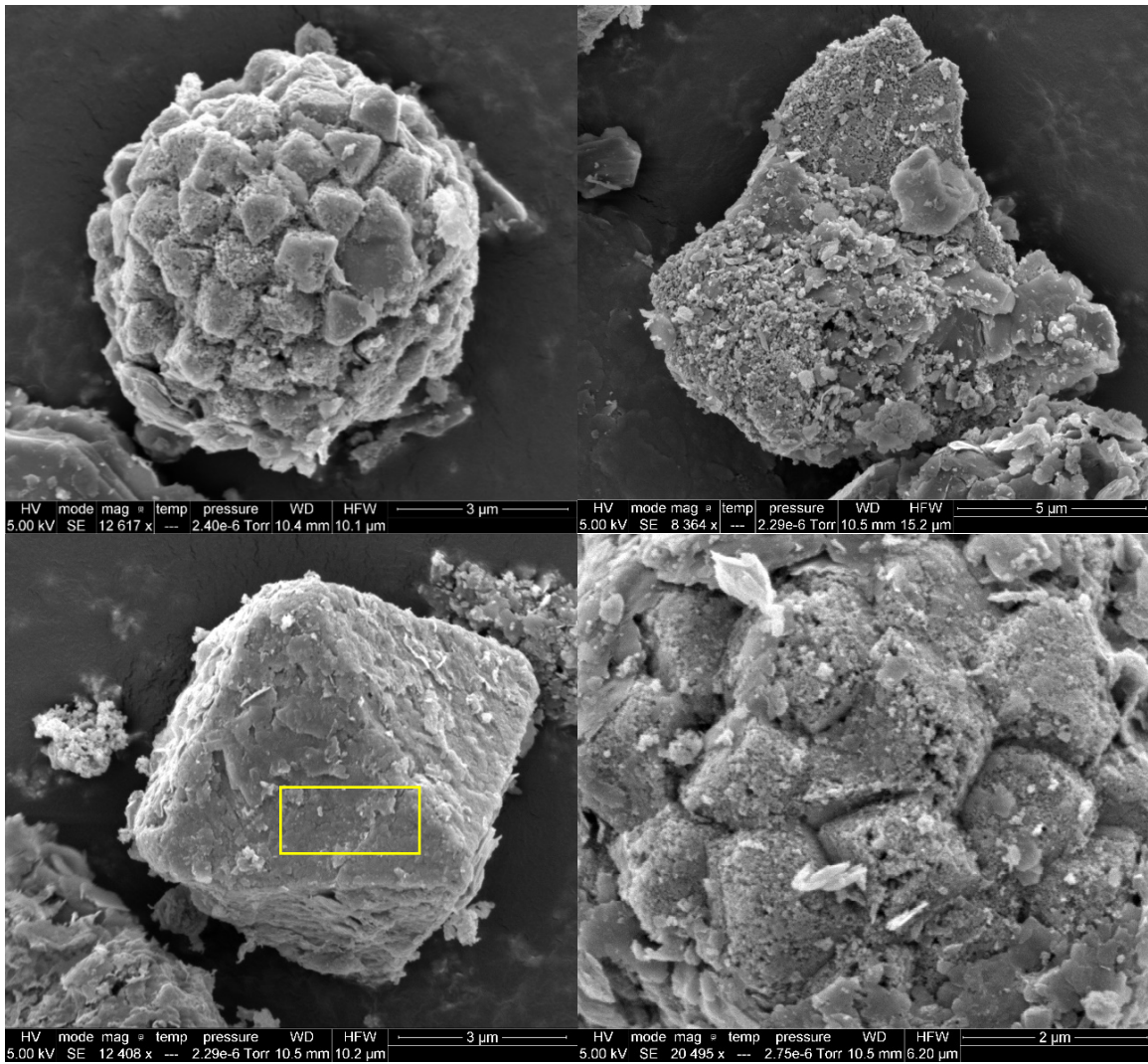


Figure 6.12. SEM analysis of the 2.20 SG sink of WK-13 calcined at 400°C. EDX analysis suggesting the formation of iron oxide and the crystal structure of pyrite being intact.

An analysis of the leaching data suggested that acid leaching of the calcination products performed at 400°C led to a 48% reduction in contaminants, particularly Fe and Ca, by using simple magnetic separation. While the overall gangue contamination reduced in the process, it was unfortunately accompanied by lower concentrations of LREEs in the initial leach solution. However, it was observed that the HREE/LREE ratio for such leaching was close to 1:1 suggesting that the process could potentially produce a better value HREE product. This observation inspired the development of an alternate process flowsheet where calcination and magnetic separation processes were incorporated to make a magnetic/non-magnetic split before acid leaching. A simplified process flow diagram outlining the various steps in this calcination-magnetic separation process alternative is shown in Figure 6.13.

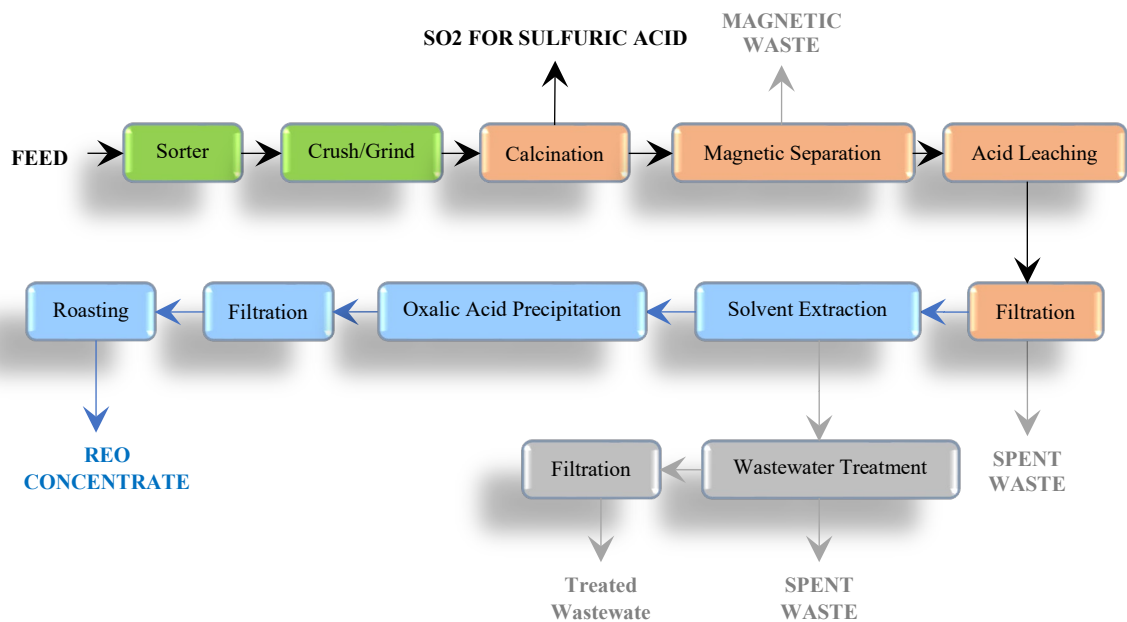


Figure 6.13. Flowsheet for single-stage calcination followed by magnetic separation in the hydrometallurgical extraction of REEs from coal-based feedstocks.

In the above flowsheet, the crushing process reduces the run-of-mine material to a top particle size of 50-mm which is subsequently sorted by an x-ray sorter to reject the lower-density fractions. The X-ray sorted product is reduced to a top particle size of 180 μm , which is suitable for calcination and magnetic separation. The calcination process liberates the REEs by thermal treatment in the presence of air. The SO_2 in the flue gasses can be captured to produce sulfuric acid if needed. The oxidized product is then

split into magnetic and nonmagnetic fractions by magnetic separation and the nonmagnetic fraction is dissolved in solution by acid leaching. The solvent extraction step concentrates the REEs in the solution and removes the buildup of contaminants. Oxalic acid precipitation by pH adjustment selectively precipitates out the REEs from the concentrated solution. The precipitate is filtered, and the solids are roasted to achieve the final REO product. The economic viability of such a process depends largely on the economic and market analysis. A relative comparison of calcination at 400°C followed by magnetic separation and only calcination at 600°C will determine the favorable process from either of the two configurations. Unfortunately, these values are subject to considerable uncertainties depending on feed composition, reagent consumption, REE prices, and cost of operation.

6.6 Conclusions

Magnetic separation tests were performed on the 2.20 SG sink fraction of the WK-13 coarse waste calcined at 400°C, 500°C, and 600°C. Acid leaching tests under standardized conditions using 1.2M sulfuric acid were performed on the magnetic and nonmagnetic fractions to assess the difference in leaching characteristics of REEs and common gangue minerals. It was found that the non-magnet portion of the calcined pyrite-rich material contained higher concentrations of REEs as compared to the magnetic fraction. A higher magnetic mass yield was observed for calcination at 400°C and decreased using elevated temperatures suggesting a phase transformation to more stable hematite with lower dissolution characteristics.

A novel flowsheet was developed based on the findings of the study which can be used to process coal-derived feedstocks with high pyrite content. For feeds containing significant amounts of pyrite, the developed process provides the benefit of removal of iron by calcinating in an oxygen atmosphere at 400°C and subsequent removal by magnetic separation. The sulfur dioxide in the flue gases from the process can be captured adding to the economic gains. Calcination at lower temperatures will allow for lower costs in the calcination operation. The lower concentration of contaminants will reduce the amounts of acid and base in solvent extraction and selective precipitation which may offset the potential losses from lower REE recoveries.

The tailings from the magnetic separation provide for an enriched feed source for the leaching operation. The mechanism of phase transformation of pyrites was established using XRD and SEM analysis to support the observations in the acid leaching tests. At lower temperatures, pyrites were decomposed to hematite, and SO₂ was released. The hematite formed as a product reported to the magnetic fraction by application of an external magnetic field. This hematite was found to have higher visible porosity which would facilitate the dissolution of associated trace elements. Additionally, a fraction of the total HREEs were found to be associated with pyrites which had different leaching characteristics as compared to the residual HREEs in the non-magnetic fraction

CHAPTER 7. EFFECT OF CALCINATION ENVIRONMENT

7.1 Introduction

Currently, the global REE supply largely comes from bastnasite in Bayan Obo and Mountain Pass and monazite from heavy-mineral placers deposits. Both REE deposits have a competitive advantage as the separation of the mineral phase from the waste rock is a relatively easy task owing to the relatively high grade and monophasic mineralogy. Therefore, the mineral processing of the conventional REE minerals provides a cost advantage in the adaptation of standard technology for exploiting a new deposit. However, to develop an economically viable REE extraction process from coal by-products, every feed must be extensively tested to obtain a unique flowsheet of optimized processing unit operations.

The most critical aspect of hydrometallurgical extraction of REEs from coal is their concentration in the PLS. To date, studies have been primarily focused on improving the leaching kinetics and recovery of the REEs contained in coal by calcination. Significant success has been achieved by calcinating the coal by-products under an oxidative environment and leaching with a mineral or organic acid [17, 36, 90]. However, the concentration of contaminant ions in the PLS is equally if not more vital as their leaching behavior influences the ionic strength of the lixiviants and can potentially result in lower REE recovery. The high-temperature calcination pretreatment however oxidizes the gangue minerals and allows for higher dissolution of contaminant ions primarily aluminum, calcium, and iron in the PLS [84]. Trivalent metal ions, Al^{+3} and Fe^{+3} , have been found to unfavorably affect the precipitation efficiency of REEs [84]. Calcium when present in a sulfate system can precipitate as gypsum [$CaSO_4 \cdot 2H_2O$] and potentially cause co-precipitation of REE ions on its surface [15]. Therefore, a holistic understanding of the effect of calcination on the leaching behavior of mineral species present in coal is required. The leaching characteristics of REEs and the most prevalent contaminant ions (Al, Ca, and Fe) associated with common mineral species such as clays and pyrites would allow for a more informed equipment selection and enhance the efficacy of the process flowsheet design. Achieving a low contaminant to REE ratio in the hydrometallurgical circuit may

eliminate the need for multistage solvent extraction and reduce reagent cost in downstream processing [61]. The knowledge of the leaching patterns of REEs along with contaminants could allow for the selection of an optimum set of calcination parameters to attain selectivity in the leaching of REEs.

Al and Fe are primarily associated with aluminosilicate clays and pyrites found as major minerals in coal. Calcium, on the other hand, originates from trace quantities of calcite found in coal beds. The clays that form the floor of the coal seam are called under-clays and can be a potential host to ion adsorbed REEs. Clay minerals such as kaolinite, halloysite, and illite have been identified to be present in bulk along with quartz in the underclay samples of Appalachian basin coal deposits [134-137]. These clay minerals are a potential host for the bulk of the REEs and a source of Al contamination. Quartz is relatively unreactive and has a very high thermal and acid stability [117, 118]. Additionally, studies have found that the REE and trace element content in quartz is two to three orders of magnitude lower than the upper crustal abundance [120, 121]. Coal deposits with high pyrite content contain appreciable amounts of both massive and fine-grained pyrites which are primarily differentiated by the size of mineralization [122]. While massive pyrite can be removed from the coal by washing, the framboidal pyrites due to their small particle size are not efficiently removed [123]. These pyrite framboids are responsible for iron contamination in the PLS and are a common host to trace elements such as Pb, As, Cd, and REEs [123, 179].

Hence, the objective of the test program and findings presented in this chapter was to understand the leaching behavior of REEs and contaminants from the calcination of common mineral species present in coal. The effect of calcination atmosphere (oxidizing/inert) was also studied on the leachability of REEs contained in coal. The thermal decomposition of the various density fractions of two coal sources along with mineral samples of clays and pyrite were also studied by TGA-DSC and XRD analysis to identify the phase transformations due to calcination.

7.2 Materials and Methods

7.2.1 Materials

Bulk samples were collected from both WK-13 and Fire Clay coarse refuse bituminous coal sources. The samples were density fractionated for characterization and testing the effect of calcination atmosphere on the leaching behavior of the contained REEs. The WK-13 samples were split using three specific gravity cut-points (1.80 SG, 2.00 SG, and 2.20 SG) which resulted in four density fractions (1.80 SG float, 1.80x2.00 SG, 2.00x2.20 SG, and 2.20 SG sink). The Fire Clay coarse refuse material was fractionated at four S.G. cut points (1.60 SG, 1.80 SG, 2.00 SG, and 2.20 SG) resulting in five density fractions (1.60 SG float, 1.60x1.80 SG, 1.80x2.00 SG, 2.00x2.20 SG, and 2.20 SG sink). The sink-float analysis for both samples was performed by SGS North America Inc.

The mass yield for fractions less than 2.20 S.G. was relatively small for both the materials, 4.9% and 12.5% for WK-13 and Fire Clay, respectively (Table 7.1). The low mass yield for the lighter fractions is indicative of the high-density cut point and the cleaning efficiency of the processing plant. The density cut point for the coal preparation plant processing for WK-13 was 1.70 and the cut point for Fire Clay material was 1.60 SG.

Table 7.1. The weight distribution of the (a) West Kentucky No.13 and (b) Fire Clay coarse refuse samples in different density fractions.

Specific Gravity	% Weight	% Cumulative Weight
West Kentucky No.13		
1.80 SG float	1.1	1.1
1.80x2.00 SG	1.0	2.1
2.20x2.20 SG	2.9	4.9
2.20 SG sink	95.1	100.0
Fire Clay		
1.60 SG float	3.0	3.0
1.60x1.80 SG	2.9	5.9
1.80x2.00 SG	2.3	8.3
2.00x2.20 SG	4.2	12.5
2.20 SG sink	87.5	100.0

Based on the results of the proximate analysis, the composition of the materials was estimated. The composite samples of both the materials were inherently dry with very low moisture content. The WK-13 composite sample had 1.2% moisture while the Fire Clay composite sample had 1.1 % moisture. The composite sample of WK-13 had 89.2% ash material with 9.6% carbon content while the composite sample of Fire Clay had 85.8 % ash material and 13.2% carbon content as shown in Table 7.2. The 2.2 SG sink fraction for both the sample had similar composition and moisture content despite having different mass yields. The results in Table 7.2 show that the composite sample of WK-13 contains significantly higher sulfur content (1.1%) as compared to Fire Clay composite sample (0.3%). This was expected as WK-13 has been shown in previous studies to contain a higher concentration of pyrite, which results in the higher sulfur content of the sample.

Table 7.2. Proximate analysis of the density fractions of the West Kentucky No.13 and Fire Clay refuse.

Sample SG	% Moisture	% Ash	% Combustible	% Sulfur
West Kentucky No.13				
1.80 SG float	2.7	22.3	75.0	2.5
1.80x2.00 SG	1.8	56.3	41.9	4.6
2.20x2.20 SG	1.9	66.1	32.0	6.2
2.20 SG sink	1.1	91.0	7.8	0.9
Composite	1.2	89.2	9.6	1.1
Fire Clay				
1.60 SG float	1.4	28.3	70.3	0.6
1.60x1.80 SG	1.8	43.1	55.1	0.6
1.80x2.00 SG	1.2	59.9	38.9	0.6
2.00x2.20 SG	1.0	72.9	26.1	0.5
2.20 SG sink	1.0	90.5	8.5	0.2
Composite	1.0	85.8	13.2	0.3

The results of the XRF analysis showed that SiO₂, Al₂O₃, and Fe₂O₃ were the major components in the ash obtained from the WK-13 sample (Table 7.3). Combined, the three components represented more than 93% of the total weight of the sample. Most of the Fire Clay samples consisted of SiO₂, Al₂O₃ and Fe₂O₃, and K₂O. The four elements together comprised more than 97% of the total weight of the samples. It was noteworthy that the iron content in the Fire Clay samples is significantly lower than that in the WK-13

samples. This observation is in line with the fact that the pyrite content in the Fire Clay material is known to be lower as compared to the West WK-13 material.

Table 7.3. XRF analysis of major and minor phases for the density fractions of the West Kentucky No.13 and Fire Clay samples on an ash basis.

Specific Gravity	SiO ₂ (%)	Al ₂ O ₃ (%)	Fe ₂ O ₃ (%)	CaO (%)	MgO (%)	Na ₂ O (%)	K ₂ O (%)	MnO (%)	P ₂ O ₅ (%)	TiO ₂ (%)	BaO (%)	SrO (%)
West Kentucky No.13												
1.80 SG float	54.7	25.8	12.7	1.5	0.9	0.1	2.7	0.0	0.2	1.4	0.1	0.1
1.80x2.00 SG	54.7	25.9	12.8	1.5	0.9	0.1	2.7	0.0	0.2	1.4	0.1	0.1
2.20x2.20 SG	52.4	26.2	15.4	0.8	1.0	0.1	2.9	0.0	0.4	1.1	0.1	0.1
2.20 SG sink	62.4	24.4	6.9	0.5	1.5	0.2	3.5	0.1	0.2	1.1	0.1	0.0
Fire Clay												
1.60 SG float	66.6	26.3	2.5	0.8	0.7	0.0	2.7	0.0	0.1	2.0	0.1	0.0
1.60x1.80 SG	66.4	25.2	2.7	1.4	0.8	0.0	2.9	0.0	0.1	1.7	0.1	0.0
1.80x2.00 SG	67.0	26.4	3.0	0.6	0.8	0.0	2.7	0.0	0.1	1.6	0.1	0.0
2.00x2.20 SG	68.0	26.9	3.0	0.3	0.8	0.0	2.3	0.0	0.2	1.4	0.1	0.0
2.20 SG sink	62.6	27.2	5.3	0.4	1.4	0.2	3.2	0.1	0.1	1.1	0.1	0.0

The REE concentrations of the different density fractions for WK-13 and Fire Clay material are shown in Table 7.4 and Table 7.5. The WK-13 composite samples contained 297.5 ppm TREEs while Fire Clay composite sample contained 365.5 ppm TREE. The light REE (LREE) dominated the overall concentration of REEs for both the materials. The lighter density fractions for both WK-13 and Fire Clay had significantly higher REE concentration than the heaviest 2.20 SG sink fraction.

A weighted average of the density fractions lighter than 2.20 had an REE concentration of 506.2 ppm for WK-13 and 727.7 ppm for Fire Clay material. This indicates that REEs can be significantly concentrated using density separation. However, it is important to note that the mass yield of the density fractions lighter than 2.20 S.G. is very low. The mass yield of density fractions lighter than 2.20 is 4.9% for WK-13 and 12.5% for Fire Clay material. This would correspond to an REE recovery of 1.70% for WK-13 and 1.99% for the Fire Clay coarse refuse material even if a density separation were made at 2.20 S.G. Therefore, it will not be economically feasible to concentrate the

REEs using density separation, even though the REE concentration in the lighter material is significantly higher than the heavier fraction.

Table 7.4. REE concentrations (ppm) by ICP-OES in each density fraction of West Kentucky No.13 coarse refuse on a dry, ash basis.

Specific Gravity	Sc	La	Ce	Pr	Nd	Sm	Eu	Gd	LREE
1.80 SG float	28.3	79.0	186.8	20.4	78.4	25.8	3.1	11.4	433.1
1.80x2.00 SG	25.2	107.8	262.8	28.8	112.2	32.0	4.3	14.2	587.2
2.20x2.20 SG	21.4	80.3	194.6	22.2	85.2	31.3	3.5	12.0	450.5
2.20 SG sink	17.2	51.7	107.3	12.8	50.5	15.2	1.9	8.2	264.8
Specific Gravity	Y	Tb	Dy	Ho	Er	Tm	Yb	Lu	HREE
1.80 SG float	6.7	2.0	9.1	4.0	7.5	1.5	6.7	1.7	39.1
1.80x2.00 SG	6.0	1.0	8.3	4.1	6.8	1.2	6.0	1.9	35.2
2.20x2.20 SG	5.3	1.3	6.4	2.6	5.8	0.9	5.3	2.1	29.8
2.20 SG sink	3.6	0.8	4.8	2.6	5.1	0.7	3.6	0.7	21.8

Table 7.5. REE concentrations (ppm) by ICP-OES of different density fractions of Fire Clay samples.

Specific Gravity	Sc	La	Ce	Pr	Nd	Sm	Eu	Gd	LREE
1.60 SG float	32.7	154.8	382.7	36.4	145.5	28.5	3.3	14.2	798.2
1.60x1.80 SG	27.9	116.4	285.5	27.9	111.6	21.9	2.8	8.7	602.6
1.80x2.00 SG	22.1	113.7	280.6	27.0	105.8	21.9	2.9	9.2	583.2
2.00x2.20 SG	19.3	106.0	264.1	25.6	97.5	20.6	2.9	9.3	545.4
2.20 SG sink	18.0	53.5	118.2	13.6	49.8	10.8	1.8	4.6	270.3
Specific Gravity	Y	Tb	Dy	Ho	Er	Tm	Yb	Lu	HREE
1.60 SG float	96.6	0.8	23.6	4.9	10.6	4.1	9.8	0.8	151.2
1.60x1.80 SG	67.3	0.8	16.9	3.6	9.1	3.0	7.1	0.4	108.2
1.80x2.00 SG	50.2	0.5	13.8	3.2	7.8	2.7	5.5	0.3	84.1
2.00x2.20 SG	39.9	0.4	11.7	2.7	7.3	2.3	4.5	0.1	68.9
2.20 SG sink	25.1	0.7	6.1	1.3	5.3	1.3	3.5	0.4	43.7

Additionally, high purity mineral specimens of pyrite, kaolinite, illite, and quartz were used for calcination tests and DSC analysis. The details of the mineral specimens used in the study are provided in Table 7.6 and Table 7.7.

Table 7.6. Details of the mineral samples used in the current study. (For Illite: x represents the variable amount of water that this group could contain)

Name	Formula	Molar Weight (gm)	Purity Grade	Source
Mineral Specimens				
Kaolinite	Al ₂ Si ₂ O ₇ .2H ₂ O	258.16	>99.9%	Fisher Sci
Pyrite	FeS ₂	119.98	> 99.9%	Fisher Sci
Quartz	SiO ₂	60.08	> 99.9%	Fisher Sci
Illite Shale	(K, H) Al ₂ (Si, Al) ₄ O ₁₀ (OH) ₂ - xH ₂ O	-	> 85.0%	Ward's Science
Calcite	CaCO ₃	100.09	>95.00	Fisher Sci

Table 7.7. XRF analysis of major and minor phases for the mineral samples on an ash basis (* Iron for pyrite is reported as % Fe).

Mineral	SiO ₂ (%)	Al ₂ O ₃ (%)	Fe ₂ O ₃ (%)	CaO (%)	MgO (%)	Na ₂ O (%)	K ₂ O (%)	MnO (%)	P ₂ O ₅ (%)	TiO ₂ (%)	Sulfur (%)	CaCO ₃ (%)	MgCO ₃ (%)
Kaolinite	50.9	41.5	0.5	0.1	0.1	0.1	0.1	0.0	0.1	1.8	0.0	0.0	0.0
Pyrite	0.5	0.0	44.4*	0.3	0.1	0.00	0.0	0.0	0.0	0.1	49.4	0.0	0.0
Quartz	100.0	0.0	0.0	0.0	0.0	0.0	0.0	0.0	0.0	0.0	0.0	0.0	0.0
Illite Shale	60.2	20.5	4.8	0.9	3.2	0.3	5.8	0.0	0.1	0.8	0.0	0.0	0.0
Calcite	0.6	0.1	0.1	0.0	0.0	0.0	0.5	0.0	0.0	0.0	0.0	96.2	0.5

Table 7.8. REE concentrations (ppm) by ICP-OES of mineral samples used in the study.

Mineral	Sc	La	Ce	Pr	Nd	Sm	Eu	Gd	LREE
Kaolinite	23.1	39.9	106.8	11.6	46.6	9.9	1.8	8.6	248.3
Pyrite	0.9	1.6	5.5	20.9	9.1	24.8	0.2	4.0	67.1
Quartz	0.0	0.2	0.2	0.6	0.5	0.7	0.0	0.3	2.4
Illite Shale	15.6	37.9	78.5	9.8	33.7	7.0	1.2	6.9	190.7
Calcite	179.4	1.8	0.0	0.0	3.6	0.0	0.0	67.5	252.4
Mineral	Y	Tb	Dy	Ho	Er	Tm	Yb	Lu	HREE
Kaolinite	4.2	0.2	2.0	1.8	6.0	0.2	0.9	0.0	15.4
Pyrite	1.3	4.1	0.0	0.0	0.0	0.0	7.2	16.0	28.6
Quartz	0.2	0.0	0.0	0.1	0.2	0.0	0.0	0.1	0.6
Illite Shale	19.1	0.6	3.6	1.2	4.3	0.5	3.1	0.5	32.8
Calcite	4.7	0.9	0.7	1.1	0.8	0.3	0.2	0.2	8.7

7.2.2 Methods

7.2.2.1 Calcination Tests

The LECO 701 thermogravimetric analyzer was used for the calcination of the different density fractions of both the feed sources and the mineral clay samples under oxidative and inert atmosphere for subsequent leaching studies. For each batch of calcination tests, a 1-2 g sample was placed in each of the six alumina crucibles. The temperature in the TGA was increased at a rate of 10 °C/min to the temperature setpoint of 600°C and held for 2 hours and three different calcination products were obtained by programming the gas flow in the TGA:

1. Calcination at 600°C under an inert atmosphere (IN);
2. Calcination at 600°C under oxidizing atmosphere (OX);
3. Calcination at 600°C under an inert atmosphere followed by calcination under an oxidizing atmosphere at 600°C (IN+OX).

Nitrogen was used as the purge and inert gas in the furnace for the calcination tests performed under inert conditions. Additionally, lids were used on crucibles to limit exposure to any atmospheric oxygen. The calcination products were subjected to a standard acid leach test with 1.2 M sulfuric acid to evaluate the effect of atmospheric conditions during calcination on the REE recovery. This information was vital for the design of the process flowsheet and the selection of a high-capacity calcination furnace. Additionally, pulverized mineral specimens were calcinated in a lab-scale Thermolyne F6020C-80 muffle furnace under different temperatures (300–800 °C). For each batch of calcination tests, a 30 g sample was distributed in six ceramic crucibles and placed into the furnace. The temperature in the muffle furnace was increased at a rate of 10 °C/min to the temperature setpoint and held at the target temperature for 2 hours. A static air condition was used during the overall calcination process and no additives were used. After cooling to room temperature, the calcination products in the crucibles were collected and used for the acid leaching tests.

7.2.2.2 *Acid Leaching Tests*

Acid leaching tests on the feed and calcined products of the coarse refuse and the mineral samples were performed in a three-neck round bottom flask with 1.2M sulfuric acid at 75°C for 5 hours at 1% w/v solid concentration. The test apparatus allowed for control over leaching temperature and stirring speed and was equipped with condensers to minimize volumetric losses due to evaporation. The leaching apparatus allowed to maintain a constant solid to volume ratio through the test. For every test, a representative sample (15 mL) was collected at the end leaching process after 1 hour. Weights of the samples were recorded for mass balance evaluation and the liquid sample was analyzed for the concentration of REEs using an ICP-OES.

7.2.2.3 *DSC Analysis*

DSC is a thermal analysis technique that measures the difference in heat flow rate between the specimen sample and the reference material as a function of temperature and time. Heat flows into the sample due to endothermic processes, evaporation, melting, glass transition, or heating in general. On the other hand, heat flows out of the specimen due to cooling, crystallization, oxidation, or other exothermic processes. DSC provides the benefit of both qualitative and quantitative measurements of the physical and chemical changes in the sample during analysis.

DSC tests using the LINSEIS TGA-DSC Simultaneous Thermal Analyzer (STA) on the density fractions of the coarse refuse samples from the Fire Clay and WK-13 were carried out under oxidizing (O₂) and inert (N₂) conditions. A 50 mg test specimen was placed into a tared alumina sample crucible with a pinhole in the lid. The sample crucible was then mounted on the platinum-rhodium thermocouple at ambient temperature and pressure. A similar empty crucible was placed on the reference position of the DSC thermocouple. A single platinum-rhodium wire is attached to the middle of the metal frame between the two positions. This thermocouple leg is shared between the sample and the reference side. Underneath the frame at each position, a platinum wire is attached to complete the thermocouple junction. This makes a total of three wires from the sensor tip to the base (Figure 7.1). The furnace was lowered and prepared for depressurization and

backfilling with inert gas. The furnace was subjected to a vacuum and subsequently repressurized with nitrogen to atmospheric pressure. With both the exit ports open heating was initiated at a rate of 10°C/min to a temperature setpoint of 1000°C. The furnace was held at the isothermal segment at 1000°C for 120 min and subsequently could cool down to room temperature. The weight loss and heat flow were measured as a function of time and temperature at a 1-sec sampling interval. The LINSEIS evaluation software was used for data analysis and calibration of the test data with materials with known melting points.

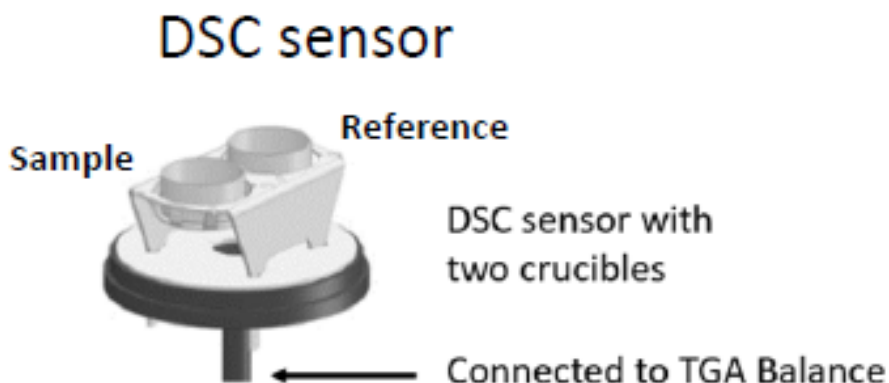


Figure 7.1. DSC Sensor setup for LINSIES STA analysis.

7.3 Results and Discussions

7.3.1 Acid Leaching Tests

The effect of calcination atmosphere on the leaching recovery of REEs was investigated by calcinating the density fractions of the two feed sources under oxidizing and inert conditions. The recovery of the LREEs and HREEs for the calcination products of WK-13 and Fire Clay sources after 1-hour leaching with 1.2M sulfuric acid at 75°C is provided in Figure 7.2 and Figure 7.3. For the calcination products of WK-13 treated under inert conditions, the ash content increased by 6-10% due to the removal of volatiles. While on the other hand calcination at 600°C under oxidizing environment resulted in the complete removal of volatiles as well as of the combustible matter.

In general, thermal treatment at 600°C on the density fractions of the WK-13 material provided increased recovery of LREEs irrespective of the environmental conditions. For the 1.80 SG float fraction, the recovery of LREEs increased by 15% points by calcination under inert conditions. Since the liberation of the mineral matter through combustion was not the likely mechanism, the increase in LREE recovery would be a result of dehydration of the clay minerals. Additionally, the increased porosity due to the removal of volatile matter upon pyrolysis could also be a contributing factor. High temperatures vaporize the volatile matter and hydrocarbons which diffuses through the particle creating large cavities [182]. On the other hand, the calcination under oxidizing conditions had a more pronounced effect on the leaching of REEs from the low-density fractions than inert conditions. The recovery of HREEs also increased by 21% upon calcination at 600°C in an oxidizing atmosphere. The significant benefit possibly resulted from the liberation of REE minerals from the mineral matter and their oxidation into REE oxides, which are more soluble. Similar findings advocating the benefits of calcination of coal rejects at 600°C for enhanced REE recovery using hydrochloric acid and nitric acid have also been reported by Zhang [90] and Yang [13].

The REE recovery in the 1.80x2.00 SG and 2.00x2.20 SG fractions suggested that, despite incomplete liberation during inert calcination, the leachability of REEs was found to be like that for calcination under oxidizing conditions. This finding suggests that the REEs in these fractions were not bound to the organic matter and were associated with mineral species. The XRF results (Table 7.3) suggested high SiO₂, Al₂O₃, and Fe₂O₃ originating from quartz, kaolinite, and pyrite as the major mineral phases as detected by XRD analysis. While quartz was the most dominant species, studies have disqualified quartz as the potential host for trace elements [120, 121]. On the other hand, REEs are associated with clays and pyrites and both undergo phase transformation under an inert as well as oxidative environment [23, 134]. Therefore, the REE leaching benefits may be associated with the transformation of REEs associated with clay and/or pyrite mineral present in the selected coal samples.

In contrast, the recovery of HREEs from a material having an SG greater than 2.00 was found to be unaffected by thermal treatment. Similar results were obtained

in Chapter 5 where the 2.20 SG sink fraction of the two feed sources were unaffected by calcination despite high temperatures and prolonged residence time. These finds together comprehensively suggest that 60-70 % of HREEs in high-density material exist in an insoluble form which is hard to leach despite thermal treatment under inert or oxidizing conditions. The higher HREE leaching recovery for the untreated 2.20 SG sink fraction WK-13 as compared to the LREEs also results in a higher concentration of HREEs in acid mine drainage samples associated with the WK-13 coal deposits[85, 172].

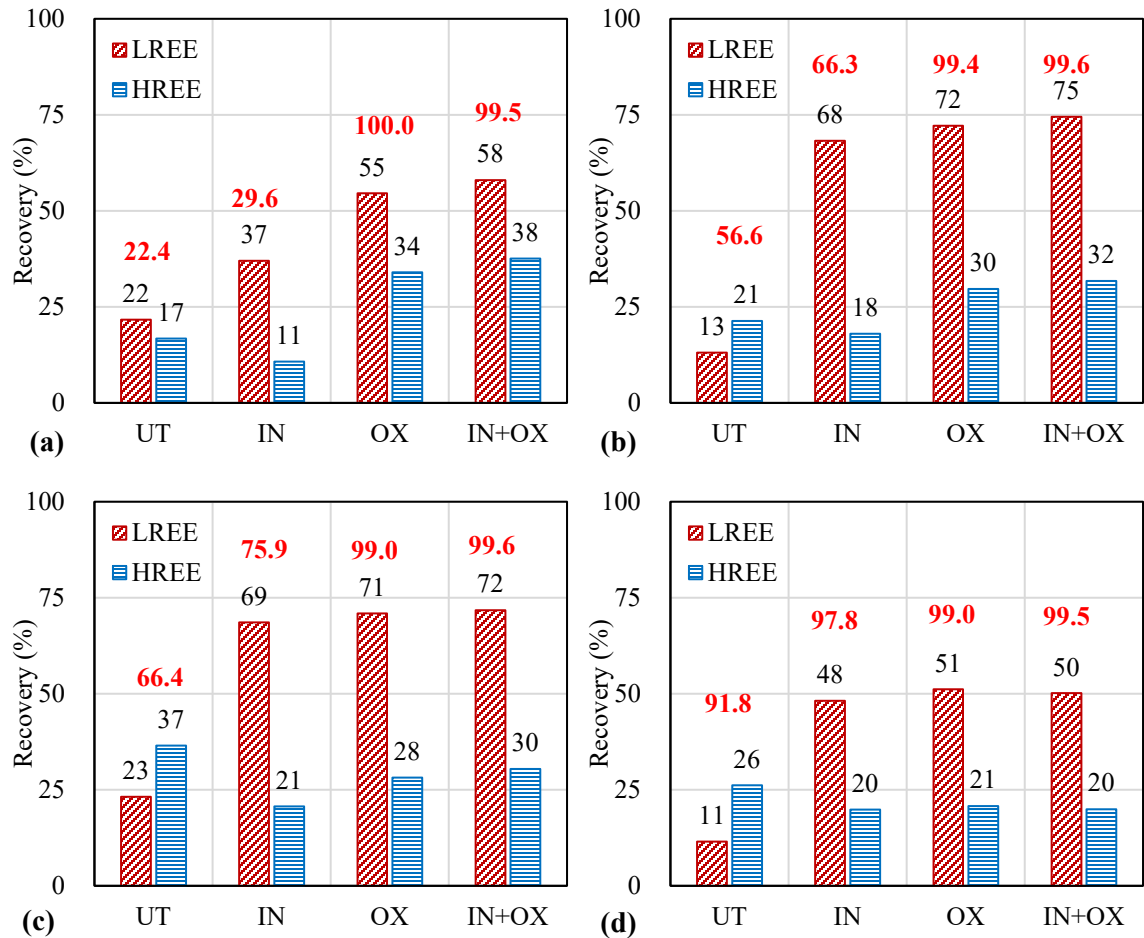


Figure 7.2. Leaching recovery for the light and heavy REEs for the (a) 1.80 SG float, (b) 1.80x2.00 SG, (c) 2.00x2.20 SG, and (d) 2.20 SG sink fractions of West Kentucky No.13 calcined at 600°C for 2 hours under different atmospheric conditions. (UT=Untreated, IN=Inert, OX=Oxidizing, IN+OX= Inert followed by Oxidizing). The number in red represents the % ash content in the calcined product.

Just like the WK-13 source, calcination in an oxidizing environment increased the recovery of LREEs for all density fractions of the Fire Clay source.

Significant benefits in the recovery of HREEs however were realized for calcination of density fractions lighter than 1.80 SG in air. It is hypothesized that the combustion of the organic matter exposed HREEs that were readily soluble under the given leach conditions. The leaching characteristics of LREEs in the 2.20 SG sink fraction of Fire Clay were significantly affected by thermal treatment in both the inert and oxygen-rich environments. This density fraction is of particular interest due to its high mass yield in the sample. LREE recoveries can be increased by 45% points by thermal treatment at 600°C.

For the calcination product obtained at 600°C by calcination under inert conditions followed by calcination under oxidizing conditions, the final ash content was the same as the single-step oxidative calcination for both the feed sources. Additionally, no significant benefit was observed on the REE recovery for calcination products of a single step (OX) and two-step calcination (IN+OX). Therefore, it can be concluded that thermal treatment alone and not the oxidation products are the primary driver for improving the recovery of LREEs in this density fraction.

The unusual behavior of the HREEs contained in each coal helps to understand the mode of association of the HREEs in coal-based byproducts. The maximum recovery of HREEs despite thermal treatment under any set of temperature and environmental conditions for both feed sources was around 40%. This would indicate that 60% of the HREEs were unaffected by thermal treatment despite relatively strong acid leaching conditions. The HREEs in heavier density fractions leach well without thermal activation while the HREEs in the lighter density fractions require liberation by removal of the combustible content for enhanced leachability.

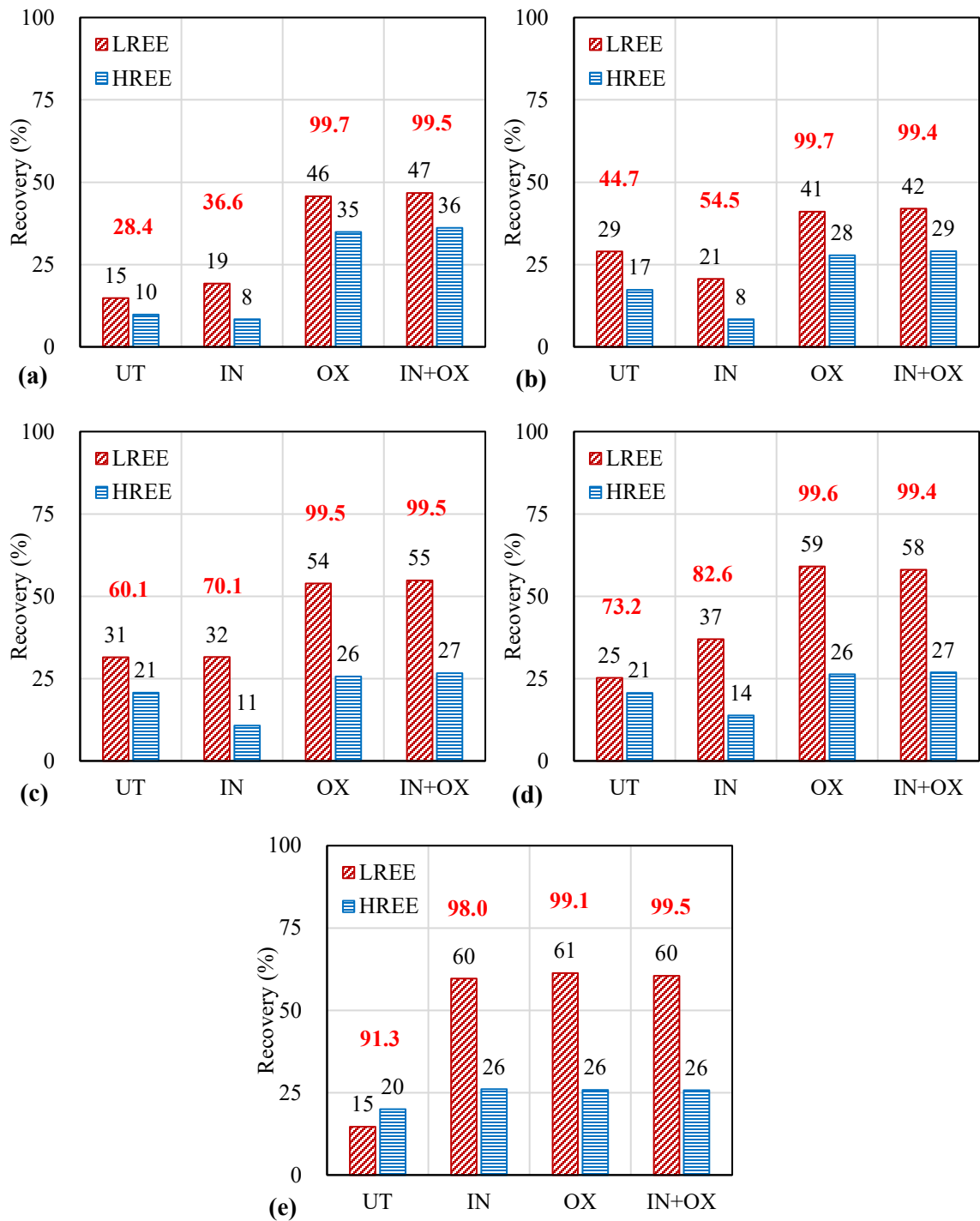


Figure 7.3. Leaching recovery for the light and heavy REEs for the (a) 1.60 SG float, (b) 1.60x1.80 SG, (c) 1.80x2.00 SG, (d) 2.00x2.20 SG, and (e) 2.20 SG sink fractions of Fire Clay calcined at 600°C for 2 hours under different atmospheric conditions. (UT=Untreated, IN=Inert, OX=Oxidizing, IN+OX= Inert followed by Oxidizing. The number in red represents the % ash content in the calcined product.

Calcination tests under oxidizing and inert conditions were also performed on mineral kaolinite and illite specimens (Figure 7.4). These clay minerals have been previously identified in Chapter 3 to be associated with the WK-13 and Fire Clay coal deposits. It was found that thermal treatment in an inert, as well as the oxidizing environment at 600°C, significantly enhanced the recovery of LREEs and HREEs associated with both the clays. The correlation between the clay samples and the heavy density fractions of the coals provides a piece of indirect evidence for the association of REEs with the clay minerals present in the heavy ash fractions of the two coal sources. Based on the XRD analysis of the calcination products under an inert and oxidizing environment, it was observed that, at 600°C, the kaolinite peak was absent for both the products. Studies have found the dehydroxylation temperature of kaolinite to be 528°C with a weight decrease of 14.4% [143]. The dehydroxylation reaction proceeds in the absence of air as:

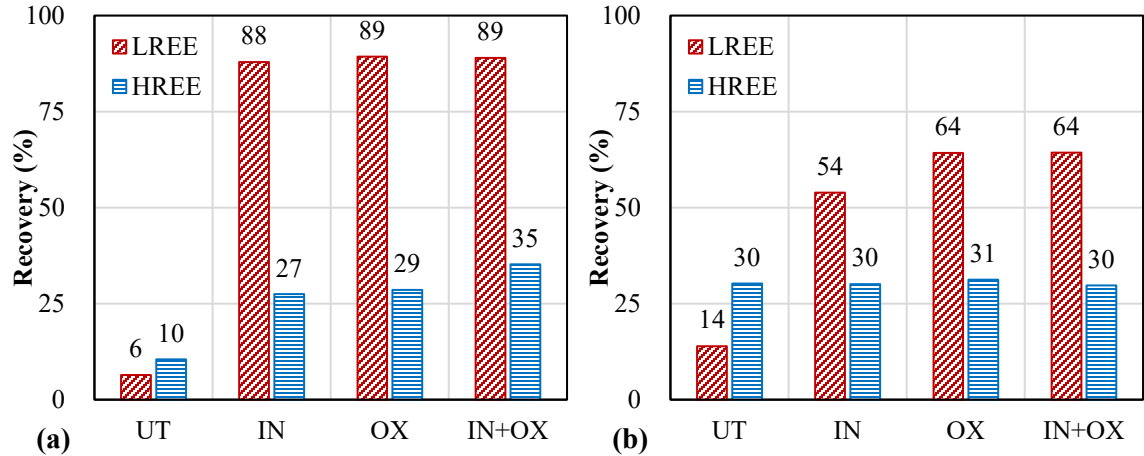
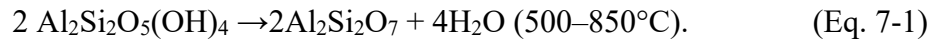


Figure 7.4. Leaching recovery for the light and heavy REEs for the mineral (a) Kaolinite (b) Illite samples calcined at 600°C for 2 hours under different atmospheric conditions. (UT=Untreated, IN=Inert, OX=Oxidizing, IN+OX= Inert followed by Oxidizing).

In an additional finding, it was observed that thermal treatment under inert conditions improved the leaching characteristics of the LREEs contained in the heavy density fractions of Fire Clay with an increase in temperature (Figure 7.5). The improvement from 15% in the untreated material to 74% in the calcined product at 1000°C

under an inert environment was possibly facilitated by the dehydration of the clay structure and the added benefit of the decomposition of REE-bearing phosphate minerals. In previous chapters, however, all density fractions have shown significantly lower REE leaching recoveries when calcination tests were performed in the presence of oxygen at 1000°C. The combination of the two findings suggests that the clays sinter at 1000°C in the presence of oxygen. The sintering effect was not observed when the samples were calcinated in an inert condition at the same temperature.

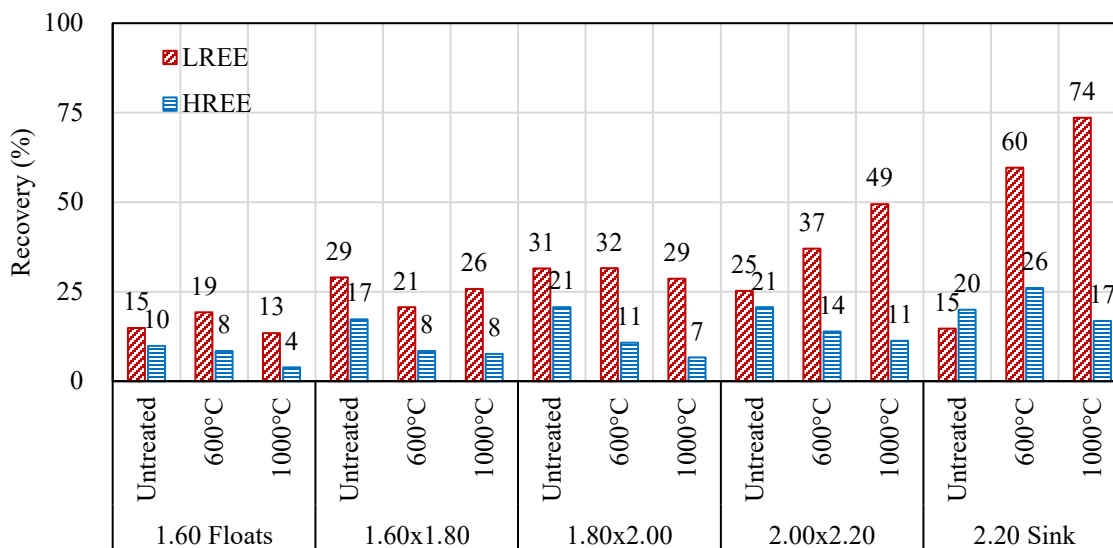


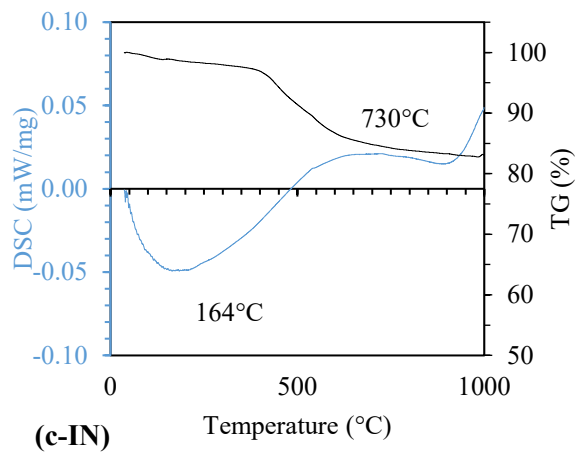
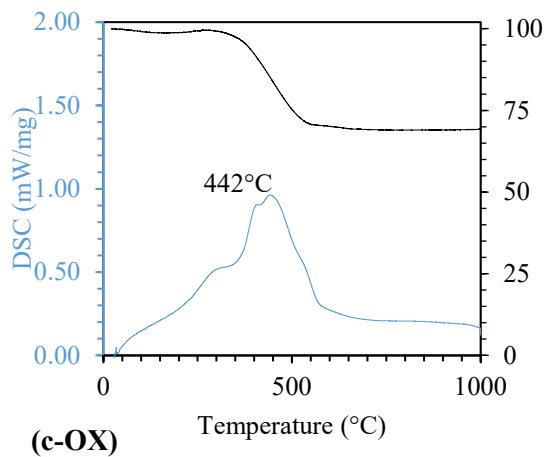
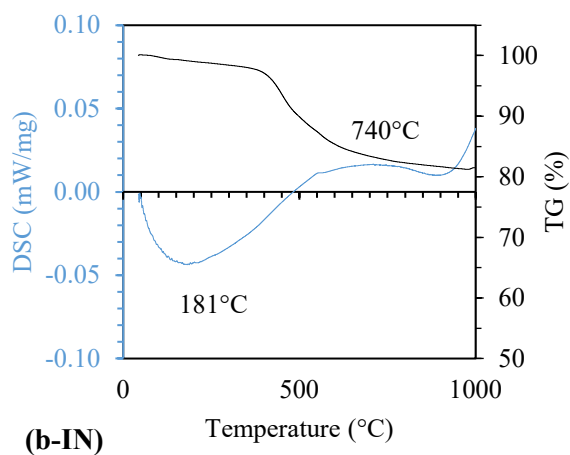
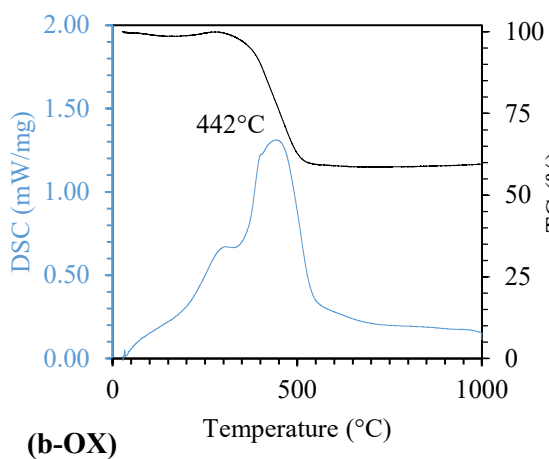
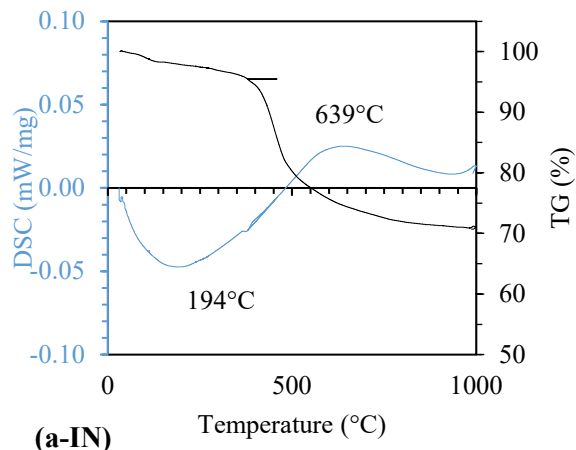
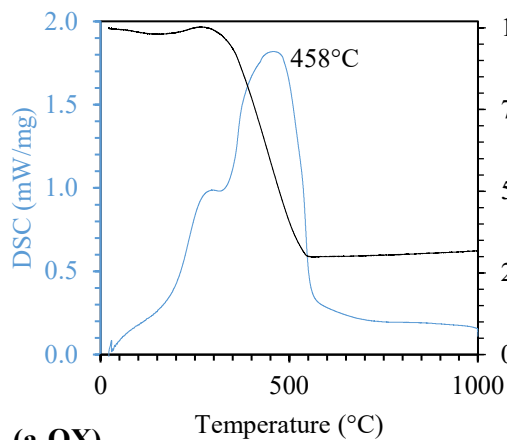
Figure 7.5. Leaching recovery for the light and heavy REEs for density fractions of Fire Clay calcined at 600°C and 1000°C for 2 hours under an inert environment.

7.3.2 DSC Analysis

The density fractions of the two coal samples were subjected to a TGA-DSC analysis under oxidizing and inert conditions separately. The results from the DSC analysis of the two source feedstocks are presented in Figure 7.6 and Figure 7.7. The coal sample was calcined from room temperature to 1000°C at a heating rate of 10°C/min. Two distinct exothermic reactions/phase transformations in both materials are observed for all density fractions when calcined under the presence of oxygen. The entire process can be divided into four stages: Stage I is characterized by mass loss by evaporation of the surface and inherent moisture (30-120°C). Due to the heat-absorbing effect of dehydration and desorption, the heat flow in this stage is endothermic. However, low-intensity oxidations between the coal surface and oxygen also existed in this stage, releasing a small amount

of heat [183]. In stage II (120-300°C), the mass increase of coal samples has been studied by researchers to be a result of the formation of oxidation complexes generated by absorbed oxygen and active functional groups on the surface of coal samples [184]. During the oxygen adsorption stage, gaseous products (CO and H₂O) are produced, and heat is released marking the start of exothermic processes. As the temperatures continue to rise the sample ignites at the start of stage III (300–550°C). During combustion, the sample undergoes intense decomposition, and most of the coal mass was consumed. During stage IV after the combustible matter in coal samples was completely burnt, at which there were no reactions, heat exchange, and further mass loss [185]. The decomposition or dehydration reactions for the constituent mineral phases such as kaolinite, illite, and coal pyrites cannot be identified and are masked by the exothermal reaction of carbon oxidation. The difference between the two feed sources can be attributed to the rank of the coal and its composition and the age of the deposit.

The weight loss in the density fractions of the WK-13 and Fire Clay sources during calcination in the absence of oxygen can be attributed to the vaporization of volatiles and dihydroxylation of clays. The endothermic peak at 160-180°C corresponds to the removal of moisture and the start of pyrolysis. Additionally, the endothermic peak at 1000°C is due to the transformation of metakaolin to mullite. Similar findings have been reported by Cao et.al when coal gangue rich in kaolinite (78%) was calcined in an argon environment [186]. The dehydroxylation of kaolinite contained in the samples from 400°C to 600°C was found to be masked by the dominant exothermal effect caused by coal pyrolysis which outweighs the endothermic effect due to kaolinite dehydroxylation [187]. However, a characteristic exothermic peak at 1000°C can be correlated to the phase transformation of meta kaolinite to mullite.



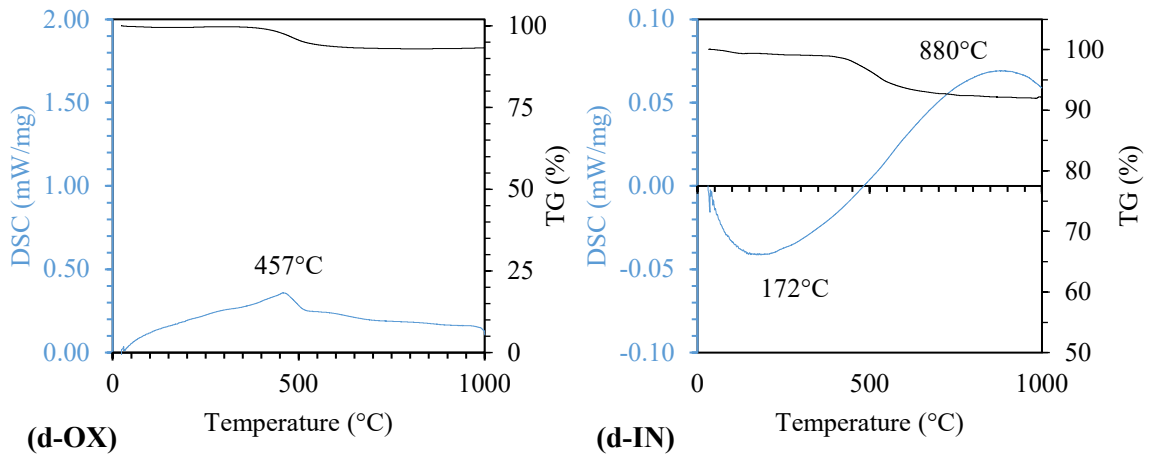
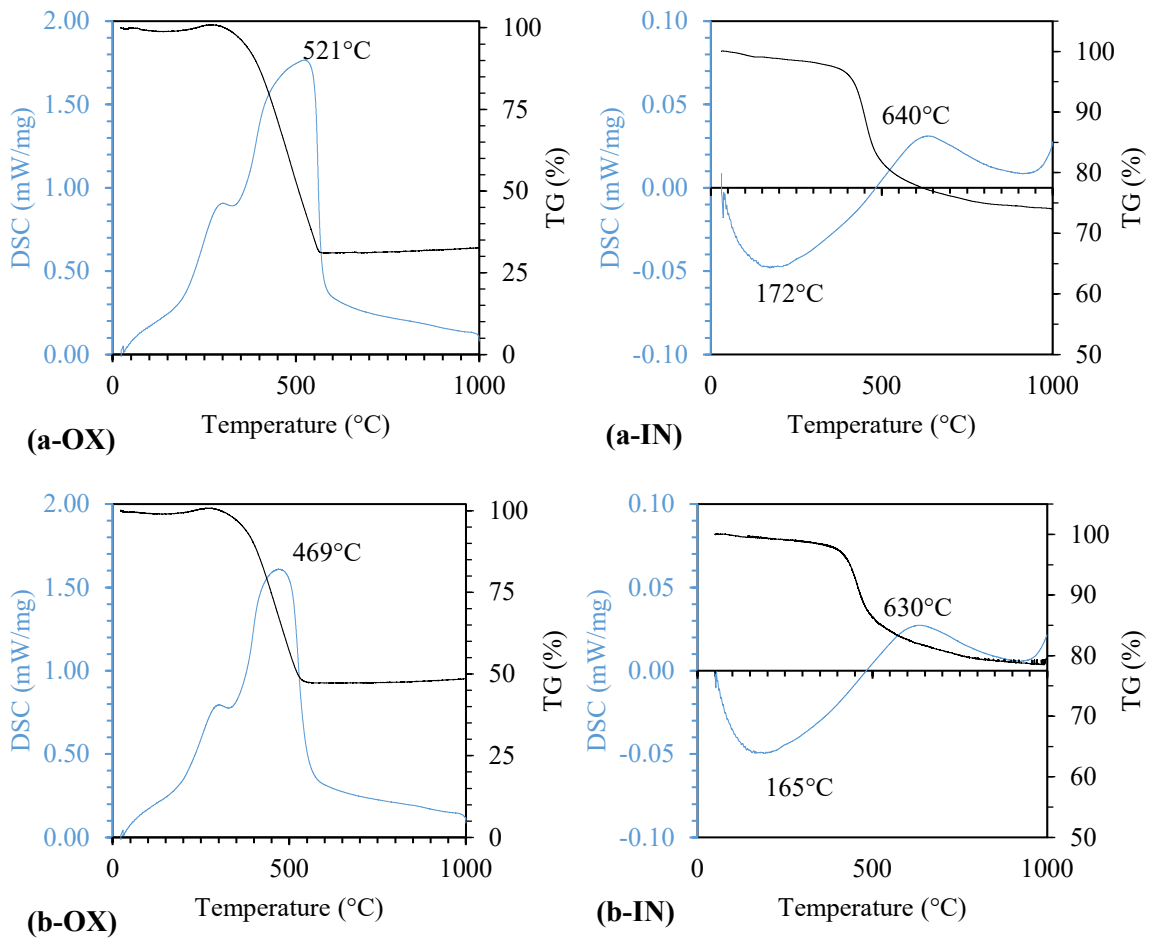


Figure 7.6. The thermogravimetric and differential scanning calorimetric (TGA-DSC) curves for (a) 1.80 SG float, (b) 1.80x2.00 SG, (c) 2.00x2.20 SG, and (d) 2.20 SG sink fractions of density fractions of West Kentucky No.13 (Exo Up: Heating rate =10°C/min) (OX=Oxidizing, IN=Inert).



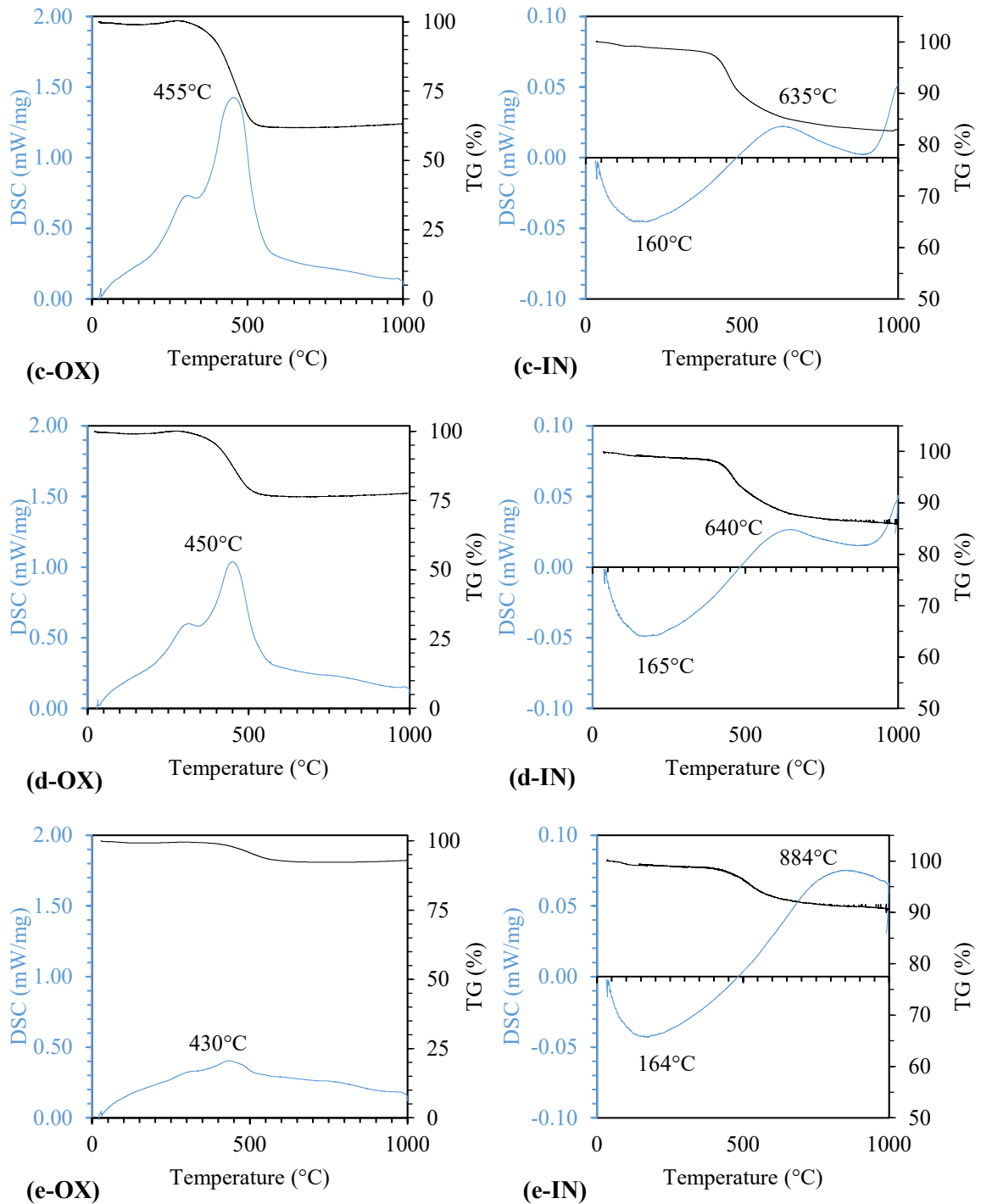


Figure 7.7. The thermogravimetric and differential scanning calorimetric (TGA-DSC) curves for the (a) 1.60 SG float, (b) 1.60x1.80 SG, (c) 1.80x2.00 SG, (d) 2.00x2.20 SG, and (e) 2.20 SG sink fractions of density fractions of Fire Clay (Exo Up: Heating rate =10°C/min) (OX=Oxidizing, IN=Inert).

7.4 Calcination and leaching of mineral clay and pyrites.

To evaluate the effect of calcination of the mineral kaolinite sample, it was calcined at different temperatures and subjected to standard acid leach tests. The recovery values of light and heavy REEs along with the concentration of Al, Ca, and Fe are shown in Figure 7.8. The recovery of light REEs remained unaffected up to 300°C but significantly increased when calcination temperature was greater than 400°C. Nearly 95% of the LREEs were recovered when the calcination temperature was 500-800°C. Also, the leaching kinetic data suggest that all the LREEs were recovered in the solution within the first 10 minutes of the test. Likewise, the HREE leaching kinetics also suggest the quick dissolution of the HREEs with no gain in recovery by prolonged leaching time. The HREEs however had a relatively small increase from 15% to 40% upon calcination at temperatures 500-800°C for 2 hours. Despite high-temperature calcination treatment, about 60% HREEs contained in the kaolinite sample were not recovered. The difference between the light and heavy REE recovery characteristics is evidence that the LREEs in the sample had a single mode of association with the kaolinite sample. The HREEs on the other hand was present in two or more forms one of which remained unaffected by thermal treatment. These results correlate well with the leaching behaviors observed for the high-density fraction in the coal sources.

Leaching characteristics of the major contaminant elements such as Al, Ca, and Fe, which are generally found in coal-based leachate, were analyzed to understand the impact of calcination and their correlation with the REEs. The concentration of contaminant ions in the leachate is a better indication of the composition of the PLS solution. Researchers have identified the negative impacts of high contaminant ion concentration in the PLS solution [84]. For example, a 1% increase in recovery of Al corresponds to a magnitude increase in the concentration of Al dissolved in the solution. The increased ionic strength consumes acid and results in lower REE recoveries. Except for Ca, the concentration of both Al and Fe were increased after calcination at 500-800°C, which correlates to the calcination behavior of the REEs. However, the leaching kinetics of the contaminants were different from those of the REEs. Al and Fe were gradually leached as the leaching reaction progressed which suggests that the calcination product

such as meta-kaolinite and iron oxides dissolved gradually with time. Hernandez et al. also reported the gradual dissolution of iron species such as magnetite, hematite, and di-iron titanium oxides contained in Beige kaolin clays using 0.50M oxalic acid at different temperatures [178]. The leaching behavior of iron associated with clays suggested higher solubility at 500-800°C which is in contrast with the findings in chapter 6 for Fe associated with coal pyrite which was maximum at 400°C.

The thermal behavior of the mineral kaolinite sample is presented in Figure 7.9. Generally, the mass change at temperatures below 200°C corresponds to the removal of surface moisture. However, as a dry kaolinite sample was procured for the studies, such a change was not observed in the thermogravimetric data. Ilić et al. measured the TGA and DTG data for high-quality kaolin clay from the Arandjelovac basin and suggested that any mass loss between 200-450°C can be attributed to the pre-dehydration process which is a result of the rearrangement of octahedral aluminosilicate layers [188]. Upon increasing the temperature further, the heating process drives the off water from mineral kaolinite and reduces the porosity resulting in an amorphous meta-kaolinite. In the temperature range, 450-650°C dehydroxylation of kaolinite occurs to produce metakaolin as explained by Meinhold [189]. The observed endothermic peak with a maximum at 547°C may be attributed to the dehydroxylation process. The mass loss flattens out at 650°C, which is indicative of complete phase transformation of kaolinite to metakaolin. An additional exothermic peak at 989°C depicts the conversion of meta-kaolinite to mullite. Similar phase transformations of kaolinite to metakaolin and mullite have been reported in the literature within +/- 20°C of the values observed in Figure 7.9.

The XRD patterns for the kaolinite sample calcined at 400°C, 600°C, and 800°C are presented in Figure 7.10. The characteristic peaks of kaolinite (2 θ : 12.41, 20.21, and 25.49°) in the untreated samples gradually disappear with an increase in temperature. The degree of dehydroxylation increases kaolinite converts to an amorphous phase, which is not detected by the XRD.

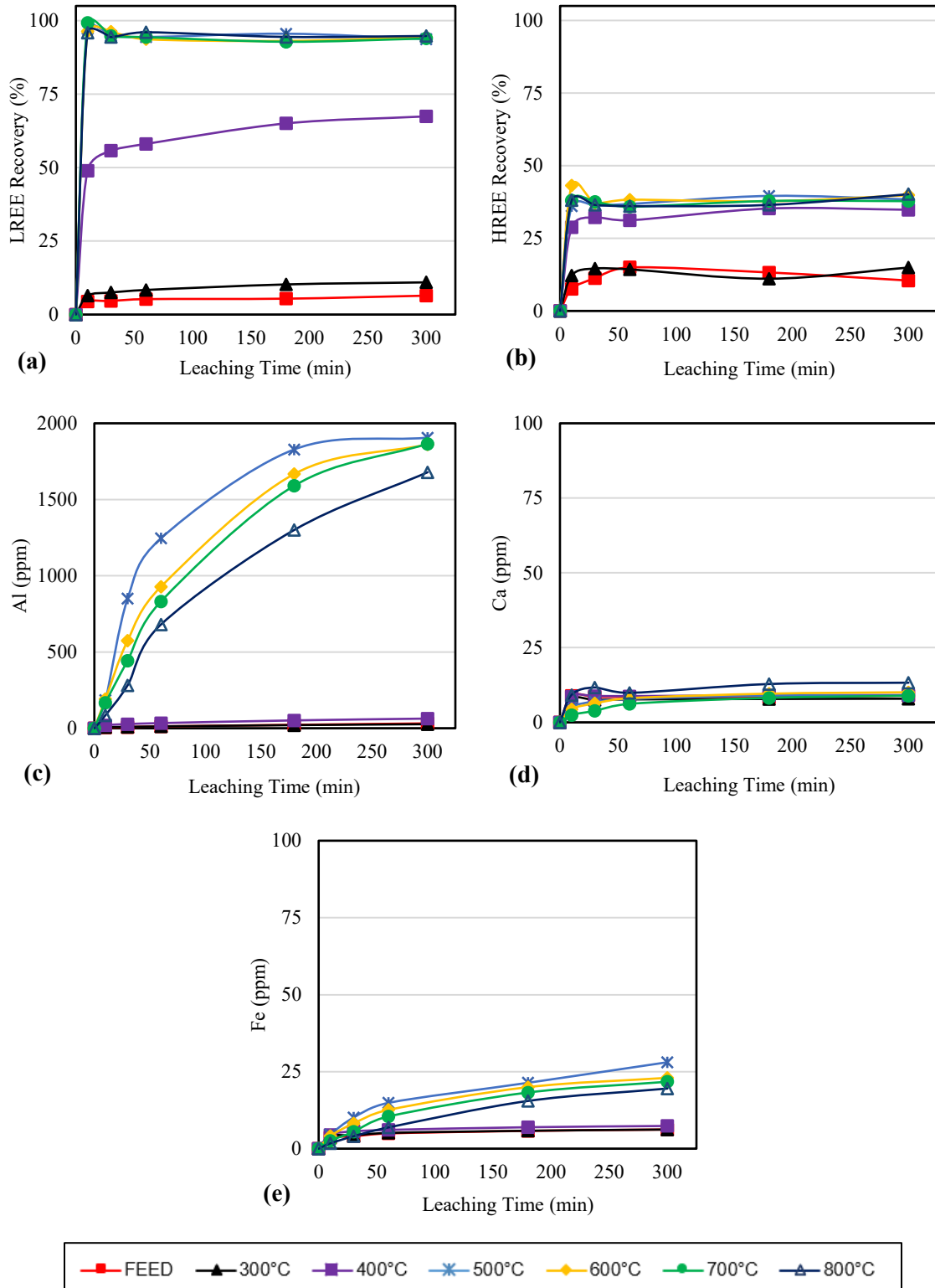


Figure 7.8. Acid Leaching Tests with 1.2M H₂SO₄ for mineral Kaolinite sample calcined at different temperatures for 2 hours (a) LREE Recovery, (b) HREE Recovery, (c) Al, (d) Ca & (e) Fe.

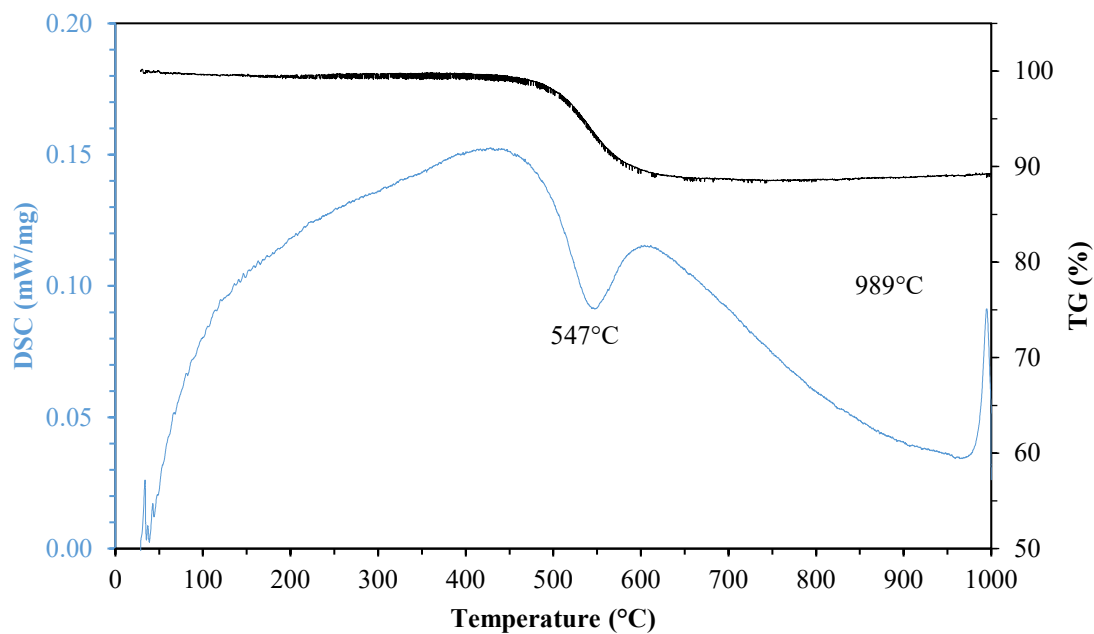


Figure 7.9. The thermogravimetric and differential scanning calorimetric (TGA-DSC) curves of mineral kaolinite (Exo Up: Heating rate =10°C/min, Oxidizing Conditions).

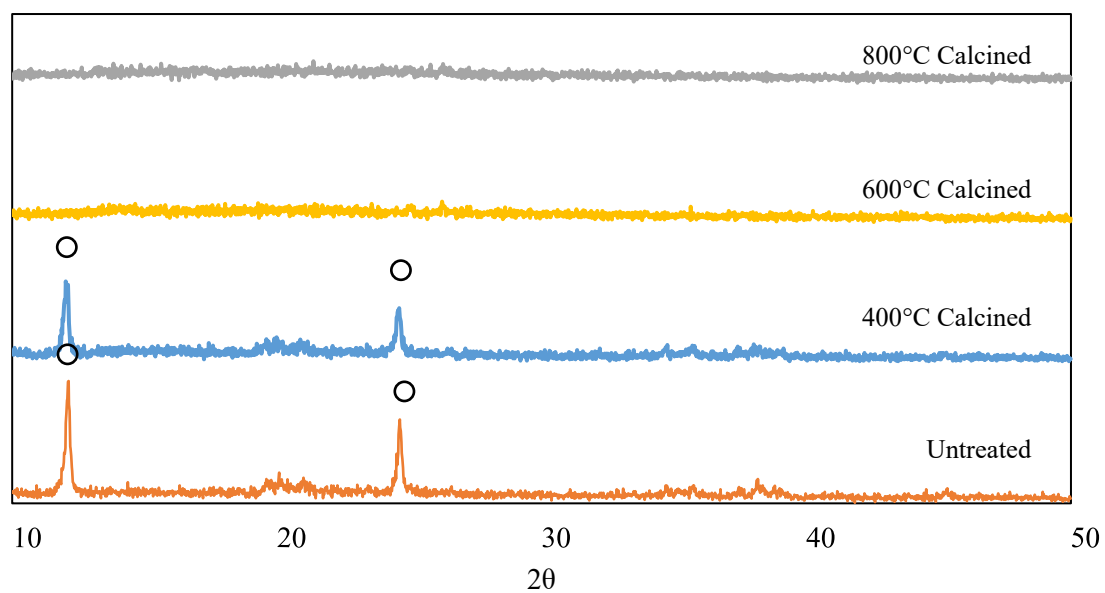


Figure 7.10. XRD Patterns of untreated kaolinite clay and calcinated at 400°C, 600°C, and 800°C for 120 minutes (○- Kaolinite).

The calcination of the illite sample at temperatures between 600 and 800°C was found to have a significant effect on the leaching characteristics of the LREEs (Figure 7.11). Like kaolinite, this benefit can also be attributed to the dehydroxylation of clay structures. Illite is more stable relative to kaolinite and is the main constituent of shales. The leaching kinetics of the REEs suggested that the REEs contained in the illite sample were leached within the first 10 minutes of the leaching reaction and no further improvements were observed after prolonged leaching times. The leaching behavior of Al and Fe suggests gradual dissolution with higher concentrations for samples calcined at 600-800°C. Hence, based on the leaching results, it can be conclusively deduced that REEs associated with clay species exhibit fast leaching kinetics. Calcium dissolution is unaffected by thermal activation. Additionally, to minimize the contamination of the coal PLS by Al and Fe, the leach reaction time should be minimized.

Based on the TGA-DSC results, the dihydroxylation reaction peak was observed at 600°C and the destruction of illite structure at 820°C (Figure 7.12). He et. al [190] studied the thermal stability of calcination of illite from Silver Hill Montana and suggested that dihydroxylation does not destroy the structure of illite. On the contrary, calcination was found to destroy the mineral structure of kaolinite samples in the current study (Figure 7.9). The findings of the study by He et. al suggest that illite clays have higher thermal stability as compared to kaolin clays. Thus, the benefits in the leaching characteristics started at 500°C calcination for illite while at 400°C for kaolinite clays (Figure 7.8).

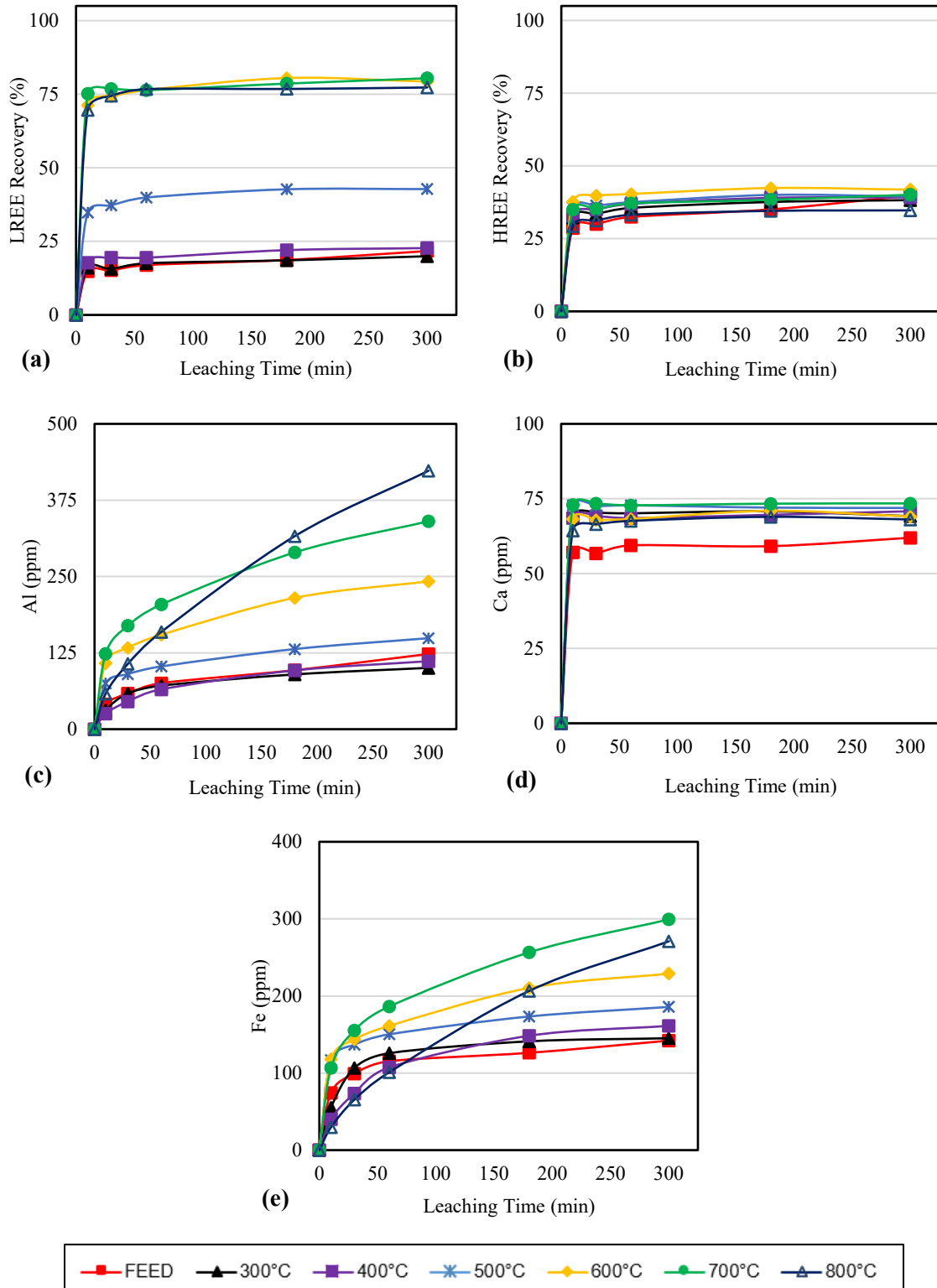


Figure 7.11. Acid leaching test results using 1.2M H₂SO₄ for mineral Illite sample calcined at different temperatures for 2 hours (a) LREE Recovery, (b) HREE Recovery, (c) Al, (d) Ca & (e) Fe.

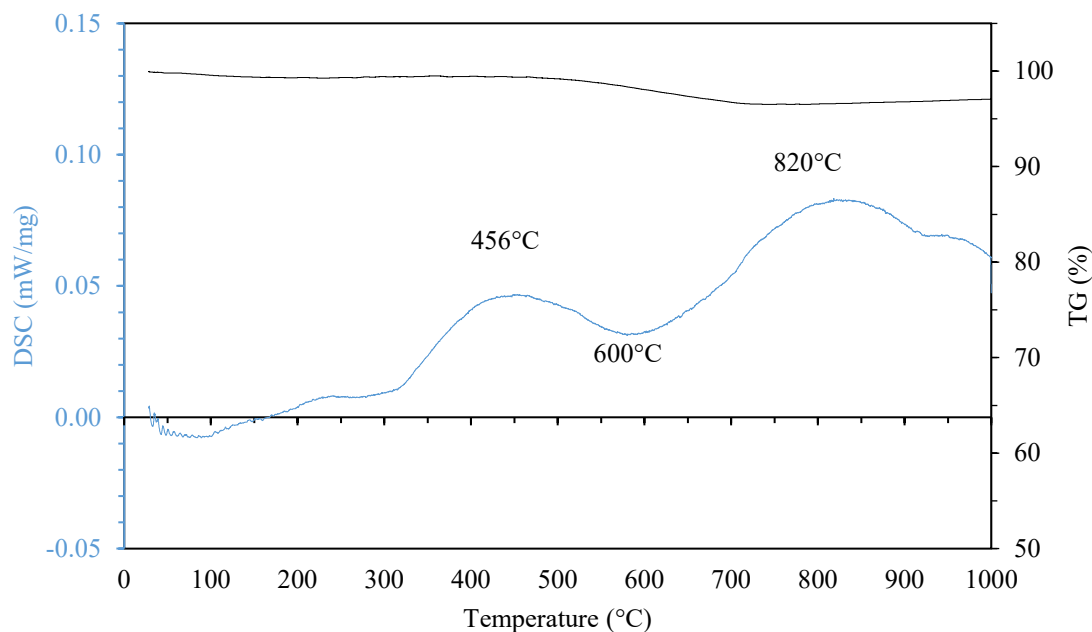


Figure 7.12. The thermogravimetric and differential scanning calorimetric (TGA-DSC) curves of mineral illite (Exo Up: Heating rate =10°C/min, Oxidizing Conditions).

Acid leaching tests with 1.2M sulfuric acid were also performed on the calcination products of mineral pyrite samples to evaluate the effect of calcination temperature on the recovery of REEs. The recovery of light and heavy REEs along with the concentration of Al, Ca, and Fe is shown in Figure 7.13. As such thermal treatment had a relatively smaller effect on the REEs associated with the pyrites. It was interesting to find that the phase transformation of pyrites allowed for increased recovery of both heavy and light group REEs only at 400°C. It was found in Chapter 6 that the calcination product of coal rejects that are rich in pyrite contained an intermediate phase that exhibits magnetic properties and was removable by magnetic separation. Li and Zhang studied the mineralogical changes in pyrite samples and found that magnetite is formed by oxidation caused by oxygen adsorbed onto the sample at 400 °C which converts to hematite after prolonged treatment [191]. However, a probable cause of the benefits in the REE leaching can be attributed to the formation of an intermediate γ -hematite which is formed by the decomposition of pyrite in the air at 400°C [192] which has ferromagnetic properties. Another magnetic intermediate in pyrite calcination is pyrrhotite, which is weakly magnetic [193]. However, based on leaching data, the intermediate phase at 400°C

crystallizes upon increasing the temperatures which correspond to a decline in REE recovery.

Despite the increasing concentration of Al with time, the concentration is less than 2 ppm and could well be within the range of the detection limit of the ICP-OES. The concentration of iron in the leachate, like the REEs, was the highest at 400°C. The intermediate phase at lower calcination temperatures thus had higher solubility in acid as compared to the crystallized hematite which was hard to leach.

The decomposition of pyrite in air starts at 300-400°C with the formation of pyrrhotite and hematite. The corresponding thermal transformation process of pyrite in an air environment can be simply summarized as pyrite → pyrrhotite → magnetite → hematite [124, 125]. Sharp exothermic peaks were observed between 400-600°C with the maximum intensity at 558°C (Figure 7.14). The exothermic phase transformation is accompanied by dramatic weight loss. Similar results for the DSC analysis of coal pyrites have been presented by Zhang et.al. [187]. In the TGA-DSC analysis, exothermal peaks were observed from 400°C to 600°C of coal gangue along with weight loss shown in the TGA curves within the same temperature interval, thereby indicating the combustion of carbon content in the coal gangue.

Mitchell studied the oxidation of iron pyrite during pulverized coal combustion. The combustion tests indicated that pyrite oxidizes through the reaction as shown below to magnetite:



The oxidation pathway starts with the transformation of pyrite (FeS₂) to troilite (FeS), which is oxidized to wustite (FeO). The troilite-to-wustite transformation involves oxidation of an oxysulfide melt (Fe-S-O) melt to an iron-oxide melt (Fe-O) melt. Magnetite (Fe₃O₄, really, FeO·Fe₂O₃) crystallizes from the oxide melt after complete melt oxidation. At high oxygen concentrations, magnetite is oxidized to hematite (Fe₂O₃) [176]. As shown in Figure 7.15 the intensity of hematite peaks increased with an increase in temperature. The intermediate phases of the calcination of pyrite however were not detected using XRD.

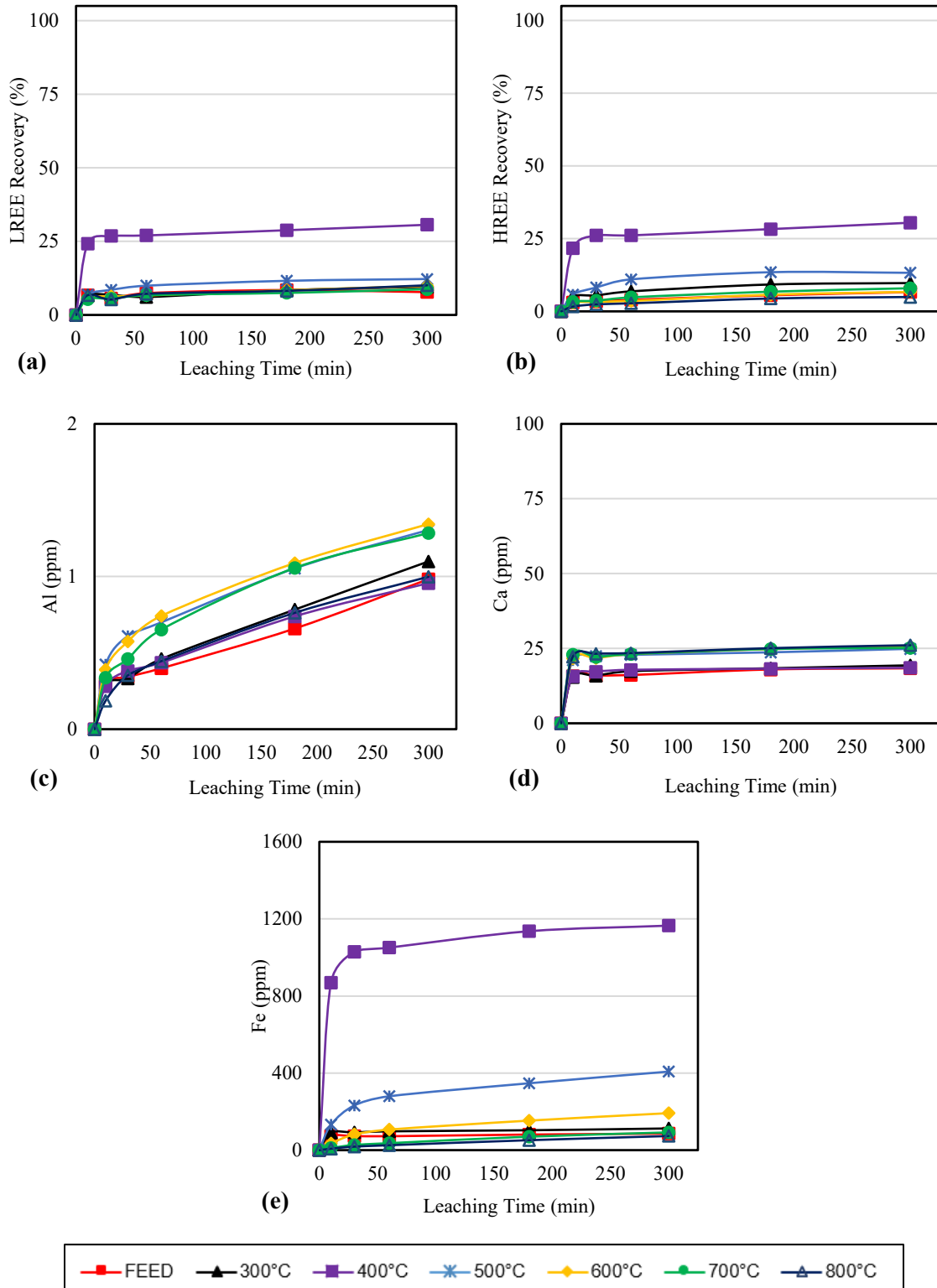


Figure 7.13. Acid Leaching Tests with 1.2M H₂SO₄ for mineral Pyrite sample calcined at different temperatures for 2 hours (a) LREE Recovery, (b) HREE Recovery, (c) Al, (d) Ca & (e) Fe

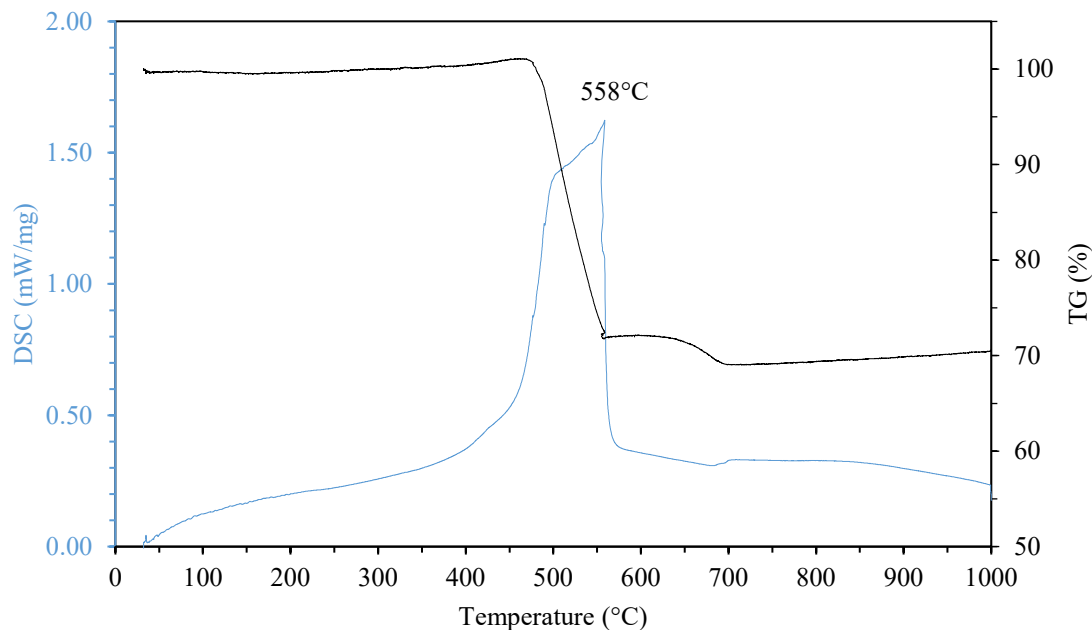


Figure 7.14. The thermogravimetric and differential scanning calorimetric (TGA-DSC) curves of mineral pyrite (Exo Up: Heating rate =10°C/min, Oxidizing Conditions).

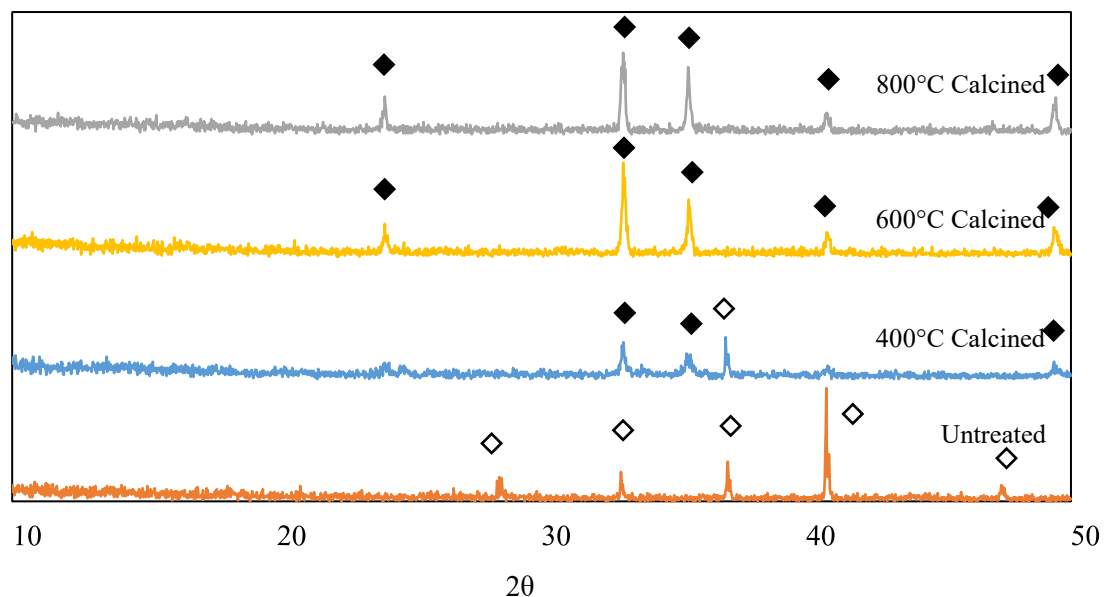


Figure 7.15. XRD Patterns of untreated mineral pyrite and calcinated at 400°C, 600°C, and 800°C for 120 minutes (\diamond - Pyrite; \blacklozenge -Hematite).

The DSC thermogram of mineral calcite is provided in Figure 7.16. It was found that that calcite has an endothermic peak at 850°C which corresponds to the

decomposition of calcite to calcium oxide. Due to the high decomposition temperature, no significant difference in the concentration of calcium was seen for the leaching tests done in Chapter 5. However, both calcite and calcium oxide readily react with acid and provide a neutralization effect in the leaching of REEs from coal sources.

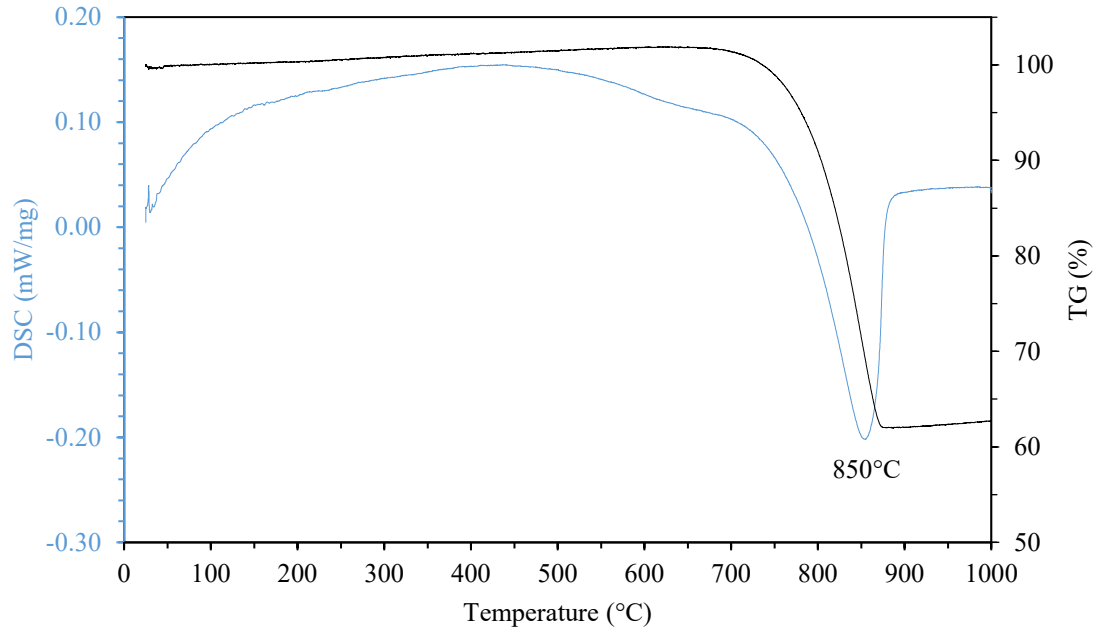


Figure 7.16. The thermogravimetric and differential scanning calorimetric (TGA-DSC) curves of the mineral calcite (Exo Up: Heating rate =10°C/min, Oxidizing Conditions).

7.5 Conclusions

The major findings from the study are as follows:

1. Significant improvements in the recovery of the 2.20 SG sink fraction of Fire Clay can be realized by calcinating in an inert atmosphere at 1000°C. Clays were found to sinter at such high temperatures under oxidizing atmosphere; however, inert atmospheres allowed for enhanced recovery of LREEs. This could be a benefit obtained from the decomposition of REE phosphate minerals that have been previously identified in fire clay deposits.
2. The kinetics of REE recovery from the calcination products of naturally occurring clays was found to be strongly correlated with the calcination products of coal-derived high

ash density fractions under the same set of calcination conditions. The comparisons have unique characteristic overlaps such as the inability of thermal treatment for enhancing the recovery of contained heavy REEs and the leaching kinetics of light REEs and contaminant elements such as Al and Fe. The thermal analysis of the natural kaolinite mineral and the coal-derived samples also presented with an overlap of a characteristic transformation peak of meta kaolinite to mullite at 950-1000°C.

3. Aluminum and iron associated with the clays dissolve gradually with time in strong acid solutions at high temperatures. The leachability of both elements increases when the clays are dehydrated and are converted to meta-kaolinite at calcination temperatures of 500-800°C. The LREEs contained in meta kaolinite were found to readily dissolve in acid with exceptionally high leaching recovery. The optimum solution to obtain selectivity while extracting REEs contained in clays is to calcinate at 500-800°C and allow shorter leaching time.
4. Calcium in coal deposits exists as calcium carbonates that readily react with acids and release carbon dioxide. The calcination product of calcite is calcium oxide which is readily soluble in an aqueous solution. Due to the high solubility of both the calcium minerals, calcination does not provide an avenue for moderating the leaching characteristics of calcium.
5. High-temperature calcination treatment irrespective of the environmental condition was found to have a preferential bias for the recovery of LREEs. Thus, the best condition to achieve a final REE product with a high HREE/LREE ratio was to opt for leaching on the untreated material. The magnitude of the benefit of recovery of the HREEs was not as pronounced as that of the LREEs for the clean coal fractions. Additionally, the HREE recovery was not affected by calcination for the high ash containing density fractions.

CHAPTER 8. CONCLUSIONS

The finely dispersed REEs associated with non-uniform mineralogy in coal result in poor leaching recovery despite harsh leaching conditions. Maximizing the recovery of the REEs and rejection of the contaminants (Al, Ca, and Fe) is very critical for the economic viability of the hydrometallurgical extraction of REEs from coal-derived sources. A systematic investigation was completed for assessing the benefits provided by an oxidation pretreatment step before leaching for improving the recovery of REEs from coal-based materials. The study involved the detailed and scientific evaluation of novel low-temperature plasma and conventional high-temperature calcination as pretreatment operations to potentially release, liberate or transform the REE-bearing minerals for enhanced recovery. The technical viability of using a low-temperature plasma (LTP) as a pretreatment unit operation with a typical hydrometallurgical circuit was established and a rare earth oxide (REO) concentrate containing greater than 97% REO was produced from both sources. Exceptional improvements in the recovery of light REEs were obtained by calcination of material within several density fractions obtained from WK-13 and Fire Clay seam coal sources at 600-800°C under oxidizing conditions after grinding to a particle size less than 165 μm . However, additional benefits were obtained for the recovery of light REEs at 1000°C for calcination under inert conditions. A good correlation between the recovery of REEs was realized for the heaviest, high ash density fractions and naturally occurring pure clay minerals supporting the hypothesis of an association between the REEs and the clay minerals found in coal. The detailed findings of the research presented in the dissertation are as follows:

1. Prolonged LTP oxidation treatment provided a significant and positive impact on the leachability of heavy REEs that are of critical importance associated with the WK-13 coal material using benign ammonium sulfate solution. The benefits were primarily realized for the 1.60 SG float fraction. An insignificant effect was found for the 2.20 SG sink fraction despite 32 hours of LTP oxidation. Based on this evidence along with other supporting facts such as the XRD analysis discussed in Chapter 4, it was concluded that the finding was due to an affinity of a portion of the HREEs with the carbonaceous material, which was removed during the LTP treatment. The affinity may

be due to a chemical bond with the natural chelating components of the organic matrix and/or the association with the micro dispersed mineral material contained within the coal.

2. The improvements in the recovery of REEs by LTP oxidation resulted in part from increased porosity and increased surface area of the treated feed, which allowed improved access for the lixivants to react and extract the REEs bound in the organic structure and the micro dispersed mineral matter. The BET surface area analysis and SEM micrographs confirmed the formation of a highly porous structure after LTP treatment.
3. The insignificant effect of the LTP on the high ash density fractions of the two coal sources suggested that REEs bound to the mineral matter were not activated by low temperatures despite a highly reactive oxidizing environment created by the oxygen plasma. As such, decomposition of the mineral matter needs to be facilitated by high-temperature oxidation methods to enhance the recovery of REEs contained in the minerals that constitute the ash in a coal seam.
4. From the high-temperature calcination tests, the recovery of heavy REEs contained in the 1.60 SG float fraction of WK-13 was maximized when the material was calcinated at 400°C in air for a longer residence time. The heavy REEs associated with coal pyrite were also found to have high recoveries at 400° due to the formation of a fissured intermediate iron oxide. When the calcination temperature was further increased, the combustible matter was completely removed, and the resulting ash exhibited high total REE recovery with more significant improvements in the recovery of the light REEs.
5. The TGA-DSC analysis of the phase transformations in the pure mineral species provided evidence that calcination at 600-800°C caused dehydroxylation of kaolinite and illite clays that were present in the WK-13 and Fire Clay seam coals. This removal of hydration water from aluminosilicate structures allowed for higher recovery of the associated REEs. However, calcination under these set of conditions also enabled higher dissolution of contaminant elements such as Al that constitute the clay and Fe which is present as an impurity due to iron oxide and as a substitution ion in the

- aluminosilicate lattice. Based on the results of the kinetic leaching tests, selectivity towards REE recovery can be achieved by exploiting the differences in the leaching kinetics of the REEs and contaminant elements. This can be accomplished by allowing a lower residence time for the calcinated feed in the leaching circuit to extract the majority of REEs within the first 10 minutes of leaching while the Al and Fe are dissolved gradually with time.
6. About 30-40% of HREEs were recovered from the 2.20 SG sink fraction of the two feed sources without any calcination pretreatment. The remainder (60-70%) of the insoluble heavy REEs possibly occurred as finely dispersed REE minerals that would require the use of chemical additives for decomposition during the calcination process. Leaching the untreated feed allowed for the highest HREE/LREE ratio in the final product as the recovery of the heavy REEs contained in the high-density ash material was found to be independent of calcination temperature, heating rates, and residence times. Calcination of the 2.20 SG sink fraction significantly improved the LREE recovery and product yield but downgraded the HREE/LREE ratio in the product.
 7. The development of a new process flowsheet using calcination at 400-500°C and magnetic separation before leaching, allowed for the removal of the bulk of the iron contained in pyrite-rich feedstocks. This was accomplished by exploiting the subtle differences in the magnetic properties of the iron oxides and the gangue minerals present in the calcination products. The magnetic fraction was generated from the calcination of the pyrite-rich 2.20 SG sink fraction of the WK-13 under an oxidizing atmosphere. The material was passed through a wet, high-intensity magnetic separator to recover the magnetic fraction, which was found to contain easy-to-leach HREEs. Additionally, the non-magnetic material was found to be enriched with about 15% higher total REEs as compared to the calcined feed.
 8. Calcination tests performed under an inert environment (nitrogen) provided improved leaching recoveries (74%) at 1000°C from the heavy density fractions of the Fire Clay source, which contrasted with the poor (22%) leaching recovery performance under oxygen. The subpar leaching performance under oxygen was likely due to sintering of

the clay surfaces which was not observed when the samples were calcinated in an inert condition at the same temperature. The benefits of REE recovery at 1000°C under an inert atmosphere were possibly facilitated by the decomposition of REE-bearing phosphate minerals like monazite and xenotime in addition to the dehydroxylation of clays.

9. The kinetics of REE recovery from the calcination products of naturally occurring clays was found to be strongly correlated with the calcination products of coal-derived high ash density fractions under the same set of calcination conditions. The comparisons have unique characteristic overlaps such as the inability of thermal treatment for enhancing the recovery of contained heavy REEs and the leaching kinetics of light REEs and contaminant elements such as Al and Fe. The thermal analysis of the natural kaolinite mineral and the coal-derived samples also presented with an overlap of a characteristic transformation peak of meta kaolinite to mullite at 950-1000°C.

CHAPTER 9. RECOMMENDATIONS FOR FUTURE WORK

The current study focused on selectively improving REE leaching characteristics from coal-derived feedstocks while rejecting the bulk of the contaminant ions by oxidation pretreatment of the feed. The effect of atmospheric conditions and temperature was evaluated for the different density fractions of the two coal coarse refuse sources. In continuation of the efforts specific suggestions for future studies are as follows:

1. A significant fraction of the HREEs associated with the high-density fractions was found to be unaffected by bank calculation pretreatment under either oxidizing or the inert environment despite calcination temperatures of 1000°C. Thus, calcination tests with chemical additives should be performed to chemically crack the HREE bearing mineral forms.
2. Calcination of the high ash density fractions was found to provide higher recovery of REEs under an inert atmosphere as compared to an oxidizing atmosphere. A detailed study of the effect of thermal treatment by calcination under an inert atmosphere should be undertaken to establish the best set of calcination parameters. A kinetic leaching study will also provide details on the benefits of inert calcination concerning the recovery with time.
3. It was found that the untreated feed had a moderate recovery of HREEs without calcination pretreatment. Investigations need to be focused on the possible mode of association of such easy-to-leach HREEs which are of critical importance with the density fractions.
4. A detailed evaluation of the proposed flowsheet should be made for a pyrite-rich source at every step of the hydrometallurgical circuit. This would prove to be an excellent exercise to test the efficacy of the flowsheet for the rejection of contaminants and evaluation of the potential benefits in downstream processing due to lower contamination in the PLS solution.

REFERENCES

1. USGS, Mineral commodity summaries 2021, in Mineral Commodity Summaries. 2021: Reston, VA. p. 200.
2. Van Gosen, B.S., P.L. Verplanck, and P. Emsbo, Rare earth element mineral deposits in the United States, in Circular. 2019: Reston, VA. p. 24.
3. Zhang, W., et al., A review of the occurrence and promising recovery methods of rare earth elements from coal and coal by-products. *International Journal of Coal Preparation and Utilization*, 2015. 35(6): p. 295-330.
4. Gupta, T., et al., Characterizing rare earth elements in Alaskan coal and ash. *Minerals & Metallurgical Processing*, 2017. 34(3): p. 138-145.
5. Luttrell, G.H., et al., A Field Survey of Rare Earth Element Concentrations in Process Streams Produced by Coal Preparation Plants in the Eastern USA. *Mining, Metallurgy & Exploration*, 2019. 36(5): p. 889-902.
6. Peelman, S., et al., Hydrometallurgical Recovery of Rare Earth Elements from Mine Tailings and WEEE. *Journal of Sustainable Metallurgy*, 2018. 4(3): p. 367-377.
7. Wang, M., et al., Catalytic leaching process of bastnaesite with hydrochloric acid after oxidation roasting pretreatment. *Journal of the Chinese Society of Rare Earths*, 2013. 31(2): p. 148.
8. Xue, B., et al., Leaching kinetics of bastnaesite concentrate in HCl solution. *Transactions of Nonferrous Metals Society of China*, 2011. 21(10): p. 2306-2310.
9. Gupta, T., Recovery of rare earth elements from Alaskan coal and coal combustion products. 2016: University of Alaska Fairbanks.
10. Beltrami, D., et al., Recovery of yttrium and lanthanides from sulfate solutions with high concentration of iron and low rare earth content. *Hydrometallurgy*, 2015. 157: p. 356-362.
11. Honaker, R., et al., Hydrometallurgical Extraction of Rare Earth Elements from Coal, in *Extraction 2018*. 2018, Springer. p. 2309-2322.
12. Zhang, W., et al., A comprehensive review of rare earth elements recovery from coal-related materials. *Minerals*, 2020. 10(5): p. 451.
13. Yang, X., J. Werner, and R. Honaker, Leaching of rare Earth elements from an Illinois basin coal source. *Journal of Rare Earths*, 2019. 37(3): p. 312-321.
14. Honaker, R.Q., et al., Conception of an integrated flowsheet for rare earth elements recovery from coal coarse refuse. *Minerals Engineering*, 2018. 122: p. 233-240.
15. Yang, X., Leaching Characteristics of Rare Earth Elements from Bituminous Coal-Based Sources. 2019.

16. Honaker, R., et al., Enhancement of a process flowsheet for recovering and concentrating critical materials from bituminous coal sources. *Mining, Metallurgy & Exploration*, 2020. 37(1): p. 3-20.
17. Ji, B., Q. Li, and W. Zhang, Leaching Recovery of Rare Earth Elements from Calcination Product of a Coal Coarse Refuse Using Organic Acids. *Journal of Rare Earths*, 2020.
18. Yanhui, X., et al., Decomposition of bastnasite and monazite mixed rare earth minerals calcined by alkali liquid. *Journal of Rare Earths*, 2012. 30(2): p. 155-158.
19. Feng, X.-l., et al., Kinetics of rare earth leaching from roasted ore of bastnaesite with sulfuric acid. *Transactions of Nonferrous Metals Society of China*, 2013. 23(3): p. 849-854.
20. Krishnamurthy, N. and C.K. Gupta, *Extractive metallurgy of rare earths*. 2004: CRC press.
21. Seredin, V.V. and S. Dai, Coal deposits as potential alternative sources for lanthanides and yttrium. *International Journal of Coal Geology*, 2012. 94: p. 67-93.
22. Dai, S., et al., Mineralogy and geochemistry of boehmite-rich coals: new insights from the Haerwusu Surface Mine, Jungar Coalfield, Inner Mongolia, China. *International Journal of Coal Geology*, 2008. 74(3-4): p. 185-202.
23. Hower, J.C., et al., Rare earth minerals in a “no tonstein” section of the Dean (Fire Clay) coal, Knox County, Kentucky. *International Journal of Coal Geology*, 2018. 193: p. 73-86.
24. Hower, J.C., L.F. Ruppert, and C.F. Eble, Lanthanide, yttrium, and zirconium anomalies in the Fire Clay coal bed, Eastern Kentucky. *International Journal of Coal Geology*, 1999. 39(1-3): p. 141-153.
25. Schulz, K.J., et al., *Critical mineral resources of the United States: economic and environmental geology and prospects for future supply*. 2018: Geological Survey.
26. Moldoveanu, G.A. and V.G. Papangelakis, Recovery of rare earth elements adsorbed on clay minerals: I. Desorption mechanism. *Hydrometallurgy*, 2012. 117: p. 71-78.
27. Gschneidner, K.A., *Rare earths: the fraternal fifteen*. 1967: US Atomic Energy Commission, Division of Technical Information.
28. De Decker, J., *Functionalized metal-organic frameworks as selective metal adsorbents*. 2017, Ghent University.
29. Lide, D.R., *Abundance of elements in the Earth’s crust and in the sea*. *CRC Handbook of chemistry and physics*, Internet version, 2005: p. 14-17.
30. Ober, J.A., *Mineral commodity summaries 2016*. 2016, US Geological Survey.
31. Kalvig, P. and E. Machacek, Examining the rare-earth elements (REE) supply–demand balance for future global wind power scenarios. *GEUS Bulletin*, 2018. 41: p. 87-90.

32. Outlook, I.G.E., Towards cross-modal electrification. International Energy Agency: Paris, France, 2018: p. 1-141.
33. Szumigala, D.J. and M.B. Werdon, Rare-earth Elements: A Brief Overview Including Uses, Worldwide Resources, and Known Occurrences in Alaska \$ nElektronische Ressource. 2011: State of Alaska, Department of Natural Resources, Division of Geological
34. Sadri, F., A.M. Nazari, and A. Ghahreman, A review on the cracking, baking and leaching processes of rare earth element concentrates. *Journal of rare earths*, 2017. 35(8): p. 739-752.
35. Jordens, A., Y.P. Cheng, and K.E. Waters, A review of the beneficiation of rare earth element bearing minerals. *Minerals Engineering*, 2013. 41: p. 97-114.
36. Zhang, W. and R. Honaker, Calcination pretreatment effects on acid leaching characteristics of rare earth elements from middlings and coarse refuse material associated with a bituminous coal source. *Fuel*, 2019. 249: p. 130-145.
37. Peiró, L.T. and G.V. Méndez, Material and energy requirement for rare earth production. *JOM*, 2013. 65(10): p. 1327-1340.
38. Parker, J.G. and C.T. Baroch, Rare-earth elements, yttrium, and thorium. A materials survey. 1971, Bureau of Mines, Washington, DC (USA).
39. Fuerstenau, D. and PRADIP. Alkyl hydroxamates as collectors for the flotation of bastnaesite rare-earth ores. in *Journal of Metals*. 1988. MINERALS METALS MATERIALS SOC 420 COMMONWEALTH DR, WARRENDALE, PA 15086.
40. Aplan, F., The processing of rare earth minerals. *Rare Earths: Extraction, Preparation and Applications*, 1989: p. 15-34.
41. Houot, R., et al. Recovery of rare earth minerals, with emphasis on flotation process. in *Materials Science Forum*. 1991. Trans Tech Publ.
42. Kul, M., Y. Topkaya, and İ. Karakaya, Rare earth double sulfates from pre-concentrated bastnasite. *Hydrometallurgy*, 2008. 93(3-4): p. 129-135.
43. Kumari, A., et al., Process development to recover rare earth metals from monazite mineral: A review. *Minerals Engineering*, 2015. 79: p. 102-115.
44. Jordens, A., et al., Processing a rare earth mineral deposit using gravity and magnetic separation. *Minerals Engineering*, 2014. 62: p. 9-18.
45. Ferron, C.J., S.M. Bulatovic, and R.S. Salter. Beneficiation of rare earth oxide minerals. in *Materials Science Forum*. 1991. Trans Tech Publ.
46. Pavez, O. and A. Peres. Flotation of monazite-zircon-rutile with sodium oleate and hydroxamates. in *XVIII International Mineral Processing Congress*. 1993.
47. Qi, D., Chapter 1 - Extraction of Rare Earths From RE Concentrates, in *Hydrometallurgy of Rare Earths*, D. Qi, Editor. 2018, Elsevier. p. 1-185.
48. Leadbetter, J., Rare Earth Separation Using Monazite and Xenotime. 2016, UC Irvine.

49. Kruesi, P.R. and G. Duker, Production of rare earth chloride from bastnasite. *JOM*, 1965. 17(8): p. 847-849.
50. Brugger, W. and E. Greinacher, A process for direct chlorination of rare earth ores at high temperatures on a production scale. *JOM*, 1967. 19(12): p. 32-35.
51. Hart, K. and D. Levins. Management of wastes from the processing of rare earth minerals. in *Chemeca 88: Australia's Bicentennial International Conference for the Process Industries; Preprints of Papers*. 1988. Institution of Engineers, Australia.
52. Kumari, A., et al., Thermal treatment for the separation of phosphate and recovery of rare earth metals (REMs) from Korean monazite. *Journal of Industrial and Engineering Chemistry*, 2015. 21: p. 696-703.
53. Krumholz, P., Brazilian practice for monazite treatment. *Proceedings of rare metals*, Indian institute of metals and Bhabha atomic research centre, Bombay, 1957: p. 78-82.
54. Topp, N.E., *The chemistry of the rare-earth elements*. Vol. 4. 1965: Elsevier Publishing Company.
55. Lange, A., *Advances in Extractive Metallurgy*. Inst. Min. Metall., 1968.
56. Hoshino, M., K. Sanematsu, and Y. Watanabe, Chapter 279 - REE Mineralogy and Resources, in *Handbook on the Physics and Chemistry of Rare Earths*, B. Jean-Claude and P. Vitalij K, Editors. 2016, Elsevier. p. 129-291.
57. Moldoveanu, G.A. and V.G. Papangelakis, An overview of rare-earth recovery by ion-exchange leaching from ion-adsorption clays of various origins. *Mineralogical Magazine*, 2016. 80(1): p. 63-76.
58. Chi, R.-a. and Z.-g. Xu, A solution chemistry approach to the study of rare earth element precipitation by oxalic acid. *Metallurgical and Materials Transactions B*, 1999. 30(2): p. 189-195.
59. Gao, Y., C.-Z. Fan, and X. Hong, Experimental Study on Adsorption of Rare Earth Elements on Kaolinite and Halloysite. *Acta Geologica Sinica-english Edition*, 2017. 91: p. 80-82.
60. Luo, X., et al., The basic research on the weathered crust elution-deposited rare earth ores. *Nonferrous Metals Science and Engineering*, 2012.
61. Chandra, A., *Thermodynamic Modeling and Equilibrium System Design of a Solvent Extraction Process for Dilute Rare Earth Solutions*. 2019.
62. Seredin, V.V., et al., Coal deposits as promising sources of rare metals for alternative power and energy-efficient technologies. *Applied Geochemistry*, 2013. 31: p. 1-11.
63. Seredin, V., Rare earth element-bearing coals from the Russian Far East deposits. *International Journal of Coal Geology*, 1996. 30(1-2): p. 101-129.
64. Hower, J.C., et al., Distribution of rare earth elements in the pilot-scale processing of fly ashes derived from eastern Kentucky coals: Comparisons of the feed and processed ashes. *Fuel*, 2021. 295: p. 120562.

65. Birk, D. and J.C. White, Rare earth elements in bituminous coals and underclays of the Sydney Basin, Nova Scotia: Element sites, distribution, mineralogy. *International Journal of Coal Geology*, 1991. 19(1): p. 219-251.
66. Zhang, F., et al., Geological Controls on Enrichment of Rare Earth Elements and Yttrium (REY) in Late Permian Coals and Non-Coal Rocks in the Xian'an Coalfield, Guangxi Province. *Minerals*, 2021. 11(3): p. 301.
67. Li, B., et al., Mineralogy and Geochemistry of Late Permian Coals within the Tongzi Coalfield in Guizhou Province, Southwest China. *Minerals*, 2020. 10(1): p. 44.
68. Blissett, R., N. Smalley, and N. Rowson, An investigation into six coal fly ashes from the United Kingdom and Poland to evaluate rare earth element content. *Fuel*, 2014. 119: p. 236-239.
69. Wagner, N.J. and A. Matiane, Rare earth elements in select Main Karoo Basin (South Africa) coal and coal ash samples. *International Journal of Coal Geology*, 2018. 196: p. 82-92.
70. Akdogan, G., et al., Characterization of rare earth elements by XRT sorting products of a South African coal seam. *International Journal of Coal Preparation and Utilization*, 2019: p. 1-17.
71. Akdogan, G. and T. Ghosh, Identification of REE in Some Alaskan Coal and Ash Samples. University of Alaska, Available at: <https://edx.netl.doe.gov>, 2014.
72. Huang, Q., et al., Characterization study of rare earths, yttrium, and scandium from various Colombian coal samples and non-coal lithologies. *International Journal of Coal Geology*, 2019. 209: p. 14-26.
73. Wang, W., et al., Partitioning of elements and macerals during preparation of Antaibao coal. *International Journal of Coal Geology*, 2006. 68(3-4): p. 223-232.
74. Seredin, V. Ashes of coals—new potential source of Y and HREE. in *Proceedings of the 29th International Geological Congress*. 1992.
75. Seredin, V., On a new type of rare-earth elements mineralization of cenozoic coal-bearing depressions. *Doklady Akademii Nauk SSSR*, 1991. 320: p. 1446-1450.
76. Ekmann, J. Rare Earth Elements in Coal Deposits—a Prospectivity Analysis. in *Adapted from poster presentations AAPG Easter Section meeting, Cleveland, Ohio*. 2012.
77. Lin, R., et al., Organic and inorganic associations of rare earth elements in central Appalachian coal. *International Journal of Coal Geology*, 2017. 179: p. 295-301.
78. Gupta, T., et al., Maximizing REE Enrichment by Froth Flotation of Alaskan Coal Using Box-Behnken Design. *Mining, Metallurgy & Exploration*, 2019. 36(3): p. 571-578.
79. Zhang, W., R. Honaker, and J. Groppo, Concentration of rare earth minerals from coal by froth flotation. *Minerals & Metallurgical Processing*, 2017. 34(3): p. 132-137.

80. Zhang, W., X. Yang, and R.Q. Honaker, Association characteristic study and preliminary recovery investigation of rare earth elements from Fire Clay seam coal middlings. *Fuel*, 2018. 215: p. 551-560.
81. Lin, R., et al., Enrichment of rare earth elements from coal and coal by-products by physical separations. *Fuel*, 2017. 200: p. 506-520.
82. Huang, Q., et al., Liberation and release of rare earth minerals from Middle Kittanning, Fire Clay, and West Kentucky No. 13 coal sources. *Powder Technology*, 2018. 332: p. 242-252.
83. Ganguli, R. and D.R. Cook, Rare earths: A review of the landscape. *MRS Energy & Sustainability*, 2018. 5.
84. Zhang, W., et al., Effects of contaminant metal ions on precipitation recovery of rare earth elements using oxalic acid. *Journal of Rare Earths*, 2020.
85. Hassas, B.V., M. Rezaee, and S.V. Pisupati, Precipitation of rare earth elements from acid mine drainage by CO₂ mineralization process. *Chemical Engineering Journal*, 2020. 399: p. 125716.
86. Honaker, R., W. Zhang, and J. Werner, Acid leaching of rare earth elements from coal and coal ash: Implications for using fluidized bed combustion to assist in the recovery of critical materials. *Energy & Fuels*, 2019. 33(7): p. 5971-5980.
87. Free, M.L., *Hydrometallurgy: fundamentals and applications*. 2013: John Wiley & Sons.
88. Gupta, C.K., *Hydrometallurgy in Extraction Processes, Volume II*. 2017: Routledge.
89. Gupta, C.K., *Chemical metallurgy: principles and practice*. 2006: John Wiley & Sons.
90. Zhang, W. and R. Honaker, Enhanced leachability of rare earth elements from calcined products of bituminous coals. *Minerals Engineering*, 2019. 142: p. 105935.
91. Zhang, W. and R. Honaker, Characterization and recovery of rare earth elements and other critical metals (Co, Cr, Li, Mn, Sr, and V) from the calcination products of a coal refuse sample. *Fuel*, 2020. 267: p. 117236.
92. Yuan, S., et al., Kinetics of Roasting Decomposition of the Rare Earth Elements by CaO and Coal. *Metals*, 2017. 7(6): p. 213.
93. Sachan, A., Enhanced bioweathering of coal for rare earth element extraction and concentration. 2019: University of Alaska Fairbanks.
94. Park, S. and Y. Liang, Bioleaching of trace elements and rare earth elements from coal fly ash. *International Journal of Coal Science & Technology*, 2019. 6(1): p. 74-83.
95. Sarswat, P.K., et al., Efficient recovery of rare earth elements from coal based resources: a bioleaching approach. *Materials Today Chemistry*, 2020. 16: p. 100246.

96. Park, D., et al., A biosorption-based approach for selective extraction of rare earth elements from coal byproducts. *Separation and Purification Technology*, 2020. 241: p. 116726.
97. Goldston, R.J. and P.H. Rutherford, *Introduction to plasma physics*. 1995: CRC Press.
98. Gomez, E., et al., Thermal plasma technology for the treatment of wastes: a critical review. *Journal of hazardous materials*, 2009. 161(2-3): p. 614-626.
99. Bárdos, L. and H. Baránková, Cold atmospheric plasma: Sources, processes, and applications. *Thin Solid Films*, 2010. 518(23): p. 6705-6713.
100. Kemp, D. and A. Cilliers, High-temperature thermal plasma treatment of monazite followed by aqueous digestion. *Journal of the Southern African Institute of Mining and Metallurgy*, 2016. 116(10): p. 901-906.
101. Patiño, P., et al., Upgrading of diesel fuels and mixtures of hydrocarbons by means of oxygen low pressure plasmas: a comparative study☆. *Fuel*, 2003. 82(13): p. 1613-1619.
102. Bond, J. and L. Giroux. Low temperature plasma ashing of coal for quantitative mineral analysis. in 2013 World Of Coal Ash (WOCA) Conference—April 22-2. 2013.
103. Graves, D. and M. Kushner. Low temperature plasma science: not only the fourth state of matter but all of them. in Report of the Department of Energy Office of Fusion Sciences Workshop Low Temperature Plasmas. 2008.
104. Semenova, S., et al., Modification of Mongolian coals using a low-temperature oxygen plasma. *Solid Fuel Chemistry*, 2013. 47(2): p. 83-87.
105. Taylor, P.R. and S.A. Pirzada, Thermal plasma processing of materials: a review. *Advanced Performance Materials*, 1994. 1(1): p. 35-50.
106. Schriver, D., M. Ashour-Abdalla, and R. Richard, On the origin of the ion-electron temperature difference in the plasma sheet. *Journal of Geophysical Research: Space Physics*, 1998. 103(A7): p. 14879-14895.
107. Gleit, C.E. and W.D. Holland, Use of Electrically Excited Oxygen for the Low Temperature Decomposition of Organic Substances. *Analytical Chemistry*, 1962. 34(11): p. 1454-1457.
108. Hozumi, K., M. Hutoh, and K. Umemoto, Identification of the source of the crude drug Tu-zhu-ye using low-temperature plasma ashing. *Microchemical journal*, 1972. 17(2): p. 173-185.
109. Adolphi, P. and M. Stör, Glow discharge excited low temperature ashing: A new technique for separating mineral matter of coals. *Fuel*, 1985. 64(2): p. 151-155.
110. McConkey, J., et al., Electron impact dissociation of oxygen-containing molecules—A critical review. *Physics Reports*, 2008. 466(1-3): p. 1-103.
111. Application for plasma etching and ashing. 2019; Available from: https://www.emsdiasum.com/microscopy/technical/datasheet/plasma_apps.aspx.

112. Kuhn, J.K., F. Fiene, and R.D. Harvey, Geochemical evaluation and characterization of a Pittsburgh No. 8 and a Rosebud seam coal. 1978: Department of Energy, [Office of the Assistant Secretary for
113. Richaud, R., A. Herod, and R. Kandiyoti, Comparison of trace element contents in low-temperature and high-temperature ash from coals and biomass. *Fuel*, 2004. 83(14-15): p. 2001-2012.
114. Allen, R.M., R.W. Carling, and J.B. VanderSande, Microstructural changes in coal during low temperature ashing. *Fuel*, 1986. 65(3): p. 321-326.
115. Miller, R.N., R.F. Yarzab, and P.H. Given, Determination of the mineral-matter contents of coals by low-temperature ashing. *Fuel*, 1979. 58(1): p. 4-10.
116. Schweinfurth, S.P., *Coal--a Complex Natural Resource: An Overview of Factors Affecting Coal Quality and Use in the United States*. 2003.
117. Scherzer, J., Dealuminated faujasite-type structures with SiO₂Al₂O₃ ratios over 100. *Journal of Catalysis*, 1978. 54(2): p. 285-288.
118. Lier, J.A.V., P.L.D. Bruyn, and J.T.G. Overbeek, THE SOLUBILITY OF QUARTZ. *The Journal of Physical Chemistry*, 1960. 64(11): p. 1675-1682.
119. Ringdalen, E., Changes in quartz during heating and the possible effects on Si production. *Jom*, 2015. 67(2): p. 484-492.
120. Zemskova, M., V. Prokofiev, and A. Bychkov, Analysis of Rare Earth Elements (REE) in vein quartz and quartz-sandstone host rock in the Zhelannoe high purity quartz deposit, Russia. 2015. p. 1007.
121. Santoro, A., et al., Assessing rare earth elements in quartz rich geological samples. *Applied Radiation and Isotopes*, 2016. 107: p. 323-329.
122. Lauf, R.J., L.A. Harris, and S.S. Rawlston, Pyrite framboids as the source of magnetite spheres in fly ash. *Environmental Science & Technology*, 1982. 16(4): p. 218-220.
123. Schweinfurth, S.P. and R.B. Finkelman, *Coal--a complex natural resource : an overview of factors affecting coal quality and use in the United States*, in Circular. 2002.
124. Wang, L., et al., Magnetic properties related to thermal treatment of pyrite. *Science in China Series D: Earth Sciences*, 2008. 51(8): p. 1144-1153.
125. Yan, J., L. Xu, and J. Yang, A study on the thermal decomposition of coal-derived pyrite. *Journal of Analytical and Applied pyrolysis*, 2008. 82(2): p. 229-234.
126. Groves, S., J. Williamson, and A. Sanyal, Decomposition of pyrite during pulverized coal combustion. *Fuel*, 1987. 66(4): p. 461-466.
127. Srinivasachar, S., J.J. Helble, and A.A. Boni, Mineral behavior during coal combustion 1. Pyrite transformations. *Progress in Energy and Combustion Science*, 1990. 16(4): p. 281-292.
128. Jovanović, D., Kinetics of thermal decomposition of pyrite in an inert atmosphere. *Journal of thermal analysis*, 1989. 35(5): p. 1483-1492.

129. Paulik, F., J. Paulik, and M. Arnold, Kinetics and mechanism of the decomposition of pyrite under conventional and quasi-isothermal—quasi-isobaric thermoanalytical conditions. *Journal of Thermal Analysis and Calorimetry*, 1982. 25(2): p. 313-325.
130. Zhou, Y., et al., Thermal phase transition of pyrite from coal. *Journal of Thermal Analysis and Calorimetry*, 2018. 134(3): p. 2391-2396.
131. Thomas, P.S., et al., Characterisation of the oxidation products of pyrite by Thermogravimetric and Evolved Gas analysis. *Journal of Thermal Analysis and Calorimetry*, 2003. 72(3): p. 769.
132. Chen, H., B. Li, and B. Zhang, Decomposition of pyrite and the interaction of pyrite with coal organic matrix in pyrolysis and hydrolysis. *Fuel*, 2000. 79(13): p. 1627-1631.
133. Waters, K., et al., The effect of heat treatment on the magnetic properties of pyrite. *Minerals Engineering*, 2008. 21(9): p. 679-682.
134. Scott, M., et al., Characterization of Rare Earth Elements in in Clay Deposits Associated with Central Appalachian Coal Seams. 2017. p. B13C-1786.
135. Verba, C., M. Scott, and A.K. Plechacek, The search for rare earths elements and critical metals in underclay deposits. 2018. p. H51P-1537.
136. Yang, J., et al., Microanalytical Approaches to Characterizing REE in Appalachian Basin Underclays. *Minerals*, 2020. 10(6): p. 546.
137. Yang, X., et al., Using yttrium as an indicator to estimate total rare earth element concentration: a case study of anthracite-associated clays from northeastern Pennsylvania. *International Journal of Coal Science & Technology*, 2020. 7(4): p. 652-661.
138. Montross, S.N., et al., Advanced characterization of rare earth element minerals in coal utilization byproducts using multimodal image analysis. *International Journal of Coal Geology*, 2018. 195: p. 362-372.
139. Fitzpatrick, M., *Coal and Underclay*. 2011.
140. J. Ambrose, S.M.-C. and J. Pera, Pozzolanic behavior of thermally activated kaolin. *ACI Symposium Publication*. 132.
141. Altiokka, M.R. and H.L. Hoşgün, Investigation of the dissolution kinetics of kaolin in HCl solution. *Hydrometallurgy*, 2003. 68(1): p. 77-81.
142. Trusilewicz, L., et al., TEM and SAED characterization of metakaolin. Pozzolanic activity. *Journal of the American Ceramic Society*, 2012. 95(9): p. 2989-2996.
143. Edomwonyi-Otu, L., et al., Influence of thermal treatment on kankara kaolinite. *Opticon* 1826, 2013(15).
144. Lemaitre, J. and B. Delmon, Study of the sintering mechanism of kaolinite at 900 and 1050° C; influence of mineralizers. *Journal of Materials Science*, 1977. 12(10): p. 2056-2064.

145. Wang, H., Q. Feng, and K. Liu, The dissolution behavior and mechanism of kaolinite in alkali-acid leaching process. *Applied Clay Science*, 2016. 132-133: p. 273-280.
146. Honaker, R., et al., Laboratory and bench-scale testing for rare earth elements. *Cell*, 2014. 724: p. 554-3652.
147. Standard, A., Standard test methods for proximate analysis of coal and coke by macro Thermogravimetric analysis. 2013, ASTM International West Conshohocken, PA.
148. Standard, A., Test methods for total sulfur in the analysis sample of coal and coke. 2002.
149. Standard, A., D1193–06. 2018.“. Standard specification for reagent water.” ASTM International, West Conshohocken, PA.
150. ITWG, ITWG GUIDELINE ON POWDER X-RAY DIFFRACTION (XRD)—GENERAL OVERVIEW. NUCLEAR FORENSICS INTERNATIONAL TECHNICAL WORKING GROUP, 2015. 1.
151. Brunauer, S., P.H. Emmett, and E. Teller, Adsorption of gases in multimolecular layers. *Journal of the American chemical society*, 1938. 60(2): p. 309-319.
152. Connelly, A., Laboratory Techniques, Science, BET surface area, <https://andyjconnelly.wordpress.com/2017/03/13/bet-surface-area/>. 2017.
153. Taggart, R.K., J.C. Hower, and H. Hsu-Kim, Effects of roasting additives and leaching parameters on the extraction of rare earth elements from coal fly ash. *International Journal of coal geology*, 2018. 196: p. 106-114.
154. Vaidyanathan, N.P., et al., Surface Treatment of Carbon Fibers Using Low Temperature Plasma. *The Journal of Adhesion*, 1995. 48(1-4): p. 1-24.
155. Sha, Z., et al., Low-temperature plasma assisted growth of vertical graphene for enhancing carbon fibre/epoxy interfacial strength. *Composites Science and Technology*, 2019. 184: p. 107867.
156. Oldham, T., et al., Highly Uniform Activation of Carbon Fiber Reinforced Thermoplastics by Low-Temperature Plasma. *ACS Applied Polymer Materials*, 2019. 1(10): p. 2638-2648.
157. Li, C.-q., H.-b. Dong, and W.-w. Zhang, Low-temperature plasma treatment of carbon fibre/epoxy resin composite. *Surface Engineering*, 2018. 34(11): p. 870-876.
158. Erdogan, S., et al., Interaction of metals with humic acid isolated from oxidized coal. *Polish Journal of Environmental Studies*, 2007. 16(5).
159. Mastalerz, M., et al., Rare earth elements and yttrium in Pennsylvanian coals and shales in the eastern part of the Illinois Basin. *International Journal of Coal Geology*, 2020. 231: p. 103620.
160. Honaker, R., et al. Recovery of rare earth minerals and elements from coal and coal byproducts. in *International Coal Preparation Conference*. 2016.

161. Honaker, R., et al., Process evaluation and flowsheet development for the recovery of rare earth elements from coal and associated byproducts. *Minerals & Metallurgical Processing*, 2017. 34(3): p. 107-115.
162. Wenyuan, W., et al., Study on roasting decomposition of mixed rare earth concentrate in CaO-NaCl-CaCl₂. *Journal of Rare Earths*, 2006. 24(1): p. 23-27.
163. Bian, X., et al., Study on decomposition of mixed rare earth concentrate by Ca (OH) 2-NaOH. *Chin. Rare Earths*, 2014. 35(4): p. 30-34.
164. Honaker, R., J.M. Werner, and W. Zhang, Apparatus and method for power generation and valuable element recovery from combustion by-products. 2020, Google Patents.
165. Zhang, W., et al., Lithium leaching recovery and mechanisms from density fractions of an Illinois Basin bituminous coal. *Fuel*, 2020. 268: p. 117319.
166. Dube, R.M., Collectors for enabling flotation of oxidized coal. 2012.
167. Dube, R. and R. Honaker, Improving the flotation performance of an oxidized bituminous coal source. *Minerals Engineering*, 2019. 142: p. 105937.
168. Arya, S., et al., Design and experimental evaluation of a flooded-bed dust scrubber integrated into a longwall shearer. *Powder Technology*, 2018. 339: p. 487-496.
169. Arya, S., J. Sottile, and T. Novak, Development of a flooded-bed scrubber for removing coal dust at a longwall mining section. *Safety Science*, 2018. 110: p. 204-213.
170. Arya, S., et al., Empirical Formulae for Determining Pressure Drop Across a 20-Layer Flooded-Bed Scrubber Screen. *Mining, Metallurgy & Exploration*, 2019. 36(6): p. 1169-1177.
171. Mendbayar, U., et al., Investigation and Quantification of Water Track Networks in Boreal Regions of Alaska. 2016.
172. Zhang, W. and R. Honaker, Process development for the recovery of rare earth elements and critical metals from an acid mine leachate. *Minerals Engineering*, 2020. 153: p. 106382.
173. Ptáček, P., et al., The kinetics and mechanism of kaolin powder sintering I. The dilatometric CRH study of sinter-crystallization of mullite and cristobalite. *Powder Technology*, 2012. 232: p. 24-30.
174. Liu, X., X. Liu, and Y. Hu, Investigation of the thermal behaviour and decomposition kinetics of kaolinite. *Clay Minerals*, 2015. 50(2): p. 199-209.
175. Karunadasa, K.S.P., et al., Thermal decomposition of calcium carbonate (calcite polymorph) as examined by in-situ high-temperature X-ray powder diffraction. *Journal of Physics and Chemistry of Solids*, 2019. 134: p. 21-28.
176. Mitchell, R.E., Mechanisms of pyrite oxidation to non-slagging species. 2002, Stanford University (US).
177. Malden, P.J. and R.E. Meads, Substitution by Iron in Kaolinite. *Nature*, 1967. 215(5103): p. 844-846.

178. Hernández, R.H., et al. Iron removal from a kaolinitic clay by leaching to obtain high whiteness index. in IOP Conference Series: Materials Science and Engineering. 2013. IOP Publishing.
179. Finkelman, R.B., Modes of occurrence of potentially hazardous elements in coal: levels of confidence. *Fuel processing technology*, 1994. 39(1-3): p. 21-34.
180. Valian, A., Characterization of Rare Earth Elements in the Illinois Basin Coals. 2020.
181. Hu, G., et al., Decomposition and oxidation of pyrite. *Progress in Energy and Combustion Science*, 2006. 32(3): p. 295-314.
182. Fu, P., et al. Effects of Pyrolysis Temperature on Characteristics of Porosity in Biomass Chars. in 2009 International Conference on Energy and Environment Technology. 2009.
183. Zhang, Y., et al., Characteristics of mass, heat and gaseous products during coal spontaneous combustion using TG/DSC–FTIR technology. *Journal of Thermal Analysis and Calorimetry*, 2018. 131(3): p. 2963-2974.
184. Zhu, H., et al., The stage analysis and countermeasures of coal spontaneous combustion based on “five stages” division. *Plos one*, 2018. 13(8): p. e0202724.
185. Liu, H. and F. Wang, Thermal characteristics and kinetic analysis of coal-oxygen reaction under the condition of inert gas. *International Journal of Coal Preparation and Utilization*, 2019: p. 1-17.
186. Cao, Z., et al., Effect of calcination condition on the microstructure and pozzolanic activity of calcined coal gangue. *International Journal of Mineral Processing*, 2016. 146: p. 23-28.
187. Zhang, Y., et al., Pyrite transformation and sulfur dioxide release during calcination of coal gangue. *Rsc Advances*, 2014. 4(80): p. 42506-42513.
188. Ilić, B.R., A.A. Mitrović, and L.R. Miličić, Thermal treatment of kaolin clay to obtain metakaolin. *Hemijska industrija*, 2010. 64(4): p. 351-356.
189. Meinhold, R., et al., Flash calcination of kaolinite studied by DSC, TG and MAS NMR. *Journal of Thermal Analysis and Calorimetry*, 1992. 38(9): p. 2053-2065.
190. He, C., E. Makovicky, and B. Øsbæck, Thermal stability and pozzolanic activity of calcined illite. *Applied Clay Science*, 1995. 9(5): p. 337-354.
191. LI, H.Y. and S.H. ZHANG, Detection of mineralogical changes in pyrite using measurements of temperature-dependence susceptibilities. *Chinese Journal of Geophysics*, 2005. 48(6): p. 1454-1461.
192. Music, S., S. Popović, and M. Ristić, Thermal decomposition of pyrite. *Journal of radioanalytical and nuclear chemistry*, 1992. 162(2): p. 217-226.
193. Vaughan, D.J., Mineral chemistry of metal sulfides. *Cambridge Earth Sci. Ser.*, Cambridge, 1978. 493.

VITA

EDUCATION

University of Alaska Fairbanks

Master of Science (M.S.) Mining Engineering, Awarded 2016

Indian Institute of Technology-Indian School of Mines, Dhanbad

B. Tech in Mining Engineering, Awarded 2012

INDUSTRIAL EXPERIENCE

Assistant Mine Manager

Coal India Limited, Madhya Pradesh, India (2012-2014)

- Planned underground mining operations and supervised a staff of 200 personnel as a part of daily management.
- Monitored roof support systems and implemented the use of two-point extensometers to proactively detect roof failures.
- Conducted safety drills and drafted technical reports for weekly production and equipment utilization.

RESEARCH EXPERIENCE

Research Assistant

University of Kentucky, Lexington, Kentucky

- Led two bench and pilot-scale projects funded by the US Department of Energy while supervising a team of four undergraduate researchers.
- Developed a novel process for the reduction of iron contamination in REE leaching and slashed processing costs by 50%
- Assisted in designing the experimental program, obliged to environmental health and safety guidelines, and managed project budgets.
- Aided for running a wide variety of analytical equipment (TGA-DSC, TGA (LECO), XRD, XRF, ICP-OES, SEM-EDX) for characterizing the samples.

Research and Teaching Assistant

University of Alaska Fairbanks, Fairbanks, Alaska

- Characterized the presence of rare earth elements in Alaskan coal deposits and developed a flowsheet for their concentration.

- Performed statistical analysis of test data, managed project milestones, and prepared financial and achievement reports.
- Assisted in designing the course structure, prepared teaching material, conducted lab sessions, and graded assignments.

PROFESSIONAL MEMBERSHIP

- Society for Mining, Metallurgy, and Exploration (SME)
- SME- Young Leaders Committee
- University of Kentucky- Graduate Student Congress

PROFESSIONAL PUBLICATIONS

- Gupta, T., Ghosh, T., Akdogan, G., & Bandopadhyay, S. (2019). Maximizing REE enrichment by froth flotation of Alaskan coal using box-Behnken design. *Mining, Metallurgy & Exploration*, 36(3), 571-578.
- Gupta, T., Ghosh, T., Akdogan, G., & Srivastava, V. K. (2017). Characterizing rare earth elements in Alaskan coal and ash. *Minerals & Metallurgical Processing*, 34(3), 138-145.
- Gupta, T. (2016). Recovery of rare earth elements from Alaskan coal and coal combustion products. University of Alaska Fairbanks.
- Mendbayar, U., Misra, D., Gupta, T., & Ghosh, T. (2016). Investigation and Quantification of Water Track Networks in Boreal Regions of Alaska.

CONFERENCE PRESENTATIONS

- Gupta T., Zhang W. and Honaker R., Oxidation Pretreatment for Enhanced Leachability of Rare Earth Elements from Bituminous Coal Sources, SME Annual Conference and Expo, February 22-26, 2020, Phoenix, AZ
- Gupta T., Zhang W. and Honaker R., Low-Temperature Plasma Treatment for Enhanced Recovery of Rare Earth Elements From Coal, SME Annual Meeting, February 24-27, 2019, Denver CO.
- Gupta T., Ghosh T, Akdogan G, Characterizing REEs in Alaskan Coal and Ash, SME Annual Meeting, February 21-24, 2016, Phoenix, AZ

AWARDS AND FELLOWSHIPS

- SME- Raja & Geetha V Ramani Graduate Thesis Award (2021)

- SME- WAAIME Scholarship (2020, 2019, 2018)
- SME- Grand Canyon Scholarship (2020, 2015)
- SME- MPD Outstanding Graduate Scholarship (2020)
- SME- Gerald V. Henderson Memorial Scholarship (2019)
- SME- Mineral Processing Division Poster session-2nd Position (2018)
- Alaska Geological Society Poster session-1st Place (2016)